

Habiba Drias
Farouk Yalaoui *Editors*

Quantum Computing: Applications and Challenges

Information Systems Engineering and Management

2

Editorial Board Members

Abdelkader Hameurlain, *Université Toulouse III - Paul Sabatier, Toulouse, France*

Ashwani Kumar Dubey, *Amity University, Noida, India*

Carlos Montenegro, *Francisco José de Caldas District University, Bogota, Colombia*

Fernando Moreira, *Portucalense University, Berlin, Germany*

Francisco Peñalvo, *University of Salamanca, Salamanca, Spain*

Gintautas Dzemyda, *Vilnius University, Vilnius, Lithuania*

Jezreel Mejia-Miranda, *CIMAT - Center for Mathematical Research, Zacatecas, Zacatecas, Mexico*

Mário Piattini, *University of Castilla-La Mancha, Albacete, Spain*

Mirjana Ivanović, *Dept. of Mathematics and Informatics, University of Novi Sad, Novi Sad, Serbia*

Mirna Muñoz, *CIMAT - Center for Mathematical Research, Progreso, Zacatecas, Mexico*

Sajid Anwar, *Institute of Management Sciences, Peshawar, Pakistan*

Tutut Herawan, *Faculty of Comp Sci & Info Tech, University of Malaya, Kuala Lumpur, Malaysia*

Valentina Colla, *TeCIP Institute, Scuola Superiore Sant'Anna, Pisa, Italy*

Vladan Devedzic, *University of Belgrade, Belgrade, Serbia*

Series Editor

Álvaro Rocha, *ISEG, University of Lisbon, Lisbon, Portugal*

The book series “Information Systems Engineering and Management” (ISEM) publishes innovative and original works in the various areas of planning, development, implementation, and management of information systems and technologies by enterprises, citizens, and society for the improvement of the socio-economic environment.

The series is multidisciplinary, focusing on technological, organizational, and social domains of information systems engineering and management. Manuscripts published in this book series focus on relevant problems and research in the planning, analysis, design, implementation, exploration, and management of all types of information systems and technologies. The series contains monographs, lecture notes, edited volumes, pedagogical and technical books as well as proceedings volumes.

Some topics/keywords to be considered in the ISEM book series are, but not limited to: Information Systems Planning; Information Systems Development; Exploration of Information Systems; Management of Information Systems; Blockchain Technology; Cloud Computing; Artificial Intelligence (AI) and Machine Learning; Big Data Analytics; Multimedia Systems; Computer Networks, Mobility and Pervasive Systems; IT Security, Ethics and Privacy; Cybersecurity; Digital Platforms and Services; Requirements Engineering; Software Engineering; Process and Knowledge Engineering; Security and Privacy Engineering, Autonomous Robotics; Human-Computer Interaction; Marketing and Information; Tourism and Information; Finance and Value; Decisions and Risk; Innovation and Projects; Strategy and People.

Indexed by Google Scholar. All books published in the series are submitted for consideration in the Web of Science.

For book or proceedings proposals please contact Alvaro Rocha (amrrocha@gmail.com).

SERIES EDITOR:

Álvaro Rocha, ISEG, University of Lisbon, Portugal

ADVISORY BOARD:

Abdelkader Hameurlain, Université Toulouse III - Paul Sabatier, France

Ashwani Kumar Dubey, Amity University, India

Carlos Montenegro, Francisco José de Caldas District University, Colombia

Fernando Moreira, Portucalense University, Portugal

Francisco Peñalvo, University of Salamanca, Spain

Gintautas Dzemyda, Vilnius University, Lithuania

Jezreel Mejia-Miranda, CIMAT - Center for Mathematical Research, Mexico

Mário Piattini, University of Castilla-La Mancha, Spain

Mirjana Ivanović, University of Novi Sad, Serbia

Mirna Muñoz, CIMAT - Center for Mathematical Research, Mexico

Sajid Anwar, Institute of Management Sciences Peshawar, Pakistan

Tutut Herawan, University of Malaya, Malaysia

Valentina Colla, Scuola Superiore Sant'Anna - TeCIP Institute, Italy

Vladan Devedzic, University of Belgrade, Serbia

Habiba Drias · Farouk Yalaoui
Editors

Quantum Computing: Applications and Challenges



Springer

Editors

Habiba Drias
Algerian Academy of Science
and Technology (AAST)
Algiers, Algeria

Head of the Computer Science Section
AAST
Algiers, Algeria

University of Science and Technology Houari
Boumediene (USTHB)
Algiers, Algeria

Head of the laboratory of Research in A.I.
(LRIA)
USTHB
Algiers, Algeria

Farouk Yalaoui
Algerian Academy of Science
and Technology
University of Technology of Troyes (UTT)
Troyes, France

ISSN 3004-958X

ISSN 3004-9598 (electronic)

Information Systems Engineering and Management

ISBN 978-3-031-59317-8

ISBN 978-3-031-59318-5 (eBook)

<https://doi.org/10.1007/978-3-031-59318-5>

© The Editor(s) (if applicable) and The Author(s), under exclusive license
to Springer Nature Switzerland AG 2024

This work is subject to copyright. All rights are solely and exclusively licensed by the Publisher, whether the whole or part of the material is concerned, specifically the rights of translation, reprinting, reuse of illustrations, recitation, broadcasting, reproduction on microfilms or in any other physical way, and transmission or information storage and retrieval, electronic adaptation, computer software, or by similar or dissimilar methodology now known or hereafter developed.

The use of general descriptive names, registered names, trademarks, service marks, etc. in this publication does not imply, even in the absence of a specific statement, that such names are exempt from the relevant protective laws and regulations and therefore free for general use.

The publisher, the authors and the editors are safe to assume that the advice and information in this book are believed to be true and accurate at the date of publication. Neither the publisher nor the authors or the editors give a warranty, expressed or implied, with respect to the material contained herein or for any errors or omissions that may have been made. The publisher remains neutral with regard to jurisdictional claims in published maps and institutional affiliations.

This Springer imprint is published by the registered company Springer Nature Switzerland AG
The registered company address is: Gewerbestrasse 11, 6330 Cham, Switzerland

If disposing of this product, please recycle the paper.

Preface

This volume contains papers from the Symposium on Quantum Sciences, Applications and Challenges (QSAC'2023), held in Algiers during September 24–25, 2023. The event was organized by the computer science section of the Algerian Academy of Science and Technology (AAST), aiming to explore the frontiers of one of the most captivating fields of modern science. Its objective was to inspire innovative research in the realm of quantum sciences. Articles from quantum computing are included in this book. The themes addressed during the scientific event revolved cover the latest developments in quantum computing and their applications. They embrace the fields of quantum machine learning, quantum cryptography, quantum optimization, and quantum artificial intelligence and applications. The book is the first of its kind among the instigators of this discipline in the world. It will allow scientific research to embark on these new and strategic domains.

Quantum computing promises exponentially faster computation and the ability to solve problems that are intractable by classical computers. This challenging field has the power to revolutionize cryptography, optimization, artificial intelligence, and simulations that could transform industries ranging from finance to drug discovery.

The opportunities of quantum technologies are enormous. The calculations carried out by quantum systems are very fast and their spin-offs in industry are very beneficial. This advance will be more talented by hybridizing it with artificial intelligence. Unlike this gainful progress for our society, quantum technologies unfortunately pose threats. The most striking example is the attack on cryptography. Computer security is highly threatened by quantum technologies.

Both opportunities and threats favor the emergence of start-ups, particularly in the fields of quantum computing, quantum communications, quantum post-cryptography and quantum artificial intelligence. Classical computing dealing with data will have to migrate to quantum computing and the sooner the better to ensure data protection.

Sixty-four submissions from quantum sciences were received following the call for papers. Each article was double-blind reviewed by at least three members of the program's international committee and external reviewers. Only 18 top-rated papers from quantum computing were selected for oral presentation, and 15 of them are included in the proceedings, as they all reflect Springer's publication policy. The accepted and presented papers deal with novel research and innovative applications and stimulated fruitful debates and knowledge acquisition. We hope the future readers find these contributions useful and inspiring.

The proceedings editors would like to thank all the contributors who made the symposium successful: the organizing group, the program committee chairs, the scientific committee, the external reviewers, the keynote speakers, the authors for submitting their work, the participants for their discussions and for the rich debates they aroused during the sessions, and our sponsors who helped in terms of logistics.

Our special thanks goes to Springer for publishing a part of the proceedings of QSAC'2023.

Habiba Drias
Farouk Yalaoui

Invited Speakers

From Einstein's Doubts To Technology: The Second Quantum Revolution

Alain Aspect

Institut d'Optique, Paris-Saclay University, France
alain.aspect@institutoptique.fr

Alain Aspect was awarded the 2022 Nobel Prize in Physics, jointly with John Clauser and Anton Zeilinger, “for experiments with entangled photons, establishing the violation of Bell inequalities and pioneering quantum information science”.

Abstract

Thanks to the mysterious concept of wave–corpuscle duality, the first quantum revolution made it possible to describe the structure of matter, its electrical, mechanical and optical properties, and its interaction with light. It then provided the technologies—transistor, laser, integrated circuits—that led to the information and communication society.

The second quantum revolution, based on the notion of entanglement, is even more surprising in conceptual terms, since it forces us to reject Einstein's cherished local realist vision of the world, as demonstrated by the violation of Bell's inequalities. It also opens up fascinating prospects for applications, with emerging technologies ranging from quantum sensors to quantum communications and quantum computers. Will these technologies bring about a new upheaval in society? If so, we could truly speak of a second quantum revolution.

Biography

Alain Aspect was awarded the 2022 Nobel Prize in Physics, jointly with John Clauser and Anton Zeilinger, “for experiments with entangled photons, establishing the violation of Bell inequalities and pioneering quantum information science”.

Prof. Alain Aspect is a former student of ENS Cachan and Paris-Sud University (currently Paris-Saclay University). He has held positions at the Institut d'Optique, ENS Yaoundé (Cameroon), ENS Cachan, ENS/Collège de France, CNRS. He is currently professor (Augustin Fresnel chair) at the Institut d'Optique Graduate School (Paris-Saclay University), professor at the Ecole Polytechnique (Polytechnic Institute of Paris) and director of research emeritus at the CNRS.

Prof. Aspect is a member of several science academies in France, Italy, the USA, Austria, Belgium, and the UK. He received numerous accolades and honors. In 2005, he was named Knight of the Legion of Honor. He received the Medal of the City of Paris, was named Commander of the Palmes academics and received the title of Officer

of the National Order of Merit in the same year (2011). In 2014, he was named Officer of the Legion of Honor. And in 2022, he received the title of commander of the Legion of Honor.

Among many awards, he received the CNRS Gold Medal (2005), the Wolf Prize in Physics (2010), the Balzan Prize for Quantum Information (2013), the Niels Bohr Gold Medal (2013), Albert Einstein Medal (2013) and Ives Medal from the Optical Society of America (2013). *Alain Aspect was awarded the Nobel Prize in Physics in 2022 by the Royal Swedish Academy of Sciences.*

Alain Aspect's experimental work focused on testing Bell's inequalities with pairs of entangled photons (PhD, 1974-1983); wave-particle duality for single photons (1984-86, with Philippe Grangier); the cooling of atoms by laser under photon recoil (1985-1992, with Claude Cohen-Tannoudji); ultra-cold atoms, quantum gases and quantum simulators (1992-, in the atomic optics group he created at the Institute of Optics).

Next Generation Secure Communication

Mohamed Bourennane

Stockholm University, Sweden

Abstract

The financial and defense sectors crucially depend on communication through channels that cannot be intercepted by unauthorized people. Today's cryptographic protocols rely on RSA or so-called elliptical curves methods. But there is no guarantee that today's cryptographic protocols will remain safe in the near future. Fortunately, quantum mechanics makes it possible to solve the key transfer problem in a new and proven safe manner. Unlike classical methods, it is the nature's laws that guarantee the security of quantum cryptography. I will introduce and review quantum secure communication advances and also the worldwide and our effort in quantum technologies.

Biography

Mohamed Bourennane is a professor at Stockholm University. He is a graduate of the University of Science and Technology—Houari Boumediene, Algiers, Algeria. He has obtained his PhD from the Royal Institute of Technology, Stockholm. He was a researcher at Ludwig Maximilians University, Munich and Max Planck Institute for Quantum Optics, Garching, Germany. He has obtained the six years senior research fellow from the Swedish Research Council (VR). Today, he has established very young and dynamics research group in quantum information and quantum optics at Stockholm University. He has initiated, managed and led projects financed from, VR, Knut and Alice Wallenberg Foundation (KAW), Stiftelsen Olle Engkvist, Carl Tryggers Foundation and the Swedish Agency for Exchange Programs (STINT), Defence Material Administration (FMV), ABB-Hitachi, EU and Polish National Foundation. He is an elected member of the Royal Swedish Academy of Sciences.

The Alchemy of Vacuum

Thomas W. Ebbesen

USIAS & ISIS, University of Strasbourg & CNRS, France

Abstract

Over the past decade, the possibility of manipulating material and chemical properties by using hybrid light–matter states has stimulated considerable interest [1-3]. Such hybrid light–matter states can be generated by strongly coupling the material to the spatially confined electromagnetic field of an optical resonator. Most importantly, this occurs even in the dark because the coupling involves the electromagnetic fluctuations of the resonator, the vacuum field. After introducing the fundamental concepts, examples of modified properties of strongly coupled systems, such as chemical reactivity, charge and energy transport, superconductivity and magnetism, will be given to illustrate the broad potential of light–matter states.

- [1] Garcia Vidal, F. J., Ciuti, C., Ebbesen, T. W.: *Science* **373**, eabd336 (2021)
- [2] Genet, C., Faist, J., Ebbesen, T. W.: *Phys. Today* **74**, 42 (2021)
- [3] Nagarajan, K., Thomas, A., Ebbesen, T. W.: *J. Am. Chem. Soc.* **143**, 16877 (2021)

Biography

Thomas W. Ebbesen is a Norwegian physical chemist who has done research in nanoscience around the world. He studied in the U.S., obtaining his bachelor's at Oberlin College in Ohio before moving to France, where he obtained his PhD at the Pierre and Marie Curie University in the early 1980s. He then moved back to the USA to work at the Notre Dame Radiation Laboratory, where he spent several years doing research in photo-physical chemistry.

His contribution to nanoscience began in 1988 when he moved to NEC in Tsukuba, Japan. He started working on the synthesis and on the properties of fullerenes, in particular, superconductivity, before drifting his attention toward carbon nanotubes. In 1992, working in collaboration with Pulickel Ajayan, he discovered an easy way to produce carbon nanotubes in large quantities. He went on to study the mechanical and electronic properties of single nanotubes.

He unexpectedly observed light propagation through holes much smaller than the light wavelength. The phenomenon was explained by the interaction of light with electron waves at the metal surfaces (plasmons), and published in 1998, just before Ebbesen returned to France.

Since 1999, Ebbesen has worked at the Institut de Science et Ingénierie Supramoléculaires (ISIS) in Strasbourg, which he directed from 2004 to 2012. His research interest

still focuses on the properties of plasmonic nanostructures and the interactions between plasmons and molecules.

He has received several awards for his contribution to nanoscience, including the Agilent Europhysics Prize in 2001 for his work on nanotubes, the France Telecom Prize of the French Academy of Sciences in 2005, and the Quantum Electronics and Optics Prize of the European Physical Society in 2009. He is also a member of the Institut Universitaire de France, the Norwegian Academy of Science and Letters, the French Academy of Science and the Royal Flemish Academy of Belgium.

Advances in Quantum Medical Image Analysis Using Machine Learning

Khaled Elleithy

Bridgeport University, Connecticut, USA

Abstract

Quantum machine learning (QML) is an interdisciplinary field combining quantum computing (QC) and machine learning (ML). It has gained increased attention due to advances in near-term hardware implementations of quantum devices. The use of QML has proven to result in a significant improvement in performance and computational speed. Consequently, QML has become an effective technique for data processing and classification. Researchers have recently proposed various QML solutions in the medical image analysis field to gain an advantage of quantum supremacy. The main objective of this speech is to present a holistic review of current leading-edge published works in the quantum medical image analysis field with a focus on supervised learning using artificial neural networks. A comparative study is used to pinpoint the potential of existing techniques, the most promising techniques and the future of research in this area.

Biography

Dr. Elleithy has worked in academia for the past 30 years in various administrative and teaching roles, including a PhD Program Director, Online MS Program Advisor, Associate Dean for Engineering, Associate Vice President for Graduate Studies and Research, Associate Dean of Engineering, Business and Education and Dean of the College of Engineering, Business and Education.

Dr. Elleithy published over 400 research papers in national/international journals and conferences with 5,000+ Google Scholar citations. His most recent research results in quantum computing, security of wireless communications, steganography and data fusion in wireless sensor networks represent noteworthy contributions to the sciences and technology fields.

Dr. Elleithy was the PI or Co-PI of over three million dollars funded research projects in the past twenty years. Sponsors include ARDEC, United Nations, Connecticut NASA Space Grant, CISCO, the University of Connecticut START program, the University of Bridgeport CTNEXT, Saudi Aramco and King Abdul Aziz City of Science and Technology (KACST).

Dr. Elleithy was the PhD dissertation advisor for 27 students. PhD students in his research group won more than forty awards at the state and national levels for their

research papers and posters. Many have participated in funded research projects and published their research results in quality journals and conferences.

Dr. Elleithy has been heavily involved with numerous professional societies during the past 30 years, including the Institute of Electrical Engineering (IEEE), the Association for Computing Machinery (ACM), and the American Society of Engineering Education (ASEE). This involvement includes conference and workshop organizations, leadership, journal editing, and other endeavors.

Dr. Elleithy is the founder and co-chair of the International Joint Conferences on Computer, Information, and Systems Sciences, and Engineering (CISEE), the most significant online engineering conference successfully running from 2005 to 2014. CISSE was technically co-sponsored by CT IEEE several times. He was the Co-chair of the 2014 Zone 1 Conference of the American Society for Engineering Education, Bridgeport, Connecticut, April 3–5, 2014, technically co-sponsored by the IEEE CT section. He was the Chairman of the IEEE Connecticut Conference on Industrial Electronics, Technology & Automation, Bridgeport, October 14–15, 2016. Dr. Elleithy was the IEEE Connecticut Communications Chapter Chair from 2006–2008. Dr. Elleithy was the Chair of the Northeast Conference of the American Society for Engineering Education, Bridgeport, Connecticut, October 16–17, 2020.

Dr. Elleithy received the Distinguished Professor of the Year Award from the University of Bridgeport in 2005. He received the 2015 Connecticut Quality Improvement Award (CQIA) Gold Innovation Award. In December 2017, he was elected Fellow of the African Academy of Sciences to recognize his contributions to Wireless Sensor Networks and Wireless Communications. In 2020, Dr. Elleithy received IEEE Connecticut Section Outstanding Member in Academia Award.

Post-Quantum Cryptography: Scientific, Technological and Geopolitical Challenges

Abdellah Mokrane

Paris 8 University, France

Abstract

Since the evidence of the reality of the quantum computer in the 90s and Peter Shor's publication of a fast quantum algorithm for solving encryption problems that had previously been considered very hard, the scientific community and especially researchers in cryptography began intense research over the last 20 years to propose new (classical) encryption algorithms resistant to quantum computing. In this talk, we will explain what are the proposed solutions to this academic and technological challenge. We will also discuss the geopolitical consequences resulting from this coming digital revolution. Along the way, based on Algeria's past experience in the field of encryption and cybersecurity, we will propose a 20-year strategy to tackle this challenge.

Biography

Abdellah Farid Mokrane received a Master's degree in Pure Mathematics from Paris Sud University in June 1988 and a PhD in the field of Algebraic Geometry from the same university in February 1992, then an "Habilitation à Diriger des Recherches" (HDR) from Paris Nord University in November 2003. He held the position Maître de Conférences at the Galilée Institute a college of University of Paris Nord from 1993 to 2004. Since 2004, he has held a full professor position at Paris 8 university. His area of expertise includes algebraic geometry, arithmetic as well as cryptography. He has supervised a dozen doctoral theses, and he was Project Manager at the Ministry of Higher Education and Research in France in charge of the evaluation of research teams and international relations. He has been a visiting professor in different universities around the world and in different international conferences (Japan, India, China, Germany, Italy, USA, UK, Lebanon, Egypt, Mali, Netherlands, Spain, etc). For 20 years, he has been in charge of the Master's degree in Mathematics at Paris 8 university, creating a speciality in arithmetic, cryptography and coding, then a speciality in big data and recently a speciality in cybersecurity and data sciences. He developed a very intense collaboration with Algeria in the fields of teaching, PhD advising, research and development through notably the following institutions: CF-DAT, IHESN, EMP, DGRSDT, USTHB, etc.

Contents

An Overview of Quantum Key Agreement Protocols <i>Youssouf Achouri, Rima Djellab, and Khaled Hamoudi</i>	1
Variational Circuit Based Hybrid Quantum-Classical Algorithm VC-HQCA <i>Mohcene Mouad Lariane and Hacene Belhadef</i>	15
Quantum Computing in Non Destructive Testing of Materials <i>Thouraya Merazi-Meksen</i>	32
Enhanced Gaussian Quantum Particle Swarm Optimization for the Clustering of Biomedical Data <i>Saida Ishak Boushaki, Omar Bendjehaba, Nadjet Kamel, and Dhai Eddine Salhi</i>	38
Quantum Inspired Grey Wolf Optimizer for Convolutional Neural Network Hyperparameter Optimization <i>Selma Kali Ali and Dalila Bougaci</i>	50
Frequent Itemsets Mining Using New Quantum Inspired Elephant Swarm Algorithm <i>Hadjer Moulai</i>	65
Quantum Slime Mould Algorithm and Application to Urgent Transportation ... <i>Celia Khelfa, Habiba Drias, and Ilyes Khennak</i>	77
Quantum FP-Growth for Association Rules Mining <i>Widad Hassina Belkadi, Yassine Drias, and Habiba Drias</i>	91
Gaussian Quantum-Behaved PSO Strategy for Lithium Battery Model Optimization <i>Walid Merrouche, Badis Lekouaghet, and Elouahab Bouguenna</i>	107
Quantum Recurrent Neural Networks for Soil Profiles Prediction in Türkiye ... <i>Yassine Drias, Alaa Eddine Siouane, and Tuna Çakar</i>	120
Q-CODA: Co-designing Quantum Codes and Architectures for Hardware-Aware Quantum Error Correction <i>Pratik Thantharate and Anurag Thantharate</i>	134

Quantum Computing for Computer Vision: Applications, Challenges, and Research Tracks	152
<i>Naoual El Djouher Mebtouche and Sarah Sahnoune</i>	
A Multiparty Efficient Semi-quantum Secret Sharing Protocol of Specific Bits	167
<i>Mustapha Anis Younes, Sofia Zebboudj, and Abdelhakim Gharbi</i>	
Quantum Convolution for Convolutional Neural Networks	179
<i>Mustapha Bourahla</i>	
A Quantum-Inspired Deep Learning Models for Skin Lesion Classification	194
<i>Mohamed Ait Mehdi, Khadidja Belattar, and Feryel Souami</i>	
Author Index	209



An Overview of Quantum Key Agreement Protocols

Youssouf Achouri^{1(✉)}, Rima Djellab², and Khaled Hamoudi³

¹ LaSTIC laboratory, University of Batna 2, 05000 Batna, Algeria
y.achouri@univ-batna2.dz

² LAMIE laboratory, University of Batna 2, 05000 Batna, Algeria
r.djellab@univ-batna2.dz

³ LIGM, ESIEE Paris, University of Gustave Eiffel, 93162 Noisy-le-Grand, France
khaled.hamoudi@esiee.fr

Abstract. Quantum Key Agreement (QKA) stands as a pivotal protocol in quantum cryptography, facilitating the shared creation of a secret key among participants over an insecure communication medium. This study explores the complex theoretical foundations and intricate mathematical frameworks integral to QKA. Additionally, it presents a structured analysis and categorization of various multi-party Quantum Key Agreement mechanisms, an increasingly significant topic in the quantum computing era. Each approach is scrutinized for its strengths and weaknesses, providing a comprehensive comparative study that covers their real-world applications and the unique challenges they face. Striking a balance between detailed technical exposition and perceptive observations on the broader implications of these quantum technologies, this paper offers a well-rounded view on advancing secure quantum communication systems. The goal of this research is to furnish readers with a thorough understanding of QKA principles and an insightful perspective on the diverse opportunities and obstacles presented by different multi-party QKA frameworks.

Keywords: quantum key agreement · multiparty quantum key agreement · quantum key distribution

1 Introduction

Key agreement protocols, also recognized as key exchange protocols, are central to the practice of cryptography. They enable parties to generate cryptographic keys collaboratively, allowing for the secure transmission of information over public channels without the prior exchange of secret keys.

The landmark research by Diffie and Hellman in 1976 unveiled a technique for two entities to share a secret key securely, thereby protecting their exchanges from unauthorized snooping [1]. This innovation spurred further investigation into expanding the protocol to include multiple parties, as documented in subsequent academic research [2–4].

Quantum cryptography introduces a transformative approach to securing communications, deeply rooted in the core principles of quantum mechanics, and offers unparalleled levels of security [5]. The introduction of the BB84 protocol for quantum key distribution by Bennett and Brassard in 1984 sparked significant excitement and progress in this field [6]. This pivotal moment led to the development of multiple quantum cryptography applications, such as techniques for distributing quantum keys [7,8], mechanisms for sharing quantum secrets [9,10], systems for secure direct quantum communication [11,12], and methods for conducting quantum comparisons in private [13,14]. Quantum Key Agreement (QKA) leverages quantum mechanics to equitably and securely generate cryptographic keys, inherently protecting against the potential risks brought by quantum computing. This is achieved through adherence to quantum phenomena like the Heisenberg uncertainty principle and the no-cloning theorem, creating an effective shield against advanced quantum threats [15,16]. The introduction of QKA was marked in 2004 with the presentation of the first protocol for quantum-based key agreement [17], which has led to the creation of a comprehensive array of protocols tailored for both dyadic [18–22] and collective frameworks [23–34].

Quantum key agreement models are generally differentiated by their design and operational efficiency [35]. This differentiation includes the Tree MQKA protocol, enabling the exchange of sensitive information through quantum communication; the Complete Graph MQKA protocol, facilitating information sharing among all protocol participants; and the Circle MQKA protocol, in which participants circulate a sequence of particles that represent their private keys to others in a circular manner, ensuring the encryption of data returns to the initiator.

This paper aims to offer a detailed exploration of quantum key agreement (QKA), beginning with an introduction to the principles of quantum computing and its specific language. We will outline QKA, contrast it with Quantum Key Distribution (QKD), and highlight the advantages of QKA for secure, sustainable communication networks. Further, we will examine the three main multi-party QKA configurations-circle, tree, and complete graph-analyzing their benefits and drawbacks. This discussion aims to provide a systematic framework for classifying QKA approaches, facilitating strategic decision-making among researchers and practitioners.

2 Preliminary Knowledge

The focal point of this section lies in comprehending quantum computing. Our exploration begins with an introduction to bra-ket notation, establishing a foundational understanding. We then delve into the captivating phenomena of superposition and entanglement. Lastly, we demystify the operation and measurement processes by delving into the realm of quantum gates [36].

2.1 Unraveling Quantum Notation: The Essence of Bra and Ket

Quantum computing operates with qubits as its core elements, which are the quantum analogs of classical bits. The handling and interaction of these qubits lay the groundwork for quantum computational processes. For the articulation of a qubit's state and its basis within this field, a distinct notation known as bra-ket notation is predominantly employed.

Understanding Bra Notation. At the forefront of Bra notation is the symbol $\langle \cdot |$, playing a pivotal role. In this setting, the symbols ‘0’ and ‘1’ under the Bra category act as essential elements on a two-dimensional vector plane. To elaborate, $\langle 0 |$ is equivalent to the vector $[1 \ 0]$, and conversely, $\langle 1 |$ aligns with the vector $[0 \ 1]$.

Exploring Ket Notation. Conversely, within the quantum realm, the notation $| \cdot \rangle$, where the dot symbolizes the core aspect, signifies Ket notation. As an example, the Ket notations can be articulated as: $| 0 \rangle = [1 \ 0]^*$ and $| 1 \rangle = [0 \ 1]^*$. It is crucial to acknowledge that Bra notation is essentially the conjugate transpose of Ket notation.

The notations $| 0 \rangle$ and $| 1 \rangle$, along with their corresponding Bra notations $\langle 0 |$ and $\langle 1 |$, establish the conventional bases on a two-dimensional plane. These notational forms are chiefly utilized to depict and define a qubit's state within quantum computational operations.

2.2 Exploring Superposition and Measurement in Quantum Systems

Quantum computing introduces the fascinating concept of superposition, where qubits are in a state that encompasses both $| 0 \rangle$ and $| 1 \rangle$ simultaneously. This state of superposition is typically expressed in the Z-basis, with a qubit's state represented as $(\alpha | 0 \rangle + \beta | 1 \rangle)$. When measuring this superposed state, the likelihood of finding the qubit in the $| 0 \rangle$ state is $|\alpha|^2$, and in the $| 1 \rangle$ state is $|\beta|^2$, ensuring the sum of these probabilities equals one, $|\alpha|^2 + |\beta|^2 = 1$.

Observing the qubit along varying axes yields different measurement outcomes. Notably, the X-basis offers an alternative perspective on the qubit's state:

Quantum States Along the Z-Axis.

$$| 0 \rangle = \frac{1}{\sqrt{2}}(| + \rangle + | - \rangle); | 1 \rangle = \frac{1}{\sqrt{2}}(| + \rangle - | - \rangle) \quad (1)$$

Quantum States Along the X-Axis.

$$| + \rangle = \frac{1}{\sqrt{2}}(| 0 \rangle + | 1 \rangle); | - \rangle = \frac{1}{\sqrt{2}}(| 0 \rangle - | 1 \rangle) \quad (2)$$

2.3 The Phenomenon of Quantum Entanglement and Its Effects

Quantum mechanics unveils that when two photons are entangled, their connection persists across vast distances, whether they are mere nanometers or several kilometers apart. Quantum entanglement suggests that the act of measuring the properties of one photon immediately influences the state of its counterpart, irrespective of the spatial gap separating them.

Entanglement's significance shines through in the example of Bell states, illustrating how the observation of one qubit instantly sets the state of its entangled partner. For example, given the Bell state $\frac{1}{\sqrt{2}}(|00\rangle + |11\rangle)_{12}$, a measurement resulting in $|0\rangle$ for the first qubit means the second qubit is also in the state $|0\rangle$, even in the absence of direct observation.

We proceed to explore the intricacies of qubits within Bell and GHZ states:

Bell States Revisited.

$$\begin{aligned} |\Phi^\pm\rangle_{AB} &= \frac{1}{\sqrt{2}}(|00\rangle \pm |11\rangle)_{AB} \\ |\Psi^\pm\rangle_{AB} &= \frac{1}{\sqrt{2}}(|01\rangle \pm |10\rangle)_{AB} \end{aligned} \quad (3)$$

GHZ States Elaborated.

$$\begin{aligned} |\Psi_{1,5}\rangle_{ABC} &= \frac{1}{\sqrt{2}}(|000\rangle \pm |111\rangle)_{ABC} \\ |\Psi_{2,6}\rangle_{ABC} &= \frac{1}{\sqrt{2}}(|001\rangle \pm |110\rangle)_{ABC} \\ |\Psi_{3,7}\rangle_{ABC} &= \frac{1}{\sqrt{2}}(|010\rangle \pm |101\rangle)_{ABC} \\ |\Psi_{4,8}\rangle_{ABC} &= \frac{1}{\sqrt{2}}(|011\rangle \pm |100\rangle)_{ABC} \end{aligned} \quad (4)$$

2.4 Quantum Gates: Building Blocks of Quantum Computation

Quantum gates play a crucial role in quantum computation, serving as the fundamental building blocks for various quantum algorithms and operations. These gates are unitary transformations that can be applied to individual qubits or multiple qubits collectively.

In some cases, a unitary operation may act on a single qubit without affecting the entire entangled state. This ability to address individual qubits independently is a significant advantage in quantum computing.

In the upcoming subsections, we will introduce the four fundamental single-qubit gates, each of which contributes to the versatility and power of quantum computing:

$$\begin{aligned} I &= \begin{pmatrix} 1 & 0 \\ 0 & 1 \end{pmatrix}, \sigma_x = \begin{pmatrix} 0 & 1 \\ 1 & 0 \end{pmatrix} \\ \sigma_y &= \begin{pmatrix} 0 & -1 \\ 1 & 0 \end{pmatrix}, \sigma_z = \begin{pmatrix} 1 & 0 \\ 0 & -1 \end{pmatrix} \end{aligned} \quad (5)$$

2.5 Assessing States in Quantum Mechanics: Bell and GHZ States

Understanding the state of qubits through measurement is pivotal in quantum mechanics. The Controlled NOT (CNOT) gate and the Hadamard (H) gate are instrumental in discerning the entangled states.

The Role of the CNOT Gate. The CNOT gate, a key quantum gate, manipulates qubits by employing one as the control and the others as target qubits. Its operation hinges on the state of the control qubit:

- When the control qubit is $|0\rangle$, the target qubits remain unaltered.
- Conversely, if the control qubit is $|1\rangle$, it triggers a NOT operation on the target qubits, inverting their states.

As an illustration, applying a CNOT gate to a pair of qubits initially in the state $|11\rangle$, with the first qubit as control and the second as target, results in the state $|10\rangle$, flipping the target qubit from ‘1’ to ‘0’ due to the control qubit’s state.

Functionality of the Hadamard (H) Gate. The Hadamard (H) gate, crucial for quantum computation, affects a single qubit as follows:

$$H|0\rangle \rightarrow \frac{(|0\rangle + |1\rangle)}{\sqrt{2}}, H|1\rangle \rightarrow \frac{(|0\rangle - |1\rangle)}{\sqrt{2}} \quad (6)$$

Applying the H gate to $|0\rangle$ generates a superposition of $|0\rangle$ and $|1\rangle$, and similarly for $|1\rangle$, but with a phase difference between the states.

For Bell states, a sequence involving the CNOT and H gates enables Bell state measurement. Initially, the CNOT gate targets the Bell states, with the first qubit as control and the second as target. Following this, the Hadamard gate acts on the resultant state for measurement. An example of this process is shown in Bell state $|\Phi^+\rangle_{AB}$ measurement.

GHZ State Measurement.

$$\begin{aligned} |\Phi^+\rangle_{AB} &= \frac{(|00\rangle + |11\rangle)}{\sqrt{2}} \xrightarrow{\text{CNOT}_{AB}} \frac{(|00\rangle + |10\rangle)}{\sqrt{2}} \\ &= \frac{1}{\sqrt{2}}(|0\rangle + |1\rangle)_A |0\rangle_B \xrightarrow{H_A} |0\rangle_A |0\rangle_B \end{aligned} \quad (7)$$

Similar methodology applies to GHZ state measurements. For example, measurement on $|\Phi_1\rangle_{ABC}$ with particle A as the control transitions $\frac{1}{\sqrt{2}}(|000\rangle + |111\rangle)_{ABC}$ to a final state of ‘000’ after H gate application on particle A, leading to outcomes ‘000’, ‘001’, ‘010’, ‘011’, ‘100’, ‘101’, ‘110’, ‘111’ for different $|\Psi_{1,2,\dots,8}\rangle_{ABC}$ states.

3 Comparative Analysis of QKA and QKD in Quantum Cryptography

Quantum cryptography has evolved remarkably, with Quantum Key Agreement (QKA) and Quantum Key Distribution (QKD) standing out as pivotal developments. Utilizing quantum mechanics, these protocols enable the secure exchange of cryptographic keys, though they are distinguished by their distinct approaches and applications. This section aims to delve into both QKA and QKD, exploring their similarities, differences, and evaluating their effectiveness under various scenarios.

3.1 Exploring Quantum Key Agreement

Quantum Key Agreement (QKA) offers a protocol within quantum cryptography that allows multiple parties to jointly generate a shared secret key, leveraging quantum mechanics' inherent unpredictability and randomness. Unlike conventional key agreement methods, QKA facilitates a key generation process where all participants equally contribute.

3.2 Understanding Quantum Key Distribution

Quantum Key Distribution (QKD), another quantum cryptographic protocol, enables two parties to generate and share a secret key securely for encrypted communication. QKD's core advantage stems from quantum mechanics' ability to alert the parties of any interception attempts by third parties.

3.3 Contrasting QKA with QKD

A comparison of Quantum Key Agreement (QKA) and Quantum Key Distribution (QKD) reveals fundamental differences. QKA is characterized by a collaborative key generation mechanism where all parties actively contribute. In contrast, QKD involves a key being generated by one party and shared with another, highlighting a unilateral approach to key generation. While QKA necessitates mutual trust among participants, QKD relies on quantum mechanics to secure communication. Notable implementations of these protocols include Zhou et al.'s model for QKA and the BB84 protocol by Bennett and Brassard for QKD. QKA is optimal for scenarios requiring joint participation in key generation, whereas QKD is suited for secure point-to-point communications, such as in Quantum-Secure Direct Communication (QSDC).

3.4 Opting for QKA over QKD: Advantages

Though QKD is renowned for its security capabilities, QKA presents preferable features in certain contexts:

- **Joint Key Production:** QKA’s multi-party key generation model promotes equality and inclusiveness among participants, ensuring everyone plays a part in securing the key [37].
- **Flexibility in Dynamic Networks:** QKA shows superior adaptability in environments with frequently changing network participants, unlike QKD’s more static approach [38, 39].
- **Distributed Trust Framework:** In situations where trust is spread across parties without centralizing key generation control, QKA’s trust model is more appropriate [37].

4 Multiparty Quantum Key Agreement Protocols

Multiparty Quantum Key Agreement (MQKA) protocols play a crucial role in establishing shared secret keys among multiple participants, ensuring secure communication in the field of quantum cryptography. In this section, we will explore the three different types of MQKA protocols that can be found in the literature [35]: the Tree MQKA Protocol, the Circle MQKA Protocol, and the Complete Graph MQKA Protocol (See Fig. 1).

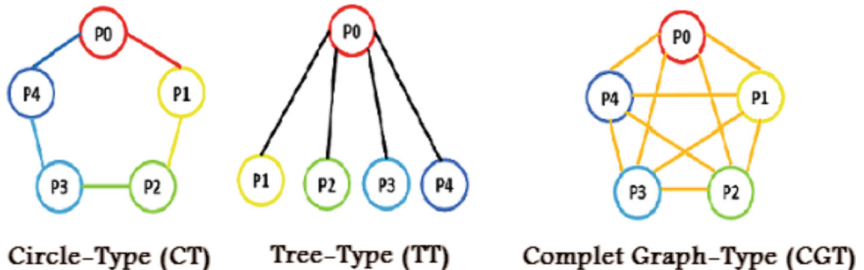


Fig. 1. Three types of (MQKA) Protocols.

4.1 The Tree-Based MQKA Protocol

The tree-based multiparty quantum key agreement (MQKA) protocol employs a hierarchical structure to facilitate secure communication among participants. This structure categorizes participants into levels, with each having a parent node and potentially multiple child nodes. The operation of this protocol is outlined as follows:

- **Initial Key Generation by Leaf Nodes:** Participants at the bottom of the hierarchy, known as leaf nodes and lacking child nodes, initiate the process by creating a series of quantum states, such as entangled photons. These states are then forwarded to their respective parent nodes.

- **Intermediate Node Processing through Bell Measurements:** Participants situated at intermediate levels, equipped with both parent and child nodes, receive quantum states from their descendants. They conduct Bell measurements on these states to derive certain outcomes, which are subsequently passed up to their parent node.
- **Finalizing the Key at the Root Node:** The root node, positioned at the pinnacle of the tree, collects outcomes from all subordinate nodes. A final round of Bell measurements on these outcomes allows for the creation of a shared secret key among the node and its immediate children.
- **Enhancement of the Established Key:** To ensure the integrity and confidentiality of the established key, the root node applies error correction and privacy amplification. This step refines the initially extracted outcomes into a secure shared key.

This hierarchical MQKA protocol enables the establishment of shared secret keys among nodes, facilitating secure quantum communication across different levels of the structure. The reliance on quantum mechanics for the protocol's security offers a robust alternative to classical cryptographic techniques, particularly in terms of scalability and flexibility in secure communications.

4.2 The Circle-Type MQKA Protocol

The circle-type multiparty quantum key agreement (MQKA) protocol is designed with a circular configuration, connecting each participant directly to two others and forming a continuous loop. This section outlines the protocol's operational steps:

- **Initial Quantum State Generation:** Participants create and distribute a sequence of quantum states, for instance, photons, to the adjacent participants in the circular arrangement.
- **Performing Measurements and Sharing Results:** After receiving quantum states, each participant employs random measurement bases to conduct observations on these states. The results of these observations are then communicated back to the original senders of the quantum states.
- **Determining Matching Bases:** Through mutual discussions, participants ascertain which observations were conducted under matching bases and discard outcomes derived from differing bases, focusing only on congruent measurement results for key derivation.
- **Refining the Shared Key:** Participants utilize the congruent measurement results to implement error correction and privacy amplification processes, culminating in the creation of a secure, shared secret key among themselves.

This circular MQKA protocol facilitates the establishment of a shared secret key among participants, enabling encrypted communication across the loop. Leveraging quantum mechanical principles, this protocol enhances security against specific threats that traditional cryptographic methods may not adequately address.

4.3 The Complete Graph-Type MQKA Protocol

The complete graph-type multiparty quantum key agreement (MQKA) protocol is established within a network where every participant is directly connected to all others, creating a complete graph structure. This protocol is designed to facilitate the creation of a shared secret key among any pair of participants within the network. The operational steps are outlined below:

- **Quantum State Distribution:** Participants initiate the protocol by preparing and distributing specific quantum states, like photons, across the network to each other participant. These states lay the groundwork for the shared secret key.
- **Observations and Sharing of Results:** Each participant, upon receiving these quantum states, selects measurement bases at random to observe the states and records the outcomes. These recorded outcomes are then communicated to the originating senders.
- **Aligning Measurement Bases:** Through mutual communication, participants identify which observations were conducted with aligning measurement bases, focusing on these congruent observations for key development.
- **Shared Key Development:** With the aligned measurement outcomes, the protocol employs error correction and privacy amplification methods to derive a refined, shared secret key, bolstering its security.

This approach ensures that each participant pair within the complete graph framework can generate a shared secret key, facilitating secure quantum cryptographic communications. The protocol's robustness, underpinned by quantum mechanical principles, offers enhanced security against specific vulnerabilities inherent in traditional cryptographic approaches.

5 Discussion

This section delves into the advantages and disadvantages of three multi-party Quantum Key Agreement (MQKA) protocols: the Tree MQKA Protocol, Circle MQKA Protocol, and Complete Graph MQKA Protocol. Each protocol presents distinctive features, and a thorough understanding of their strengths and limitations is crucial for selecting the most appropriate one based on specific quantum communication scenarios.

5.1 Protocol for Multi-party Quantum Key Agreement in Tree Topology

The Multi-Party Quantum Key Agreement (MQKA) Protocol designed with a hierarchical tree structure, known as the Tree MQKA Protocol, organizes participants with each having a parent node and potentially one or more child nodes. An analysis of its advantages and disadvantages is presented below:

Advantages:

- **Efficient Scalability:** The hierarchical tree structure facilitates efficient scalability, allowing for the addition of more participants without a significant increase in communication complexity.
- **Reduced Resource Usage:** In comparison to the Complete Graph, the Tree QKA Protocol typically requires fewer quantum states to be transmitted, resulting in reduced resource consumption.
- **Parent-Child Key Distribution:** The protocol enables the establishment of shared secret keys between the root node and each child node, introducing an additional layer of security.

Disadvantages:

- **Single Point of Failure:** The root node serves as a potential single point of failure. If compromised, it could jeopardize the security of the entire tree.
- **Limited Connectivity:** Participants can only communicate with their parent and child nodes, restricting direct communication possibilities.
- **Increased Latency:** As the tree size grows, the latency of communication between distant nodes may increase, impacting real-time applications.

The choice of an MQKA protocol depends on specific quantum communication requirements. The Tree MQKA Protocol offers efficient scalability and reduced resource consumption, making it suitable for scenarios where these advantages outweigh concerns about limited connectivity and potential single points of failure.

5.2 Protocol for Multi-party Quantum Key Agreement in Circular Topology

The Multi-party Quantum Key Agreement (MQKA) Protocol designed with a circular topology, known as the Circle MQKA Protocol, establishes connections where each participant is linked to two neighboring participants. An examination of its merits and drawbacks is presented below:

Advantages:

- **Improved Connectivity:** Participants, in contrast to the Tree Protocol, benefit from connections with two neighbors, enhancing direct communication and reducing latency.
- **Decentralized Structure:** The absence of a single point of failure enhances the protocol's resilience against potential attacks.
- **Intermediate Node Resilience:** Even if certain intermediate nodes are compromised, communication can persist through the remaining nodes.

Disadvantages:

- **Limited Scalability:** As the participant count rises, managing the circular topology may become unwieldy, potentially impacting scalability.
- **Complex Key Agreement:** Establishing shared secret keys among all participants in the circle can become intricate and resource-intensive.
- **Higher Resource Consumption:** Compared to the Tree Protocol, the Circle Protocol may necessitate a larger number of quantum states to be transmitted.

The selection of an MQKA protocol depends on the specific requirements and constraints of the quantum communication scenario. The Circle MQKA Protocol offers improved direct communication and resilience, making it suitable for small to medium-sized networks, though careful consideration is advised regarding scalability challenges and resource consumption.

5.3 Protocol for Multi-party Quantum Key Agreement in Complete Graph Topology

The Multi-Party Quantum Key Agreement (MQKA) Protocol designed for Complete Graph topology establishes a fully connected network where each participant is directly linked to every other participant. An exploration of its merits and drawbacks follows:

Advantages:

- **Optimal Connectivity:** The Complete Graph ensures the highest level of connectivity, facilitating direct communication between any pair of participants without intermediaries.
- **Robust Resilience:** With no single point of failure, the protocol exhibits strong resilience against node compromise, enhancing overall system reliability.
- **Versatile Communication:** Participants enjoy efficient and direct communication regardless of their relative positions within the network.

Disadvantages:

- **Resource Intensity:** Implementing the Complete Graph necessitates a substantial number of quantum state transmissions, leading to resource-intensive operations and potential cost implications.
- **Scalability Challenges:** The protocol encounters increased complexity and resource requirements as the number of participants grows, posing challenges to scalability.
- **Privacy Concerns:** Given the direct connections between all participants, higher privacy concerns may arise compared to alternative protocols.

The selection of an appropriate QKA protocol hinges on the specific requirements and constraints of the quantum communication scenario at hand. For expansive hierarchical networks with limited connectivity needs, the Tree MQKA Protocol may prove optimal. Conversely, circular topologies in small to medium-sized networks may benefit from the enhanced connectivity and decentralized structure offered by the Circle MQKA Protocol. Lastly, the Complete Graph MQKA Protocol is most fitting for compact applications prioritizing direct communication and maximum resilience.

We summarize the characteristics of each protocol in a table (Table 1) for easy comparison:

Table 1. Comparison of Different MQKA Protocols

Protocols	Examples	Advantages	Disadvantages
Tree MQKA Protocols	– [26] – [40]	– Efficient Scalability – Reduced Resource Usage – Parent-Child Key Distribution	– Single Point of Failure – Limited Connectivity – Increased Latency
Circle MQKA Protocols	– [32] – [33]	– Enhanced Connectivity – Decentralized Nature – Intermediate Node Resilience	– Limited Scalability – Complex Key Agreement – Higher Resource Consumption
Complete Graph MQKA Protocols	– [23] – [24]	– Maximum Connectivity – Highly Resilient – Versatile Communication	– Resource-Intensive – Scalability Challenges – Privacy Concerns

In practice, a comprehensive evaluation of the network's size, topology, security requirements, and available resources is essential to make an informed decision regarding the QKA protocol. As quantum communication technologies continue to advance, these protocols will play a crucial role in ensuring secure and efficient quantum key agreement in various real-world applications.

6 Conclusion

This study has conducted a comprehensive exploration of quantum key agreement (QKA) and its pivotal role in advancing secure communication. Through a solid understanding of quantum computing and its unique notation, we have defined QKA and performed an extensive comparison with quantum key distribution (QKD), highlighting the specific advantages of QKA in establishing enduringly secure communication channels. The research has thoroughly examined the three primary categories of multi-party QKA schemes, namely the circle, tree, and complete graph schemes, carefully assessing their respective strengths and limitations. The adoption of a standardized approach to categorize multi-party QKA schemes equips researchers and practitioners with a framework for making informed decisions when implementing quantum cryptographic protocols. As the landscape of quantum technologies progresses, the insights derived

from this investigation emphasize the promising and indispensable role of QKA in ensuring robust and long-term security in forthcoming communication systems.

References

1. Diffie, W., Hellman, M.: New directions in cryptography. In: Democratizing Cryptography: The Work of Whitfield Diffie and Martin Hellman, pp. 365–390 (2022)
2. Ingemarsson, I., Tang, D., Wong, C.: A conference key distribution system. *IEEE Trans. Inf. Theory* **28**, 714–720 (1982)
3. Burmester, M., Desmedt, Y.: A secure and efficient conference key distribution system. In: De Santis, A. (ed.) Advances in Cryptology - EUROCRYPT'94. Lecture Notes in Computer Science, vol. 950, pp. 275–286. Springer, Berlin (1995). <https://doi.org/10.1007/BFb0053443>
4. Steiner, M., Tsudik, G., Waidner, M.: Key agreement in dynamic peer groups. *IEEE Trans. Parallel Distrib. Syst.* **11**, 769–780 (2000)
5. Shor, P., Preskill, J.: Simple proof of security of the BB84 quantum key distribution protocol. *Phys. Rev. Lett.* **85**, 441 (2000)
6. Bennett, C., Brassard, G.: Quantum cryptography: public key distribution and coin tossing. ArXiv Preprint: [arXiv:2003.06557](https://arxiv.org/abs/2003.06557) (2020)
7. Bennett, C.: Quantum cryptography using any two nonorthogonal states. *Phys. Rev. Lett.* **68**, 3121 (1992)
8. Bennett, C., Wiesner, S.: Communication via one-and two-particle operators on Einstein-Podolsky-Rosen states. *Phys. Rev. Lett.* **69**, 2881 (1992)
9. Gottesman, D.: Theory of quantum secret sharing. *Phys. Rev. A* **61**, 042311 (2000)
10. Hillery, M., Bužek, V., Berthiaume, A.: Quantum secret sharing. *Phys. Rev. A* **59**, 1829 (1999)
11. Boström, K., Felbinger, T.: Deterministic secure direct communication using entanglement. *Phys. Rev. Lett.* **89**, 187902 (2002)
12. Deng, F., Long, G., Liu, X.: Two-step quantum direct communication protocol using the Einstein-Podolsky-Rosen pair block. *Phys. Rev. A* **68**, 042317 (2003)
13. Tseng, H., Lin, J., Hwang, T.: New quantum private comparison protocol using EPR pairs. *Quantum Inf. Process.* **11**, 373–384 (2012)
14. Sun, Z., Long, D.: Quantum private comparison protocol based on cluster states. *Int. J. Theor. Phys.* **52**, 212–218 (2013)
15. Gisin, N., Ribordy, G., Tittel, W., Zbinden, H.: Quantum cryptography. *Rev. Mod. Phys.* **74**, 145 (2002)
16. Tajima, A., Tanaka, A., Maeda, W., Takahashi, S., Tomita, A.: Practical quantum cryptosystem for metro area applications. *IEEE J. Sel. Top. Quantum Electron.* **13**, 1031–1038 (2007)
17. Zhou, N., Zeng, G., Xiong, J.: Quantum key agreement protocol. *Electron. Lett.* **40**, 1 (2004)
18. Chong, S., Tsai, C., Hwang, T.: Improvement on “quantum key agreement protocol with maximally entangled states”. *Int. J. Theor. Phys.* **50**, 1793–1802 (2011)
19. Chong, S., Hwang, T.: Quantum key agreement protocol based on BB84. *Opt. Commun.* **283**, 1192–1195 (2010)
20. Huang, W., Wen, Q., Liu, B., Gao, F., Sun, Y.: Quantum key agreement with EPR pairs and single-particle measurements. *Quantum Inf. Process.* **13**, 649–663 (2014)

21. Huang, W., Su, Q., Wu, X., Li, Y., Sun, Y.: Quantum key agreement against collective decoherence. *Int. J. Theor. Phys.* **53**, 2891–2901 (2014)
22. Shen, D., Ma, W., Wang, L.: Two-party quantum key agreement with four-qubit cluster states. *Quantum Inf. Process.* **13**, 2313–2324 (2014)
23. Liu, B., Gao, F., Huang, W., Wen, Q.: Multiparty quantum key agreement with single particles. *Quantum Inf. Process.* **12**, 1797–1805 (2013)
24. Yin, X., Ma, W., Shen, D., Wang, L.: Three-party quantum key agreement with Bell states. *Acta Phys. Sinica* **62** (2013)
25. He, Y., Ma, W.: Quantum key agreement protocols with four-qubit cluster states. *Quantum Inf. Process.* **14**, 3483–3498 (2015)
26. Xu, G., Wen, Q., Gao, F., Qin, S.: Novel multiparty quantum key agreement protocol with GHZ states. *Quantum Inf. Process.* **13**, 2587–2594 (2014)
27. Shi, R., Zhong, H.: Multi-party quantum key agreement with bell states and bell measurements. *Quantum Inf. Process.* **12**, 921–932 (2013)
28. Yin, X., Ma, W., Liu, W.: Three-party quantum key agreement with two-photon entanglement. *Int. J. Theor. Phys.* **52**, 3915–3921 (2013)
29. Sun, Z., Zhang, C., Wang, B., Li, Q., Long, D.: Improvements on “multiparty quantum key agreement with single particles”. *Quantum Inf. Process.* **12**, 3411–3420 (2013)
30. Shukla, C., Alam, N., Pathak, A.: Protocols of quantum key agreement solely using Bell states and Bell measurement. *Quantum Inf. Process.* **13**, 2391–2405 (2014)
31. Zhu, Z., Hu, A., Fu, A.: Improving the security of protocols of quantum key agreement solely using Bell states and Bell measurement. *Quantum Inf. Process.* **14**, 4245–4254 (2015)
32. Sun, Z., Yu, J., Wang, P.: Efficient multi-party quantum key agreement by cluster states. *Quantum Inf. Process.* **15**, 373–384 (2016)
33. Sun, Z., Zhang, C., Wang, P., Yu, J., Zhang, Y., Long, D.: Multi-party quantum key agreement by an entangled six-qubit state. *Int. J. Theor. Phys.* **55**, 1920–1929 (2016)
34. Huang, W., Wen, Q., Liu, B., Su, Q., Gao, F.: Cryptanalysis of a multi-party quantum key agreement protocol with single particles. *Quantum Inf. Process.* **13**, 1651–1657 (2014)
35. Liu, B., Xiao, D., Jia, H., Liu, R.: Collusive attacks to “circle-type” multi-party quantum key agreement protocols. *Quantum Inf. Process.* **15**, 2113–2124 (2016)
36. Chen, K., Chang, Z., Zeng, G., Chou, Y.: Multiparty quantum key agreement with GHZ state. In: 2015 IEEE International Conference on Systems, Man, and Cybernetics, pp. 1589–1594 (2015) Oct 2017
37. Xu, Y., Wang, C., Cheng, K., Zhu, H.: A novel three-party mutual authentication quantum key agreement protocol with GHZ states. *Int. J. Theor. Phys.* **61**, 245 (2022)
38. Eftekhari, S., Nikooghadam, M., Rafighi, M.: Security-enhanced three-party pairwise secret key agreement protocol for fog-based vehicular ad-hoc communications. *Veh. Commun.* **28**, 100306 (2021)
39. Altaf, I., Arslan Akram, M., Mahmood, K., Kumari, S., Xiong, H., Khurram Khan, M.: A novel authentication and key-agreement scheme for satellite communication network. *Trans. Emerg. Telecommun. Technol.* **32**, e3894 (2021)
40. Yang, H., Lu, S., Zhu, J., Wu, J., Zhou, Q., Li, T.: A tree-type multiparty quantum key agreement protocol against collusive attacks. *Int. J. Theor. Phys.* **62**, 7 (2022)



Variational Circuit Based Hybrid Quantum-Classical Algorithm VC-HQCA

Mohcene Mouad Lariane^(✉) and Hacene Belhadef

NTIC Faculty, University of Abdelhamid MEHRI Constantine 2, Constantine, Algeria
{mouad.lariane,hacene.belhadef}@univ-constantine2.dz

Abstract. Quantum machine learning (QML) has emerged as a promising field that combines principles from quantum computing and machine learning. This work investigates the influence of variational circuit design on the performance of QML hybrid models. A novel classification system is introduced to categorize variational circuit designs based on their architectural properties. Specifically, the research focuses on exploring the “ONE-TO-ONE-VC” and analyzes the diverse effects of different combinations of quantum gates on the circuit’s performance.

Moreover, the research delves into the study of hyper-parameters and their impact on the performance of QML models. By systematically varying hyper-parameters, the objective is to understand their influence on the overall performance and efficiency of the models. Additionally, a hybrid quantum-classical classifier is built and bench-marked against current classifiers implemented in Qiskit, a widely-used quantum computing framework.

The findings of this research provide compelling evidence for the significance of variational circuit design in QML models. By demonstrating the impact of circuit design on model performance.

Keywords: Quantum machine learning · Variational circuit design · Hybrid models · Classification · Architectural properties · Quantum gates · Hyper-parameters · Quantum-classical classifier

1 Introduction

QML, or Quantum Machine Learning, is a new and emerging field that aims to leverage the power of quantum computing to enhance classical machine learning algorithms. It employs quantum circuits, which can be trained using optimization algorithms to minimize a cost function. This approach has demonstrated effectiveness in various applications, including supervised and unsupervised learning, classification, and regression [13].

QML algorithms are considered variational circuit-based hybrid quantum-classical algorithms [6]. They utilize quantum gates to manipulate qubits and apply quantum theory to perform computations [13]. Classical optimization algorithms are also employed to adjust the circuit parameters and train the model

[6]. The optimization process involves iteratively adjusting the parameters based on measurement results until the cost function is minimized [6]. The design of the quantum circuit is crucial, as it needs to be expressive enough to handle the problem's complexity while remaining amenable to efficient optimization using classical techniques [19].

Similar to classical machine learning, QML requires careful tuning of hyper-parameters to achieve optimal results. Hyper-parameters are parameters that are set before training and are not learned from the data. In the context of QML, these hyper-parameters include the depth of the variational circuit, the number of qubits used, and the learning rate of the classical optimizer. Properly setting these hyper-parameters is essential for achieving the best possible performance in QML [18].

Problem

The problem of choosing the right variational circuit design for hybrid quantum-classical algorithms is a significant challenge in the field of quantum machine learning [6]. Variational circuits are crucial components of these algorithms as they determine how quantum states are prepared and manipulated during the learning process [6].

One of the main difficulties is the vast design space of variational circuits. There are numerous parameters, such as gate types, connectivity patterns, and layer structures, that can be adjusted to create different circuit architectures. Each choice affects the expressiveness and computational efficiency of the algorithm, making the selection process complex and nontrivial [6].

Moreover, the impact of variational circuit design on algorithm performance is not yet fully understood. The relationship between circuit design choices and learning outcomes is highly dependent on the specific problem being addressed. There is a lack of clear guidelines or established best practices for choosing the optimal circuit design for a given task [19].

The computational cost of evaluating different circuit designs further exacerbates the challenge. Quantum simulations and experiments are resource-intensive, requiring substantial computational power and access to quantum hardware. The exploration of different circuit designs can be time-consuming and costly, limiting the scalability and practicality of the search process [9].

Addressing the problem of choosing the right variational circuit design is crucial for advancing the field of hybrid quantum-classical algorithms. It requires a combination of theoretical analysis, experimental validation in quantum computing, and machine learning. By understanding the impact of circuit design choices and developing guidelines or automated tools for selection, researchers can enhance the efficiency, accuracy, and applicability of hybrid quantum-classical algorithms in practical settings.

Proposed Solutions

One approach involves exploring a wide range of variational circuit designs to understand their impact on algorithm performance. By systematically investigating different circuit architectures, researchers can gain insights into the relationship between circuit design choices and the model's capabilities.

In addition, a new classification for variational circuit designs is introduced based on their structural properties, connectivity patterns, and other relevant characteristics. This classification framework consists of 4 classes based on the number of gates used for encoding the data and parameterizing the circuit; this provides a structured way to compare and analyze different designs, facilitating the identification of circuit architectures that are well-suited for specific tasks.

Another important aspect is the consideration of hyperparameters in hybrid quantum-classical algorithms. Hyperparameters, such as the learning rate and a number of optimization iterations, can significantly affect the performance of the model, where it is needed to carefully tune these hyperparameters to find the optimal settings for a given variational circuit design. Understanding the interplay between hyperparameters and circuit design is crucial for achieving desirable results.

To demonstrate the importance of the choice of variational circuit design, a comparison has been held of the performance of a simple hybrid quantum-classical algorithm with more advanced and established algorithms. These comparisons showcase the benefits and limitations of different circuit designs in terms of accuracy. By highlighting the superiority or distinct advantages of a specific variational circuit design, the significance of making informed choices in designing hybrid quantum-classical algorithms is underscored.

By combining the exploration of variational circuit designs, introducing new classification schemes, considering the impact of hyperparameters, and conducting comparative evaluations, aiming to establish guidelines and insights for selecting the most suitable circuit design for hybrid quantum-classical algorithms. These efforts contribute to advancing the field of quantum machine learning and enable the development of more efficient, accurate, and scalable algorithms with broad applications in various domains.

2 State of the Art

QML algorithms are designed to exploit the quantum mechanical properties of quantum systems to solve complex problems more efficiently than classical algorithms [7]. The field of QML holds great promise for a wide range of applications, including optimization, classification, and regression, and is likely to play a crucial role in the development of future quantum computing technologies [13].

2.1 Quantum Computing

Quantum computing is a new paradigm in computing that makes use of quantum-mechanical phenomena, such as superposition and entanglement, to

perform operations on data. It is fundamentally different from classical computing, which uses binary digits (bits) to represent information, with each bit either being in the state of 0 or 1 [20]. In contrast, quantum computing makes use of quantum bits (qubits), which can be in a superposition of both 0 and 1 at the same time, allowing quantum computers to perform certain tasks exponentially faster than classical computers [24].

2.2 Qubits

The quantum version of classical bits, serve as the basic building blocks of a quantum computer. Unlike classical bits, qubits can assume a range of values represented by a quantum state $|\psi\rangle = \alpha|0\rangle + \beta|1\rangle$, where $|\alpha|^2$ represents the probability of measuring the qubit to 0 and $|\beta|^2$ represents the probability of measuring the qubit to 1. Two special states of a qubit are $|0\rangle$ with $\alpha = 1$ and $\beta = 0$ and $|1\rangle$ with $\alpha = 0$ and $\beta = 1$, which are referred to as the computational basis states. A quantum state is expressed as a vector in a high-dimensional Hilbert space [8]. The Qubit sphere representation is shown in Fig. 1.

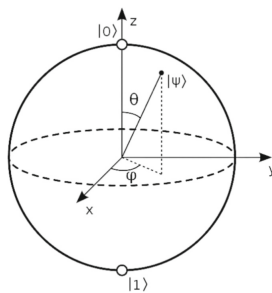


Fig. 1. Qubit sphere

2.3 Quantum Gates

In quantum computing, quantum gates are analogous to logic gates in classical computing, and they operate on qubits to perform various quantum operations. They are represented as matrices that operate on quantum states and can transform the state of a single qubit or multiple qubits at the same time. Quantum gates can perform a variety of operations, such as rotations around an axis, phase shifts, and flips. Figure 2 shows some of the commonly used quantum gates [8].

2.4 Quantum Circuit

A quantum circuit is an ordered sequence of quantum gates that are applied to qubits to perform quantum computations [14]. The input of the quantum circuit is a qubit which is a quantum state, and the output is also another quantum state [17]. The choice of quantum gates used in a quantum circuit can have a

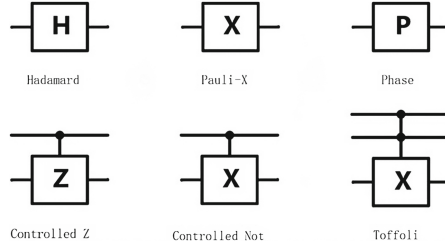


Fig. 2. Graphical representation of the quantum logic gates

significant impact on the behavior and performance of the circuit [15]. Therefore, selecting the right set of gates is crucial to achieving the desired quantum computation task [11]. Along with Hadamard gate, Controlled Hadamard gate, Pauli X, and Controlled Pauli X gate are heavily used to develop quantum circuits for positively or negatively correlated quantum entanglement. The following are the components needed to build a quantum circuit:

Feature Map. The feature map is a quantum circuit layer that prepares the input data to be processed by the variational circuit. It is responsible for encoding the input data into the quantum state representation that can be further manipulated and optimized by the variational circuit [7].

Variational Circuit (VC). A variational circuit is a type of quantum circuit where the gate parameters are chosen as variables to be optimized [23].

2.5 Quantum Machine Learning (QML)

QML is a rapidly growing interdisciplinary field that combines principles of quantum mechanics and machine learning to enable more efficient and accurate solutions to complex problems [13]. QML algorithms use quantum circuits to perform tasks such as classification, regression, clustering, and dimensional reduction on quantum data. The quantum data is often encoded as quantum states or quantum measurements of classical data [13]. The output of a QML algorithm is usually a set of quantum states that can be measured to obtain the final result. The key advantage of QML over classical machine learning is the ability to perform certain tasks, such as feature mapping and optimization, much faster on a quantum computer [13].

2.6 Hybrid Quantum-Classical Models (HQCM)

HQCM are a type of computational model that combines the strengths of classical and quantum computing to solve complex problems [7] by using quantum proprieties for computations and classical algorithms for optimization. Figure 3 presents QML model types [22].

		Type of the algorithm	
		Classical	Quantum
Type of the optimizer	Classical	CC	CQ
	Quantum	QC	QQ

Fig. 3. QML models types

3 Contributions

In this contribution, a novel classification for variational circuits (VCs) is introduced, it provides a structured framework for analyzing and comparing different circuit architectures. Specifically, it focuses on exploring the “one-to-one VC” class and investigating the design possibilities by employing various combinations of Pauli X, Y, and Z gates. Additionally, we propose a new Hybrid quantum-classical algorithm (VC-HQCA) that leverages the power of the use of variational circuits in combination with a simple gradient descent optimizer. Furthermore, an examination has been held on the impact of hyper-parameters on the performance of the algorithm, considering factors such as learning rate and number of iterations and shots. To highlight the significance of choosing an appropriate variational circuit design and hyper-parameter selection, the VC-HQCA against state-of-the-art Qiskit advanced algorithms was bench-marked. Demonstrating through this comparative analysis the critical role of variational circuit design and hyper-parameter optimization in achieving optimal performance for quantum machine learning tasks.

3.1 New Variational Circuit Level of Classification

When it comes to designing variational circuits specifically for Machine Learning (ML) tasks, the choice of Pauli gates can have a substantial impact on the performance of the resulting model. To establish a clear cause-and-effect relationship between these variables, an experimental and methodical approach was implemented in order to create a new classification system that accounts for the design complexity of variational circuits with their various unlimited designs. This classification system will enable us to derive valid conclusions and establish robust guidelines for designing variational circuits tailored for Machine Learning tasks. Through thorough testing, as a result, the most optimal combination of Pauli gates and design configuration for achieving optimal performance in ML applications is identified, which can provide researchers and developers with a

solid framework for designing variational circuits that are optimized for a range of Machine Learning tasks.

The following classes were suggested “Table 1” to simplify the approach for designing variational circuits; the problem is broken down into two main factors. These factors include the number of qubits used for encoding data (state preparation), the number of qubits used for parameterizing the quantum variational circuit, and the number of entanglements. It is important to note that the number of qubits used for encoding data is independent of the number of features in the dataset.

Table 1. Variational circuit classes based on the number of gates used for encoding and parameterization

Parametrization	Encoding	
	<i>One gate</i>	<i>Multiple gates</i>
<i>One gate</i>	ONE-TO-ONE-VC	N-TO-N-VC
<i>Multiple gates</i>	ONE-TO-N-VC	N-TO-N-VC

ONE-TO-ONE Variational Circuit (ONE2ONE-VC). This specific variational circuit design, tailored for machine learning (ML) tasks, is the most straightforward one. It adheres to the subsequent guidelines:

In case of One Qubit Variation Circuit: (see Fig. 4) To encode classical data, you can utilize only two Pauli gates X/Y/Z in this scenario. The first gate rotates the Qubit on one of the three axes (X/Y/Z), while the second optimizes the VC to produce the desired output.

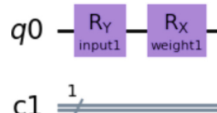


Fig. 4. Example of a One Qubit ONE-TO-ONE-VC

In case of Multiple Qubit Variational Circuit: (see Fig. 5) It consists of using two Pauli gates X/Y/Z for each Qubit in this instance. The initial gate encodes the input, while the second is responsible for optimizing the VC. Finally, a correlation between these qubits is created by applying entanglement between them.

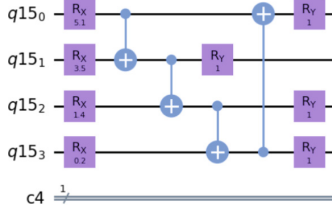


Fig. 5. Example of a Multiple Qubit ONE2ONE-VC

Single and Multiple Entanglement. In the case of a “one qubit variational circuit,” entanglement is not required as it is only applied to two or more qubits. However, in a “multiple qubits variational circuit,” one or more entanglements can be applied to establish a relationship between the features by transferring the quantum data from one qubit to another. The provided examples illustrate a multiple qubits variational circuit with a single entanglement as shown in Fig. 5 and double (multiple) entanglement as illustrated in Fig. 6.

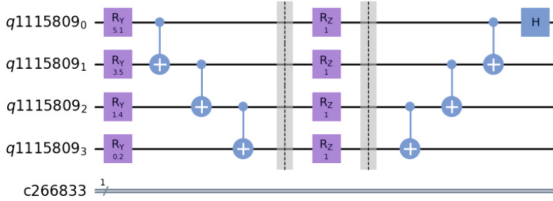


Fig. 6. ONE2ONE-VC with double entanglement VC design

3.2 Variational Circuit Based Hybrid Quantum-Classical Algorithm (VC-HQCA)

In this section, a Variational Circuit-based Hybrid quantum-classical algorithm (VC-HQCA) based on a simple parameterized quantum circuit (PQC) is introduced.

VC-HQCA Pipeline. The pipeline of such algorithms refer to Fig. 7, typically involves several steps that are carefully designed to maximize the computational power of quantum computers [7]. At the heart of these algorithms lies the variational circuit, which is a parameterized quantum circuit that can be optimized through classical optimization techniques [6].

The first step in the pipeline is to prepare the initial state of the system, followed by the implementation of the variational circuit. The next step involves measuring the output of the circuit and using classical optimization techniques to update the parameters. This step is repeated iteratively until the desired accuracy is achieved.

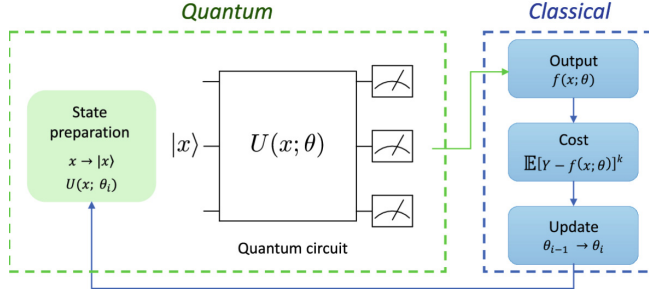


Fig. 7. VC-HQCA architecture

Variational Circuit. In our study, using a straightforward and effective ONE-TO-ONE-VC with single and double entanglement. The primary objective of selecting this particular variational circuit design was to investigate and test various combinations of Pauli X/Y/Z.

Optimisation Function. Since it's a hybrid quantum-classical model, we use classical computing to optimize the PVC parameters to get the desired results, a.k.a training our model by adjusting the PVC parameters. Therefore, a simple gradient descent function is used for optimizing the parameters with the following Eq. (1) [3]

$$\theta = \theta - \alpha \nabla J(\theta) \quad (1)$$

- θ is a vector of parameters
 - α is the learning rate (a hyper-parameter that determines the step size in each iteration)
 - $J(\theta)$ is the cost function (a measure of how well the model fits the training data)
 - $\nabla J(\theta)$ is the gradient of the cost function with respect to the parameters θ (a vector that points in the direction of steepest increase of the cost function).
- The Gradient function is presented in Eq. (2).

$$\nabla J(\theta) = \left[\frac{\partial J(\theta)}{\partial \theta_1}, \frac{\partial J(\theta)}{\partial \theta_2}, \dots, \frac{\partial J(\theta)}{\partial \theta_n} \right] \quad (2)$$

- $J(\theta)$ is the cost function to be minimized by adjusting the model parameters θ .

- $\theta_1, \theta_2, \dots, \theta_n$ are the individual components of the parameter vector θ .
- $\frac{\partial J(\theta)}{\partial \theta_i}$ represents the partial derivative of the cost function with respect to the i -th component of the parameter vector θ .

The Loss function L is presented in Eq. (3).

$$L(y_i - \hat{y}_i) = (y_i - \hat{y}_i)^2 \quad (3)$$

- y_i is the target (true) value for the i th sample
- \hat{y}_i the predicted value for the i th sample

Environment Setup. The code for the implementation is executed on the IBM Quantum Platform ([Link](#)), written in Python language and utilized the Qiskit library ([Link](#)). To carry out the simulation, The Aer QASM simulator was employed and operated on the IBM experience platform. For the study, a real-world classical Iris dataset Iris dataset was chosen ([Link](#)) obtained from the Sklearn library ([Link](#)). This dataset was selected for its simplicity, as it only has four features. This implies that only four Qubits VC are required to encode the features, making it suitable for this research as multiple simulations will be held with a high number of epochs using different VC designs and hyper-parameters. Additionally, the same dataset was used to compare the performance of VC-HQCA with the Qiskit classifiers; it is also the same one that the Qiskit team had already used to benchmark the VQC performance against the classical SVM model. For more information, you can check the link to the Qiskit benchmark in the following ([Link](#)).

3.3 Pauli X/Y/Z Gates Choice Impact on One-to-one VC-Based Model's Performance

Using the previous environment setup and the variational circuit-based Hybrid quantum-classical algorithm, all different possible combinations were tried for designing the used one-to-one VC. And the following results were obtained in Fig. 8.

the obtained results show that Pauli RZ gates are not suitable for designing ONE2ONE-VCs. However, RX-RX and RY-RY gates combinations are suitable for designing ONE2ONE-VCs with increasing accuracy after each iteration, whereas RX-RY and RY-RX gates are the ideal gates combination.

3.4 Hyper-parameters Impact on VC-HQCA's Performance

Using the previous environment setup and the variational circuit based Hybrid quantum-classical algorithm, the values of different Hyper-parameter such as the learning rate and the numbers shot, were constantly updated in order to observe their impact on the VC-HQCA's performance.

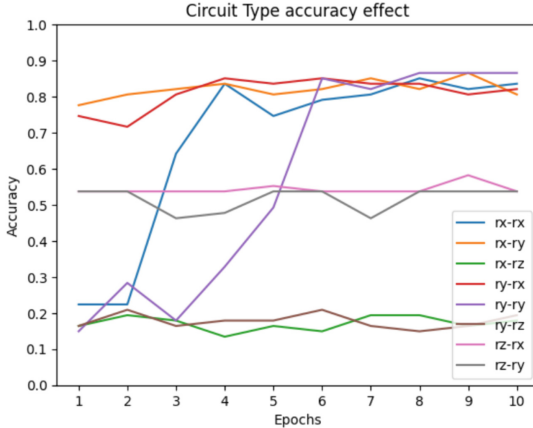


Fig. 8. Pauli X/Y/Z gates choice impact on the VC-HQCA’s performance

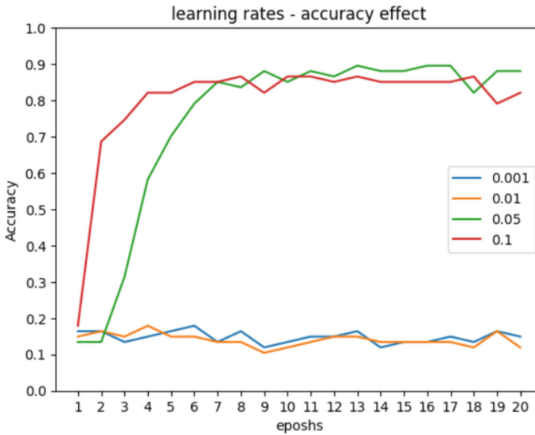


Fig. 9. Learning rate impact on the model’s performance

Learning Rate. [21] the obtained results show that it is better to avoid using small learning rates (< 0.05). Whereas the ideal learning rate is 0.1. However, 0.05 as a learning rate has good results as well as shown in Fig. 9.

Shots Number. “Shots” refer to the number of times a quantum algorithm or circuit is executed to gather statistical data, which helps estimate the probabilities of different outcomes and make meaningful quantum computations [1] the obtained results show that the smaller the number of shots is the faster it is to achieve good results. Therefore the choice of the shots number depends on the number of epochs that has been chosen. Therefore, in order to obtain better results, the smaller the number of epochs, the smaller the number of shots should be (see Fig. 10).



Fig. 10. Number of shots impact on the model's performance

Epoch's Number. [10] the obtained results show that a high number of epochs doesn't necessarily mean a higher accuracy and model's performance. So the number of epochs is irrelevant and has no impact on the model's accuracy, at least for this kind of the variational circuits design used for hybrid quantum-classical machine learning algorithms as depicted in Fig. 11.

3.5 Benchmarking the VC-HQCA

Qiskit Classifiers. For comparison, the VC-HQCA was compared with the following Qiskit Quantum classifiers:

- Variational Quantum Classifier (VQC) [4].
- Quantum Support Vector Classifier (QSVC)/ Quantum Support Vector Machine (QSVM) [16].
- Pegasos Quantum Support Vector Classifier (Pegasos QSVC) [5].
- Estimator Quantum Neural Network (EstimatorQNN) [12].
- Sampler Quantum Neural Network (SamplerQNN) [12].

In this comparison, two ONE2ONE-VC designs were used. The first one is the one used to test the hyper-parameters' impact on the model's performance which is a ONE2ONE-VC with single entanglement (see Fig. 5). Also, another yet simple VC design ONE2ONE-VC with double entanglement (see Fig. 6), is used with the intention of comparing their performance with the performances of the previously mentioned classifiers.

However, it is important to mention that the previously mentioned qiskit quantum classifiers use more complex and advanced VC designs, such as the ONE-TO-N-VC, which is used by the VQC algorithm. Not only that but also they employ advanced optimizers such as COBYLA optimizer [2] while VC-HQCA uses a simple gradient descent function for the VC parameter optimization.

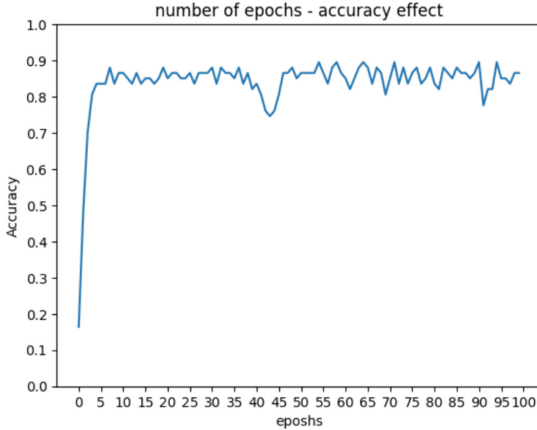


Fig. 11. Number of epochs impact on the model’s performance

The goal behind this comparison is to prove how crucial is the choice of the right variational circuit design. By using a simple yet efficient variational circuit design and outperforming advanced models with complex and advanced variational circuit designs and good optimization algorithms.

Bench-Marking. All the results in the following table “Table 2”

Table 2. Bench-marking algorithms

Algorithm	Optimizer	Variational Circuit	Train accuracy	Test accuracy
VC-HQCA	Gradient descent	ONE2ONE-VC with single entanglement	85%	94%
VC-HQCA	Gradient descent	ONE2ONE-VC with double entanglement	76%	76%
VQC	COBYLA	Advanced	82%	70%
QSVC (QSVM)	stochastic gradient descent	Advanced	100%	85%
Pegasos QSVC	Pegasos algorithm	Advanced	54%	42%
EstimatorQNN	COBYLA	Advanced	51%	24%
SamplerQNN	COBYLA	Advanced	76%	67%

4 Conclusion

Shots number, Learning rate, and Number of Epochs, These three main hyper-parameters play a crucial role in finding a balance between convergence speed, accuracy, and generalization in hybrid quantum-classical machine learning algorithms. Selecting suitable values for these hyper-parameters often involves experimentation and fine-tuning to achieve optimal results.

The obtained results show that the VC-HQCA with the “ONE2ONE-VC with single entanglement” outperformed all of the qiskit classifiers when performing a binary classification task on the Iris Sklearn dataset. It is important to note that even though the Qiskit algorithms use more advanced and complex variational circuit designs and good advanced optimizers, but it was still outperformed by the VC-HQCA that used a more simple and abstract variational circuit design and a simple gradient descent function.

The choice of variational circuit design plays a crucial role in hybrid quantum-classical algorithms, as it directly impacts the performance and efficiency of the algorithm. While more advanced algorithms and complex variational circuit designs may seem appealing, it is important to recognize that simplicity can often lead to surprising and impressive results.

In some cases, a simpler variational circuit design can exhibit surprising capabilities. The use of a basic gradient descent optimizer, which iteratively updates the parameters based on the gradient of the objective function, allows for continuous refinement of the variational circuit. This process can guide the algorithm towards an optimal solution.

In some cases, the simplicity of a basic gradient descent optimizer paired with a simple variational circuit can lead to better performance. The simplicity of the design may allow for faster convergence, better avoidance of local optima, and improved generalization properties. It is often the case that complex algorithms may suffer from overfitting or difficulties in exploring the solution space due to their intricate structures.

Moreover, the choice of the variational circuit design must be aligned with the specific problem at hand. A simple variational circuit design can be more suitable for certain problems where the complexity of a more advanced design may not be necessary or may even be detrimental. The simplicity of the variational circuit can reduce the risk of overfitting and improve the interpretability of the results.

In conclusion, the choice of the variational circuit design is crucial in hybrid quantum-classical algorithms. While advanced algorithms and complex variational circuit designs may seem appealing, simplicity can often yield impressive results. A simple hybrid quantum-classical algorithm with a basic gradient descent optimizer and a simple variational circuit can outperform more advanced algorithms with complex designs. The simplicity of the design can lead to faster convergence, better generalization properties, and improved interpretability. Ultimately, the selection of the variational circuit design should be tailored to the problem at hand, taking into account the specific requirements and constraints of the problem and the available computational resources.

5 Limitations

While our study and results provide valuable insights into the performance of the chosen hybrid quantum-classical algorithm with a simple gradient descent optimizer and a simple variational circuit, it is important to acknowledge certain limitations that were encountered during our research. These limitations have

impacted the scope and breadth of our study. The main limitation was faced was the hardware computational limitation, which prevented us from further exploring and expanding our research in the following areas:

5.1 Limited Dataset Selection

In our study, a specific dataset to evaluate the performance of our algorithm was used. However, due to hardware limitations, it was not possible to incorporate a larger variety of datasets. Using more datasets would have allowed us to strengthen the generalizability and robustness of our findings. It would have provided a broader understanding of how our algorithm performs across different domains and problem types.

5.2 Exploration of Different Variational Circuits

Variational circuits come in various designs and structures, each with its own strengths and weaknesses. Unfortunately, due to computational limitations, it was not possible to explore and study more types of variational circuits in our research. Incorporating different variational circuit designs would have allowed us to investigate their impact on the performance and efficiency of our algorithm, providing a more comprehensive understanding of the variational circuit landscape.

5.3 Resource Constraints

Quantum computing resources, including hardware availability and computational power, present inherent limitations in conducting research in this field. The limited access to quantum computers and their associated computational resources restricted the scale and depth of our experiments. More computational resources would have allowed us to conduct larger-scale simulations, accommodate additional datasets, and explore more complex variational circuit designs.

Despite these limitations, our research and findings contribute to the understanding of hybrid quantum-classical algorithms based on simple variational circuits and gradient descent optimization. Our study demonstrates the potential and effectiveness of such algorithms in specific contexts. It provides a foundation for future research to expand and overcome these limitations by incorporating larger datasets, benchmarking against a wider range of algorithms, and exploring more diverse variational circuit designs.

6 Perspectives

This study serves as an initiation into the exploration of a new level of classification using variational circuits (VCs) in the context of quantum computing. It aims to provide a comprehensive guideline that incorporates key quantum computing concepts and quantum theory while designing quantum circuits by

adopting a methodical approach to explore new categorical classifications based on the complexity of VC designs, specifically focusing on categorical classification.

However, there are still numerous avenues for future research and investigation in this emerging field. Building upon our initial findings, it is possible to extend the exploration and explore additional classifications that can be studied in future research endeavors. Some potential classifications include ONE2ONE-VC with single entanglement/multiple entanglements, ONE2N-VC with single entanglement/multiple entanglements, N2ONE-VC with single entanglement/multiple entanglements, and N2N-VC with single entanglement/multiple entanglements. These classifications can provide further insights into the relationship between VC designs, entanglement patterns, and their impact on categorical classification.

Moreover, the variety of quantum gates available for designing VCs presents another avenue for future investigations. Different combinations of quantum gates can lead to distinct VC designs, each with its own unique characteristics. Exploring these combinations and their influence on the performance and effectiveness of VC-based quantum machine learning (QML) models can advance our understanding and optimization of VC-based approaches.

The main motivation behind this study is to establish a comprehensive guideline for designing VCs in order to optimize VC-based QML models. By expanding our knowledge in this field, the full potential of quantum computing will be unlocked in order to solve complex classification problems within the realm of artificial intelligence (AI).

References

1. Alsharabi, N., Shahwar, T., Rehman, A.U., Alharbi, Y.: Implementing magnetic resonance imaging brain disorder classification via AlexNet-quantum learning. *Mathematics* **11**(2), 376 (2023)
2. Armaos, V., Badounas, D.A., Deligiannis, P., Lianos, K., Yordanov, Y.S.: Efficient parabolic optimisation algorithm for adaptive VQE implementations. *SN Comput. Sci.* **3**(6), 443 (2022)
3. Bergholm, V., et al.: PennyLane: automatic differentiation of hybrid quantum-classical computations. arXiv preprint: [arXiv:1811.04968](https://arxiv.org/abs/1811.04968) (2018)
4. Blance, A., Spannowsky, M.: Quantum machine learning for particle physics using a variational quantum classifier. *J. High Energy Phys.* **2021**(2), 1–20 (2021)
5. Chatterjee, S., Das, A.: An ensemble algorithm using quantum evolutionary optimization of weighted type-II fuzzy system and staged Pegasos quantum support vector classifier with multi-criteria decision making system for diagnosis and grading of breast cancer. *Soft. Comput.* **27**(11), 7147–7178 (2023)
6. Chen, S.Y.C., Yang, C.H.H., Qi, J., Chen, P.Y., Ma, X., Goan, H.S.: Variational quantum circuits for deep reinforcement learning. *IEEE Access* **8**, 141007–141024 (2020). <https://doi.org/10.1109/ACCESS.2020.3010470>
7. Havlíček, V., et al.: Supervised learning with quantum-enhanced feature spaces. *Nature* **567**(7747), 209–212 (2019). <https://doi.org/10.1038/s41586-019-0980-2>

8. Hughes, R.: Quantum computation. *Comput. Sci. Eng.* **3**(2), 26 (2001). <https://doi.org/10.1109/MCISE.2001.908998>
9. Hussain, N.H.M., et al.: Machine learning of the reverse migration models for population prediction: a review. *Turk. J. Comput. Math. Educ. (TURCOMAT)* **12**(5), 1830–1838 (2021)
10. Kim, D.: Deep learning neural networks for automatic vehicle incident detection. *Asia-Pac. J. Convergent Res. Interchange* **4**(3), 107–117 (2018)
11. Lanyon, B.P., et al.: Simplifying quantum logic using higher-dimensional Hilbert spaces. *Nat. Phys.* **5**(2), 134–140 (2009)
12. Mac-Kay Cisternas, C.A.: Quantum machine learning for predictive maintenance (2023)
13. Mitarai, K., Negoro, M., Kitagawa, M., Fujii, K.: Quantum circuit learning. *Phys. Rev. A* **98**(3), 032309 (2018). <https://doi.org/10.1103/PhysRevA.98.032309>
14. Nielsen, M.A., Chuang, I.L.: Programmable quantum gate arrays. *Phys. Rev. Lett.* **79**, 321–324 (1997). <https://doi.org/10.1103/PhysRevLett.79.321>
15. Ono, T., Okamoto, R., Tanida, M., Hofmann, H.F., Takeuchi, S.: Implementation of a quantum controlled-swap gate with photonic circuits. *Sci. Rep.* **7**(1), 45353 (2017)
16. Pai, A.G., Buddhiraju, K.M., Durbha, S.S.: Multiclass classification of hyperspectral remote sensed data using QSVC. In: *Remote Sensing for Agriculture, Ecosystems, and Hydrology XXIV*, vol. 12262, pp. 104–108. SPIE (2022)
17. Plesch, M., Brukner, I.C.V.: Quantum-state preparation with universal gate decompositions. *Phys. Rev. A* **83**, 032302 (2011). <https://doi.org/10.1103/PhysRevA.83.032302>
18. Salehi, T., Zomorodi, M., Plawiak, P., Abbaszade, M., Salari, V.: An optimizing method for performance and resource utilization in quantum machine learning circuits. *Sci. Rep.* **12**(1), 16949 (2022)
19. Schuld, M., Bocharov, A., Svore, K.M., Wiebe, N.: Circuit-centric quantum classifiers. *Phys. Rev. A* **101**, 032308 (2020). <https://doi.org/10.1103/PhysRevA.101.032308>
20. Soiguine, A.: Two shaky pillars of quantum computing. *J. Appl. Math. Phys.* **11**(2), 448–456 (2023)
21. Stein, S.A.: Quantum computing aided machine learning through quantum state fidelity (2021)
22. Temme, K., Bravyi, S., Gambetta, J.M.: Error mitigation for short-depth quantum circuits. *Phys. Rev. Lett.* **119**, 180509 (2017). <https://doi.org/10.1103/PhysRevLett.119.180509>
23. Tilly, J., et al.: The variational quantum eigensolver: a review of methods and best practices. *Phys. Rep.* **986**, 1–128 (2022)
24. Weigold, M., Barzen, J., Leymann, F., Salm, M.: Encoding patterns for quantum algorithms. *IET Quantum Commun.* **2**(4), 141–152 (2021)



Quantum Computing in Non Destructive Testing of Materials

Thouraya Merazi-Meksen^{1,2(✉)}

¹ Faculty of Electrical Engineering, University of Science and Technology Houari Boumediene, Bab Ezzouar, Algeria
tmeksen@usthb.dz

² USTHB, Bp 32, El Alia, Bab Ezzouar, Algiers, Algeria

Abstract. Non-Destructive Testing (NDT) is a set of methods and techniques to verify the integrity of a structure without damaging it. It concerns mechanical structures, as well as civil engineering constructions... Since the reliability of the results is closely dependent on the quality of the instrumentation used, NDT research is continuously evolving with technological advances. Indeed, inspections by ultrasonic waves or eddy currents have seen their instrumentation highly miniaturized and connected in recent decades. This paper sheds light on work toward exploiting quantum computing and the Internet of Things in the field of materials control.

Keywords: Non Destructive Testing · Industry 4.0 · Quantum computing

1 Introduction

The aim of non-destructive testing (NDT) is to detect defects inside a material without damaging it. Research in this domain has taken on great importance with the growth of the aerospace and nuclear industries. These methods and techniques were then adopted by all fields for the detection of discontinuities, manufacturing defects, or damage such as cracks.

The most common NDT methods are: radiography, ultrasound, magnetic particle inspection, thermography, and eddy current [1]. For all methods, suitable sensors and instrumentation are required, and their quality has a major influence on the reliability of the diagnosis. This means that NDT research is closely linked to technological advances such as the miniaturization of equipment, robotization, and artificial intelligence. Indeed, the increasing affordability of miniaturized wireless sensors, their interconnectivity over the Internet, the cost of storing and processing data in the cloud, and the rapid improvement in analysis and decision-making are all driving researchers to begin working on this so-called Industry 4.0 path [2].

Industrie 4.0 refers to a new generation of connected, robotized, and intelligent factories. The Industry 4.0 term first appeared at Hannover Messe in 2011 when Professor Wolfgang Wahlster, Director of the German Research Center for Artificial Intelligence, addressed the opening ceremony audience. This gave a name to all the ongoing activities

that will eventually lead to the fourth Industrial Revolution. NDT 4.0 will be integrated into the world provided by the results of Industry 4.0.

Nano-diagnostics is also of the most promising scientific directions of NDT. Non-destructive testing of the new generation is the use of known nano-effects, nano-sensors and nano-transformers [3].

This paper describes the project to develop our precedent works toward these new technologies. Indeed, we have proposed some imaging ultrasonic testing methods to help in decision making [4] and we are looking to exploit Internet of Things and quantum computing in non destructive testing research. Indeed, in situations where the required ultrasound wavelengths are of the order of the dimensions of the structural grains of the material, the signal observed in conventional methods is drowned in noise. In these cases, even advanced signal processing methods are ineffective because the grains of the material also interact with the waves and behave like discontinuities, just like any defects.

After the introduction, we will give a reminder of the ultrasonic and eddy current inspections in Sect. 2. In Sect. 3, Industry 4.0 and NDT 4.0 are described. Section 4 shows how quantum computing can be used to improve NDT of materials. Finally, a conclusion is given.

2 Non Destructive Testing Overview

Among the most used NDT methods, we can mention gammagraphy, ultrasonic inspection, and eddy currents. Regarding gammagraphy, this method is increasingly being replaced by the other two because of the harmfulness of radiation. We can summarize their principles as follows.

2.1 Ultrasonic Inspection

Ultrasonic waves are used in non-destructive testing (NDT) to determine the internal characteristics of a material or to detect a defect that may be present in the structure. Evaluation consists of emitting ultrasonic waves into the area to be explored and studying the reflected, refracted, or scattered echoes [5]. Manual systems have been used successfully since the end of the Second World War. These systems use one or more ultrasonic transducers delivering so-called A-Scan (Amplitude Scanning) signals which an operator has to analyze and interpret by considering the characteristics of the signal (position, amplitude, rise time, etc.).

When large structures are inspected, the amount of data produced can be too great, and interpreting the results of ultrasonic inspection becomes a delicate operation requiring a high degree of technical skill on the part of the operators. This has led to great interest in the development of automatic systems.

The graphic performance of computers, and the development of algorithms have made it possible to represent data in image form. In addition to the ease with which results can be displayed, ultrasound imaging can be used to automate the detection, location, and sizing of defects in many situations using conventional signal and image processing tools. However, in the case of materials with a high level of structural noise, the

interpretation of signals and images can be very complex, particularly when detection and characterization are based on the analysis of diffracted echoes, which are often confused with echoes due to structural noise. Figure 1 summarizes the ultrasonic NDT principle (see Fig. 2).

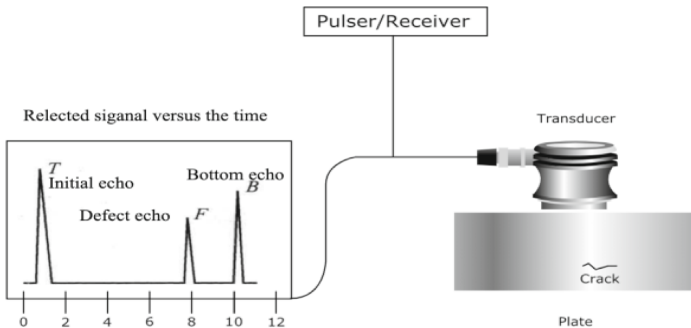


Fig. 1. Ultrasonic NDT principle

2.2 Eddy Current NDT

An eddy current is a swirling electrical current that is created in a conducting metal such as steel by moving the metal through a magnetic field or a magnetic field over the metal. The currents generated produce their own magnetic field. When a defect is present in the metal (a crack for example), the eddy current is influenced, and the measures of the changes are exploited to locate and characterize this defect (Fig. 3).

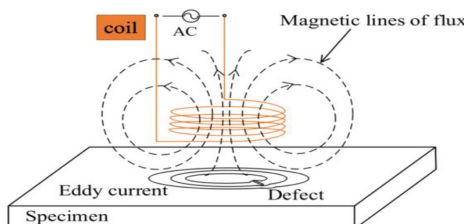


Fig. 2. Eddy current NDT principle

In the eddy-current testing of tubes, an inspector will run a probe through the length of a tube in order to identify tiny defects [6]. Eddy current tests can also help identify defects on the surface of materials, with the use of pulsed eddy current testing equipment. The potential applications of eddy current non-destructive testing are:

- Conductivity Testing
- Surface Inspection
- Detection of Corrosion
- Bolt Hole Inspection
- Tubing inspection

3 NDT 4.0

Nondestructive Testing 4.0 has been defined by Schulenburg as “the concept of cyber-physical non-destructive testing arising from Industry 4.0 digital technologies, and physical inspection methods” [7]. It seeks to enhance inspection performance, integrity engineering and decision making for safety, sustainability, and quality assurance, as well as provide timely and relevant data to improve design, production, and maintenance characteristics.

3.1 From Industry 1.0 to Industry 4.0

The first industrial revolution (Industry 1.0) began in the 18th century with the harnessing of steam power and the mechanization of production. Developments such as steam-powered ships and steam locomotives have made a major contribution to human life [8].

The second industrial revolution (Industry 2.0) began in the 19th century with the discovery of electricity. Countless motorized objects came into being, such as the motor car, the aeroplane, etc.

The third industrial revolution (Industry 3.0) began in the 1970s. It concerns partial automation using computers driving programmable controllers. Since the introduction of these technologies, it has become possible to automate various processes.

The fourth Industrial Revolution is currently underway. It is characterized by the application of information and communication technologies to industry. It is known as “Industry 4.0”. It stems from developments in Industry 3.0. Production systems already equipped with IT technology are extended by a network connection and connected via Internet. This enables communication with other installations and the networking of systems for the exchange of information and the creation of intelligent systems. The figure below summarizes the four principal phases of industrialization.

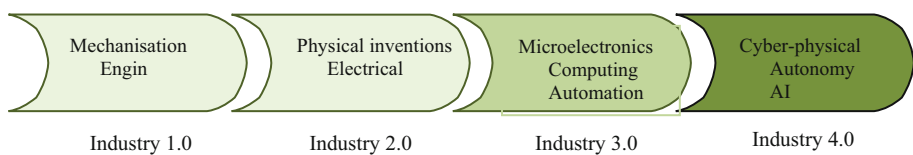


Fig. 3. The four phases of industry evolution

Industry 4.0 is not the emerging technologies, but their integration for a purpose that was not achievable up until now: The increase in communication bandwidth from 5G, the ability to manage terabytes of data, computational processing speed and capacity, and mobile devices [9].

4 Quantum Computing in NDT

Quantum is introducing innovative and advanced methods in the field of Non Destructive Testing.

The greatest development of nano-diagnostic systems occurs with the use of scanning probe microscopy. In this joint future all elements of digitalization will be applied, e.g. modeling and simulation, real-time inspection, internet of things, machine learning, digital twin, and artificial intelligence.

Quantum elastic scattering of ultrasonic waves and phonons by defects is recent fields of research for different cases. It is based on the study of the vibrations of atoms. [10, 11] caused by an elementary excitation (quasi-particle) called phonon. Phonons can interact with each other, electrons, magnons, and other quasi-particles. Phonons also interact with point and linear defects, surface imperfections, and volume disorders: cracks, vacancies, dislocations, insertions, pores, inhomogeneities, microstructure imperfections, grain boundaries, delaminations, discontinuities, cavities, all reflection surfaces, and so on (Fig. 4).

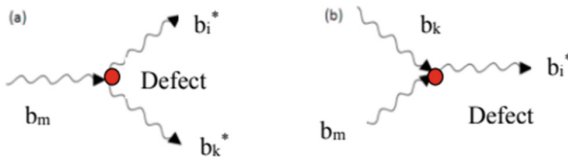


Fig. 4. Phonon-defect interaction

Ultrasonic waves can be considered as a phonon-phonon interaction from quantum point of view. The nonlinear nature of the phonon scattering is caused by the nonlinearity of the medium density and elastic modulus variations and defects in the material.

In conventional methods of ultrasonic testing, a wave is disturbed by a discontinuity only when its half wavelength is smaller than the dimension of the obstacle. Thus, for the detection of cracks (very thin) it would be necessary to use very short wavelengths, therefore very high frequencies. The problem then, is that high frequencies have very low penetrating power. This is why the use of quantum computing is a very promising prospect.

In the case of eddy current inspection, novel magneto-vision systems was developed based on miniature, highly sensitive sensors Called Quantum Well Hall Effect (QWHE) [12, 13]. This system consists of small size sensors arrays, and an adjustable electromagnet. Linear magnetic flux density. That makes them well suited for electromagnetic NDT imaging methods when multiplexing these sensors through simultaneous time and frequency division multiplexing. Thus, they are conducted in order to improve measurement times over previous arrays.

5 Conclusion

The control of materials and structures is a field greatly dependent on the instrumentation used. Every advance in technology and computing allows for progress in instrumentation (sensors), data acquisition, and processing. The miniaturization, the wireless and the communication systems have to be exploited in industry. In this article, we study the possibilities of exploiting quantum computing to detect very small defects (cracks for

example) present in the structures under control. In those cases, the grains of the material also interact with the ultrasound beam, consequently generating signals that are too noisy to distinguish defects. Quantum computing must also be considered in the detection of defects present on the surface of structures. Indeed, when the crack is emerging, the classical methods remain difficult to exploit, both by ultrasonic methods and eddy currents.

References

1. Hellier, C.: Handbook of Nondestructive Evaluation. McGraw-Hill, New York, p. 1.1 (2003). ISBN: 978-0-07-028121-9
2. Lasi, H., Fettke, P., Kemper, H.G., Feld, T., Hoffmann, M.: Industry 4.0. Bus. Inf. Syst. Eng. **6**, 239–242 (2014)
3. Mandayam, S., Sagar, S.P. (eds.): Advances in Non Destructive Evaluation: Proceedings of NDE 2020. Springer Nature, Cham (2022)
4. Merazi Meksen, T., Boudraa, B., Drai, R., Boudraa, M.: Automatic crack detection and characterization during ultrasonic inspection. J. Nondestr. Eval. **29**(3), 169–174 (2010)
5. Taheri, H., Hassen, A.: Nondestructive ultrasonic inspection of composite materials: a comparative advantage of phased array ultrasonic. Appl. Sci. **9**(8), 1628 (2019)
6. Garcia Martin, J.: Non Destructive testing based on Eddy current testing. Sensors **11**, 2525–2565 (2011)
7. Schulenburg, L.: NDT 4.0: opportunity or threat. Mater. Eval. **78**(7), 852–860 (2020)
8. Lau, Y.W., Yeung, K.C.: From industrial revolution (Industry 1.0) to surgery 4.0. Chin. J. Dig. Surg., 919–924 (2020)
9. Claycomb, J.R., Tralshawala, N., Cho, H.M., Boyd, M., Miller Jr, J.H.: Superconducting quantum interference devices for nondestructive testing. Futuristic Aircrafts., 155 (1989)
10. Karpelson, A.: Linear and nonlinear classical and quantum elastic scattering of ultrasonic waves and phonons by defects. e-J. Nondestr. Test. ISSN: 1435–4934
11. Shulyakovskiy, R., Garkun, A., Levchuk, M., Nevmerzhitsky, M., Shaplov, A.: Quantum-mechanical uncertainty in NDT (Example of Scanning Tunnel Microscopy). In: International Conference NDT Days 2018, Sozopol, Bulgaria (2018)
12. Liang, C.W., Ahmad, E., Balaban, E., Sexton, J., Missous, M.: A quantum well Hall effect Magnetovision system for non-destructive testing. In: 19th World Conference on Non-Destructive Testing (2016)
13. Missous, M.: Real time magnetic imaging of paramagnetic and ferromagnetic materials using time frequency division multiplexed quantum well Hall effect sensor arrays. In: 59th Annual Conference of the British Institute of Non-Destructive Testing, NDT 2022, pp. 235–247. British Institute of Non-Destructive Testing (2022)



Enhanced Gaussian Quantum Particle Swarm Optimization for the Clustering of Biomedical Data

Saida Ishak Boushaki^{1(✉)}, Omar Bendjeghaba², Nadjet Kamel³,
and Dhai Eddine Salhi⁴

¹ Computer Science Department, University M'Hamed Bougara, 35000 Boumerdes, Algeria
s.boushaki@univ-boumerdes.dz

² LREEI, University M'Hamed Bougara, 35000 Boumerdes, Algeria

³ Faculty of Technology, University Ferhat Abbas Setif 1, Setif, Algeria

⁴ LIMOSE Laboratory, University Mhamed Bougara, Boumerdes, Algeria

Abstract. The clustering is a crucial procedure that has several applications, including bioinformatics. It automatically extracts relevant knowledge from data by grouping homogeneous objects into the same group.

Biomedical data clustering-focused metaheuristic algorithms are a field of current study due to their power to achieve global solutions instead of local ones. An intriguing metaheuristic technique that has been applied extensively in several fields of study is particle swarm optimization.

In this paper, Gaussian Quantum Particle Swarm Optimization (GQPSO), inspired by quantum theory, is employed to resolve the clustering problem. First, it is adapted for the clustering of biomedical data. Then, the GQPSO search mechanism is reinforced by an acceleration strategy to increase the internal cluster cohesion. The experimental outcomes on well-known biomedical datasets are encouraging and support the recommended algorithm's dominance over the cuckoo search method, genetic algorithm and both all typical and quantum particle swarm with regard to the quality of internal clustering.

Keywords: Clustering · Gaussian Quantum Particle Swarm Optimization · Quantum Theory · Biomedical data · Datamining · Metaheuristic

1 Introduction

The technique of data mining involves automatically extracts relevant knowledge from raw data by generating a model. It offers a number of techniques that fall into descriptive and predictive categories. In predictive methods, the classes are known in advance, and the produced model is used to predict unclassified objects. However, descriptive methods extract features and hidden information without any prior knowledge [1]. One of the most commonly used descriptive methods is clustering [2]. Its aim is to group homogeneous objects in the same group. It has several applications, including bioinformatics [3, 4].

Classical clustering techniques are divided into hierarchical clustering methods and partitioning ones. Hierarchical approaches require excessive complexity to explore data

at various levels of detail, while partitioning approaches are typically linear in complexity. For this reason, partitioning procedures are frequently preferred over hierarchical approaches [2].

K-means is the most widely used partitioning clustering technique [5]. It is easy to implement and has successfully addressed various problems. However, it can converge to local minima. On the other hand, clustering algorithms based on metaheuristics have demonstrated their ability to find global solutions, including particle swarm optimization (PSO), genetic algorithms (GA), and cuckoo search (CS) [6].

Recently, an interesting theory called quantum theory emerged from physics. Its primary goal is to investigate fundamental physical events, particularly at the level of atomic and subatomic particles. The Schrödinger equation is the most distinguished concept in this theory [7,8]. It has important applications in several scientific disciplines, including evolutionary computation [9]. Gaussian Quantum Particle Swarm Optimization (GQPSO) is an improved version of conventional PSO inspired by this theory [10].

The goal of this research is first to adapt GQPSO for the clustering of biomedical data. Then, an enhanced version of GQPSO is proposed, named EGQPSO. The search mechanism of EGQPSO is reinforced by an acceleration strategy to increase the internal cluster cohesion. The experimental outcomes on biomedical data are encouraging and support the effectiveness of the suggested methodology.

This study's remaining sections are organized as follows: In Sect. 2, related works are displayed. Gaussian quantum particle swarm optimization's main underlying ideas are covered in Sect. 3. In Sect. 4, the suggested approach is detailed, and its key phases are described. Section 5 provides numerical experimentation and outcomes. Finally, Sect. 6 draws conclusions and outlines our future study.

2 Related Works

Numerous articles have been published on clustering biomedical data using metaheuristic algorithms. In this section, we outline the methods most closely associated with the suggested algorithm.

In 2003, a novel method was presented for the unsupervised classification of biomedical data that emphasized the advantages of Simulated Annealing and Genetic Algorithm. Employing medoids helps increase exterior cluster separation and internal cluster cohesion. The suggested approach performs better than its rivals with regard to accuracy and stability [11].

Next, in 2008, a novel proposed algorithm described how Quantum Particle Swarm Optimization (QPSO) can be applied to cluster biomedical data. The experimental tests demonstrate the suitability of the QPSO-based clustering algorithm for this research area [12].

More recently, in 2019, a hybrid algorithm using Fuzzy C-Means Clustering (FCM) and a kidney-inspired algorithm created for clustering biomedical data was presented. The experimental findings demonstrate how effective the suggested strategy is over conventional methods in producing compact clusters [13].

In the same year, the rough fuzzy cuckoo search algorithm was employed to tricluster genes in parallel between samples and time points. The provided solution outperformed other approaches when compared to current triclustering algorithms [14].

While hybrid algorithms improve clustering results, they are often sophisticated and require more processing power. Other techniques, instead of endorsing a particular metaheuristic, utilize novel ideas generated by cutting-edge theories like quantum theory to enhance their own performance more easily.

In this study, quantum theory is used to enhance the capabilities of the standard PSO.

3 Background of GQPSO

Particle swarm optimization (PSO) is an intriguing metaheuristic algorithm [15]. It draws modeling ideas from the movement and social behavior observed in swarm-like groups of fish or bird flocks. A collection of particles makes up the PSO population, each one standing for a possible resolution, they navigate the search space in quest of the best one. Based on both its own and its neighbors' experiences, each particle modifies its location. The particle's current optimal location with the highest fitness value is considered the global best. Through iterations, particles continuously explore and exploit the search space, progressively converging towards the optimal solution.

The position and velocity of each particle are used to update its position. The following formula is used to determine particle i 's new location at iteration $it + 1$:

$$ps_i(it + 1) = ps_i(it) + vlc_i(it + 1) \quad (1)$$

where: $ps_i(it)$ is particle i 's present location at iteration it . $Vlc_i(it + 1)$ is particle i 's velocity at iteration $it + 1$.

Each particle's velocity is modified in accordance with its present velocity, best prior location ($PsBt$), and the best position of all the particles in the swarm (Glb s). The new velocity of particle i at iteration $it + 1$ is calculated as follows:

$$vlc_i(it + 1) = iw \times vlc_i(it) + cst1 \times rd() \times (PsBt_i - ps_i(it)) + cst2 \times rd() \times (Glb - ps_i(it)) \quad (2)$$

where: $vlc_i(it)$ represents the current particle i velocity at iteration it . iw is constant that regulates how much the particle's prior velocity affects its current velocity. $Cst1$ and $cst2$ are the acceleration coefficients for the social and cognitive components, respectively. $rd()$ produces a random number in the range between 0 and 1. $PsBt_i$ is the best place that particle i has discovered thus far. Glb is the optimal location inside the swarm for all particles.

The Quantum Particle Swarm Optimization (QPSO) algorithm combines principles from quantum mechanics with the traditional PSO algorithm to enhance its global search capabilities and improve optimization performance [16]. In the QPSO version, the update of the particle is described by a wavefunction called the Schrödinger equation:

$$\begin{cases} ps_i(it + 1) = LA + \alpha \cdot |MoyBt - ps_i(it)| \cdot \ln(1/\theta) & \text{if } \lambda \geq 0.5 \\ ps_i(it + 1) = LA - \alpha \cdot |MoyBt - ps_i(it)| \cdot \ln(1/\theta) & \text{if } \lambda \leq 0.5 \end{cases} \quad (3)$$

where: α is a contraction-expansion coefficient, a design factor, The values θ and λ are produced inside the interval $[0, 1]$ by means of the uniform probability distribution functions. $MoyBt$, which stands for Mean Best of the population, is the average of all particles' $PsBt$ placements. LA is the local attractor and it is given by following equation:

$$LA = \frac{cst1 \times PsBt_i + cst2 \times GlBs}{cst1 + cst2} \quad (4)$$

In Gaussian Quantum Particle Swarm Optimization (GQPSO) [10], the random numbers are produced by employing Gaussian distribution sequences with zero mean and unit variance for the stochastic PSO coefficients. Therefore, it might be possible to strike a good balance between the likelihood of having many small amplitudes around the current points (fine-tuning) and the likelihood of having higher amplitudes, which might allow particles to move away from the current point and escape from local minima. The following is an explanation of the latest GQPSO update:

$$\begin{cases} ps_i(it+1) = LA + \alpha \cdot |MoyBt - ps_i(it)| \cdot \ln(1/Gos) & \text{if } \lambda \geq 0.5 \\ ps_i(it+1) = LA - \alpha \cdot |MoyBt - ps_i(it)| \cdot \ln(1/Gos) & \text{if } \lambda \leq 0.5 \end{cases} \quad (5)$$

where Gos is a random number, generating by Gaussian distribution sequences with zero mean and unit variance.

4 The Proposed Algorithm

Finding the most significant groupings is the primary objective of the clustering procedure, based on the similarities between them. The literature defines several similarity metrics; nevertheless, the most conventional measurement is the Euclidean distance. Using this method, clustering is viewed as an optimization issue where the goal is to select the best possible partition from a large number of potential ones by refining an objective function. To produce compact groups, the total similarity inside a cluster is calculated using the Euclidean distance. This function minimizes the distance between each item and the allocated cluster's centroid. The formula below describes the goal function employed in this study:

$$Fitness = \text{Minimise} \sum_{i=1}^n \min\{D_{1i}, D_{2i}, \dots, D_{ki}\} \quad (6)$$

where: n is the number of objects, D_{ji} is the distance between object i and cluster number j .

Organizing clusters turns into a minimization issue depending on the chosen objective function. The following outlines the primary steps of the planned Enhanced Quantum Particle Swarm Optimization (EGQPSO):

- 1. Initial population and encoding:** In this study, particles represent solutions to the problem. Each solution divides the dataset into k clusters, with clusters defined by their centroids. Therefore, k centroids constitute a solution. As the dataset under consideration has m characteristics, each centroid is represented as a vector of m

dimensions. Therefore, each particle is represented by a matrix of k rows and m columns ($k \times m$). Like other metaheuristics, a random selection is made from the search space to create the starting population..

2. **Fitness evaluation:** To create dense clusters, we employ fitness explained in Eq. (6). The cost of each particle is calculated, and the best particle is selected.
3. **Gaussian Quantum Particle Swarm update:** In QPSO, the wavefunction (Schrödinger equation) is used to represent a particle's state, with the probability density function providing the likelihood of the particle appearing in a given position. When using the Monte Carlo approach, particles move in accordance with Eq. (3). While the QPSO version uses a uniform probability distribution to generate random numbers, the GQPSO employs Gaussian probability as indicated in Eqs. (5) and (4). Using Gaussian distribution sequences for random number generation can strike a harmony between big amplitudes and numerous tiny amplitudes close to current locations (fine-tuning). This might allow particles to escape local minima and migrate away from the current location.
4. **Adjusting new solutions:** The boundary management procedure's goal is to ensure that particles remain within the available search space. In our work, we used a technique based on the classical strategy [17] for managing limit values. This technique operates by capping the particle's location at the limit when it exceeds it.
5. **Fitness evaluation:** Find the optimal solution by calculating the objective functions for each one, as mentioned earlier.
6. **Comparing new and old solutions:** Replace the old solution with the new one if it is superior.
7. **Enhanced mechanism:** To expedite the search mechanism, an additional local mechanism is applied to the obtained solutions. First, the closest centroid is assigned to each dataset item. Next, the following formula is used to determine the center of each recently created cluster:

$$\text{ClusterCenter}_i = \frac{1}{NbCl_i} \sum \text{Object}_l \quad (7)$$

where, ClusterCenter_i is the center of the group number i . Object_l denotes dataset item from cluster i , $NbCl_i$ is the number of dataset items that are a part of cluster number i .

Afterward, each particle's optimal location is updated with its corresponding cluster center, as determined by equation (7).

1. **Fitness Evaluation:** Find the optimal solution by calculating the objective functions for each one.
2. Repeat steps 3 through 8 until a termination criterion is met.
3. Finally, display the ideal position and the ideal goal function.

Pseudocode for the EGQPSO clustering algorithm is presented in Fig. 1.

Gaussian Quantum Particle Swarm Clustering Algorithm

1. Establish the starting settings;
2. Start up the swarm at random;
3. Use equation (6) to determine the swarm's fitness and choose the optimal particle;

While (stop criteria are not satisfied), **do**

 4. Determine the new particle positions using the Gaussian Quantum Particle Swarm update, as given in Equations (5) and (4);
 5. Ensure that particles remain within the available search space using the boundary management procedure;
 6. Calculate the fitness of the new particle positions by employing the equation (6) and select the best particle;
 7. Replace the positions of the old particles with the new ones if they are superior;
 8. Enhance the search mechanism by conducting an additional local search. First, assign each dataset object to the closest particle position. Then, calculate the center of each new generated cluster using Equation 7. Next, update the swarm's information;
 9. Calculate the fitness of the new particle positions by employing the equation (6) and select the best particle;

End While;

 10. Show the fitness value and the final best position.

Fig. 1. The main steps of EGQPSO clustering algorithm.

5 Experiments and Results

Five algorithms: quantum particle swarm optimization (QPSO), enhanced Gaussian quantum particle swarm optimization (EGQPSO), cuckoo search algorithm (CS), genetic algorithm (GA), and standard PSO, are compared in order to assess the efficacy of the suggested EGQPSO. Ten runs of each assessed algorithm were conducted. Every tested method also has a predetermined population size and total number of iterations. One hundred iterations were allotted to all programs, with ten being the population size. For accurate comparisons, the most popular configurations and the best performance were taken into consideration while setting the settings for the different experimental procedures. These were chosen in line with the recommendations made by the original publications.

5.1 Datasets

Three common biomedical datasets (Breast A, NOVARTIS, and LEUKEMIA) were used in the study, and it references Table 1 as a source for the key traits of these datasets.

Table 1. Details of the tested biomedical datasets.

Datasets	Number of genes	Number of samples	Number of clusters
Breast A	98	1213	3
NOVARTIS	103	1000	4
LEUKEMIA	248	985	6

5.2 Results and Discussion

Table 2 displays the fitness measured using various clustering techniques in relation to distinct standards: the Standard Deviation (Std), Mean, Worst, and Best. Please note the bolded reporting of the best values.

This table clearly demonstrates that, for all the datasets considered, QPSO outperforms PSO. This indicates a diverse population and the exploration of new areas. Furthermore, for all the experimental datasets, EGQPSO performed better than the other approaches. This can be attributed to the use of Gaussian probability distribution in QPSO, which proves to be a potent technique for enhancing QPSO's ability to avoid premature convergence to local maxima. Additionally, the local search mechanism has accelerated the search process while improving global search. However, GA's optimization outcomes for almost all datasets were poor.

It is evident from the same table that EGQPSO has, with the exception of the standard deviation, produced the best optimization outcomes across all examined criteria, which consistently ranks as the second best. However, this latter criterion does not significantly influence the clustering results. This is because, for a given Std, the values fall within the range of Mean-Std and Mean + Std. For instance, with the Breast A dataset, the best Std is achieved by QPSO (2.144), indicating that the values are between 1,110.170 and 1,114.458. In contrast, EGQPSO has a Std of 7.574, with values between 873.493 and 888.641.

A comparison of the convergence behavior of all the experimented algorithms on the Breast A, NOVARTIS, and LEUKEMIA datasets is seen in Figs. 2, 3, and 4, in that order. It is clear from these results that the suggested EGQPSO converges more quickly than CS., GA, PSO, and QPSO. Therefore, EGQPSO is the optimal algorithm.

To determine if the means of three or more groups are different, ANOVA, or the Analysis of Variance test, is performed. Figures 5, 6, and 7 display the ANOVA test findings for Novartis, Leukemia, and Breast A, respectively.

Additionally, pairwise comparisons from a multiple comparison test were conducted. Figures 8, 9, and 10 show the outcomes of these comparisons for Novartis, Leukemia, and Breast A, respectively.

Table 2. Fitness comparison of different clustering algorithms (GA, CS, PSO, QPSO, and EGQPSO) on all tested datasets.

Breast A				
Algorithms	Best	Worst	Mean	Std
GA	1,600.350	1,741.472	1,663.267	45.650
CS	1,091.285	1,165.688	1,115.471	21.029
PSO	1,448.578	1,484.346	1,459.784	11.787
QPSO	1,107.385	1,114.360	1,112.314	2.144
EGQPSO	872.003	893.711	881.067	7.574
LEUKEMIA				
GA	146,028,907.350	155,921,193.327	151,659,272.862	2,997,269.587
CS	84,619,412.857	92,460,719.673	89,698,253.610	2,101,861.564
PSO	148,482,187.368	168,282,935.375	158,286,250.238	5,665,143.487
QPSO	138,151,538.050	149,890,045.139	145,082,784.199	3,366,416.893
EGQPSO	67,047,054.027	74,688,782.505	70,444,274.288	2,588,973.788
NOVARTIS				
GA	5,530,315.205	6,128,272.793	5,818,032.718	191,464.251
CS	2,968,944.289	3,418,404.588	3,154,530.818	118,657.855
PSO	6,554,726.189	7,297,107.719	6,886,720.413	279,279.775
QPSO	4,241,797.842	4,385,449.657	4,330,938.626	43,954.016
EGQPSO	2,267,507.617	2,448,341.153	2,361,098.355	77,873.077

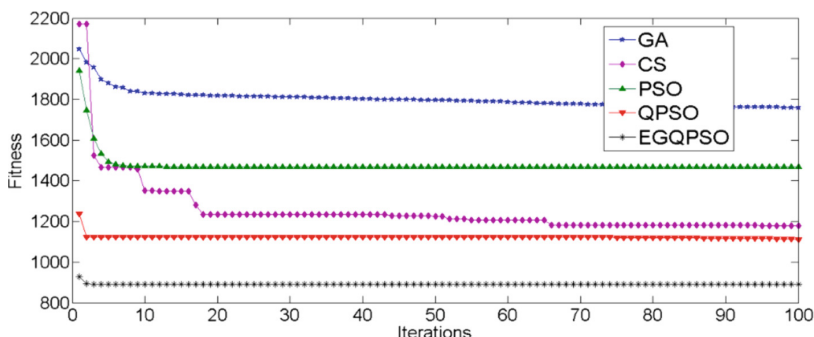


Fig. 2. The Fitness function variation of different clustering algorithms (GA, CS, PSO, QPSO, and EGQPSO) on Breast A dataset.

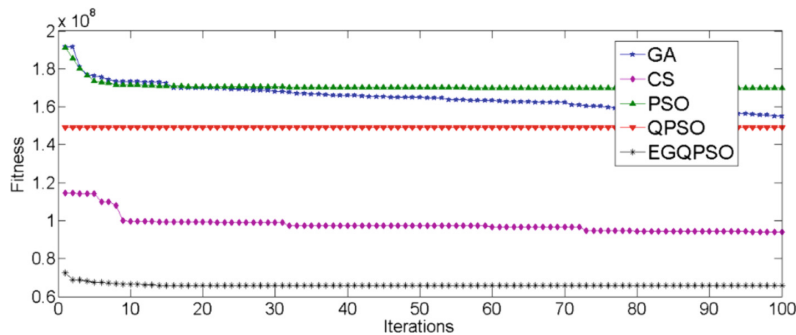


Fig. 3. The Fitness function variation of different clustering algorithms (GA, CS, PSO, QPSO, and EGQPSO) on LEUKEMIA dataset.

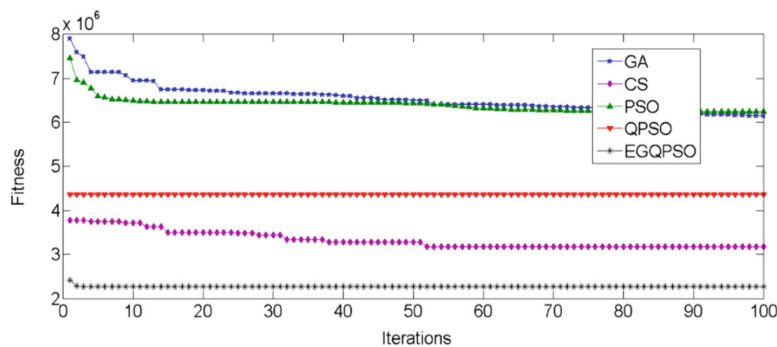


Fig. 4. The Fitness function variation of different clustering algorithms (GA, CS, PSO, QPSO, and EGQPSO) on NOVARTIS dataset.

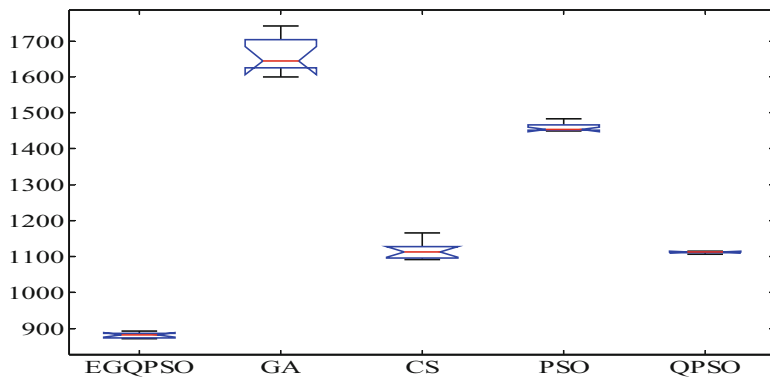


Fig. 5. Results of ANOVA test on Breast A.

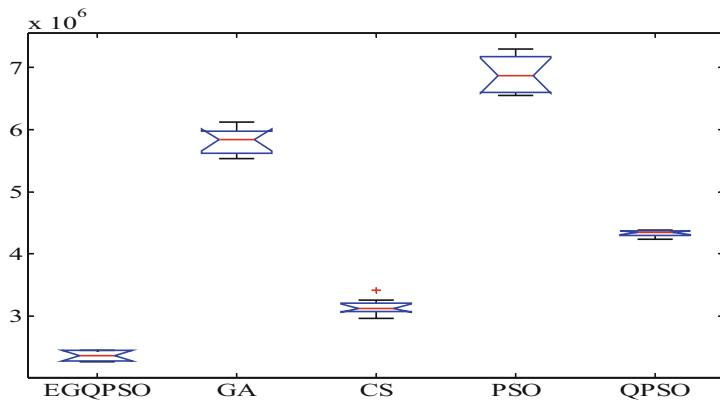


Fig. 6. Results of ANOVA test on NOVARTIS.

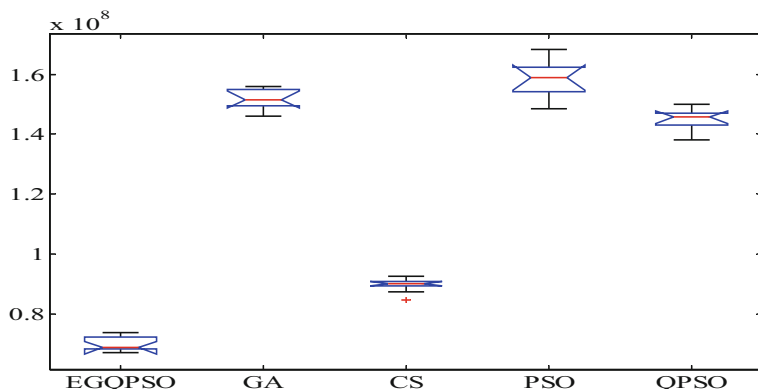
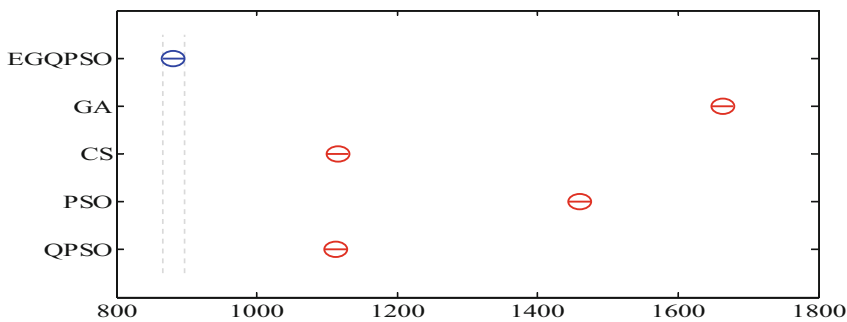


Fig. 7. Results of ANOVA test on LEUKEMIA.



GA, CS, PSO and QPSO have means significantly different from EGQPSO

Fig. 8. Results of pairwise comparison on Breast A.

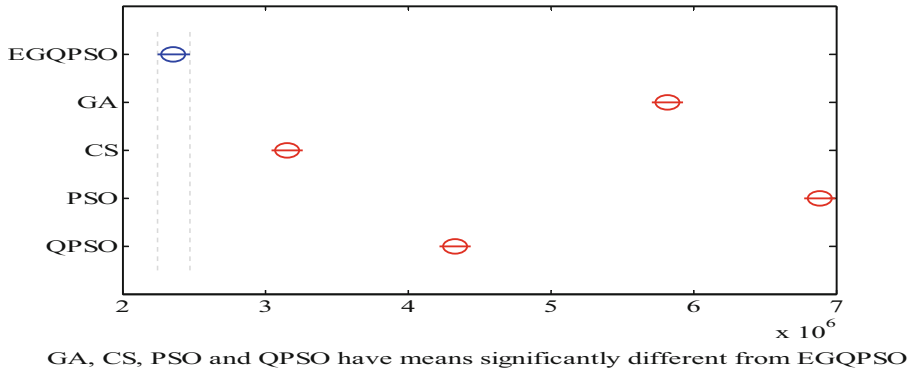


Fig. 9. Results of pairwise comparison on NOVARTIS.

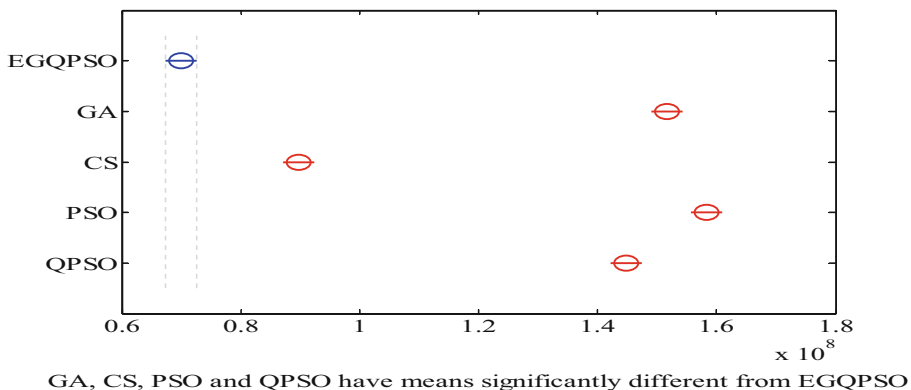


Fig. 10. Results of pairwise comparison on LEUKEMIA.

6 Conclusion

In this study, a novel approach for clustering biomedical data is presented: Enhanced Gaussian Quantum Particle Swarm Optimization (EGQPSO). The method is built upon the well-established metaheuristic methodology referred to as Particle Swarm Optimization (PSO), which has been enhanced with a quantum update, Gaussian distribution sequences, and an additional local search mechanism. The quantum update diversifies the population and explores new areas, while the use of Gaussian probability distribution in EGQPSO improves the algorithm's ability to avoid premature convergence to local maxima. Furthermore, the local search mechanism significantly accelerates the search process.

The effectiveness of EGQPSO in increasing the convergence rate is demonstrated through simulation studies on real-world biomedical datasets. When compared to several other well-known metaheuristic clustering algorithms, including GA, CS, PSO, and QPSO, EGQPSO consistently produces some among the top grouping outcomes for the datasets under examination.

In conclusion, the encouraging outcomes obtained on widely used datasets encourage us to investigate the integration of quantum operators and subroutines in specialized domains like image segmentation.

References

1. Coenen, F.: Journal Article Title - Review: data mining: Past, present and future. 26 (2011). <https://doi.org/10.1017/S0269888910000378>
2. Xu, R., Wunsch, D.: Survey of clustering algorithms. IEEE Trans. Neural Netw. **16**(3), 645–678 (2005). <https://doi.org/10.1109/TNN.2005.845141>
3. Xu, R., Wunsch, D.C., 2nd.: Clustering algorithms in biomedical research: a review. IEEE Rev. Biomed. Eng. **3**, 120–154 (2010). <https://doi.org/10.1109/RBME.2010.2083647>. PMID: 22275205
4. IshakBoushaki, S., Kamel, N., Bendjehaba, O.: Biomedical document clustering based on accelerated symbiotic organisms search algorithm. Int. J. Swarm Intell. Res. **12**(4), 169–185 (2021)
5. Sinaga, K.P., Yang, M.S.: Unsupervised K-means clustering algorithm. IEEE Access, **8**, 80716–80727 (2020) <https://doi.org/10.1109/ACCESS.2020.2988796>
6. Hruschka, E.R., Campello, R.J., Freitas, A.A.: A survey of evolutionary algorithms for clustering. IEEE Trans. Syst. Man, Cybernet. Part C (Appl. Rev.) **39**(2), 133–155 (2009). <https://doi.org/10.1109/TSMCC.2008.2007252>
7. Schrödinger, E.: An undulatory theory of the mechanics of atoms and molecules. Phys. Rev. **28**(6), 1049 (1926). <https://doi.org/10.1103/PHYSREV.28.1049>
8. Ursin, R., Hughes, R.J.: Quantum information: sharing quantum secrets. **501** (2013). <https://doi.org/10.1038/501037A>
9. Takata, T., Isokawa, T., Matsui, N.: Performance analysis of quantum-inspired evolutionary algorithm. 15 (2011). <https://doi.org/10.20965/JACHI.2011.P1095>
10. Coelho, L. dos S.: Gaussian quantum-behaved particle swarm optimization approaches for constrained engineering design problems. 37, (2010). <https://doi.org/10.1016/J.ESWA.2009.06.044>
11. Pan, H., Zhu, J., Han, D.: Genetic algorithms applied to multi-class clustering for gene expression data. Genomics, Proteomics Bioinform. **1**(4), 279–287 (2003). [https://doi.org/10.1016/S1672-0229\(03\)01033-7](https://doi.org/10.1016/S1672-0229(03)01033-7)
12. Chen, W., Sun, J., Ding, Y., Fang, W., Xu, W.: Clustering of gene expression data with quantum-behaved particle swarm optimization, In: Proceedings of the 21th International Conference on Industrial, Engineering & Other Applications of Applied Intelligent Systems, pp. 388–396 (2008)
13. Nayak, J., Vakula, K., Dash, P.B., Naik, B.: Kidney-Inspired Algorithm and Fuzzy Clustering for Biomedical Data Analysis (2019). <https://doi.org/10.1016/B978-0-12-818146-1.00011-8>. Presented at the January 1
14. Palaniswamy, S.: Rough fuzzy cuckoo search for triclustering microarray gene expression data. Turkish J. Electr. Eng. Comput. Sci. **27**(6), 4328–4339 (2019). <https://doi.org/10.3906/elk-1809-86>
15. Kennedy, J., Eberhart, R.C.: Particle swarm optimization **1** (1995). <https://doi.org/10.1007/S11721-007-0002-0>
16. Sun, J., Feng, B., Xu, W.-B.: Particle swarm optimization with particles having quantum behavior. In: Proceedings of 2004 Congress on Evolutionary Computation, Piscataway, NJ, pp.325–331 (2004)
17. Cheng, S., Shi, Y., Qin, Q.: Experimental study on boundary constraints handling in particle swarm optimization: from population diversity perspective. Int. J. Swarm Intell. Res. (IJSIR) **2**(3), 43–69 (2011). <https://doi.org/10.4018/JSIR.2011070104>



Quantum Inspired Grey Wolf Optimizer for Convolutional Neural Network Hyperparameter Optimization

Selma Kali Ali^(✉) and Dalila Boughaci

Department of Artificial Intelligence, University of Science and Technology Houari Boumediene (USTHB), Algiers, Algeria
`{skaliiali, dboughaci}@usthb.dz`

Abstract. Convolutional Neural Networks (CNNs) have revolutionized the field of computer vision and achieved remarkable success in various image-related tasks. However, their performance heavily depends on the correct tuning of hyperparameters, which can be challenging and time-consuming due to the vast search space. Recent advances in metaheuristic optimization algorithms have demonstrated their effectiveness in estimating the hyperparameters of deep learning networks. On the other hand, introducing Quantum Computing (QC) concepts into metaheuristic algorithms has further propelled this research field. This paper proposes a novel approach, qGWO-CNN, to fine-tune CNN hyperparameters. Our proposed qGWO-CNN method uses an improved variant of the Grey Wolf Optimizer (GWO), inspired by QC principles, to search for optimal hyperparameter values efficiently. To evaluate qGWO-CNN performance, we conduct experiments on the CIFAR-10 dataset using the AlexNet architecture. Comparison with other GWO-based approaches shows the excellent performance of the proposed algorithm in terms of classification accuracy. Furthermore, the numerical results indicate the potential of qGWO-CNN to be a promising approach for improving CNN performance.

Keywords: Convolution Neural Network · Hyperparameter Optimization · Grey Wolf Optimizer · Quantum-Inspired Metaheuristics

1 Introduction

Convolutional Neural Networks [14] (CNNs) have emerged as one of the most essential and powerful deep learning algorithms of recent years. Initially designed for image-processing tasks, CNNs have caused a paradigm shift in computer vision, achieving extraordinary success in various visual data tasks like image recognition and object detection. However, their applications extend beyond image analysis, as they have made significant advances in other fields, such as natural language processing [1] and speech recognition [18].

Over the years, several CNN architectures have been proposed, each contributing to different insights into computer vision tasks. Popular CNN architectures include LeNet [14], AlexNet [13], VGGNet [19], GoogLeNet [23], and ResNet [8]. While these architectures differ in complexity, depth, and layer count, they all share fundamental elements crucial to their excellent performance.

Despite the remarkable performance of CNNs, their effectiveness depends on correctly setting hyperparameters such as the number of layers, kernel size, learning rates, and dropout rates. The selection of hyperparameters involves exploring a high-dimensional space, making manual tuning impractical due to the vast number of possibilities. Consequently, several hyperparameter optimization approaches have been proposed to automate this process, including grid search, random search [4], Bayesian optimization [15], and metaheuristic algorithms. Among these, metaheuristic algorithms have gained popularity due to their effectiveness in handling non-convex and high-dimensional optimization problems. Recent studies have exploited metaheuristic algorithms such as Particle Swarm Optimization (PSO) [5, 9, 20, 26, 27], Genetic Algorithm (GA) [2], and Firefly Algorithm (FA) [3] for CNN hyperparameter optimization. The research results highlight their potential to improve the performance of CNN models significantly.

The Grey Wolf Optimizer [17] (GWO) is a metaheuristic optimization algorithm inspired by the social behavior and hunting strategies of grey wolves in nature. Thanks to its simplicity, efficiency, and robustness in solving various optimization problems, it has shown competitive performance compared to traditional optimization methods. However, it is prone to a few issues, such as slow convergence speed and the risk of stagnation in local optima. Numerous modifications and hybridizations with other optimization techniques have been proposed to overcome its limitations and enhance performance [10, 24].

Quantum Computing (QC) is an emerging field encompassing elements from mathematics, physics, and computer science. Integrating QC concepts into metaheuristic algorithms has significantly improved the performance of conventional metaheuristics. These quantum-inspired metaheuristic algorithms exhibit improved convergence speed and strike a good balance between exploration and exploitation during optimization.

Given the importance of CNNs, more work must be done to optimize their hyperparameters. Inspired by the high performance of GWO and quantum-inspired metaheuristics, we introduce a novel approach named qGWO-CNN. An improved variant of the quantum-inspired GWO algorithm (qGWO) is proposed in this work. qGWO is also inspired by the hybrid GWO-MVO algorithm, which has proven effective in estimating the optimal dropout rate value [10]. GWO-MVO amalgamates the GWO and Multi-Verse Optimizer (MVO) algorithms [16]. This study focuses on the image classification task and evaluates the proposed qGWO-CNN method on the CIFAR-10 benchmark dataset. The experimental results are promising, demonstrating the effectiveness of qGWO-CNN in achieving improved performance in CNN hyperparameter optimization.

The paper is structured as follows: Sect. 2 provides an overview of fundamental metaheuristic techniques for optimizing CNN hyperparameters and quantum-inspired metaheuristics. Section 3 explains the basic concepts used in the study. Section 4 presents a detailed explanation of our proposed method. Section 5 discusses our experiments and the obtained results. Finally, Sect. 6 concludes the paper, highlights its limitations and discusses potential future research directions.

2 Literature Overview

2.1 Optimizing CNN Hyperparameters with Metaheuristic

Hyperparameter optimization is critical in designing efficient Machine Learning (ML) models. It has a significant influence on the overall performance of the model and its ability to generalize to new data. Metaheuristics are optimization techniques that provide robust and efficient solutions to complex optimization problems. Applying metaheuristics to optimize deep learning hyperparameters has been a topic of interest due to their effectiveness in saving time and resources. Recently, several studies investigated using metaheuristics to solve hyperparameter optimization problems in CNN models. The results reveal that metaheuristic algorithms make it possible to design proper CNN models automatically.

Yamasaki et al. [27] introduced an automated approach to finding optimal hyperparameters for CNN using the Particle Swarm Optimization (PSO) algorithm. This work focused solely on optimizing the hyperparameters of the convolutional and pooling layers. The experimental results on five image datasets, including CIFAR-10, CIFAR-100, and three Imagenet subsets, demonstrate significant improvements over the standard Alexnet configuration.

A novel variant of PSO swarm optimization called cPSO-CNN was proposed to optimize the hyperparameter configuration of pre-determined CNN architectures in [26]. this method was evaluated on the CIFAR-10 dataset using five well-known CNN architectures (AlexNet, VGGNet-16, VGGNet-19, GoogleNet, ResNet-52, RestNet-101, and DenseNet-121). Experimental results reveal that using cPSO-CNN to optimize the hyperparameters of the first CNN layer leads to outperforming standard architectures in terms of classification error rate.

Authors in [9] presented a new PSO-based algorithm for automatically searching CNN architectures in image classification tasks. The proposed psocCNN simplifies the optimization process and enhances the performance of the PSO algorithm through its innovative direct encoding strategy and speed operator. Results indicate the effectiveness and efficiency of the proposed algorithm in automating the search for optimal CNN architectures for image classification tasks.

In [20], Singh et al. introduced a Multi-level Particle Swarm Optimization (MPSO) algorithm that simultaneously optimizes the architecture and hyperparameters of a CNN. The proposed approach uses multiple swarms at two levels: individuals at level 1 optimize the architecture, including the number of convolutional, pooling, and fully connected layers, while swarms at level 2 optimize

the hyperparameters of these layers. The evaluation of five benchmark datasets, including MNIST, CIFAR-10, CIFAR-100, Convex Sets, and MDRBI, shows the effectiveness of MPSO in learning optimal CNN architectures.

Another variant of PSO called PSO without velocity (PSWV) was proposed in [5]. PSWV achieved rapid convergence to the best CNN architecture. The proposed approach on nine benchmark datasets for image classification tasks confirmed that PSWV efficiently identifies CNN architectures that achieve performance comparable to the best existing designs.

Besides the widely used PSO, other metaheuristics like Genetic Algorithm (GA) [2] and Firefly Algorithm (FA) [3] have also been employed with success to optimize CNN hyperparameters.

2.2 Quantum-Inspired Metaheuristics

Quantum mechanics is a field of physics that focuses on particle behavior at the atomic and subatomic levels. Some fundamental concepts of quantum mechanics, such as superposition and entanglement, have been exploited to improve the efficiency of optimization techniques. Quantum-inspired metaheuristics are a class of optimization algorithms that draw on the principles of quantum mechanics to solve complex optimization problems. Unlike quantum metaheuristics, these algorithms have been designed to run on classical computers.

Kim and Han [7] introduced the first quantum-inspired algorithm, which applied the idea of quantum bits and quantum superposition states to GA. Their work paved the way for subsequent contributions, significantly enhancing conventional QGA [25].

Motivated by the promising outcomes of QGA, researchers have extended the concepts of QC to various other metaheuristics, such as PSO [22], GWO [24], and Ant Colony Optimization (ACO) [11]. This hybridization of quantum-inspired ideas has led to advancements in these metaheuristics, improving their efficiency and performance in solving complex optimization problems. The reader may refer to [6], where a detailed survey is provided.

3 Background

3.1 Convolution Neural Network

The Convolutional Neural Network (CNN) is one of the most widely used deep learning algorithms, specifically designed for processing and analyzing visual data. CNNs have revolutionized the field of computer vision and have achieved state-of-the-art performance in various image-related tasks. Moreover, CNNs have also demonstrated success in other domains, such as natural language processing [1] and speech recognition [18], when adapted and extended to handle sequential data. Some of the well-known CNN architectures include LeNet [14], AlexNet [13], VGGNet [19], GoogLeNet [23], and ResNet [8]. In every CNN architecture, the primary components consist of three types of layers: convolutional, pooling, and fully connected layers.

Convolutional layers are the fundamental components of a CNN, responsible for automatically learning and extracting relevant visual features from the input data. The primary operation performed by a convolutional layer is called “convolution.” It involves sliding a set of learnable filters (kernels) across the input data. These filters detect specific features or patterns in the image, such as edges, corners, or textures, which leads to creating a feature map.

Typically, after a convolutional layer, a pooling layer is employed. Pooling layers reduce the spatial dimensions of the feature maps while preserving the most relevant information. There are two standard pooling methods: average pooling and max pooling, which keep the average and maximum value in a local region, respectively. The pooling technique helps decrease computational complexity and control overfitting by focusing on the most relevant features.

Towards the network’s end, fully connected layers perform classification or regression tasks based on the extracted features. These layers are similar to those found in traditional neural networks.

CNNs are trained through a process called supervised learning. Like other deep learning networks, training a CNN involves forward propagation, where the input data passes through the layers to make predictions, and backpropagation, where the network learns from prediction errors to update the learnable parameters (weights and biases).

Hyperparameters are the configuration settings before training the network. These settings determine the network’s architecture and affect its training process and performance. They can be categorized into model hyperparameters (e.g., number of layers, kernel size, padding stride) and algorithm hyperparameters (e.g., learning rate, dropout rate, activation function type). Selecting appropriate hyperparameters affects the performance and generalization ability of the CNN. However, finding the optimal hyperparameters can be time-consuming. Thus, hyperparameter optimization techniques are often employed to automate this process instead of manual tuning.

3.2 Grey Wolf Optimizer

The Grey Wolf Optimizer (GWO) is a swarm intelligence optimization algorithm inspired by the social hierarchy and hunting behavior of grey wolves in the wild. The algorithm was proposed by Seyedali Mirjalili et al. in 2014 [17]. The GWO algorithm is based on three main social behaviors observed in grey wolves:

- **Leadership hierarchy:** In a wolf pack, there is a hierarchy of leadership where α , β , and δ wolves represent the leaders who guide the group. These three wolves are considered the best solutions found so far.
- **Prey hunting:** Grey wolves employ a cooperative and communicative capture strategy within their pack to effectively surround and capture prey. The three leaders, α , β , and δ , guide this hunting mechanism. Hence, each wolf updates its position using Eq. (1).

$$X_{(t+1)} = \frac{X_1 + X_2 + X_3}{3} \quad (1)$$

$$X_1 = X_\alpha - A_\alpha \cdot D_\alpha \quad (2)$$

$$X_2 = X_\beta - A_\beta \cdot D_\beta \quad (3)$$

$$X_3 = X_\delta - A_\delta \cdot D_\delta \quad (4)$$

$$D_{\alpha/\beta/\delta} = |C_{\alpha/\beta/\delta} \cdot X_{\alpha/\beta/\delta} - X_{(t)}| \quad (5)$$

where X_α , X_β , X_δ represent α , β , and δ wolf positions respectively. D mathematically models the hunting encirclement behavior employed by grey wolves during their hunting activities. A and C are coefficient vectors, calculated as follows:

$$A_w = 2 \cdot a \cdot r_w - a \quad (6)$$

$$C_i = 2 \cdot r_i \quad (7)$$

a is a vector that decreases linearly from 2 to 0 as the iteration progresses. r_w and r_i are random vectors generated from a uniform distribution within the $[0, 1]$ range for each α , β , and δ wolf.

- **Exploration and exploitation:** The wolves balance between exploring new areas for potential prey and exploiting known hunting grounds. This behavior is mimicked in GWO through a combination of random exploration and targeted exploitation of promising regions in the search space. The random values of A contribute to both the exploitation and exploration mechanisms. When $|A| < 1$, exploitation is encouraged, whereas $|A| > 1$ promotes exploration. Additionally, the random behavior of component C ensures exploration as well.

3.3 Schrödinger Equation

The Schrödinger wave equation is one of the most fundamental equations in quantum mechanics. It describes the time evolution of quantum systems and provides the basis for understanding various quantum phenomena. The time-dependent Schrödinger equation is given as follows [22]:

$$i\hbar \frac{\partial}{\partial t} \Psi(\mathbf{X}, t) = \hat{H} \Psi(\mathbf{X}, t) \quad (8)$$

where i is the imaginary unit ($i^2 = -1$) and \hbar is the reduced Planck's constant. $\Psi(\mathbf{X}, t)$ is the particle's wave function, representing its quantum state at position X and time t . \hat{H} is the Hamiltonian operator, representing the particle's total energy in the quantum system.

$$\hat{H} = -\frac{\hbar^2}{2m} \nabla^2 + V(\mathbf{X}) \quad (9)$$

m is the mass of the particle. ∇^2 is the Laplacian operator, representing the spatial second derivative of the wave function. $V(\mathbf{X})$ is the potential energy function that depends on the spatial coordinates \mathbf{X} .

Solving the time-dependent Schrödinger equation can ascertain the wave function that characterizes the system's quantum state at any specific time t and position X . This enables us to make informed predictions concerning its behavior and properties.

4 Proposed Method

4.1 qGWO Algorithm

The GWO algorithm has become a subject of considerable interest in recent years due to its easy implementation, minimal parameter requirements, and robust convergence performance. However, when applied to real optimization tasks, it encounters challenges such as slow convergence speed and the risk of stagnation in local optima. Motivated by the promising outcomes of incorporating quantum-based concepts into metaheuristics, we introduce a novel variant of GWO with quantum behavior. The foundation of our algorithm relies mainly on the principles of quantum dynamics used in Quantum-behaved Particle Swarm Optimization (QPSO) [22]. Our algorithm sets itself apart from previous versions of qGWO by leveraging the effectiveness of GWO-MVO, which has shown its ability to estimate an optimal dropout rate for the CNN model [10].

In quantum space, the wave function $\Psi(\mathbf{X}, t)$ describes the quantum state of a wolf, which depends on the wolf's position. In three-dimensional space, it satisfies the following relation:

$$|\Psi(\mathbf{X}, t)|^2 dx dy dz = Q dx dy dz \quad (10)$$

where $Q dx dy dz$ is the probability that the gray wolf appears in the infinitesimal element around the point (x, y, z) . In other words, $|\Psi(\mathbf{X}, t)|^2 = Q$ is the probability density function satisfying:

$$\int_{-\infty}^{+\infty} |\Psi(\mathbf{X}, t)|^2 dx dy dz = \int_{-\infty}^{+\infty} Q dx dy dz = 1 \quad (11)$$

In the algorithm, we assume that each wolf moves in a spin-less way in an N -dimensional Hilbert space with specified energy. To simplify the description, we first consider a one-dimensional space where the wolf's position is denoted by X and the center of the potential well $g_{i,t}$ by g . The potential energy in the one-dimensional δ potential well can be represented as follows [22]:

$$V(X) = -\gamma \cdot \delta(X - g) = -\gamma \cdot \delta(Y) \quad (12)$$

here, we define $Y = X - g$, and γ defines the intensity of the potential well.

Like [22], we employ the Monte Carlo method to derive the update function for each wolf's position. Each dimension is bounded in a δ potential well and updated independently. Equation (13) is used to measure the j th ($1 \leq j \leq N$) component of the position of individual i ($1 \leq i \leq M$) at the $(t+1)$ th iteration. For a more comprehensive understanding of the method used to derive this equation, refer to [22].

$$X_{i,t+1}^j = g_{i,t}^j \pm \frac{L_{i,t}^j}{2} \ln\left(\frac{1}{u_{i,t+1}^j}\right) \quad (13)$$

where $u_{i,t+1}^j$ is a sequence of random numbers uniformly distributed on $[0, 1]$, varying for each component and dimension across iterations. $g_{i,t}^j$ corresponds to the wolf's local attractor, which depends on the average of the best three wolves as described in Eq. (1). Unlike [24], the local attraction of a wolf depends only on the average of the three best wolves without any additional exploitation. Thus, the expression for $g_{i,t}^j$ can be given as follows:

$$g_{i,t}^j = x_{m,t}^j - \frac{1}{3}(A_{\alpha,t} \cdot D_{\alpha,t}^j + A_{\beta,t} \cdot D_{\beta,t}^j + A_{\delta,t} \cdot D_{\delta,t}^j) \quad (14)$$

where $x_{m,t}^j$ denotes the j th mean component of the position of the best three wolves(α, β, δ) at iteration t . The parameter D_k is defined as in traditional GWO (Eq. (5)). Inspired by our previous GWO-MVO algorithm, we calculate the A_k parameter using the same concept. Here, a decreases non-linearly to ensure a good balance between exploration and exploitation.

$$a = 2 \times \left(1 - \frac{t^{\frac{1}{p_1}}}{T^{\frac{1}{p_1}}}\right) \quad (15)$$

where t indicates the current iteration, and T is the maximum number of iterations. The constant p_1 controls the level of exploitation throughout the iterations.

To reinforce the exploitation towards the alpha wolf rather than the average position of the gray wolves as in [24], the value of $L_{i,t}^j$ can be determined by :

$$L_{i,t}^j = 2 \cdot \mu \cdot |X_{i,t}^j - X_{\alpha,t}^j| \quad (16)$$

Here, μ isn't a fixed constant, as seen in the standard QPSO algorithm. Instead, it decreases non-linearly over iterations, departing from previous quantum-inspired GWO algorithms. Equation (17) draws inspiration from calculating the MVO parameter (Travelling_distance_rate) used in GWO-MVO.

$$\mu = 1 - \frac{t^{\frac{1}{p_2}}}{T^{\frac{1}{p_2}}} \quad (17)$$

p_2 is a control parameter of the exploitation around wolf α .

Finally, the position of a wolf is updated as follows:

$$X_{i,t+1} = \begin{cases} g_{i,t}^j + \mu \cdot |X_{i,t}^j - X_{\alpha,t}^j| \times \ln\left(\frac{1}{u_{i,t+1}^j}\right) & \text{if } R > 0.5 \\ g_{i,t}^j - \mu \cdot |X_{i,t}^j - X_{\alpha,t}^j| \times \ln\left(\frac{1}{u_{i,t+1}^j}\right) & \text{else} \end{cases} \quad (18)$$

$R \in [0, 1]$ is a random number chosen from a uniform distribution.

The proposed quantum-inspired GWO is outlined in Algorithm 1.

4.2 qGWO-CNN

The proposed qGWO-CNN method assumes a pre-determined CNN architecture and focuses on optimizing specific hyperparameters like kernel size and padding.

Algorithm 1: Quantum Inspired Grey Wolf Optimizer

```

/* Initialization */  

Initialize parameters:  $T$ ,  $p_1$  and  $p_2$   

Initialize the grey wolf population  

/* Evaluation */  

Evaluate the fitness of each wolf  

Select the leaders' positions  $X_\alpha$ ,  $X_\beta$  and  $X_\delta$   

while  $t < T$  do  

  for each wolf do  

    | Determine the position of the current wolf's local attractor by Eq. (14)  

    | Update the position of the current wolf by Eq. (18)  

  end for  

  Evaluate the fitness of each wolf  

  Update the leaders' positions  $X_\alpha$ ,  $X_\beta$  and  $X_\delta$   

   $t = t + 1$   

end while  

return  $X_\alpha$ 

```

qGWO algorithm is used to estimate the values of these hyperparameters. The optimization process involves updating each individual in the population based on its position and the positions of the three leaders in the search space. Further, the range of each hyperparameter is considered to ensure that values falling outside the specified range are adjusted. Evaluating each wolf includes generating a corresponding CNN model, training it on a training sample, and testing its performance on a validation sample. The optimization process flow is depicted in Fig. 1.

In the following, we provide a detailed explanation of the fundamental aspects of our approach, including solution representation, population initialization, and the fitness function.

Solution Encoding: A wolf position is encoded as a numerical vector whose length equals the number of selected hyperparameters. Each vector element corresponds to a specific hyperparameter, and its value represents a possible setting for that hyperparameter. The vector elements can be integers or real numbers, depending on the type of associated hyperparameter. Consider the following hyperparameters for optimizing a CNN: kernel size of a convolution layer, kernel size of a pooling layer, and dropout rate. A potential solution, representing a wolf's position, can be denoted as $(5, 3, 0.5)$, where the kernel size of the convolution layer is 5, the kernel size of the pooling layer is 3, and 0.5 is the dropout rate.

Population Initialization: Hyperparameter values are randomly generated in the initial stage, and each wolf in the swarm represents a distinct set of hyperparameters. To enable an adequate search, a lower and upper bound limit

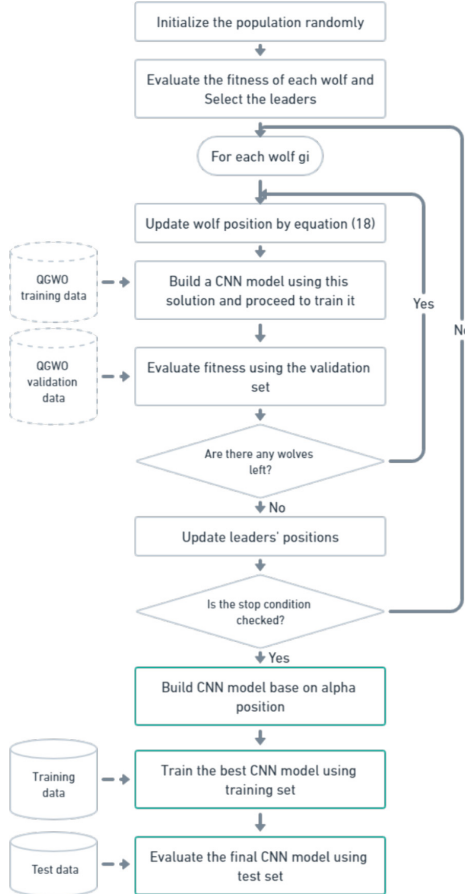


Fig. 1. Flowchart of the proposed qGWO-CNN approach.

the search space of each dimension. The selection of these limits depends on the nature of the hyperparameter.

Fitness Functions: A classifier model is created to evaluate a given solution using the corresponding hyperparameter values. Each potential solution is estimated based on the performance of its CNN model. After training the CNN model with a fixed number of epochs, the classification error rate (CER) is computed on the validation set. Thus, the fitness function is determined by the CER and is calculated as follows:

$$CER = 1 - Accuracy \quad (19)$$

$$Accuracy = \frac{tp + tn}{tp + fn + fp + tn} \quad (20)$$

where, tp is the true positive, tn is the true negative, fp is the false positive and fn is the false negative.

5 Experiments

Experiments are conducted on a desktop computer with an AMD RYZEN 7 3700X CPU, 16 GB of RAM, a Nvidia RTX 2060 super GPU card, and an Ubuntu 18.04 operating system. The programs are implemented in Python using Keras, scikit-learn, NumPy, SciPy, and pandas.

We selected the basic AlexNet for CNN architecture since it represents a typical CNN with moderate complexity. For the experiment dataset, we opt for CIFAR-10 [12] as it is a well-known and commonly used benchmark dataset for CNN evaluations.

Since evaluating each position involves training a CNN model, qGWO-CNN can be very time-consuming. To limit this problem, we set the number of training epochs to 5. We train the models using only 1/5 of the training set (i.e., 10000), while 128 instances are reserved for validation.

5.1 Selected Hyperparameters

Considering our constrained test environment, we focused on optimizing the first convolutional layer and the dropout rate values. The first convolutional layer plays a vital role in extracting features from raw data, and the dropout technique has demonstrated its effectiveness in addressing overfitting issues in CNNs. As a result, we focused on optimizing four hyperparameters in the AlexNet architecture (since there are two dropout rates). Table 1 describes the hyperparameters we aimed to optimize, along with their respective minimum and maximum values, which control the search space.

Table 1. Hyperparameters to optimize.

Hyperparameter	Type	Range
Kernel size	Integer	[3,11]
Stride size	Integer	[1,5]
Dropout rate	Real	[0,1]

5.2 Metaheuristic Parameters

Multiple tests were conducted to determine the input parameters for our proposed algorithm. Additionally, GWO and GWO-MVO parameters were configured to highlight the improvements of qGWO over these two algorithms. The specific parameter settings are shown in Table 2.

Table 2. Metaheuristic parameters.

Algorithm	#iterations	#wolves	p_1	p_2
GWO-CNN	10	20	-	-
GWO-MVO-CNN	10	20	2	10
qGWO-CNN	10	20	2	9

5.3 Results Analysis

We conducted ten independent tests for the three approaches: GWO-CNN, GWO-MVO-CNN, and qGWO-CNN. The results obtained are shown in Table 3. From the numerical outcomes, it is evident that the qGWO-CNN method significantly outperforms GWO-CNN and GWO-MVO-CNN. Specifically, qGWO-CNN achieved an accuracy of 84.71% on the CIFAR-10 dataset using the AlexNet architecture, surpassing GWO-CNN and GWO-MVO-CNN by 4.89% and 4.6%, respectively.

Table 3. Experimental results obtained out of ten independent runs.

Approach	Average accuracy	Best accuracy	Worst accuracy	SD
GWO-CNN	79.58%	79.82%	79.11%	0.21%
GWO-MVO-CNN	80.11%	80.3%	79.74%	0.19%
qGWO-CNN	84.18%	84.71%	84.01%	0.18%

Figure 2 illustrates a box plot of the test accuracy distribution on CIFAR-10 for the three approaches: GWO-CNN, GWO-MVO-CNN, and qGWO-CNN. The box plot indicates that qGWO-CNN achieved the highest-quality performance over the ten independent runs compared to the other two approaches. On the other hand, GWO-CNN showed the worst performance.

Table 4 compares average test accuracies on the CIFAR-10 dataset for different hyperparameter optimization approaches. qGWO-CNN is compared with standard AlexNet [27], PSO-CNN [27], PSO-b [21], MPSO-CNN [20], and cPSO-CNN [26]. Our qGWO-CNN method demonstrates significant improvement over the standard AlexNet configuration, achieving a gain of 6.43%. Moreover, it outperforms PSO-CNN, which is applied to optimize AlexNet hyperparameters, and PSO-b, proposed for selecting convolutional neural network parameters, including architecture. Although qGWO-CNN is less efficient than MPSO-CNN and cPSO-CNN, it remains competitive, considering that our focus was on optimizing only the first convolutional layer in this study. Thus, optimizing all layers has the potential to enhance qGWO-CNN performance further.

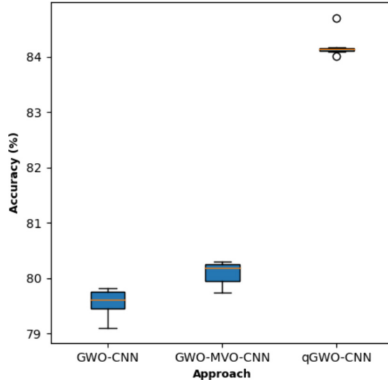


Fig. 2. Boxplots of the test accuracies achieved on CIFAR-10. These accuracies were obtained out of ten independent runs.

Table 4. Performance comparison in terms of average accuracy between qGWO-CNN and different approaches on CIFAR-10.

Approach	Network	Optimization	Accuracy
Standar AlexNet [27]	AlexNet	-	77.75%
PSO-CNN [27]	AlexNet	Hyperparameter optimization	80.15%
PSO-b [21]	13-CNN	Architecture optimization	81.47%
MPSO-CNN [20]	DCNN	Architecture optimization	87.34%
cPSO-CNN [26]	AlexNet	Hyperparameter optimization	91.33%
qGWO-CNN	AlexNet	Hyperparameter optimization	84.18%

6 Conclusion

This paper focuses on fine-tuning CNNs’ hyperparameters, an essential step in achieving optimal performance. We propose a novel approach, qGWO-CNN, which uses an enhanced variant of the GWO algorithm inspired by QC. Through experiments on the CIFAR-10 dataset with the AlexNet architecture, we demonstrated the efficacy of qGWO-CNN in accurately estimating hyperparameter values. The results revealed that qGWO outperforms basic GWO and the hybrid GWO-MVO algorithm, showing reduced chances of being stuck in local optima. However, our comparison with prior work indicates the need for optimizing more network layers beyond just the first convolutional layer.

In future work, we plan to investigate additional hyperparameters and optimize all network layers. Additionally, evaluating qGWO-CNN on diverse types of CNN architectures and other datasets will be essential. Future efforts will also involve optimizing the CNN architecture, not only the hyperparameters. Furthermore, developing a quantum GWO by including quantum operators could significantly improve this work.

References

1. Abas, A.R., Elhenawy, I., Zidan, M., Othman, M.: BERT-CNN: a deep learning model for detecting emotions from text. *Comput. Mater. Continua* **71**(2) (2022)
2. Anaraki, A.K., Ayati, M., Kazemi, F.: Magnetic resonance imaging-based brain tumor grades classification and grading via convolutional neural networks and genetic algorithms. *Biocybern. Biomed. Eng.* **39**(1), 63–74 (2019)
3. Bacanin, N., Bezdan, T., Tuba, E., Strumberger, I., Tuba, M.: Optimizing convolutional neural network hyperparameters by enhanced swarm intelligence metaheuristics. *Algorithms* **13**(3), 67 (2020)
4. Bergstra, J., Bengio, Y.: Random search for hyper-parameter optimization. *J. Mach. Learn. Res.* **13**(2) (2012)
5. Elhani, D., Megherbi, A.C., Zitouni, A., Dornaika, F., Sbaa, S., Taleb-Ahmed, A.: Optimizing convolutional neural networks architecture using a modified particle swarm optimization for image classification. *Expert Syst. Appl.* **229**, 120411 (2023)
6. Gharehchopogh, F.S.: Quantum-inspired metaheuristic algorithms: comprehensive survey and classification. *Artif. Intell. Rev.* **56**(6), 5479–5543 (2023)
7. Han, K.H., Kim, J.H.: Genetic quantum algorithm and its application to combinatorial optimization problem. In: Proceedings of the 2000 Congress on Evolutionary Computation. CEC00 (Cat. No. 00TH8512), vol. 2, pp. 1354–1360. IEEE (2000)
8. He, K., Zhang, X., Ren, S., Sun, J.: Deep residual learning for image recognition. In: Proceedings of the IEEE Conference on Computer Vision and Pattern Recognition, pp. 770–778 (2016)
9. Junior, F.E.F., Yen, G.G.: Particle swarm optimization of deep neural networks architectures for image classification. *Swarm Evol. Comput.* **49**, 62–74 (2019)
10. Kali Ali, S., Boughaci, D.: Hybrid approach based on grey wolf optimizer for dropout regularization in deep learning. In: Chikhi, S., Diaz-Dascalzo, G., Amine, A., Chaoui, A., Saidouni, D.E., Kholladi, M.K. (eds.) *Modelling and Implementation of Complex Systems. LNNS*, vol. 593, pp. 121–134. Springer, Cham (2023). https://doi.org/10.1007/978-3-031-18516-8_9
11. Khudair Madhloom, J., Abd Ali, H.N., Hasan, H.A., Hassen, O.A., Darwish, S.M.: A quantum-inspired ant colony optimization approach for exploring routing gateways in mobile ad hoc networks. *Electronics* **12**(5), 1171 (2023)
12. Krizhevsky, A., Nair, V., Hinton, G.: Cifar-10 (canadian institute for advanced research) (2010). <http://www.cs.toronto.edu/~kriz/cifar.html>, **5**(4), 1
13. Krizhevsky, A., Sutskever, I., Hinton, G.E.: Imagenet classification with deep convolutional neural networks. *Commun. ACM* **60**(6), 84–90 (2017)
14. LeCun, Y., Bottou, L., Bengio, Y., Haffner, P.: Gradient-based learning applied to document recognition. *Proc. IEEE* **86**(11), 2278–2324 (1998)
15. Martinez-Cantin, R.: Bayesopt: a Bayesian optimization library for nonlinear optimization, experimental design and bandits. *J. Mach. Learn. Res.* **15**(1), 3735–3739 (2014)
16. Mirjalili, S., Mirjalili, S.M., Hatamlou, A.: Multi-verse optimizer: a nature-inspired algorithm for global optimization. *Neural Comput. Appl.* **27**, 495–513 (2016)
17. Mirjalili, S., Mirjalili, S.M., Lewis, A.: Grey wolf optimizer. *Adv. Eng. Softw.* **69**, 46–61 (2014)
18. Passricha, V., Aggarwal, R.K.: A hybrid of deep CNN and bidirectional LSTM for automatic speech recognition. *J. Intell. Syst.* **29**(1), 1261–1274 (2019)
19. Simonyan, K., Zisserman, A.: Very deep convolutional networks for large-scale image recognition. arXiv preprint [arXiv:1409.1556](https://arxiv.org/abs/1409.1556) (2014)

20. Singh, P., Chaudhury, S., Panigrahi, B.K.: Hybrid MPSO-CNN: multi-level particle swarm optimized hyperparameters of convolutional neural network. *Swarm Evol. Comput.* **63**, 100863 (2021)
21. Sinha, T., Haidar, A., Verma, B.: Particle swarm optimization based approach for finding optimal values of convolutional neural network parameters. In: 2018 IEEE Congress on Evolutionary Computation (CEC), pp. 1–6. IEEE (2018)
22. Sun, J., Feng, B., Xu, W.: Particle swarm optimization with particles having quantum behavior. In: Proceedings of the 2004 Congress on Evolutionary Computation (IEEE Cat. No. 04TH8753), vol. 1, pp. 325–331. IEEE (2004)
23. Szegedy, C., et al.: Going deeper with convolutions. In: Proceedings of the IEEE Conference on Computer Vision and Pattern Recognition, pp. 1–9 (2015)
24. Vijay, R.K., Nanda, S.J.: A quantum grey wolf optimizer based declustering model for analysis of earthquake catalogs in an ergodic framework. *J. Comput. Sci.* **36**, 101019 (2019)
25. Wang, H., Liu, J., Zhi, J., Fu, C., et al.: The improvement of quantum genetic algorithm and its application on function optimization. *Math. Probl. Eng.* **2013** (2013)
26. Wang, Y., Zhang, H., Zhang, G.: CPSO-CNN: an efficient PSO-based algorithm for fine-tuning hyper-parameters of convolutional neural networks. *Swarm Evol. Comput.* **49**, 114–123 (2019)
27. Yamasaki, T., Honma, T., Aizawa, K.: Efficient optimization of convolutional neural networks using particle swarm optimization. In: 2017 IEEE Third International Conference on Multimedia Big Data (BigMM), pp. 70–73. IEEE (2017)



Frequent Itemsets Mining Using New Quantum Inspired Elephant Swarm Algorithm

Hadjer Moulai^(✉)

LRIA, Faculty of Computer Science, Departement of Artificial Intelligence and Data Science, USTHB, Algiers, Algeria
hamoulai@usthb.dz

Abstract. In this paper, an original quantum inspired swarm intelligence approach for solving discrete problems is presented, namely Quantum-inspired Discrete Elephant Herding Optimization (QDEHO). The proposed approach takes advantage of quantum computing characteristics which are studied and analyzed in order to inspire a novel algorithm based on the new Discrete Elephant Herding Optimization (DEHO). As an illustration on how our proposal can be applied on real-life discrete problems, a case study on frequent itemsets mining (FIM) is carried out where the algorithm is modeled and applied on the problem in order to extract interesting patterns from large-scale databases. In order to validate our work, extensive experiments on six relevant datasets with increasing sizes were carried out. The obtained results prove the effectiveness and applicability of our approach. Furthermore, a comparative study of QDEHO with well-known state of the art algorithms such as Particle Swarm Optimization (PSO) and Bat algorithm (BAT) was undertaken, where the results showed that QDEHO is superior to the competing algorithms in almost all datasets.

Keywords: Swarm intelligence · Discrete optimization · Elephant herding optimization · Quantum computing · Data mining · Frequent itemsets

1 Introduction

With the rapid growth of generated data, conventional analysis techniques proves to be excessively resource-consuming in terms of physical memory, which significantly impacts temporal complexity and hence decision making.

To tackle that, evolutionary computation and algorithms offer a robust and efficient approach to explore vast search spaces to solve complex optimization problems. On the other hand, quantum computing is a novel field of research in computer science aimed at harnessing the possibilities offered by quantum physics. It is a promising field that incorporates unique mechanics concepts of

quantum physics (e.g. superposition, entanglement, etc.) into classical computing for information processing.

The aim of this paper is to exploit the principles of quantum computing, such as *quantum bit*, *superposition of states*, and *quantum gates*, in conventional evolutionary algorithms in order to propose a novel efficient technique.

Our choice for the swarm approach is Discrete Elephant Herding Optimization [15], which is a method inspired by the behavior of elephants when in group in order to solve discrete optimization problems.

DEHO have proved to be very effective on problems such as association rule mining in comparison with both single and multi-objective techniques such as Particle Swarm Optimization (PSO) [13] and Non-dominated Sorting Genetic Algorithm II (NSGA2) [4].

However, we think that DEHO can be further improved if we incorporate quantum computing concepts into the resolution process.

The remainder of this paper is organized as follows: next section reviews state of the art algorithms and provides required background knowledge on quantum computing, Sect. 3 gives a detailed explanation of our proposal, in Sect. 4 we show how the proposed algorithm can be applied for the task of frequent itemsets mining, Sect. 5 illustrates numerical results and a comparative study. And finally, in Sect. 6 we conclude this work and discuss perspectives.

2 Background and Related Work

2.1 Preliminaries on Quantum Computing

In this section we'll present some basic concepts of quantum computing which are essential for the understanding of our proposal.

A Quantum Bit. In classical computer science, a “bit” represents the elementary unit of information, used to manipulate data. It can be in one of two states, 1 or 0, like a switch, open or closed.

The quantum version of a bit of information, called a “Qubit” and used in quantum computing, can be in both states at the same time. These states can be represented by an arrow, which points to a position on the surface of a sphere as shown in the Fig. 1 [5].

Mathematically speaking, a qubit is represented as a complex vector of size 2: $|\psi\rangle = \alpha|0\rangle + \beta|1\rangle$.

α and β represent the amplitudes or probabilities of the qubit being in states 0 and 1 respectively. The amplitudes must satisfy the following normalization condition: $|\alpha|^2 + |\beta|^2 = 1$.

States 0 and 1 are represented as column vectors: $|0\rangle = [1, 0]$ and $|1\rangle = [0, 1]$

The observation of this state will give the value 0 with a probability equal to α^2 and the value 1 with a probability equal to β^2 .



Fig. 1. A classical bit and a qubit [1]

A Quantum Register. A quantum register can be described as a set or vector of qubits, which is an arbitrary superposition of n qubits.

A qubit can be in the state 0 or 1, but also in both at the same time. Therefore, a register of n qubits can hold 2^n distinct values.

2.2 Related Work

Quantum-inspired metaheuristics are solvers that incorporate principles inspired from quantum mechanics into classical-approximate algorithms using non-quantum machines. The recent literature presents new approaches that use the concepts of quantum mechanics and swarm intelligence for different applications

In [9], the authors proposed a novel evolutionary computing method called a genetic quantum algorithm (GQA), based on genetic algorithm and quantum computing. GQA's performance was tested on the well-known knapsack problem, where it proved its effectiveness over conventional genetic algorithm.

In [6], the authors proposed a new algorithm, called QUAntum Particle Swarm Optimization (QUAPSO) based on quantum computing and particle swarm optimization. Another improvement, inspired by Kangaroo Algorithm (KA), was added to PSO in order to optimize its efficiency in local search. The experimental results show that QUAPSO outperforms the six different well-known algorithms on a set of 30 test functions.

In [3], the authors presented three novel quantum-inspired algorithms based on Lorentz (QPSO-LR), Rosen-Morse (QPSO-RM) and Coulomb-like Square Root (QPSO-CS) potential fields. The algorithms are used to solve 24 benchmark functions. A comparative study is conducted with the classical particle swarm optimization (PSO), genetic algorithm (GA), and firefly algorithm (FFA).

While these algorithms borrow ideas from quantum mechanics, they are implemented on classical computers and do not take full advantage of the speed-up offered by quantum computing. Nonetheless, they have shown promising

results in solving complex optimization problems efficiently and may serve as useful alternatives to traditional metaheuristics. That's what inspired us to propose a quantum-inspired DEHO [15] as it has proved to be a very effective algorithm recently.

3 Quantum Inspired DEHO (QDEHO)

The following approach is based on the new discrete EHO proposed in [15]. In the latter, each elephant is represented by its position/solution and velocity.

A quantum inspired DEHO namely QDEHO, is an evolutionary algorithm where the elephants' positions are represented by quantum registers.

3.1 Solution Encoding

Each elephant in the swarm carries a quantum solution represented as a string of n qubits, which forms what is known as a quantum register.

Table 1. Structure of a quantum solution in QDEHO

α_1	α_2	α_3
β_1	β_2	β_3

In Table 1, is an example of a quantum register that would represent an elephant's solution in QDEHO.

Thanks to this superposition of states, a quantum individual can simultaneously represent an entire population of individuals, each with a probability. Therefore, in such a representation of individuals, there will be no need to have a large population size, which provides more diversity while using a small population [9]. However, in the act of observing a quantum state, it collapses to a single state.

3.2 Solution Measurement

In order to effectively exploit the superposition of states in a qubit, we need to read each bit. This operation leads to the extraction of a binary solution from a quantum solution. The aim is to allow the evaluation of the elephants swarm, depending on the binary solutions extracted.

As shown in Algorithm 1, for each Qubit a random number $rand$ in the range of $[0, 1]$ is generated. Depending on this value, the algorithm returns either 0 or 1 (Fig. 2).

Each solution is then evaluated using a fitness function specific to the problem to solve. The next step is to update each elephant's quantum solution.

Algorithm 1: The measure function

```

Input: Qubit  $Q_i = (\alpha_i, \beta_i)$ ;
Output: Binary solution  $X_i$ ;
1 if  $rand > \alpha_i^2$  then
2   | return 1;
3 else
4   | return 0;
5 end

```

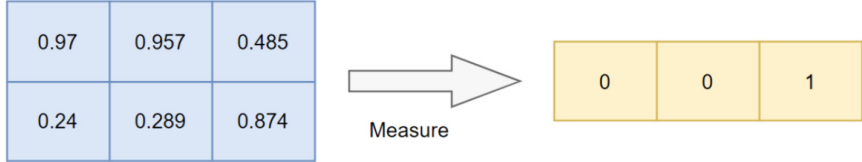


Fig. 2. Example of measuring a binary solution from a quantum register

3.3 Solution Update

Each elephant's register $R_{c_i,j}$ is updated at each iteration using Eq. 1 such as:

$$R_{new,c_i,j} = R_{c_i,j} + \alpha \times (X_{c_i,best} - X_{c_i,j}) \times r \quad (1)$$

- $X_{c_i,j}$: the elephant current solution
- $X_{c_i,best}$: the best elephant in clan c_i .
- α and r are empirical parameters.

For the best elephant in each clan, Eq. 2 is used to calculate its new register. $X_{center,c_i,d}$ represents the center of gravity of the i^{th} clan and β is an empirical parameter.

$$R_{new,c_i,j} = R_{c_i,j} + (X_{c_i,best} + (\beta \times X_{c_i,center})) \quad (2)$$

The center of gravity of each clan is calculated using Eq. 3.

$$X_{center,c_i,d} = \frac{1}{n_{c_i}} \sum_{j=1}^{n_{c_i}} x_{c_i,j,d} \quad (3)$$

$$R_{c_i,worst} = R_{c_i,worst} + (x_{min} + (x_{max} - x_{min} + 1) \times rand) \quad (4)$$

Finally, at each generation the worst elephant $R_{c_i,worst}$ in each clan c_i is replaced using Eq. 4, such as:

- x_{min} : the minimum size of a solution.
- x_{max} : the maximum size of a solution.

Register Update. At each iteration, each elephant's register has to be updated. Which means that a number of qubits have to be modified in Q_i^t to obtain the updated new Q_i^{t+1} . This operation is done through the application of a quantum single qubit gate. The choice of the quantum gate highly depends on the problem to solve. The most common quantum gates allowing transformations on single qubits are the following [16]:

- simple quantum gates: identity transformation, negation, phase shift, the combination of phase shift and negation.
- the square root gate of NOT: \sqrt{NOT}
- the controlled-NOT gate (CNOT).

Algorithm 2: The qubit update

Input: Qubit $Q_i = (\alpha_i, \beta_i)$

Output: Updated Qubit

1 Obtain the new (α_i, β_i) :

2 $(\alpha_i, \beta_i)^{(t)} == (X)(\alpha_i, \beta_i)^{(t-1)}$

3.4 The Proposed Algorithm

Algorithm 3 resumes the main steps of the proposed QDEHO approach.

In the next section we will explain how the proposed algorithm is applied for frequent itemsets mining.

4 Frequent Itemsets Mining (FIM) Using Quantum-DESWSA

4.1 Preliminaries on FIM

Frequent itemsets are a fundamental concept in data mining, used to uncover associations in large datasets. These patterns help businesses and researchers gain valuable knowledge for decision making [12].

Let T be a set of M transactions $T = \{t_1, t_2, \dots, t_M\}$, representing a transactional database, and I a set of N different items (or attributes) $\{i_1, i_2, \dots, i_N\}$. An itemset X is simply a set of items, i.e., $X \subseteq I$.

The support of an itemset $Sup(X)$ is the number of transactions that contains X divided by M . An itemset X is frequent if its support is no less than $MinSup$, where $MinSup$ is a threshold chosen by the user.

The discovery of frequent itemsets is typically accomplished through algorithms like Apriori[2] or FP-Growth[8]. These algorithms explore the dataset and find

Algorithm 3: Quantum inspired DEHO (QDEHO)

Input: N_c : number of clans, N : number of elephants, X_{min} : Minimum size of a solution; X_{max} : Maximum size of a solution; t_{max} : maximum number of generations;

Output: best solutions

```

1  for  $i=1$  to  $N_c$  do
2    for  $j=1$  to  $N$  do
3      Randomly initialize the Register of Qbits  $R_i$  for each elephant
4      Generate current solution  $X_{c_i,j}$  using  $R_i$ 
5    end
6  end
7  for  $t=1$  to  $t_{max}$  do
8    for  $i=1$  to  $N$  do
9      for  $i=1$  to  $N_c$  do
10        Update each elephant's register  $R_{i,c_i}$  using a quantum gate in each
11        clan using equation 1
12        Update the best elephant's register  $R_{best,c_i}$  in each clan using
13        equation 2
14        Replace the worst elephant's register  $R_{worst,c_i}$  in each clan using
15        equation 4
16        Update local best and global best if needed;
17        If the number of generations is reached stop and return best
18        solutions.
19      end
20    end
21  end
22 end

```

the itemsets that meet a user-defined minimum support threshold. However, these approaches are very time consuming and not suitable for large datasets.

To overcome this performance issue of exact approaches, several algorithms have been proposed that use bio-inspired techniques, such as genetic algorithms [18] or PSO [14], that proved their performance in comparison with brute force approaches. In the next sections we'll explain how we applied our quantum inspired approach QDEHO to solve the frequent itemset mining problem.

4.2 Solution Representation

A solution is represented by a vector of n qubits called register, such as n is the number of items in the dataset.

At each iteration, the corresponding itemset is obtained by applying Algorithm 1 on the current register.

4.3 Solution Update

Each register is updated using Algorithm 2. For the problem of frequent itemsets mining we have chosen the NOT gate which inverts α_i and β_i in a single qubit.

The NOT gate in quantum computing is known as the Pauli-X gate, and it acts on a single qubit to flip its state between 0 and 1.

Mathematically, the Pauli-X gate is represented by the following 2×2 matrix:

$$X = \begin{pmatrix} 0 & 1 \\ 1 & 0 \end{pmatrix}$$

4.4 Fitness Function

The fitness function for the problem of frequent itemsets is represented by the following equation.

$$f(X) = Support(X) = \frac{N^o \text{ of transactions that contain } X}{N^o \text{ of transactions in the database}} \quad (5)$$

The fitness function is to be maximized.

5 Performance Evaluation

In this section, we are going to measure the performance of our proposals on different datasets of various sizes and compare the obtained results with state of the art algorithms.

All the algorithms were scripted in Java and executed on intel core i7 machine with 16 GB of main memory running under Windows 10.

5.1 Datasets Description

In order to better demonstrate how QDEHO works on real life data, a series of experiments were carried out on six datasets from various and well known repositories, such as Frequent and mining dataset Repository [7,17].

Table 2 describes the datasets in terms of number of transactions and number of items .

The empirical parameters of our approach and those of state of the art algorithms are fixed through extensive experiments.

Each algorithm is then executed while variating the number of iterations from 100 to 1000 iterations. Maximum number of iterations is the same for all algorithms.

The final obtained results are the average of 10 consecutive executions for each iteration number, giving us the mean fitness performance of each algorithm.

Table 2. Datasets description

Dataset	N^o of transactions	N^o of items
IBM Quest 1	2,041	999
Chess	3,196	75
Mushroom	8,124	119
IBM Quest 2	18,905	999
Pumsbs star	40,385	7,116
Connect	100,000	999

Table 3. Comparing average fitness for extracted frequent itemsets

Dataset	QDEHO	PSO	GA	BAT
IBM Quest 1	0.007	0.001	0.001	0.001
Chess	0.99	0.37	0.14	0.86
Mushroom	0.75	0.19	0.13	0.34
IBM Quest 2	0.03	0.003	0.001	0.01
Pumsbs star	0.06	0.004	0.004	0.04
Connect	0.62	0.19	0.13	0.79

Table 4. Comparing average cpu time for extracted frequent itemsets

Dataset	QDEHO	PSO	GA	BAT
IBM Quest 1	5.96	0.01	0.12	28.08
Chess	1.43	0.004	0.03	7.62
Mushroom	2.41	0.04	0.03	12.1
IBM Quest 2	1.3	0.004	0.28	6.14
Pumsbs star	77.8	0.007	2.64	402.56
Connect	29.6	0.03	0.13	188.76

5.2 Numerical Results and Discussion

Tables 3 and 4 exhibit the average fitness and CPU time respectively, for our proposal in comparison with PSO[13], GA[11] and BAT[10]. The results are illustrated in Figs. 3 and 4.

Table 3 shows that QDEHO yields superior results in terms of average fitness in comparison with PSO and GA on all datasets. And outperform BAT as well excepts on one case only where BAT performs slightly better. Figure 3 confirms these conclusions.

When it comes to the average CPU time, we notice that QDEHO results are satisfying in comparison with GA and PSO although higher. However, QDEHO is faster than BAT, with which it competes in terms of solution's quality.

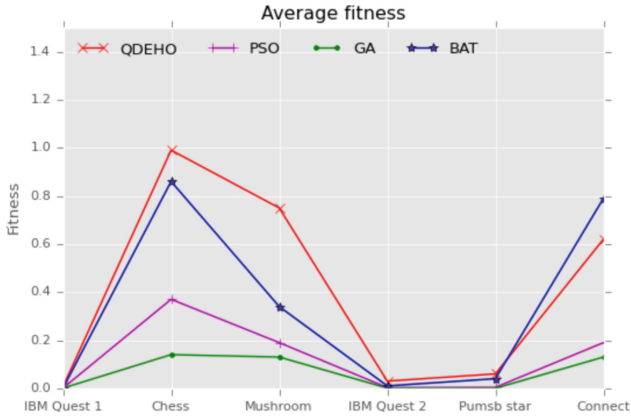


Fig. 3. Average fitness values for QEDHO in comparison with PSO, GA and BAT

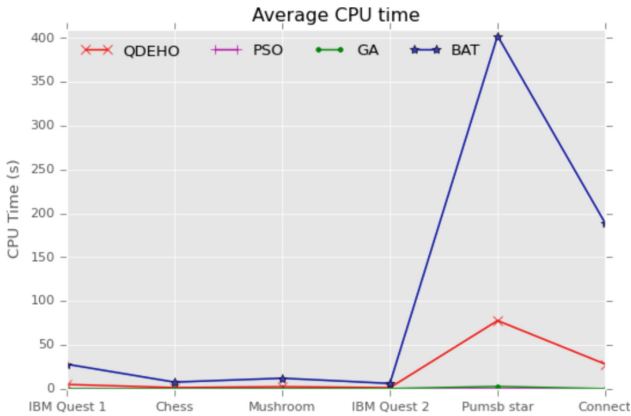


Fig. 4. Average CPU time in seconds for QEDHO in comparison with PSO, GA and BAT

We conclude that the experimental results demonstrate the effectiveness and the applicability of QDEHO.

6 Conclusion and Perspectives

In this paper we have proposed a new original quantum inspired elephant swarm algorithms namely QDEHO. The originality of this work lies into the challenging task of implementing quantum concepts into the discrete swarm approach DEHO. Our proposal is supported by an illustration on how frequent itemsets mining can be solved using QDEHO. The experiments on six different benchmarks with increasing sizes, showed that our proposal yields satisfying results that outperform well-known state of the art algorithms.

As a future work, we would like to compare QDEHO with more recent state of the art algorithms and work on applying it to other data mining problems such as clustering. A further perceptive would be to explore utilizing frameworks like Qiskit for QDEHO implementation and testing on an actual quantum computer.

Acknowledgements. We would like to express our special thanks of gratitude to the Directorate General for Scientific Research and Technological Development (DGRSDT), for the support of this work under the grant number C0662300.

References

1. 1Qbit: A bit or two about qubits (2022). <https://1qbit.com/blog/quantum-computing/a-bit-or-two-about-qubits/>. Accessed July 2023
2. Agrawal, R., Imielinski, T., Swami, A.: Fast algorithms for mining association rules. In: Proceedings of the 20th International Conference on Very Large Data Bases, pp. 487–499 (1994)
3. Alvarez-Alvarado, M.S., Alban-Chacón, F.E., Lamilla-Rubio, E.A., et al.: Three novel quantum-inspired swarm optimization algorithms using different bounded potential fields. *Sci. Rep.* **11**, 11655 (2021). <https://doi.org/10.1038/s41598-021-90847-7>
4. Deb, K., Pratap, A., Agarwal, S., Meyarivan, T.: A fast and elitist multiobjective genetic algorithm: NSGA-II. *IEEE Trans. Evol. Comput.* **6**(2), 182–197 (2002). <https://doi.org/10.1109/4235.996017>
5. Deutsch, D., Ekert, A.: Quantum computation. *Phys. World* **11**(3), 47–52 (2006)
6. Flori, A., Oulhadj, H., Siarry, P.: Quantum particle swarm optimization: an auto-adaptive PSO for local and global optimization. *Comput. Optim. Appl.* **82**(2), 525–559 (2022). <https://doi.org/10.1007/s10589-022-00362-2>
7. Hämäläinen, W.: Datasets (2019). <http://www.cs.uef.fi/~whamalai/datasets.html>. Accessed 10 Aug 2019
8. Han, J., Pei, J., Yin, Y.: Mining frequent patterns without candidate generation: a frequent-pattern tree approach. In: Proceedings of the 2000 ACM SIGMOD International Conference on Management of Data, pp. 1–12 (2000)
9. Han, K.H., Kim, J.H.: Genetic quantum algorithm and its application to combinatorial optimization problem, vol. 2, pp. 1354 – 1360 vol.2 (2000). <https://doi.org/10.1109/CEC.2000.870809>
10. Heraguemi, K., Kamel, N., Drias, H.: Multi-swarm bat algorithm for association rule mining using multiple cooperative strategies. *Appl. Intell.* **45** (2016). <https://doi.org/10.1007/s10489-016-0806-y>
11. Holland, J.H.: Genetic algorithms. *Sci. Am.* **267**(1), 66–73 (1992). <http://www.jstor.org/stable/24939139>
12. Jiawei, H., Kamber, M.: Data Mining: Concepts and Techniques. Morgan Kaufmann Publishers, Burlington (2011)
13. Kennedy, J., Eberhart, R.: Particle swarm optimization. In: Proceedings of ICNN'95 - International Conference on Neural Networks, vol. 4, pp. 1942–1948 vol.4 (1995). <https://doi.org/10.1109/ICNN.1995.488968>
14. Lin, J.C.W., et al.: Mining high-utility itemsets based on particle swarm optimization. *Eng. Appl. Artif. Intell.* **55**, 320–330 (2016). <https://doi.org/10.1016/j.engappai.2016.07.006>, <https://www.sciencedirect.com/science/article/pii/S0952197616301312>

15. Mouhai, H., Drias, H.: Association rule mining using new discrete elephant swarm approaches. *Expert. Syst.* **40**(2), e13159 (2023). <https://doi.org/10.1111/exsy.13159>
16. Rieffel, E., Polak, W.: An introduction to quantum computing for non-physicists. *ACM Comput. Surv.* **32**(3), 300–335 (2000)
17. Tapia, E.M.: Activity recognition in the home setting using simple and ubiquitous sensors (2018). <http://courses.media.mit.edu/2004fall/mas622j/04.projects/home/>
18. Yan, X., Zhang, C., Zhang, S.: Genetic algorithm-based strategy for identifying association rules without specifying actual minimum support. *Exp. Syst. Appl.* **36**(2, Part 2), 3066–3076 (2009). <https://doi.org/10.1016/j.eswa.2008.01.028>, <https://www.sciencedirect.com/science/article/pii/S0957417408000195>



Quantum Slime Mould Algorithm and Application to Urgent Transportation

Celia Khelfa^(✉), Habiba Drias, and Ilyes Khennak

Laboratory for Research in Artificial Intelligence, USTHB, Algiers, Algeria
`{ckhelfa,hdrias,ikhennak}@usthb.dz`

Abstract. The Slime Mould Algorithm (SMA) is a Swarm Intelligence (SI) technique inspired by the foraging behavior of slime moulds in nature. SMA demonstrates promise as an optimization method and researchers are actively exploring ways to improve its performance, including integrating hybrid strategies. Concurrently, quantum computing (QC) has emerged as a rapidly expanding research area, leveraging quantum mechanics principles for computation. This study presents QSMA, a quantum version of the slime mould algorithm, which combines classical SMA with the quantum Grover's algorithm. We apply this algorithm to the ambulance dispatching problem, a critical challenge in emergency medical services, where the objective is to allocate ambulances to respond to emergency calls efficiently. Our implementation of QSMA using the IBM Qiskit simulator is compared with the classical approach. This evaluation is performed using real-world COVID-19 data from Chicago. The experimental analysis reveals that the proposed quantum algorithm for ambulance dispatching is highly competitive, exhibiting significant improvements and converging to the optimal solution faster than the classical algorithm.

Keywords: Slime Mould Algorithm · Quantum Computing · Grover Algorithm · Quantum Slime Mould Algorithm · COVID-19 · Ambulance Dispatching Problem

1 Introduction

Quantum computing stands out as a highly promising and exciting field of research, offering numerous advantages over classical computing [5]. By harnessing the principles of quantum mechanics, it presents a diverse collection of potent theories that introduce revolutionary concepts such as state superposition, interference, and quantum algorithms, which hold the potential to drive exponential advancements in solving intricate scientific and industrial challenges [7]. In particular, quantum computing showcases its exceptional capabilities in cryptography, optimization, and machine learning, where classical computers face limitations [2]. Its ability to solve complex problems exponentially faster than its classical counterparts underscores the transformative potential of quantum computing in various practical applications.

Solving real-world problems inevitably encounters challenges in providing the best solution. These issues are due to the dimension, constraints, and hypotheses defining the problem [3]. As a real-world optimization challenge, the ambulance dispatching problem is no exception to these difficulties. It is a specialized version of the Vehicle Routing Problem (VRP) with several additional complexities that make it even more challenging than the standard VRP, such as the dynamic nature of the demands and taking into account hospital capacity and traffic conditions [10]. The problem is considered an NP-complete problem because it is a variant of the NP-complete problem VRP [11]. These complexities further contribute to the difficulty of solving the problem and finding an exact solution. As a result, researchers have explored various approaches, particularly heuristic and metaheuristic algorithms, to provide high-quality solutions in a reasonable amount of time [1]. Swarm Intelligent (SI) algorithms are a powerful class of soft computing techniques and are extensively employed in optimization and computational intelligence tasks [14]. Among these, the Slime Mould Algorithm (SMA) stands out as a recent SI approach inspired by the extraordinary foraging abilities of slime moulds in nature [13]. Slime moulds, being simple organisms, demonstrate impressive skills in finding optimal paths to reach food sources. The SMA employs a population-based strategy, generating and iteratively updating individual solutions while incorporating exploration and exploitation to achieve an optimal solution.

Recent research has explored methods to enhance the SMA for more efficient and effective solutions to complex optimization problems. Some studies have introduced an optimized version of the SMA using quantum strategies. Yu et al. [21] proposed an improved SMA, called WQSMA, incorporating two innovative techniques: the quantum rotation gate and a water cycle-inspired operation. These additions were aimed at bolstering the exploration and exploitation capabilities of the original SMA. Still in the same direction, Zhang et al. [22] presented an enhanced version of the Slime Mould Algorithm (SMA) known as DQOBLSMA (Dynamic Quantum Rotation Gate and Opposition-Based Learning SMA). This approach introduced two mechanisms: the dynamic quantum rotation gate and opposition-based learning. However, it is worth noting that these studies still need to provide concrete quantum implementations.

One promising approach involves combining SMA with the renowned quantum Grover's search algorithm to leverage the speedup benefits of quantum computing. Drawing inspiration from the weight (w) principle in the SMA, the Grover algorithm efficiently searches the entire population, mitigating classical SMA limitations. In this study, we propose a quantum version of the SMA specifically tailored to address the ambulance dispatching problem. We delve into quantum computing concepts to effectively achieve our objectives. Our proposed approach is implementable on a quantum simulator like the Quantum Assembly (QASM) simulator provided by Qiskit, an open-source Python library for quantum computing, allowing us to showcase the performance advantage of the Quantum Slime Mould Algorithm (QSMA). By comparing the results obtained from the quantum version to the classical SMA, we will assess the efficacy of our

quantum approach in optimizing ambulance dispatching using real COVID-19 data recorded in Chicago.

The paper is structured into seven sections. The next section provides an introduction to the SMA and basic quantum subroutines. In Sect. 3, we introduce the ambulance dispatching problem and its mathematical modeling. Section 4 outlines our proposed quantum slime mould algorithm, followed by Sect. 5, which describes QSMA for solving the addressed problem. Section 6 presents the experimental results. Lastly, Sect. 7 provides the conclusion of the paper.

2 Background

This section overviews the fundamental ideas utilized in formulating our proposals. Firstly, we discuss the SMA, followed by an introduction to the core quantum concepts that contributed to the development of QSMA.

2.1 Slime Mould Algorithm

The SMA is one of the latest swarm intelligence algorithms [16] mimicking the behavior of slime molds or the physarum polycephalum in nature. The primary steps in SMA for food searching encompass three key stages: approach, wrap, and grabble the food [13]. During the initial stage, the SMA searches and approaches the food source guided by the odor present in the air. In the second phase, the wrap phenomenon emulates the contraction mode of venous tissue structure in slime mold. Subsequently, the grabble stage is reached, wherein decisions are made regarding whether to pursue the current food source or explore alternative food sources. The mathematics corresponding to the main steps in the SMA are introduced subsequently.

Approaching Food: The slime mould employs Eq. (1) [16] to navigate toward the food source by tracking environmental odors. Higher food concentrations lead to an increase in the weight assigned to a region, prompting the organism to explore that area. Conversely, lower food concentrations result in a decrease in the weight of the region, leading it to shift its exploration towards other areas.

$$X^{t+1} = \begin{cases} X_b^t + v_b(W.X_A^t - X_B^t) & \text{if } r < p \\ v_c.X^t & \text{else} \end{cases} \quad (1)$$

where:

- X^t and X^{t+1} are the position of the slime mould during iterations (t) and (t+1), respectively.
- v_c linearly decreases from 1 to 0, v_b is converted in $[-a, a]$, X_b the best solution so far.
- During iteration t, X_A^t and X_B^t denote respectively the position vectors of randomly selected individuals from the slime mould.
- W is the weight of the slime mould.

- r is a random value, and p is calculated on Eq. (2), where B_f is the best fitness value obtained and S_i indicates the fitness value of $i(i \in 1, 2, 3, ..n)$.

$$p = \tanh[f(S_i^t) - B_f] \quad (2)$$

The W formula can be described in Eq. (3), S_f refers to the sequence of fitness values, r is a random value and W_f is the worst fitness value.

$$W_i = \begin{cases} 1 + r.\log\left(\frac{B_f - f(S_i^t)}{B_f - W_f} + 1\right) & \text{if } i \in S_f \\ 1 - r.\log\left(\frac{B_f - f(S_i^t)}{B_f - W_f} + 1\right) & \text{else} \end{cases} \quad (3)$$

Wrapping Food: The act of wrapping food is the result of the contraction patterns of the slime mould venous tissue structure in their search for food. The mathematical model proposed to simulate wrap phenomena is represented in Eq. (4), where (u_b) and (l_b) are the upper and lower bounds of the search space, respectively.

$$X^{t+1} = \begin{cases} \text{rand.}(ub - lb) + lb & \text{if } \text{rand} < z \\ X_b^t + v_b(W.X_A^t - X_B^t) & \text{if } r < p \\ v_c.X^t & \text{if } r \geq p \end{cases} \quad (4)$$

Oscillation: W , v_b , and v_c are used to simulate the variation in the vein width of the slime mold. The rate at which food is updated is determined by W , which evaluates the nutritional value of the food and models the oscillatory frequency of the slime mold. This allows the slime mold to identify the most suitable food source effectively.

Additional information regarding the SMA can be found in [16].

2.2 Basic Quantum Concepts and Techniques

In contrast to classical computers, which deterministically assign each computation unit to either a zero or one, quantum computers utilize a fundamental unit known as a “qubit”. The qubit represents the smallest unit of quantum information storage and aims to embody a superposition of the states 0 and 1. This results in a quantum state, represented by the vector $|\psi\rangle = \sum_i \alpha_i |b_i\rangle$, α_i for all i are complex numbers such as $\sum_i \alpha_i^2 = 1$ according to Dirac notation [6].

Superposition is a fundamental and powerful concept that endows qubits with the ability to exist in multiple states simultaneously. It involves a combination, $\alpha_1|0\rangle + \alpha_2|1\rangle$, of two basis states, $|0\rangle$ and $|1\rangle$, with the constraint that $|\alpha_1|^2 + |\alpha_2|^2 = 1$. Utilizing n qubits, a superposition can encompass 2^n states. As a result, when an operator is applied to this set of qubits, it simultaneously affects all 2^n states, effectively enabling a parallel calculation on a vast amount of data [7].

Quantum registers can simultaneously store and process multiple quantum states, utilizing superposition and entanglement phenomena. The size of the quantum register, represented by n , corresponds to the required number of qubits for the desired quantum state. In Dirac notation, a quantum register with n qubits is denoted as $|\psi\rangle = \alpha|00\dots0\rangle + \beta|00\dots1\rangle + \gamma|00\dots01\rangle + \dots + \delta|11\dots1\rangle$, with $\alpha, \beta, \gamma, \dots$, and δ being complex probability amplitudes determining the probabilities of obtaining corresponding basis states when the quantum register is measured.

Grover's algorithm, introduced by Grover in 1996 [9], is a quantum search algorithm designed to efficiently find a target element within an unsorted list of N elements. It achieves this task with a time complexity of $O(\sqrt{n})$ and a space complexity of $O(\log(n))$. Consequently, the algorithm exhibits a quadratic speedup compared to classical search methods [17]. In this context, the quantum oracle phase, represented as a function and enclosed within an interrogatable box, flips a target qubit when the desired output is obtained. Grover's algorithm aims to search for the input(s) that cause this phase flip, enabling the identification of the target element in the unsorted list [18].

The Search of the Minimum: Grover's algorithm is not well-suited for finding the minimum element. However, the authors in [18] introduced a modified version of Grover's algorithm, a generalization, that can efficiently determine the minimum of an unsorted set with a computational complexity of $O(\sqrt{n})$. Additionally, Supasil et al. [20] proposed a technique to find the maximum elements (which can also be applied to finding the minimum) using an adapted version of Grover's algorithm. By iteratively applying the Grover diffusion operator and the quantum oracle, the amplitude of the maximum element(s) in the quantum superposition can be amplified. After running the algorithm for the appropriate number of iterations, measuring the quantum state will result in identifying the element(s) with the maximum (minimum) value(s) in the list.

3 Description of the Emergency Medical Services (EMS) Problem

Due to the sudden nature of requests for emergency transportation, EMS systems are structured to respond promptly to such circumstances. A quick response time is particularly crucial since it is usually linked to better patient outcomes. This allows EMS personnel to promptly administer medical care, potentially enhancing survival rates in specific scenarios [12].

The EMS dispatch process is designed to ensure that emergency medical resources are quickly and effectively deployed to provide high-quality care to those in need [12]. When an emergency call is received by phone, a dispatcher enters all pertinent information into the dispatching system and uses a standard set of questions to determine the emergency location, priority of the call, and any unique patient needs. If an available ambulance is found, it is immediately assigned and dispatched to the emergency location. Response time is defined as

the duration between receiving the emergency call and the ambulance arriving at the emergency site. Once the ambulance arrives at the scene, it transports the patient to the hospital for treatment [4].

The problem addressed can be viewed as an optimization problem aiming to minimize the total distance between a set of demands and the locations of ambulances, as defined in Eq. (5) [15]:

$$\min \sum_{i=1}^c \sum_{j=1}^a x_{ij} d_{ij} \quad (5)$$

where:

- C and a are the total number of emergency calls and ambulances respectively.
- d_{ij} is the distance between the position of the emergency call i and the ambulance j .
- The binary decision variable x_{ij} takes a value of 1 when an ambulance j is assigned to Call i , and it takes a value of 0 otherwise.

4 The Proposed Quantum Slime Mould Algorithm (QSMA)

This paper introduces a novel algorithm called the Quantum Slime Mould Algorithm (QSMA) that draws inspiration from the Quantum Genetic Algorithm (QGA) [19] and combines elements from quantum computing and swarm intelligence. The fundamental principle of our approach is to leverage the Grover algorithm, specifically the Quantum Minimum Finding Algorithm based on the Grover algorithm [19, 20], for selecting the best individuals from the population without relying on traditional update phases of swarm intelligence algorithms, such as Approaching and Wrapping Food in SMA.

In QSMA, the variation stage of the evolutionary strategy is eliminated as all potential individuals are generated as a superposition of basis states using qubits to represent the slime mould. By employing Grover's algorithm in the selection method, the techniques used for developing new individuals become redundant, as it allows for the identification of the T best individuals from the entire population.

In contrast to classical SMA, where the population size limits the availability of the best individual fitness pair, we utilize two quantum registers to represent all the population individuals [20]. Equation (6) illustrates this representation, where $|u_i\rangle^{\text{individual}}$ contains the individuals and $|p_i\rangle^{\text{fitness}}$ represents their corresponding fitness values. Next, the application of Grover's Search algorithm involves taking the unsorted table as input and measuring the best fitness value in the fitness register. As a result, the output consists of the T best individuals from the population. The correlation between registers plays a crucial role, leading to a post-measurement state in the individual register. This state contains superposed basis states that encode individuals with the best fitness.

$$|\text{Population}\rangle = |u_i\rangle^{\text{individual}} + |p_i\rangle^{\text{fitness}} \quad (6)$$

The Grover's Search algorithm employs a customized oracle to identify a set of good solutions that "marks" all the primary states below a specific threshold, as depicted in Fig. 1. This process is challenging because the exact number of suitable solutions T is unknown. Then, determining the optimal number of oracle calls becomes a complex task [19]. Employing an incorrect number of oracle calls can diminish the probability of discovering the desired solution, potentially leading to a higher likelihood of obtaining incorrect solutions. Our approach initializes the oracle number to 1 and selects L random solutions from the population. We then set the threshold in the oracle function to the minimum fitness value among these individuals. This approach is intended to improve the quality of solutions in subsequent iterations.

In determining the number of oracle calls, we draw inspiration from the weight (W) principle in the SMA. This principle involves assigning numerical values to represent the significance or importance of specific entities or components within the slime mould. By applying this concept, we can influence the behavior and interactions of the slime mould during the algorithm's execution, specifically to modify the number of oracle calls. Our strategy prioritizes solutions with higher weight (W) values, indicating better fitness. To achieve this, we dynamically adjust the number of oracle calls based on the ratio of average weight values between iterations. We can conduct a more focused and efficient search by specifically targeting solutions with higher weight values, increasing the likelihood of discovering promising solutions.

Classical Slime Mould Algorithm

- (1) Initialize the population of L individuals (usually random)

While (Not(Stopping Criteria))

- (2) Calculate the fitness of the slim mould
- (3) Update the best fitness value and calculate w
- (4) Variation phase (Approaching and Wrapping Food)
- (5) New individuals L

(a)

Quantum Slime Mould Algorithm

- (1) Initialize all the population
- (2) Create the registers $|ui>^{individual} + |pi>^{fitness}$ and initial L individuals

While(Not(Stopping Criteria))

- (3) Find the minimum of L individuals
- (4) Use Grover Algorithm to find the new L best items with O oracle calls
- (5) Use the principle of weight (w) in SMA to update the oracle calls

The Oracle expression:
 $O(x) = \begin{cases} -|x> & \text{if } x < \text{Boundary} \\ |x> & \text{else} \end{cases}$

(b)

Fig. 1. A comparison between the SMA and the proposed QSMA.

Figure 1 illustrates the fundamental contrast between SMA and QSMA. SMA and QSMA entail a selection phase, but SMA introduces variability by altering the randomly chosen solution during the truncation phase to approximate the optimal solution. In contrast, the quantum algorithm efficiently searches the entire population for the best solution, resulting in the minimum of samples being updated as the threshold. This approach enhances the algorithm’s ability to converge toward the optimal solution more effectively.

Pseudo-code 1 provides a detailed description of the proposed approach.

Algorithm 1. Pseudo-code of QSMA

Input: Max_iteration: The maximum number of iterations, Dimension of the Solution.
Output: L: list of best solutions
 Initialize all the population S
 Create the registers $|u_i\rangle^{\text{individual}} + |p_i\rangle^{\text{fitness}}$
 Initial L individuals and the number of oracle calls to 1
while ($t < \text{Max_iteration}$) **do**
 | Min = the minimum of L individuals
 | **if** ($\text{Min} < \text{Boundary}$) **then**
 | | Boundary = Min
 | **end**
 | **else**
 | | $L = \text{Grover_Algorithm} (S, O)$
 | **end**
 | Calculate the average of W (Equation (3)) in R
 | **if** ($R < 1$) **then**
 | | $O = \min \left\{ \frac{5}{6}m, \left(\frac{\pi}{4}\right) \sqrt{N} \right\}$
 | **end**
end

5 QSMA for Urgent Transportation

In this section, we adapt the QSMA algorithm to the ambulance dispatching problem. To determine the most suitable emergency vehicles to dispatch, we explore a search space encompassing all conceivable allocations of ambulances to calls. In other words, for C calls and A ambulances, the total number of potential allocations is A^C , and each of these allocations represents a potential solution to the problem.

5.1 Solution Encoding

Our modeling approach represents a viable solution S for the ambulance dispatching problem as a vector consisting of P elements, where P corresponds to the total number of emergency calls. Each element “ i ” within the vector corresponds to an ambulance, allowing us to denote the assignments as (c_i, a_j) ,

where “ c_i ” belongs to the list of incoming emergency calls and “ a_j ” refers to the ambulance assigned to handle the call “ c_i ”.

In order to execute the algorithm within a quantum computation environment, our initial step involves generating all potential solutions. These solutions are then represented using quantum registers, as described in Eq. (6). Utilizing quantum registers enables us to encode a superposition of numerous individuals and their associated fitness values. The application of this concept to our particular problem is exemplified in Fig. 2.

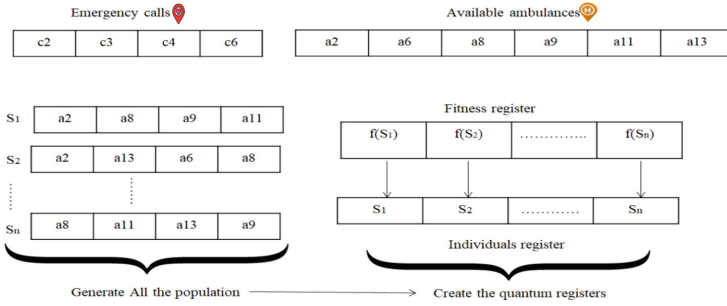


Fig. 2. Population Representation in Quantum Registers for Ambulance Dispatching Problem.

5.2 Dynamicity Modeling

The dispatch center responsible for coordinating ambulance responses receives emergency calls at varying intervals, making the ambulance dispatching problem dynamic in nature. To address this, our model allows for updates to the occupation time of ambulances and the frequency of incoming calls in each period. During these distinct time intervals, the QSMA searches for the best patient-to-ambulance assignments based on the objective function in Eq. (5). This process also updates the lists of available ambulances and unserved calls.

Pseudocode 2 outlines the proposed approach, which dynamically handles incoming calls stored in a dataset and efficiently manages ambulance utilization.

Algorithm 2. Adapting QSMA for Ambulance Dispatching in a Dynamic Setting

Input: List of Calls, UnitTime, Empirical Parameters.

Output: Solution after improvement

```

for each  $t$  in (UnitTime) do
    // Update the data
    Calls[ $t$ ] = UnservedCalls[ $t - 1$ ] + Dataset[ $t$ ] // Update the occupation time of
        ambulances
    Launch QSMA to find the best solution
end
  
```

6 Experiments and Results

6.1 Dataset

COVID-19 pandemic has had a global impact, including Chicago, which is one of the largest cities in the United States. Being a vibrant urban center with a diverse population, Chicago offers valuable insights into understanding the effects of the pandemic in an urban environment. For our proposed method's experiments, we treated real-world data from a case study focused on daily COVID-19 cases in Chicago [8]. This dataset includes a comprehensive collection of data that offers valuable insights into the number of confirmed COVID-19 cases, conducted tests, and deaths specifically attributed to COVID-19. We worked in three specific zones, namely, Washington Park Zone, Belmont Cragin, and Douglas, during the week with a high number of reported COVID-19 cases (December 21, 2021, to December 27, 2021). As a result, our dataset comprises 298 instances, where each instance represents an emergency call. The format of each instance includes an $\langle ID, ZIPcode, LONGITUDE, LATITUDE \rangle$. During our scenario, emergency calls were received at regular intervals of 10 min, resulting in a quantifiable number of calls during each interval, giving rise to 144 time intervals within a 24-hour period. Along with the calls, our dataset includes information about hospitals in Chicago. Each hospital is represented by $\langle ID, HOSPITAL, LONGITUDE, LATITUDE \rangle$. Figure 3 illustrates the distribution of hospitals and emergency calls throughout the selected zones in the Chicago region.

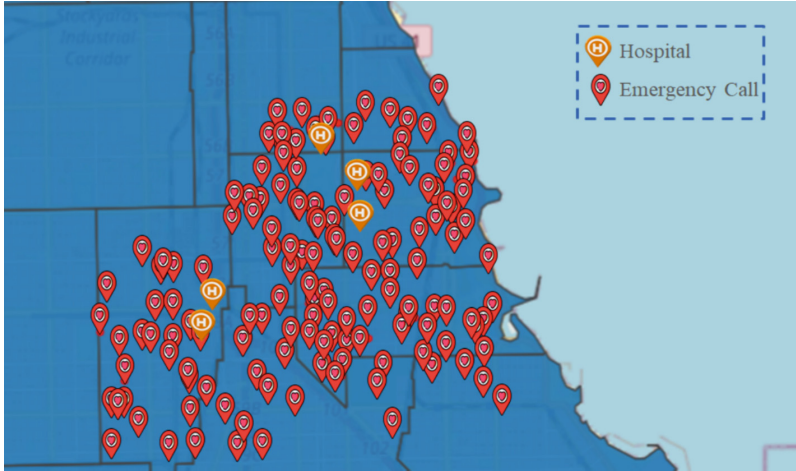


Fig. 3. The distribution of hospital and emergency calls in the selected zones in Chicago.

6.2 Empirical Results and Comparative Study

We have developed and executed a quantum slime mold algorithm for ambulance dispatching, leveraging actual data from Chicago. Our proposed algorithm was implemented on the quantum assembly (QASM) simulator. We performed a comparative analysis of the simulation outcomes between the classical slime mold algorithm and our quantum algorithm. In the classical approach, we fixed the population size at $N = 20$ and set the constant $z = 0.05$. In contrast, we initialized the oracle calls to 1 for the quantum algorithm, and the list L was set to a size of 20. Subsequently, we simulated both algorithms for 40 iterations.

In the first phase of experiments, we ran QSMA and SMA for 15 emergency calls and 20 ambulances to compare the fitness cost based on the total number of iterations. The results of Fig. 4 show that the proposed approach converges to the global minimum faster.

Next, we compared the performance of QSMA and SMA with dynamic ambulance dispatching, exploring scenarios with 3, 5, and 6 ambulances per hospital. The number of ambulances chosen directly affects the response to emergency calls and, consequently, influences the overall fitness value for each approach. Analyzing the results in Fig. 5, we observed that the proposed QSMA outperforms the classical SMA, showcasing its effectiveness in optimizing ambulance dispatching. This performance disparity can be attributed to the inherent capacity of the quantum approach to more effectively traverse and explore the entire search space.

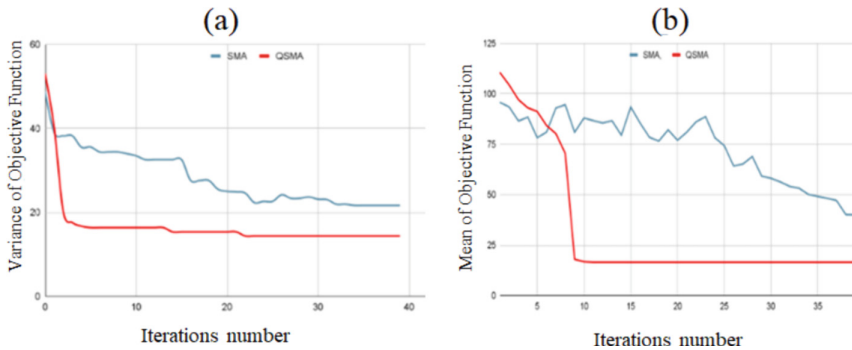


Fig. 4. Quantum vs. Classical slime mould algorithm: Comparison of Objective Function Variance (a) and Mean (b).

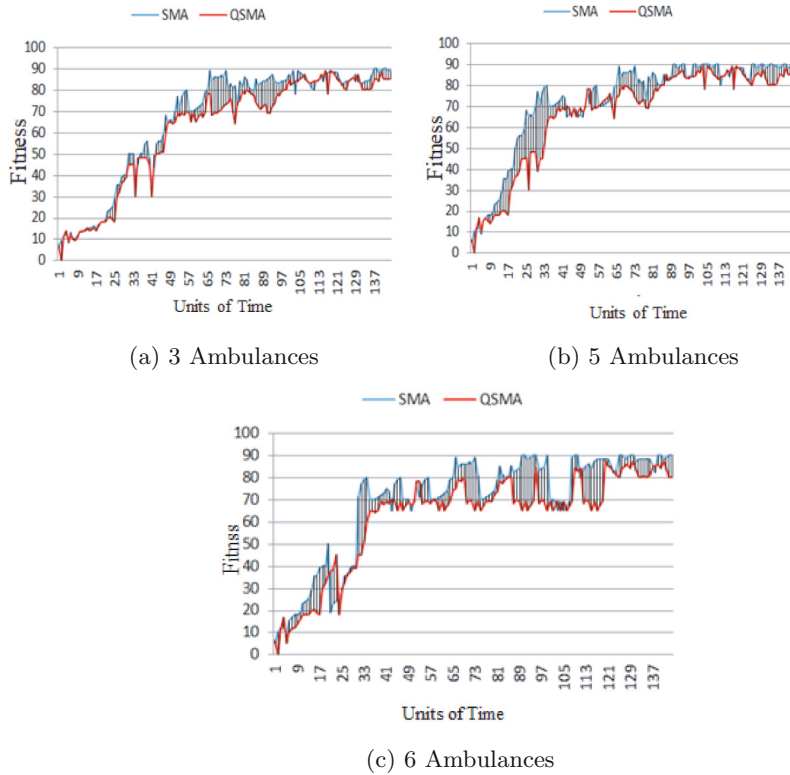


Fig. 5. Performance comparison of QSMA and SMA regarding fitness with 3, 5, and 6 ambulances per hospital.

7 Conclusions

This paper presents a novel approach called the Quantum Slime Mould Algorithm (QSMA) designed to address the ambulance dispatching problem. The QSMA combines elements from the classical slime mould algorithm and the quantum Grover's search algorithm to search for the optimal solution efficiently. We conducted experiments applying the QSMA to diverse Emergency Transportation scenarios and a real case study in Chicago. The results demonstrate the superiority of QSMA over classical SMA in terms of result quality. Moreover, the QSMA showcases a lower likelihood of being trapped in local minimums, enhancing its effectiveness in navigating complex solution spaces.

For future work, we plan to compare QSMA with other quantum optimization algorithms to assess its performance and capabilities further. Another possible research direction is testing the proposed approach on large datasets, such as those encompassing the entire Chicago region, to gauge its scalability and real-world applicability.

References

1. Aboubi, Y., Drias, H., Kamel, N.: BAT-CLARA: BAT-inspired algorithm for clustering large applications. *IFAC-PapersOnLine* **49**(12), 243–248 (2016)
2. Ajagekar, A., You, F.: Quantum computing for energy systems optimization: challenges and opportunities. *Energy* **179**, 76–89 (2019)
3. Bendimerad, L.S., Drias, H.: Intelligent contributions of the artificial orca algorithm for continuous problems and real-time emergency medical services. *Evol. Intell.* 1–36 (2023)
4. Bendimerad, L.S., Houacine, N.A., Drias, H.: Swarm intelligent approaches for ambulance dispatching and emergency calls covering: application to COVID-19 spread in Saudi Arabia. In: Abraham, A., Engelbrecht, A., Scotti, F., Gandhi, N., Manghirmalani Mishra, P., Fortino, G., Sakalauskas, V., Pllana, S. (eds.) *SocCPaR* 2021. LNNS, vol. 417, pp. 617–626. Springer, Cham (2022). https://doi.org/10.1007/978-3-030-96302-6_58
5. Daley, A.J., et al.: Practical quantum advantage in quantum simulation. *Nature* **607**(7920), 667–676 (2022)
6. Drias, H., Drias, Y., Bendimerad, L.S., Houacine, N.A., Zouache, D., Khennak, I.: Quantum ordering points to identify the clustering structure and application to emergency transportation. In: Abraham, A., Gandhi, N., Hanne, T., Hong, T.-P., Nogueira Rios, T., Ding, W. (eds.) *ISDA* 2021. LNNS, vol. 418, pp. 306–315. Springer, Cham (2022). https://doi.org/10.1007/978-3-030-96308-8_28
7. Drias, H., Drias, Y., Houacine, N.A., Bendimerad, L.S., Zouache, D., Khennak, I.: Quantum optics and deep self-learning on swarm intelligence algorithms for Covid-19 emergency transportation. *Soft Comput.* 1–20 (2022)
8. Gottlieb, M., Sansom, S., Frankenberger, C., Ward, E., Hota, B.: Clinical course and factors associated with hospitalization and critical illness among Covid-19 patients in Chicago, Illinois. *Acad. Emerg. Med.* **27**(10), 963–973 (2020)
9. Grover, L.K.: A fast quantum mechanical algorithm for database search. In: *Proceedings of the Twenty-Eighth Annual ACM Symposium on Theory of Computing*, pp. 212–219 (1996)

10. Hemici, M., Zouache, D., Brahmi, B., Got, A., Drias, H.: A decomposition-based multiobjective evolutionary algorithm using simulated annealing for the ambulance dispatching and relocation problem during Covid-19. *Appl. Soft Comput.* **141**, 110282 (2023)
11. Ibri, S., Drias, H., Nourelfath, M.: A parallel hybrid ant-tabu algorithm for integrated emergency vehicle dispatching and covering problem. *Int. J. Innov. Comput. Appl.* **2**(4), 226–236 (2010)
12. Khelfa, C., Khennak, I.: A survey on recent optimization strategies in ambulance dispatching and relocation problems. In: Drias, H., Yalaoui, F., Hadjali, A. (eds.) AID 2022. CCIS, vol. 1852, pp. 192–203. Springer, Singapore (2023). https://doi.org/10.1007/978-981-99-4484-2_15
13. Khelfa, C., Khennak, I., Drias, H., Drias, Y., Belharda, Y., Smail, M.: Slime mould algorithm for solving ambulance dispatching problem. In: Abraham, A., Hanne, T., Gandhi, N., Manghirmalani Mishra, P., Bajaj, A., Siarry, P. (eds.) SoCPaR 2022. LNNS, vol. 648, pp. 822–831. Springer, Cham (2023). https://doi.org/10.1007/978-3-031-27524-1_80
14. Khennak, I., Drias, H.: An accelerated PSO for query expansion in web information retrieval: application to medical dataset. *Appl. Intell.* **47**, 793–808 (2017)
15. Khennak, I., Drias, H., Khelfa, C., Drias, Y., Bourouhou, N.H., Zafoune, I.: Multi-objective Harris hawks optimization for optimal emergency vehicle dispatching during a pandemic. In: Abraham, A., Hanne, T., Gandhi, N., Manghirmalani Mishra, P., Bajaj, A., Siarry, P. (eds.) SoCPaR 2022. LNNS, vol. 648, pp. 852–861. Springer, Cham (2023). https://doi.org/10.1007/978-3-031-27524-1_83
16. Li, S., Chen, H., Wang, M., Heidari, A.A., Mirjalili, S.: Slime mould algorithm: a new method for stochastic optimization. *Futur. Gener. Comput. Syst.* **111**, 300–323 (2020)
17. Mandviwalla, A., Ohshiro, K., Ji, B.: Implementing Grover’s algorithm on the IBM quantum computers. In: 2018 IEEE International Conference on Big Data (Big Data), pp. 2531–2537. IEEE (2018)
18. Preston, R.H.: Applying Grover’s algorithm to hash functions: a software perspective. *IEEE Trans. Quantum Eng.* **3**, 1–10 (2022)
19. Supasil, J., Pathumsoot, P., Suwanna, S.: Simulation of implementable quantum-assisted genetic algorithm. In: Journal of Physics: Conference Series, vol. 1719, p. 012102. IOP Publishing (2021)
20. Udrescu, M., Prodan, L., Vlăduțiu, M.: Implementing quantum genetic algorithms: a solution based on Grover’s algorithm. In: Proceedings of the 3rd Conference on Computing Frontiers, pp. 71–82 (2006)



Quantum FP-Growth for Association Rules Mining

Widad Hassina Belkadi¹ , Yassine Drias² , and Habiba Drias¹

¹ LRIA, USTHB, BP 32 El Alia, Bab Ezzouar, 16111 Algiers, Algeria

wbelkadi@usthb.dz, habiba.drias@usthb.edu.dz

² MEF University, Istanbul, Türkiye

driasy@mef.edu.tr

Abstract. Quantum computing, based on quantum mechanics, promises revolutionary computational power by exploiting quantum states. It provides significant advantages over classical computing regarding time complexity, enabling faster and more efficient problem-solving. This paper explores the application of quantum computing in frequent itemset mining and association rules mining, a crucial task in data mining and pattern recognition. We propose a novel algorithm called Quantum FP-Growth (QFP-Growth) for mining frequent itemsets. The QFP-Growth algorithm follows the traditional FP-Growth approach, constructing a QF-list, then the QFP-tree, a quantum radix tree, to efficiently mine frequent itemsets from large datasets. We present a detailed analysis of each step in the QFP-Growth algorithm, providing insights into its time complexity and computational efficiency. Our algorithm outperforms classical FP-Growth with a quadratic improvement in error dependence, showcasing the power of quantum algorithms in data mining. To validate the effectiveness of our approach, we conducted experiments using the IBM QASM simulator, qiskit. The results demonstrate the efficiency and effectiveness of our QFP-Growth algorithm in mining frequent itemsets from a transactional database.

Keywords: Quantum Machine learning · Frequent Itemset Mining · Association Rules Mining · FP-growth · IBM QASM Simulator · Qiskit

1 Introduction

Quantum computing, built on quantum mechanics, has seen remarkable advancements and has the potential to solve problems exponentially faster than classical computers. Prominent quantum algorithms like Grover's search have demonstrated groundbreaking achievements. Quantum machine learning, a growing field, explores the synergy between quantum computing and machine learning, promising novel approaches for complex optimization and data analysis tasks with unparalleled computational speed and capacity.

Within the domain of data mining, frequent itemset mining plays a critical role in extracting associations and patterns from vast datasets [5, 6, 13].

Frequent itemset mining is the process of discovering frequent patterns from a dataset. It involves scanning the dataset and identifying sets of items that meet a specified support threshold. Traditional algorithms like Apriori and FP-growth are commonly employed for this task. While Apriori utilizes an iterative approach to generate candidate itemsets, FP-growth uses a more efficient method by constructing an FP-tree and directly mining frequent itemsets without candidate generation. FP-growth has shown considerable performance advantages over Apriori, especially when handling large datasets. However, despite its efficiency, the FP-growth algorithm still needs to be improved, mainly when dealing with increasingly massive datasets and complex patterns. The exponential growth of data demands even faster and more scalable algorithms to uncover valuable insights and associations. In light of these challenges, we propose “Quantum FP-Growth (QFP-growth)” as an innovative fusion of quantum computing principles and the efficiency of the classical FP-growth algorithm. With Quantum FP-Growth, we seek to harness quantum principles such as superposition and entanglement to achieve exponential speedup and efficiently explore vast itemset combinations.

The remainder of this paper is structured as follows. In Sect. 2, we begin with a comprehensive review of the fundamental concepts underlying classical FP-growth, followed by an exploration of the principles of Quantum Computing. In Sect. 3, we introduce our novel algorithm, Quantum FP-Growth, step by step, delving into an in-depth analysis of its time complexity. To demonstrate the practicality of our approach, we implement the QFP-Growth algorithm using the qiskit library and perform experiments with a market transactional database using the QASM simulator. Our findings and discussions are detailed in Sect. 4, and we conclude this work in Sect. 5, highlighting the potential impact and prospects of QFP-Growth in association rules mining and beyond.

2 Background

2.1 FP-Growth Algorithm

The FP-growth algorithm [12] is an efficient method for finding frequent itemsets in a dataset, outperforming the Apriori algorithm [1]. It eliminates the need for candidate generation and uses a divide-and-conquer approach with a data structure called FP-tree. The algorithm recursively builds conditional FP-trees for each frequent item, efficiently mining frequent itemsets without extensive candidate generation steps. Figure 1 provides an illustrative example demonstrating the algorithm’s steps. The FP-growth algorithm (see Algorithm 1) can be summarized in three main steps:

1. F-list Construction: The algorithm, shown in Algorithm 3, scans the dataset to identify the frequency of each unique item and creates an F-list containing only the elements with frequency above the minimum support. The F-list is sorted in descending order of frequency, eliminating infrequent elements early in the process. An example of this list is illustrated in Fig. 1b.

2. FP-tree Construction: The algorithm scans the dataset again and builds the FP-tree vertically, preserving frequency information and item order from the F-list. Figure 1d represents an example of this structure.
3. Mining Frequent Itemsets: After constructing the FP-tree, the algorithm mines frequent itemsets using a depth-first search starting with the least frequent item from the F-list, as depicted in Fig. 12. This step involves three substeps for each leaf item in the tree, shown in Algorithm 5, as follows:
 - (a) Build the conditional pattern base: A conditional pattern base is the set of prefix paths in the FP-tree containing the item being considered a suffix. The prefix paths are extracted from the FP tree using pointer-chasing [19].
 - (b) Generate the conditional FP-Tree: The conditional FP-Tree is structurally similar to an FP-tree but is used to find frequent itemsets ending with a specific suffix [19] (the selected item). Some items may no longer be frequent and need to be pruned.
 - (c) Search for frequent itemsets: The conditional FP-tree for the desired item is used to solve the subproblems of finding frequent itemsets for the prefix paths discovered in the conditional pattern base. If the conditional FP-tree represents a single path, all path combinations are determined. These combinations represent the desired frequent itemsets for the selected node. If the path is not a single path, the FP-growth method is recursively called.

The FP-growth algorithm efficiently discovers frequent patterns in a dataset without candidate generation, making it faster and more scalable than traditional algorithms like Apriori. The time complexity is $O(NM \log N + k2^m)$ [12], where N is the number of transactions, M is the maximum number of items in a transaction, and k is the average size of frequent itemsets.

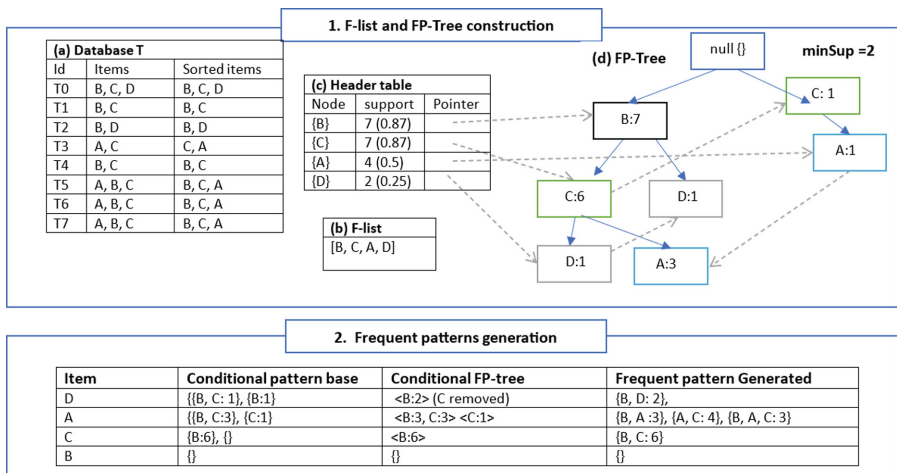


Fig. 1. Fp-growth execution illustration

2.2 Quantum Computing Concepts

Quantum Computing (QC) utilizes principles from quantum mechanics like superposition and entanglement, enabling high-speed computation and parallelism in tailored algorithms for efficient problem-solving [23]. Quantum Machine Learning (QML) combines QC and Machine Learning (ML), creating quantum versions of ML algorithms and using classical ML algorithms to analyze quantum systems.

Implementing classical ML algorithms on quantum computers involves three phases: encoding (state preparation), quantum computation (unitary transformation), and decoding (measurement) [14]. In the encoding phase, classical data is transformed and mapped onto quantum states, ensuring effective representation in the quantum system. Quantum computation exploits quantum operations like quantum gates and oracles to manipulate quantum states, benefiting from superposition and entanglement for parallel processing and potential speedups. In the measurement phase, the quantum output is mapped back to classical states for interpretable results in classical algorithms and problem domains.

2.2.1 Qubit

The fundamental concept of quantum computing revolves around the quantum bit, a qubit. Unlike classical bits, which can only exist in the 0 or 1 state, a qubit can simultaneously exist in a superposition of both states. In the computational basis, the two states of a qubit are denoted as $|0\rangle$ and $|1\rangle$. Mathematically, the state of a qubit, denoted as $|\Psi\rangle$, can be represented as $|\Psi\rangle = \alpha|0\rangle + \beta|1\rangle$ where α and β are complex numbers that represent the probability amplitudes, these amplitudes determine the likelihood of measuring the qubit as $|0\rangle$ or $|1\rangle$. In a broader context, the superposition of a collection of states denoted as $|\Psi_1\rangle, \dots, |\Psi_n\rangle$, can be expressed as in Eq. 1, where λ_i are complex coefficients representing probability amplitudes verifying $\sum_{i=1}^n \lambda_i^2 = 1$, these amplitudes determine the probabilities associated with each state within the superposition.

$$\sum_{i=1}^n \lambda_i |\Psi_i\rangle \quad (1)$$

2.2.2 Quantum Gates

Quantum gates are unitary operations applied to qubits, transforming their states [14]. Single-qubit gates like Pauli gates (X, Y, Z) for rotations and flips and the Hadamard gate to create superpositions [1]. Controlled gates operate on multiple qubits, relying on control qubits for conditional transformations, enabling entanglement and complex computations. Examples include the controlled-NOT (CNOT) and Toffoli gates, which are essential for reversible classical computations and simulating classical logic circuits [7].

2.2.3 Quantum Subroutines

After achieving an equal superposition state in a quantum algorithm, the next step is to selectively modify the probabilities (amplitudes) within the superposition to create an unequal distribution, favoring the desired answer or solution.

This is achieved using a combination of operations, including oracles and subroutines. Quantum subroutines are like functions in classical computing, but they operate on quantum states, leveraging the unique properties of quantum systems. They encapsulate a series of quantum gates to achieve specific transformations. The Quantum FP-growth algorithm utilizes specific subroutines, which are detailed below.

2.2.3.1 Quantum Search Algorithms

Grover's algorithm [10] is a quantum subroutine that enables the efficient search of an element within an unsorted database. It achieves a time complexity of $O(\sqrt{N})$, providing a quadratic speedup compared to classical algorithms. Quantum Amplitude Amplification (QAA) [3] is a technique that enhances the amplitudes of specific quantum states, like marked states in Grover's algorithm. It involves preparing the quantum state in a superposition of all possible states, applying Grover's operator with reflection and phase-shift operations to manipulate the amplitudes. Repeating this process significantly increases the amplitude of the marked state, leading to a higher probability of obtaining the desired element in a measurement. In addition to the original Grover algorithm, our algorithm incorporates the depth-first Grover search [11], an extension of the original Grover algorithm. This variant addresses inefficiencies in multi-solution search problems by introducing amplitude interception and combining quantum and classical techniques [11].

2.2.3.2 Quantum Counting Algorithms

Quantum Amplitude Estimation (QAE), also referred to as the Quantum Counting algorithm, is a robust quantum subroutine utilized to estimate the amplitude of a specific state within a quantum superposition. Its primary objective is to extract precise information about the probability distribution of a target state. By accurately estimating the amplitudes, QAE enables efficient counting of the number of solutions for a given search problem. The original QAE algorithm proposed by [3] combines the Grover operator [10] and quantum phase estimation (QPE) [17]. It estimates θ in $|\Psi\rangle = \cos(\theta)|w\rangle^\perp + \sin(\theta)|w\rangle$, where $|w\rangle^\perp$ and $|w\rangle$ represent bad and good solutions (states), respectively, using QPE, which includes the inverse Quantum Fourier Transform (QFT) and controlled Grover operators[22]. One practical application of QAE is counting the support of an item set, a task first explored by [21].

2.2.4 QASM Simulator

To overcome challenges related to limited qubit availability, noise, and error rates in physical quantum computers, quantum simulators are essential tools in quantum computing research. In this work, we utilize Qiskit [8], an open-source software development kit for quantum computing, along with its QASM simulator. Qiskit provides a comprehensive framework for developing and executing quantum programs, while the QASM simulator allows us to simulate quantum circuits on classical computers. This approach enables us to explore and exper-

iment with the QFP-growth algorithm, assess its performance, and validate its functionality before considering implementation on actual quantum hardware.

3 Quantum FP-Growth Algorithm

In Sect. 2.1, we discussed the three main steps of the FP-growth algorithm: F-list construction, FP-tree construction, and mining frequent itemsets from the FP-tree. The quantum version of this algorithm aims to retain the core principles and steps of FP-growth while leveraging the principles of quantum computing to address its limitations.

Let's consider a database T with N transactions and M items, and the set of items denoted by $C = \{item_j | j = 1, 2, \dots, M\}$. Alternatively, it can be represented as an $N \times M$ binary matrix, denoted by D (shown in Fig. 2), where the element $D_{ij} = 1$ (or 0) indicates the presence (or absence) of item I_j in transaction T_i . The Quantum FP-growth (QFP-growth) algorithm is depicted in Algorithm 2. It begins by constructing the QF-list, which is represented as a quantum circuit. Next, the QFP-tree is built. Finally, we invoke the hybrid quantum-classical algorithm QGrowth to mine the frequent itemsets in a superposition. In the subsequent sections, we will provide a detailed explanation of the three steps.

Algorithm 1. FP-growth

```

1:  $F\text{-list} \leftarrow \text{construct\_F-List}(DB, \text{minSup})$ 
2:  $FPT \leftarrow \text{construct\_FP-Tree}(DB, F\text{-list}, \text{minSup})$ 
3: for each  $item_j \in F\text{-list}$  do
4:    $F \leftarrow F \cup \text{Growth}(FPT, item_j, \text{minSup})$ 
5: end for
6: Return  $F$ 
```

Algorithm 2. QFP-GROWTH

```

1:  $QF\text{-list} \leftarrow \text{construct\_QF-List}(DB, \text{minSup})$ 
2:  $F \leftarrow \text{QGrowth}(QF\text{-list}, DB, \text{minSup})$ 
3: Return  $F$ 
```

Remark 1. We follow the query complexity model to estimate the complexity of QFP-growth. In that model, we focus solely on the number of times it interacts with the oracles responsible for input data retrieval, which are the most resource-intensive. In the following, we will estimate the query complexity of QFP-growth, in the worst-case scenario, by assessing the number of queries at each step and the total steps.

3.1 QF-List Construction

The classical algorithm to construct the F-list is outlined in Algorithm 3. This step involves two main sub-steps. Firstly, the database is scanned to calculate the support of each item, and subsequently, infrequent items are removed. The F-list construction represents one iteration of the Apriori algorithm to extract the 1-frequent itemsets. On the other hand, our QF-list construction algorithm, see Algorithm 4, inspired from [21], follows a schematic approach. It begins by estimating the supports of all individual items in the database in parallel, utilizing quantum amplitude estimation (QAE) as described in [21]. Next, QAA is

employed to search for items with supports equal to or greater than the minimum support in order to obtain the QF-list. In the subsequent discussion, we will detail these two sub-phases.

Algorithm 3. construct_F-List

```

1: F-list  $\leftarrow$  DatabaseItems(DB)
2: for each transaction $t_i \in DB$  do
3:   for each item $j \in t_i$  do
4:     F-list[item $j$ ] ++
5:   end for
6: end for
7: F-list  $\leftarrow$  removeInfrequentItems(F-list)
8: Sort F-list
9: Return F-list

```

Algorithm 4. construct_QF-List

```

1: Prepare state in superposition
2: Parallel QAE to count support of items [3]
3: Parallel QAA to search for items having
   support  $\geq \text{minSup}$  [3]
4: Measure the first register as QF-list and
   the third register as supports
5: Sort QF-list       $\triangleright$  classically (heap sort)
6: Return QF-list, QF-list _supports

```

3.1.1 Support Estimation of Each Item

Here we name QF-list with K elements, where $\text{QF-list} \subseteq C$, C is the set of all items in database T. Estimating the support sup_j of each $item_j$ in C is a computationally intensive task in the FP-growth algorithm. We employ the quantum subroutine of QAE [3] to optimize this process.

1. To start, three quantum registers are prepared: one for transaction indices, one for item indices, and an ancillary qubit for the phase oracle. The input to the QAE is a quantum state $|\Psi\rangle$, representing the superposition of the target state, encoded using Hadamard gates.
2. Grover operator is applied to enhance the target state's amplitude in the superposition. This step involves applying that phase oracle that increases the probability of measuring the target states. We define a phase oracle that determines either a transaction $|i\rangle$ contains an item $|j\rangle$ as follows [21]:

$$O|i\rangle|j\rangle = (-1)^{D_{ij}}|i\rangle|j\rangle \quad (2)$$

If $item_j \subseteq T_i$, the phase would be flipped; otherwise, nothing happens. This oracle will be used to construct Grover's operator, which is defined as follows [21]: $G = [(2|\Psi\rangle\langle\Psi| - \mathbf{1}_i) \otimes \mathbf{1}_j]O$, where $|\Psi_N\rangle = \sum_{i=0}^{N-1} \frac{|i\rangle}{\sqrt{N}}$, $\mathbf{1}_i$ and $\mathbf{1}_j$ are identity gates on the first quantum register of $|i\rangle$ storing transaction indices, and on the second register of $|j\rangle$ storing the item indices of items and the O represents the oracle represented in Eq. 2.

3. The QAE algorithm (described in paragraph 2.2.3.2) is utilized to approximate the support corresponding to the target state's amplitude in the superposition, employing the Grover operator. The first measured register is used to estimate the associated supports. We calculate the value of θ using Eq. 3, where *measured_int_value* is the decimal conversion of the measured value, and c represents the number of counting qubits (first register qubits). Then, the support of an item j is obtained using Eq. 4.

$$\theta = \frac{\pi \times \text{measured_int_value}}{2^c} \quad (3)$$

$$sup_j = \sin^2(\theta) \quad (4)$$

3.1.2 Search for Frequent Items

After estimating the support of each item, we utilize QAA to search for items with support greater than or equal to the specified minimum support threshold. The resulting QF-list circuit, produces two registers as output. The first register represents the calculated supports, while the last contains frequent items. After measuring the QF-list, the items need to be sorted in descending order based on their support values. While no quantum sorting algorithm currently outperforms the best classical sorting methods, we will use the classical heap sort algorithm for this task, which has an efficient time complexity of $O(N \log N)$ for sorting large datasets, where N is the size of the dataset.

Lemma 1. *The computational complexity of construct-QF-list (Algorithm 4) is $O\left(\sqrt{\frac{M}{M_{freq}}}\right)$ where M is the number of items, and M_{freq} is the number of frequent items.*

Proof. We first estimate the support of each item using the QAE. The error for estimating the support sup_j on average is $\Theta(\frac{sup_j(\sqrt{(1-sup_j)})}{T})$ where T is the number of repetitions [21]. If we want to estimate sup_j with absolute error ϵ , we will need to have $T = \frac{2\pi}{\epsilon}$; thus, the asymptotic runtime of this subroutine is $O(\frac{1}{\epsilon})$, the whole proof is explained in detail in [18]. The next step is the QAA to remove infrequent items; we search for M_{freq} solutions over the M item. Therefore, this subroutine takes $O(\sqrt{\frac{M}{M_{freq}}})$ [3]. Taking into account all of these factors, our algorithm requires $O\left(T\sqrt{\frac{M}{M_{freq}}}\right) = O\left(\frac{\sqrt{\frac{M}{M_{freq}}}}{\epsilon}\right)$ [21].

3.2 QFP-Tree Construction

Without a header table, the FP-tree can be visualized as a trie [20], a prefix tree-based data structure designed to store strings from a specific alphabet [20]. It can also be represented as a binary radix tree or Patricia tree, organizing keys based on their common prefixes [16, 20]. By using the horizontal transactional matrix, an example is shown in Fig. 2, and ordering items based on their support, we create ordered sequences, which are then inserted into the binary radix tree to form the FP-tree [16]. We have broadened this concept by employing a quantum radix tree [4, 15] to portray the QFP-tree. We must note that each node within the classical FP-tree stores two key pieces of information: the item itself and its corresponding support (count) in the prefixes. To construct the QFP-tree, we utilize an enhanced version of the quantum radix tree known as the augmented quantum radix tree [15]. This augmented tree allows us to incorporate the support information into the nodes. The resulting QFP-tree is represented in Fig. 2.

Definition 1. (*Quantum FP-tree*): Let D be the horizontal transactional matrix with size $n \times l$, where n is the number of transactions and l is the number of items and m is the number of unique transactions, and $m \leq n$. We assume that the numbers l , n , and m are of powers of 2 and $S \subset \{0, 1\}^l \times \{0, 1\}^l$ be a set of key-value pairs of size m . Let O be the set of valid tree nodes encoding elements of S , defined as:

$$O = \{0, 1\}^l \times \{0, 1\}^l \times \{0, \dots, N\} \times (\{0, 1\}^{\leq l} \times [m]) \quad (5)$$

So, a node has the form $(z, v, c, L_1, p_1, L_2, p_2, L_3, p_3)$, with z the key, and v the value, here, the key and the value are the same. Next, the c represents the support of the itemset. Then p_1, p_2 , and p_3 represent pointers to the parent, left child, and right child, in memory of m cells, and L_1, L_2 , and L_3 are the labels of the corresponding edges from the parent, to the left and right child, respectively. A root node has $L_1 = \emptyset$, all nodes have initially $c = 0$, and at the end, root node will have $c = n$, and leaves have $p_2 = p_3 = L_2 = L_3 = 0$.

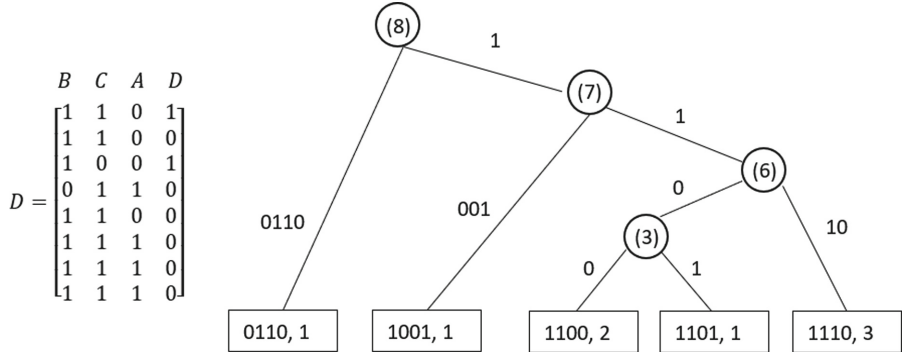


Fig. 2. QFP-tree representing transactions from the database T (Fig. 1). Internal nodes store counters of values below them. Leaves store transaction bit strings along with their corresponding support.

Corollary 1. Consider the QFP-tree $|FPT_Q(S)\rangle$, which stores m bit-strings of length $l = \log m$. The data structure operations such as insert, delete, lookup, and constructing a uniform superposition over elements of S have a time complexity of $O(\log m)$. Additionally, checking if the QFP-tree is empty or a single path can be done in constant time, $O(1)$.

Lemma 2. Classically the FP-tree construction takes $O(NM \log N)$ times. Quantumly, the computational complexity of construct_QFP-Tree is $O(N \log N)$ where N is the number of transactions.

Proof. The cost of inserting one transaction is $O(\log N)$, and we need to insert N transactions. Thus, the complexity is $O(N \log N)$.

In the classical FP-growth algorithm, a header table is constructed along with the FP-tree to enable quick and direct access to nodes associated with each item. This facilitates efficient traversal of the tree and identification of frequent itemsets. Similarly, we introduce the concept of a quantum header table (QHT) for efficient retrieval of conditional pattern bases. To represent the QHT, we utilize a quantum dictionary [9] where the item indexes serve as keys, and the corresponding values are lists of paths containing each item. This data structure allows for effective management and retrieval of conditional pattern bases in the quantum setting.

3.3 Mining Frequent Itemsets

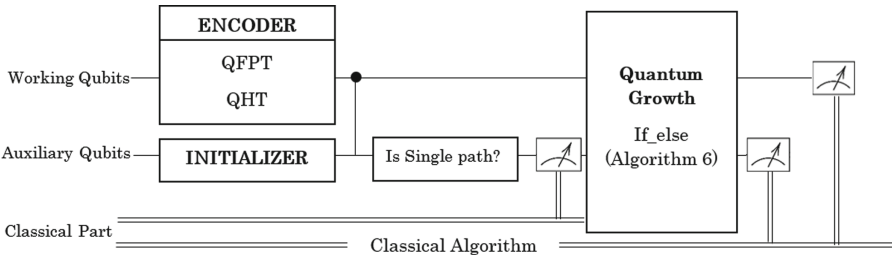


Fig. 3. Global structure of Growth (Algorithm 6). The components QFPT and QHT represent the QFP-tree and QHeaderTable, respectively. The “Is Single Path” gate determines if the QFPT is a single path (dynamic circuit)

In the classical Growth (see Algorithm 5), a depth-first search is performed on the FP-tree, starting with the least frequent item. The goal is to adapt this algorithm onto a hybrid quantum-classical approach called Depth-First Grover Search [11]. The global structure of our hybrid quantum-classical algorithm is illustrated in Fig. 3, based on [11]. The procedure is outlined in Algorithm 6. The QFP-tree, along with the QHeaderTable (QHT), represents the encoder component of the algorithm. The QHeaderTable contains the items and their associated conditional pattern bases, which are the paths in the tree containing that item. If the QFP-tree is not a single path, the conditional pattern bases are retrieved from the QHeaderTable. The QGrowth algorithm is then called recursively, constructing a conditional FP-tree (QFP-tree) as indicated in step 2. The algorithm continues until the QFP-tree is empty or becomes a single path. If the QFP-tree is a single path, measurements are taken along the path with the suffixes, and the frequent itemsets are found using the Grover search. Dynamic circuits can be employed to implement conditional statements, such as if tests and if-else conditions, found on lines 3, 4, and 12 of the algorithm. Dynamic circuits refer to quantum circuits incorporating mid-circuit measurements, which influence the subsequent execution of gates by enabling feed-forward operations [8]. In other words, these circuits allow measurements to be performed during the computation, and the measurement results can dynamically guide the flow of control in the circuit.

Lemma 3. *The time complexity of QGrowth (Algorithm 6), in the worst-case scenario, is $O\left(k(N \log N + \sqrt{\frac{2^M}{\mu}})\right)$, where k is the maximum size of frequent itemsets, and μ is the average number of frequent itemsets.*

Proof. The QGrowth algorithm is recursive, with a maximum recursive depth of k . The algorithm checks if the QFPT is empty or a single path in each recursion step. These conditional statements have a complexity of $O(1)$. If the tree is a single path, we need to apply QAA to search for the μ frequent itemsets within the set of combinations, which has a size of 2^M . The complexity of QAA is $O(\sqrt{\frac{2^M}{\mu}})$. Otherwise, if the tree is not a single path, we need to construct the QFP-tree, which has a complexity of $O(N \log N)$ in the worst-case scenario. By summing up all together, we end up with $O\left(k(N \log N + \sqrt{\frac{2^M}{\mu}})\right)$.

Theorem 1. $O\left(\frac{\sqrt{\frac{M}{M_{freq}}} + \left(k(N \log N + \sqrt{\frac{2^M}{\mu}})\right)}{3}\right)$ is the running time of QFP-growth.

Algorithm 5. Growth

```

1: Begin
2: if FPT is a single path or empty then
3:    $P \leftarrow N$ 
4:   for each combinaison C in path do
5:      $P \leftarrow P \cup N$ 
6:     P.support  $\leftarrow$  minimum
      _support(P \setminus N)
7:     if P.support  $> minSup$  then
8:       Return P
9:     end if
10:   end for
11: else
12:   for each item i in FPT do
13:      $M_i \leftarrow \{i\} \cup N$ 
14:      $CPB_i \leftarrow$  conditional _pattern
      _base(FPT, i)
15:      $CPB_i \leftarrow$  remove _infrequent
      _items(CPBi, minSup)
16:      $FPT_i \leftarrow$  construct_FPTree(CPBi)
17:     if FPTi is not empty then
18:       Return
         Growth(FPTi, minSup, Mi)
19:     end if
20:   end for
21: end if
22: End

```

Algorithm 6. QGrowth

```

1: Begin
2: QFPT  $\leftarrow$  construct _QFP-tree(DB)  $\triangleright$ 
  Quantum encoder
3: if QFPT is empty then
4:   Return []
5: end if
6: if FPT is a single path then
7:   path  $\leftarrow$  Measure QFPT
8:   combs  $\leftarrow$  combinasions(path)  $\triangleright$ 
  classically
9:   supports  $\leftarrow$  Quant _Min(combs.support)
10:  Parallel QAA to search for combi-
    naisons having support  $\geq minSup$  [3]
     $\triangleright$  quantum circuit 1
11:  P  $\leftarrow$  Measure the registers to get the
    frequents itemsets
12:  Return P
13: else
14:   CPB  $\leftarrow$  superposition of QHead-
    erTable (item with paths)  $\triangleright$  quantum
    circuit 2
15:   F  $\leftarrow$  F  $\cup$  Growth(CPB, minSup)  $\triangleright$ 
    Recursivity
16: end if
17: Return F
18: End

```

Table 1 compares the algorithm's classical and quantum time complexity, detailing the complexity of each step. Our proposed quantum version of each step outperforms the classical ones, with a significant quadratic speedup, especially in the QF-list construction.

Table 1. Comparisons of our QFP-growth algorithm and the classical FP-growth

Algorithm	Classical FP-Growth	Quantum FP-growth
(Q)F-list construction	$O(NM)$ (see Algorithm 3)	$O\left(\frac{\sqrt{\frac{M}{M_{freq}}}}{\epsilon}\right)$ (see Algorithm 4)
(Q)F-tree construction	$O(NM \log N)$	$O(N \log N)$
(Q)Growth	$O(k(MN \log N + 2^M))$ (see Algorithm 5)	$O\left(k(N \log N + \sqrt{\frac{2M}{\mu}})\right)$ (see Algorithm 6)
(Q)FP-growth	$O\left(NM \log N + k2^M\right)$ (see Algorithm 1)	$O\left(\frac{\sqrt{\frac{M}{M_{freq}}} + \left(k(N \log N + \sqrt{\frac{2M}{\mu}})\right)}{\epsilon}\right)$ (see Algorithm 2)

4 Experimental Implementation

In this section, we demonstrate the implementation of QFP-Growth on the database transaction, represented in Fig. 1, by an 8×4 matrix. The experiments are conducted on the QASM simulator, chosen for its ability to mimic an ideal noise-free quantum computer. The QFP-Growth algorithm utilizes a quantum radix tree known as the QFP-tree for efficient frequent itemset mining. Although quantum data structures like the quantum radix tree hold great potential, practical implementations are still ongoing research endeavors, and no concrete progress has been reported in the literature. Thus, we focus on implementing the QF-list (frequent 1-itemset), an essential step in classical FP-growth. By addressing this component, we aim to demonstrate the feasibility and advantages of quantum approaches in association rule mining. The QF-list circuit comprises three quantum registers. The first register contains four counting qubits used to obtain the supports, the second contains three qubits encoding the eight transaction indices (000 to 111), and the third has two qubits encoding the item indices (00 to 11). The minimum support threshold is set to 0.8. The final circuit is illustrated in Fig. 5. It estimates the supports using the QAE circuit and searches for frequent items using the QAA circuit, which employs the QAE as a state preparation gate. The development of the QAE circuit requires the design of an oracle to detect the solutions. While theoretically, implementing oracles does not require explicit specification; practical considerations necessitate careful design to ensure accurate results. In our case, we designed the oracle using one ancilla qubit and Toffoli gates. The oracle marks the transactions containing an item; for instance, if transaction T_4 (100) has the item B (01), then the bitstring 10001 is marked. Additionally, we developed the Grover operator for use in the QAE circuit, as depicted in Fig. 6a. To validate the accuracy of the designed oracle, we conducted a Grover search using the Grover operator and measured the second register (for the items). The measurement results are shown in Fig. 6b, demonstrated that the observed item distribution corresponds to the actual distribution in the dataset, thus providing evidence of its correctness.

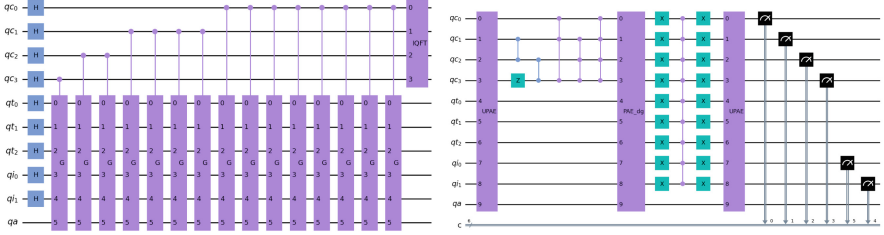


Fig. 4. The QAE circuit, G is the Grover operator showed in Fig. 6a

Fig. 5. The QF-list circuit, UPAE represents the circuit represented in Fig. 4 and PAE-dg represent its inverse.

Afterward, we constructed the QAE circuit (see Fig. 4) and incorporated it into the final Quantum Amplitude Amplification (QAA) circuit for searching frequent items. Within the QAA, we designed an oracle to detect supports greater than or equal to 0.8. To compute each item's support based on the measurement outcomes, we utilized the Eqs. 3 and 4. Consequently, the oracle needs to flip the states $|0110\rangle$, $|0111\rangle$, $|1000\rangle$, $|1001\rangle$, and $|1010\rangle$ (in decimal, they correspond to 6, 7, 8, 9, and 10 respectively). To obtain optimal results, the QAA might require several iterations. Ultimately, we performed measurements on the first and last registers, yielding a 6-bit output denoted as $i_0, i_1, e_0, e_1, e_2, e_3$, where i_0 and i_1 represent the four items (A, B, C, D), and e_0, e_1, e_2 , and e_3 are used to estimate the associated supports.

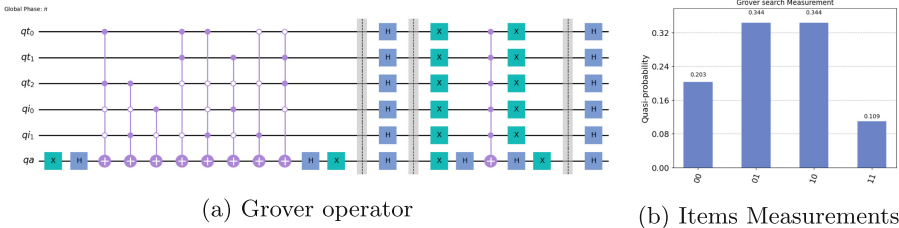


Fig. 6. Quantum circuit and results of the Grover Operator (G) containing the oracle (O) for the transaction database T of Fig. 1.

We executed the QF-list circuit on the IBM QASM simulator with 1024×32 shots and two iterations of the QAA circuit. Figure 7 shows the measurement outcomes' distribution, where items B and C, exhibiting the highest probabilities, meet the minimum support threshold. The outputs 010110 and 101010 correspond to the frequent items $|01\rangle$ (B) and $|10\rangle$ (C), respectively. By evaluating Eqs. 3 and 4, we computed the supports of items B and C to be $0.853 \approx 0.87$. For item A ($|00\rangle$), the output is 000100, resulting in a support of 0.5. The highest probability output for item D ($|11\rangle$) is 110011, yielding support of 0.30,

remarkably close to the real support of 0.25. This demonstrates the successful implementation of the QFP-list algorithm for mining frequent 1-itemsets using quantum computing techniques.

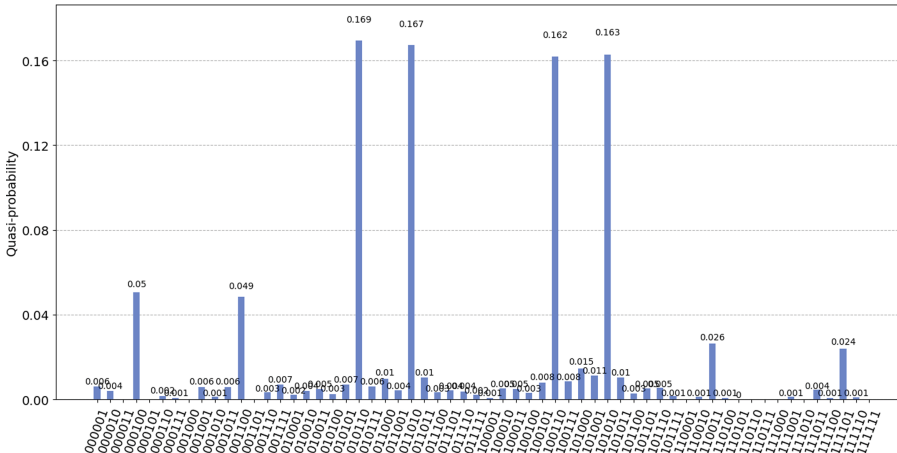


Fig. 7. Measurement outcomes of running the QF-list circuit of Fig. 5

5 Conclusion and Future Outlook

In this paper, we introduced a novel QFP-Growth algorithm for mining frequent itemsets, leveraging the power of quantum computing concepts. The proposed algorithm closely follows the steps of the classical FP-Growth approach, involving the construction of the QF-list, QFP-tree, and extraction of frequent itemsets from the QFP-tree. Each step was meticulously detailed, and its complexity was thoroughly analyzed. Our algorithm exhibited remarkable efficiency and speed, outperforming the classical approach with a quadratic improvement in error dependence. The results firmly establish the power of our quantum approach, enabling us to navigate the exponentially growing space of itemset combinations efficiently. To validate the effectiveness of our proposed method, we implemented the QF-list on the IBM QASM simulator, yielding promising results.

As we look toward future directions, we aim to explore and compare various variants of QAE [22] further to enhance the efficiency and speed of the QF-list implementation. Additionally, we plan to extend our implementation to mine all frequent k-itemsets using the QFP-tree. Real-world applications are also part of our future goals, particularly exploring the algorithm's performance on larger datasets, such as Digital soil mapping applications [2].

References

1. Agrawal, R., Srikant, R., et al.: Fast algorithms for mining association rules. In: Proceedings of the 20th International Conference on Very Large Data Bases, VLDB, Santiago, Chile, vol. 1215, pp. 487–499 (1994)
2. Belkadi, W.H., Drias, Y.: Advancements in digital soil mapping: from data acquisition to uncertainty estimation - a comprehensive review. In: Drias, H., Yalaoui, F., Hadjali, A. (eds.) AID 2022. CCIS, vol. 1852, pp. 162–177. Springer, Singapore (2023). https://doi.org/10.1007/978-981-99-4484-2_13
3. Brassard, G., Hoyer, P., Mosca, M., Tapp, A.: Quantum amplitude amplification and estimation. *Contemp. Math.* **305**, 53–74 (2002)
4. Buhrman, H., Loff, B., Patro, S., Speelman, F.: Memory compression with quantum random-access gates. arXiv preprint [arXiv:2203.05599](https://arxiv.org/abs/2203.05599) (2022)
5. Djenouri, Y., Drias, H., Bendjoudi, A.: Pruning irrelevant association rules using knowledge mining. *Int. J. Bus. Intell. Data Min.* **9**(2), 112–144 (2014)
6. Djenouri, Y., Drias, H., Habbas, Z.: Hybrid intelligent method for association rules mining using multiple strategies. *Int. J. Appl. Metaheuristic Comput. (IJAMC)* **5**(1), 46–64 (2014)
7. Drias, H., Drias, Y., Houacine, N.A., Bendimerad, L.S., Zouache, D., Khennak, I.: Quantum optics and deep self-learning on swarm intelligence algorithms for Covid-19 emergency transportation. *Soft Comput.* 1–20 (2022)
8. Gadi, A., Thomas, A., Panagiotis, B., Luciano, B., Yael, B.H., David, B.: Qiskit: an open-source framework for quantum computing (software library) online access (2020). <https://qiskit.org/>
9. Gidney, C.: Quantum dictionaries without QRAM. arXiv preprint [arXiv:2204.13835](https://arxiv.org/abs/2204.13835) (2022)
10. Grover, L.K.: A fast quantum mechanical algorithm for database search. In: Proceedings of the Twenty-Eighth Annual ACM Symposium on Theory of Computing, pp. 212–219 (1996)
11. Guo, H.: Depth-first Grover search algorithm on hybrid quantum-classical computer. arXiv preprint [arXiv:2210.04664](https://arxiv.org/abs/2210.04664) (2022)
12. Han, J., Pei, J., Yin, Y.: Mining frequent patterns without candidate generation. *ACM SIGMOD Rec.* **29**(2), 1–12 (2000)
13. Heraguemi, K.E., Kamel, N., Drias, H.: Multi-objective bat algorithm for mining interesting association rules. In: Prasath, R., Gelbukh, A. (eds.) MIKE 2016. LNCS (LNAI), vol. 10089, pp. 13–23. Springer, Cham (2017). https://doi.org/10.1007/978-3-319-58130-9_2
14. Houssein, E.H., Abohashima, Z., Elhoseny, M., Mohamed, W.M.: Machine learning in the quantum realm: the state-of-the-art, challenges, and future vision. *Expert Syst. Appl.* **194**, 116512 (2022)
15. Jeffery, S.: Frameworks for quantum algorithms (2014)
16. Karras, T.: Maximizing parallelism in the construction of BVHs, octrees, and k-d trees. In: Proceedings of the Fourth ACM SIGGRAPH/Eurographics Conference on High-Performance Graphics, pp. 33–37 (2012)
17. Kitaev, A.Y.: Quantum measurements and the abelian stabilizer problem. arXiv preprint [quant-ph/9511026](https://arxiv.org/abs/quant-ph/9511026) (1995)
18. Luongo, A.: Quantum algorithms for data analysis (2020). <https://quantumalgorithms.org>
19. Tan, P.N., Steinbach, M., Karpatne, A., Kumar, V.: Introduction to data mining (what's new in computer science) (2018)

20. Wang, F., Yuan, B.: Parallel frequent pattern mining without candidate generation on GPUs. In: 2014 IEEE International Conference on Data Mining Workshop, pp. 1046–1052. IEEE (2014)
21. Yu, C.H., Gao, F., Wang, Q.L., Wen, Q.Y.: Quantum algorithm for association rules mining. *Phys. Rev. A* **94**(4), 042311 (2016)
22. Yu, K., Lim, H., Rao, P., Jin, D.: Comparison of amplitude estimation algorithms by implementation. arXiv preprint [arXiv:2005.05300](https://arxiv.org/abs/2005.05300) (2020)
23. Zhang, Y., Ni, Q.: Recent advances in quantum machine learning. *Quantum Eng.* **2**(1), e34 (2020)



Gaussian Quantum-Behaved PSO Strategy for Lithium Battery Model Optimization

Walid Merrouche¹ (✉) Badis Lekouaghet² , and Elouahab Bouguenna¹

¹ Center for Renewable Energies Development, CDER, Bouzareah, Algiers, Algeria
w.merrouche@cder.dz

² Research Center in Industrial Technologies, CRTI, Cheraga, Algiers, Algeria

Abstract. The integration of quantum-inspired techniques into optimization algorithms allows for enhanced exploration of complex parameter spaces, enabling efficient convergence toward optimal solutions. This article presents the application of Gaussian Quantum-behaved Particle Swarm Optimization (GQPSO) strategy, tailored for optimizing the parameters of the Lithium Battery Extended Thevenin model. Inspired by the principles of swarm intelligence and quantum mechanics, the GQPSO leverages Gaussian distributions to enhance the exploration of parameter spaces, capitalizing on the advantages offered by quantum-inspired optimization techniques. Through tests on high-accuracy data, the effectiveness of the GQPSO strategy is demonstrated. The optimized Lithium Battery Extended Thevenin model showcases remarkable accuracy, with an RMSE of $2.06116086e-02$ and a standard deviation of $1.27510624e-02$. The GQPSO strategy's exceptional performance showcases the advantages of combining quantum mechanics' principles and Gaussian distributions with swarm intelligence for accurate and efficient lithium battery modeling, paving the way for improved energy storage system applications.

Keywords: Quantum Computation · Particle Swarm Optimization · Gaussian Distribution · Lithium-ion Battery · Equivalent Circuit Model · Thevenin Model

1 Introduction

In our ever-evolving world of technology and innovation, the quest for efficient and sustainable energy storage solutions has become a paramount concern. The widespread adoption of electric vehicles, renewable energy sources, and portable electronic devices has fueled the demand for high-performance batteries [1–3]. However, the optimization and accurate extraction of Equivalent Circuit Model (ECM) parameters, crucial for enhancing battery performance, have remained formidable challenges.

Conventional optimization methods have shown limitations in accurately handling the intricate and high-dimensional parameter spaces associated with ECMs. In this context, the remarkable promise of quantum computing and its potential to revolutionize problem-solving has piqued the interest of researchers across diverse domains [4]. Quantum algorithms, in particular, offer a paradigm shift in computational capabilities by harnessing the principles of quantum mechanics.

One groundbreaking approach that holds immense promise for models parameter extraction is the quantum-inspired metaheuristics [5, 6]. The wellspring of inspiration for most quantum-inspired metaheuristics originates from Genetic and Evolutionary algorithms, followed by swarm-based algorithms. Applications span a wide spectrum, encompassing areas as diverse as image processing, computer networks, flight control, and structural design. The promising results of quantum-inspired metaheuristics fuel optimism that in the future, the fusion of conventional algorithms with the principles of quantum mechanics could unlock novel solutions for optimization challenges across multifarious disciplines [5].

Swarm-based metaheuristic techniques draw inspiration from nature's collaborative behavior observed in animals working together to forage for food [7]. Originating from birds' flocking patterns, particle swarm optimization (PSO) is one of the most popular swarm techniques that has undergone many evolutions since its emergence in 1995 [8, 9]. PSO presents a distinct advantage with its minimal parameter tuning and its ability to extract optimal solutions through particle interactions. However, when dealing with a high number of dimensions or complex, large datasets, PSO's effectiveness in uncovering the global optimal solution diminishes, often accompanied by a sluggish convergence rate. Ref. [10] introduced the Quantum-behaved PSO (QPSO) as a remedy to enhance the convergence rate of the original PSO. QPSO combines the strengths of both quantum computing principles and the PSO technique, creating a powerful tool for tackling complex optimization problems. Over the subsequent decades, QPSO has garnered significant attention from scholars, finding application in diverse fields including engineering inverse problems, grey level image clustering, numerical optimization, multimodal multi-objective problems, and optimization of virtual machines in smart computing cloud placement [5].

Despite the promise of QPSO, its application, along with its extensions, within the realm of battery modeling optimization remains relatively scarce. A handful of works have ventured into this space. For instance, [11] study focused on optimizing Tremblay's battery model parameters for plug-in hybrid electric vehicle applications. Similarly, [12] research harnessed QPSO to optimize unknown parameters of a simplified first-order fractional-order model (FOM). This scarcity of application in battery modeling optimization highlights an exciting avenue for research and innovation.

To address this existing gap and recognizing the ongoing need for innovative optimization algorithms, as underscored by the No Free Lunch Theorems [13–16], we aim to introduce a novel approach in this study. This approach involves the application of the Gaussian Quantum-behaved Particle Swarm Optimization (GQPSO) strategy for optimizing the Lithium Battery ECM. GQPSO is an innovative approach, as proposed by [17], that harnesses the power of Gaussian distributions and quantum-inspired principles within the PSO framework. By amalgamating these advanced techniques, we endeavor to enhance the accuracy, efficiency, and convergence capabilities of battery model parameter estimation.

The contributions of this study unfold in two key dimensions. First, we introduce the GQPSO for the first time in the realm of parameter estimation for the Extended Thevenin ECM of Lithium-ion Battery. Secondly, the effectiveness of the GQPSO algorithm is demonstrated through a high-quality battery test profile, meticulously constructed using real-world driving data sourced from RWTH Aachen University.

Given the potential of QPSO to enhance convergence rates and explore complex parameter spaces, its integration into battery modeling holds promise for advancing energy storage solutions and optimizing battery performance across various applications.

The rest of this paper is organized as follows:

- Section 2 presents the methodology, encompassing details about the Basic PSO algorithm, the QPSO algorithm, the Gaussian QPSO applied in this paper, and insights into the Lithium-ion battery's ECM.
- Section 3 delves into the findings derived from the simulation based on real-world driving data, encompassing both the results and the ensuing discussion.
- Finally, Sect. 4 offers a conclusion based on the presented research.

2 Methods

2.1 Particle Swarm Optimization Algorithm (PSO)

The Particle Swarm Optimization (PSO) is a metaheuristic swarm intelligence algorithm, introduced by [8]. PSO is inspired by the behavior of animals in large populations such as birds flocking and fishes schooling, with a swarm of particles. Numerous versions have been suggested to enhance its performance through optimization. In PSO, the candidate solutions are called particles. Each particle moves around within a specified dimensional search space N , aiming to locate the sub-optimal or optimal position. The speed of movement of each particle is affected by its previous position, its personal best position ($pbest : P_i = (P_{i1}, P_{i2}, P_{i3}, \dots, P_{iN})$), and the global best ($gbest : P_g = (P_{g1}, P_{g2}, P_{g3}, \dots, P_{gN})$).

The positions and velocities of particles are given as follows:

$$x_i^{k+1} = x_i^k + v_i^{k+1} \quad (1)$$

$$v_i^{k+1} = wv_i^k + c_1r_1(P_{best,i} - x_i^k) + c_2r_2(G_{best} - x_i^k) \quad (2)$$

where, x_i^{k+1} is the new position of particle i , x_i^k is the previous position of particle i , v_i^{k+1} is the new velocity of particle i , variables c_1 and c_2 are the cognitive and social parameter that controls the impact of each particle's personal best information ($pbest$) and social information ($gbest$) on the search process at every iteration, w is the inertia weight, r_1 and r_2 are random numbers uniformly distributed between 0 and 1, $P_{best,i}$ is the personal best position of particle i , and G_{best} is the best position of the entire swarm.

The method to implement the global version of PSO involves a systematic series of steps. Firstly, the process initiates with the creation of a population of particles, each assigned random positions and velocities within the problem space applying a uniform probability distribution. Subsequently, the fitness of each particle is rigorously evaluated to gauge its performance. Following this, comparisons are made between the fitness of each particle and its personal best (pbest), as well as with the overall best fitness value within the population (gbest). If a particle's fitness surpasses its pbest or gbest, the corresponding values are updated accordingly. Additionally, the velocity and position of each particle are adjusted based on predetermined equations, enabling iterative refinement of the particle trajectories within the problem space. Finally, the evolutionary cycle is repeated by returning to Step 2 until reaching a stop criterion: typically a sufficiently optimized fitness or a limited number of iterations [18].

2.2 Quantum-Behaved Particle Swarm Optimization Algorithm (QPSO)

Noting that the global convergence of PSO cannot be guaranteed, and it needs conscious efforts in parameter tuning: Ref. [10] proposed the Quantum-behaved Particle Swarm Optimization (QPSO) algorithm to improve the performance of PSO and to further reduce the number of tuning parameters and increase the convergence rate. This is done by introducing the quantum theory into the existing standard PSO with its concept inspired by quantum mechanics and physics. Unlike in standard PSO, the state of the particles is represented by a wave function that is only a function of position, i.e. particle velocity is not required.

The equations for updating the positions of particles are presented as follows:

$$\begin{cases} x_i^{k+1} = P_i^k + \beta \cdot |mBest^k - x_i^k| \cdot \ln\left(\frac{1}{u}\right), & k < 0.5 \\ x_i^{k+1} = P_i^k - \beta \cdot |mBest^k - x_i^k| \cdot \ln\left(\frac{1}{u}\right), & k \geq 0.5 \end{cases} \quad (3)$$

where,

$$P_i^k = (r_1 \cdot P_{best,i} + r_2 \cdot G_{best}) / (r_1 + r_2) \quad (4)$$

$$mBest^k = \frac{1}{N} \sum_{i=1}^N P_{best,i} \quad (5)$$

In the aforementioned equation, $mBest^k$ represents the mean best position, calculated as the average of all personal best positions within the swarm. The variables r_1, r_2, k and u denote random numbers uniformly distributed on the interval $(0, 1)$.

The sole tuning parameter, denoted as β serves as the adaptive contraction or shrinkage coefficient, crucial for regulating the search time of the algorithm. A diminutive β value may lead the algorithm to converge prematurely to a local optimum solution. Consequently, the parameter β significantly influences the estimation outcome of the QPSO algorithm. In the initial optimization stages, higher β values are preferred to facilitate global exploration, while lower values are prioritized in subsequent stages to yield more precise results during local search processes.

$$\beta = (w_2 - w_1) \frac{maxIter - t}{maxIter} + w_1 \quad (6)$$

where, the inertia weight w_1 and w_2 helps to achieve a balance between global and local search ability while the ***maxIter*** is the maximum number of iterations.

2.3 Quantum-Behaved Particle Swarm Optimization Using Gaussian Mutation

Several novel iterations of QPSO have been introduced over the recent years. The majority of QPSO algorithms employ a uniform probability distribution for generating random numbers. Nonetheless, innovative methodologies have arisen, suggesting the utilization of Gaussian, Cauchy, and exponential probability distributions for the generation of random numbers. In this paper, we present new results based on the new approach proposed by [17]. This method is based on the mutation operator in QPSO using Gaussian probability distribution.

Employing Gaussian distribution sequences characterized by a mean of zero and a variance of one for the stochastic coefficients within PSO could offer a favorable balance. This balance resides between the likelihood of encountering numerous minor deviations around present points (facilitating precise adjustments) and the infrequent occurrence of more substantial deviations. Such deviations facilitate particle movement away from the current point, potentially aiding in evading local minima.

In this study, the initial step involves the generation of random numbers by utilizing the absolute values of a Gaussian probability distribution characterized by a mean of zero and a variance of one, i.e., $abs(N(0, 1))$. The ensuing sub-section delineates the novel G-QPSO strategies, which have been integrated with a mutation operator, in the subsequent manner:

Approach 1 – G-QPSO (1): parameter u of Eq. 3 is modified by the following equation:

$$\begin{cases} x_i^{k+1} = P_i^k + \beta \cdot |mBest^k - x_i^k| \cdot \ln\left(\frac{1}{G}\right), & k < 0.5 \\ x_i^{k+1} = P_i^k - \beta \cdot |mBest^k - x_i^k| \cdot \ln\left(\frac{1}{G}\right), & k \geq 0.5 \end{cases} \quad (7)$$

where $G = abs(N(0, 1))$.

Approach 2 – G-QPSO (2): parameters r_1 and r_2 of Eq. 4 are modified by the following equation:

$$P_i^k = (G.P_{best,i} + g.G_{best})/(G + g) \quad (8)$$

where $g = abs(N(0, 1))$.

Approach 3 – G-QPSO (3): This approach uses both Eq. 7 and 8.

2.4 ECM of Li-ion Battery

The Equivalent Circuit Model (ECM) is an advanced representation of a battery's behavior, designed to capture its complex dynamics and non linearities more accurately than traditional models [19]. Unlike simple ECMs, where the model contains only one RC, the Extended Thevenin ECM integrates additional elements such as diffusion impedance, charge transfer resistance, and other parameters that play a crucial role in characterizing a battery's response. This model offers a higher level of accuracy in modeling a battery's behavior with relatively medium level of complexity [20]. With its richer parameter set, the Extended Thevenin ECM offers better opportunities for parameter estimation. This is particularly beneficial in cases where data-driven approaches are used to calibrate the model [21–24].

Illustrated in Fig. 1, the Extended Thevenin model consists of two RC branches arranged in series, accompanied by the internal ohmic resistance R_0 , and supplemented by an Open Circuit Voltage source (V_{oc}).

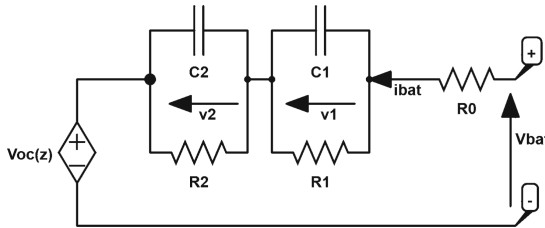


Fig. 1. Extended Thevenin battery model Schematic

To seamlessly incorporate the extended Thevenin model into a final algorithm, a discrete-time formulation can be employed, outlined as follows:

$$v_{bat}[k] = V_{oc}(z[k]) - R_0 i_{bat}[k] - \sum_{i=1}^{i=2} v_i[k] \quad (9)$$

here, v_{bat} represents the terminal battery voltage, i_{bat} stands for the input/output current, v_i signifies the voltage of the respective RC branch, and i is the number of the RC branch (1 or 2 in this context).

The state equations are as follows:

$$z[k + 1] = z[k] - \frac{\eta \Delta t}{Q_C} i_{bat}[k] \quad (10)$$

$$v_i[k + 1] = e^{\frac{-\Delta t}{R_i C_i}} v_i[k] + R_i \left(1 - e^{\frac{-\Delta t}{R_i C_i}}\right) i_{bat}[k] \quad (11)$$

where z symbolizes the State of Charge (SoC), Δt corresponds to the sampling period, R_i and C_i denote the resistance and capacitor values associated with the respective RC branch, η represents the charge coefficient (considered as 1 within this article), and Q_C signifies the nominal battery capacity in ampere-hours (Ah).

Mathematically depicting the non-linear connection between V_{oc} and SOC, we find it aptly characterized by a sixth-order polynomial exponential function:

$$V_{oc} = a_0 + a_1z + a_2z^2 + a_3z^3 + a_4z^4 + a_5z^5 + a_6z^6 \quad (12)$$

In this context, the factors a_0 to a_6 constitute the polynomial coefficients.

2.5 The Fitness Function

The fitness function is a crucial component in most optimization algorithms, serving as the benchmark to either minimize or maximize during the iterative updating process. In the context of this study, the fitness function is defined as the difference between computed data (estimated battery voltage V_{est}), obtained through model simulation, and real data acquired from measurements (experimental battery voltage V_{exp}). The quantification of this overall disparity is achieved through the computation of the minimum Root Mean Square Error (RMSE) for N samples, as outlined below:

$$F_{RMSE}(x) = \text{Min} \left\{ \sqrt{\frac{1}{N} \sum_{i=1}^N [V_{exp}(i) - V_{est}(i)]^2} \right\} \quad (13)$$

Based on the preceding subsections, we present a comprehensive flowchart (Fig. 2) illustrating the process of estimating variables using the G-QPSO algorithm. To summarize, the data collection phase involved the gathering of experimental data. Following this, we selected and modeled the Extended Thevenin ECM using Eq. 9. An initial assessment was performed to validate this model using real-world data, with a specific focus on aligning the ECM with the defined objective function. This crucial step laid the foundation for initiating the variable extraction process employing the G-QPSO algorithm.

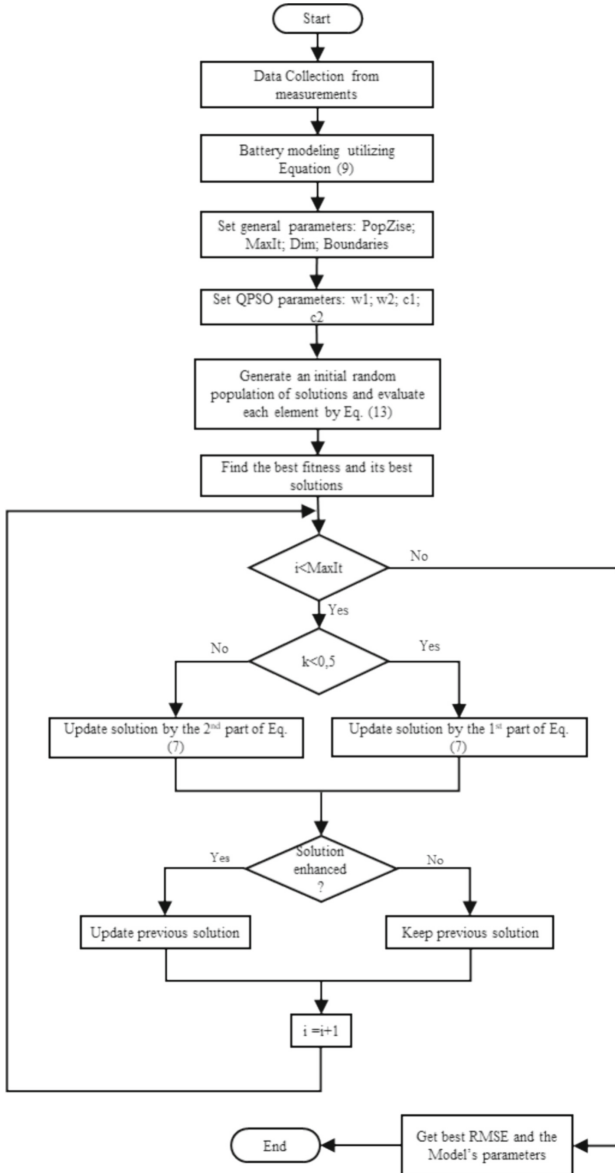


Fig. 2. Parameters optimization via the G-QPSO algorithm.

3 Results and Discussions

This article delves into the exploration of the potential of quantum-inspired metaheuristics, with a specific focus on G-QPSO in efficiently and accurately extracting parameters from the Extended Thevenin ECM.

For this purpose, we employ the G-QPSO algorithm to optimize the twelve key parameters of the ECM, which encompass R_0, R_1, C_1, R_2, C_2 , as well as coefficients a_0 to a_6 . The overarching framework of our methodology unfolds in the following phases:

- 1. Battery Model Selection:** In this study it is specifically the Extended Thevenin ECM. As previously discussed, this model encompasses the internal resistance R_0 , two serially connected RC pairs, and parameters related to $V_{oc}(z)$.
- 2. Data Collection:** To ensure robust parameter identification, our approach relies on a high-accuracy dataset drawn from Ref. [25, 26]. We utilize specifications from the Samsung 35e Lithium-ion Battery, which are outlined in Table 1. The dataset's test profile is rooted in real-world driving data, encompassing both discharging currents reaching up to 8 A and charging currents up to 2 A. Measurements of the battery's currents (depicted in Fig. 3a) and voltages are directly collected using the Digatron battery tester, with a sampling period (Δt) set at 0.1 s. Calculations of SOC are conducted through the Coulomb counting method. Notably, the SOC data predominantly covers low SOC values, ranging approximately from 35% to 15% (Fig. 3b).
- 3. Parameter Identification:** The final phase culminates in the identification of model parameters. Our approach aims to achieve convergence towards an optimal point, symbolizing the ECM parameters that minimize the objective function. In this study, the chosen objective function is the RMSE, serving to effectively reduce discrepancies between the estimated voltage V_{est} derived from potential parameters and the experimental voltage V_{exp} obtained from real-world data.

Table 1. Main specifications of the tested Lithium-ion Battery

Specification	Description
Manufacturer	Samsung SDI
Model	INR18650-35e
Nominal voltage	3.6 V
Nominal capacity	3400 mAh
Dimensions	18.55mm x 65.25mm
Figure	

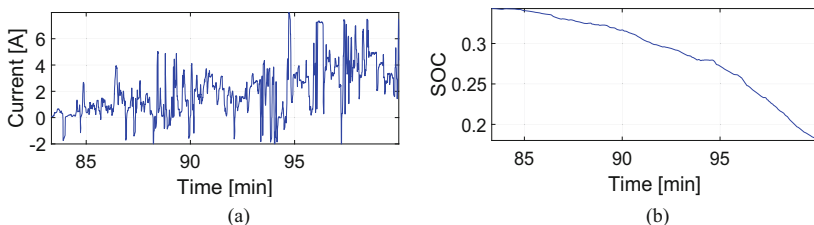


Fig. 3. Current and low SOC curves for the Real-driving world tests data

To conduct a comprehensive evaluation of the G-QPSO-based estimation algorithm's behavior and performance, we executed the algorithm in ten separate runs, as depicted in Fig. 4. This multi-run approach serves as a valuable metric for assessing the algorithm's consistency and reliability in parameter estimation.

The RMSEs of the G-QPSO algorithm, encompassing minimum, mean, and maximum values, are as follows: $2.06116086e-02$, $6.71196056e-02$, and $3.67409304e-02$, respectively. These indices furnish essential insights into the algorithm's effectiveness in minimizing discrepancies between the estimated parameters and the actual experimental data.

The Standard Deviation (SD) index indicates the distribution or spread of the deviation values. The lower calculated SD, recorded at $1.27510624e-02$, signifies accepted level of stability in the estimation process.

Figure 5 provides a visual comparison between the experimental voltage measurements and the voltage estimates obtained through the G-QPSO-based estimation algorithm, specifically corresponding to the minimum RMSE of $2.06116086e-02$. This graphical representation serves as a valuable tool to assess the accuracy of the estimation method.

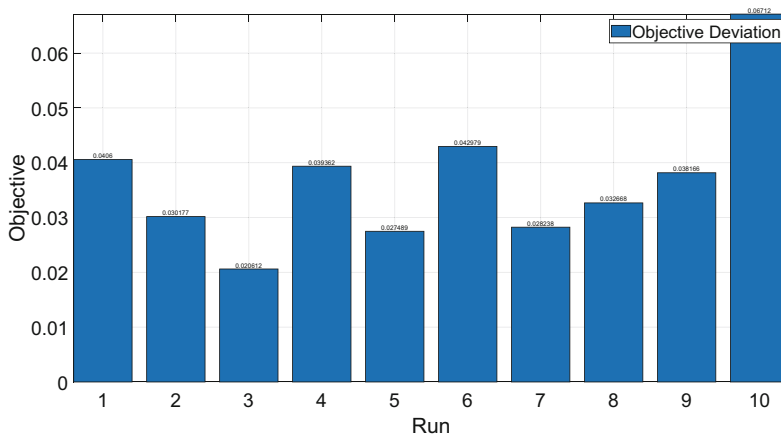


Fig. 4. Deviation of Objective values within the 10 Runs of GQPSO

The optimal optimization parameters, pinpointed through the GQPSO method, are elaborated in Table 2. These parameters emanate from the third algorithm run, resulting in a minimal RMSE. This outcome distinctly highlights the prowess of the G-QPSO algorithm in successfully identifying optimal parameter values for the ECM.

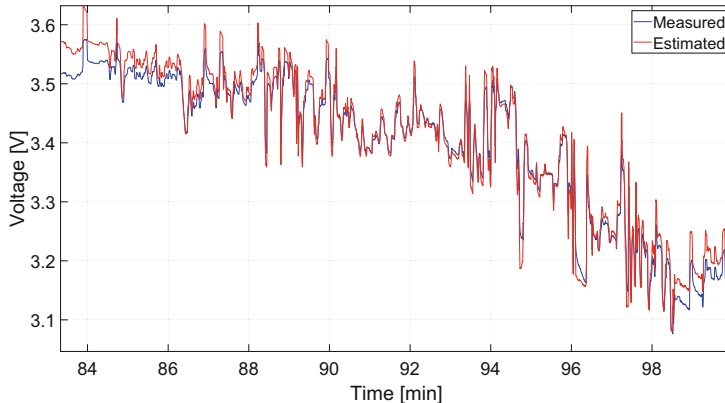


Fig. 5. Comparison between the best GQPSO-based estimated voltage and the measured voltage

Table 2. Estimated parameters of the ECM corresponding to the best optimization run

Parameters	values
R0 (Ω)	0.03467453278
R1 (Ω)	0.0264780298
C1 (F)	7352.405641
R2 (Ω)	0.02304900088
C2(F)	23614.89463
a0	3.300879825
a1	0.7987011175
a2	-0.004156364003
a3	0.0009338053178
a4	-3.358412456e-05
a5	3.860503353e-06
a6	-4.283675354e-08

4 Conclusion

In summary, this article delves into battery modeling optimization using the innovative Gaussian Quantum-behaved Particle Swarm Optimization (G-QPSO) technique. Through meticulous evaluation and experimentation, we highlight the G-QPSO's potential to significantly enhance parameter estimation accuracy in the Extended Thevenin Equivalent Circuit Model (ECM) of a Li-ion battery. The method's reliability is confirmed through multi-run analysis, and convergence behavior visualization showcases its good convergence and efficiency. Our findings underscore the algorithm's potential for real-world applications, offering a promising avenue for refining battery performance and energy applications.

References

1. von Bülow, F., Meisen, T.: A review on methods for state of health forecasting of lithium-ion batteries applicable in real-world operational conditions. *J. Energy Storage* **57**, 105978 (2023). <https://doi.org/10.1016/J.EST.2022.105978>
2. Elmahallawy, M., Elfouly, T., Alouani, A., Massoud, A.M.: A comprehensive review of lithium-ion batteries modeling, and state of health and remaining useful lifetime prediction. *IEEE Access* **10**, 119040–119070 (2022). <https://doi.org/10.1109/ACCESS.2022.3221137>
3. Merrouche, W., et al.: Improved model and simulation tool for dynamic SOH estimation and life prediction of batteries used in PV systems. *Simul. Model. Pract. Theory* **119**, 102590 (2022). <https://doi.org/10.1016/j.simpat.2022.102590>
4. Kadam, P.P., Kadam, S.: Quantum optimization techniques and it's comparison with classical optimization. In: Senju, T., So-In, C., Joshi, A. (eds.) SMART 2023. LNCS, vol. 645, pp. 639–647. Springer, Singapore (2023). https://doi.org/10.1007/978-981-99-0769-4_55
5. Hakemi, S., Houshmand, M., KheirKhah, E., Hosseini, S.A.: A review of recent advances in quantum-inspired metaheuristics (2022). <https://doi.org/10.1007/s12065-022-00783-2>
6. Gharehchopogh, F.S.: Quantum-inspired metaheuristic algorithms: comprehensive survey and classification. *Artif. Intell. Rev.* (2023). <https://doi.org/10.1007/s10462-022-10280-8>
7. Reddy, K., Saha, A.K.: A review of swarm-based metaheuristic optimization techniques and their application to doubly fed induction generator (2022). <https://doi.org/10.1016/j.heliyon.2022.e10956>
8. Kennedy, J., Eberhart, R.: Particle swarm optimization. In: Proceedings of ICNN 1995 - International Conference on Neural Networks, pp. 1942–1948. IEEE (1995). <https://doi.org/10.1109/ICNN.1995.488968>
9. Gad, A.G.: Particle swarm optimization algorithm and its applications: a systematic review. *Arch. Comput. Methods Eng.* (2022). <https://doi.org/10.1007/s11831-021-09694-4>
10. Yang, S., Wang, M., Jiao, L.: A quantum particle swarm optimization. In: Proceedings of the 2004 Congress on Evolutionary Computation (IEEE Cat. No. 04TH8753), pp. 320–324. IEEE (2004). <https://doi.org/10.1109/CEC.2004.1330874>
11. Zhang, Y., Lyden, S., De La Barra, B.A.L., Haque, M.E.: Optimization of Tremblay's battery model parameters for plug-in hybrid electric vehicle applications. In: 2017 Australasian Universities Power Engineering Conference, AUPEC 2017 (2018). <https://doi.org/10.1109/AUPEC.2017.8282405>
12. Solomon, O.O., Zheng, W., Chen, J., Qiao, Z.: State of charge estimation of Lithium-ion battery using an improved fractional-order extended Kalman filter. *J. Energy Storage* (2022). <https://doi.org/10.1016/j.est.2022.104007>
13. Service, T.C.: A No Free Lunch theorem for multi-objective optimization. *Inf. Process. Lett.* **110**, 917–923 (2010). <https://doi.org/10.1016/j.ipl.2010.07.026>
14. Joyce, T., Herrmann, J.M.: A review of no free lunch theorems, and their implications for metaheuristic optimisation. In: Yang, X.-S. (ed.) Nature-Inspired Algorithms and Applied Optimization. SCI, vol. 744, pp. 27–51. Springer, Cham (2018). https://doi.org/10.1007/978-3-319-67669-2_2
15. Haddad, S., Lekouaghet, B., Benghanem, M., Soukkou, A., Rabhi, A.: Parameter estimation of solar modules operating under outdoor operational conditions using artificial hummingbird algorithm. *IEEE Access* (2022). <https://doi.org/10.1109/ACCESS.2022.3174222>
16. Lekouaghet, B., Khelifa, M.A., Boukabou, A.: Adolescent identity search algorithm for parameter extraction in photovoltaic solar cells and modules. *J. Comput. Electron.* (2022). <https://doi.org/10.1007/s10825-022-01881-1>
17. dos Santos Coelho, L.: Gaussian quantum-behaved particle swarm optimization approaches for constrained engineering design problems. *Expert Syst. Appl.* **37**, 1676–1683 (2010). <https://doi.org/10.1016/j.eswa.2009.06.044>

18. dos Santos Coelho, L.: A quantum particle swarm optimizer with chaotic mutation operator. *Chaos Solitons Fractals* (2008). <https://doi.org/10.1016/j.chaos.2006.10.028>
19. Plett, G.L.: Battery Management Systems: Equivalent-Circuit Methods (2016)
20. Plett, G.L.: Battery Management Systems, Volume I: Battery Modeling. Artech (2015)
21. Merrouche, W., Lekouaghet, B., Bouguenna, E., Himeur, Y.: Parameter estimation of ECM model for Li-ion battery using the weighted mean of vectors algorithm. *J. Energy Storage* **76**, 109891 (2024). <https://doi.org/10.1016/j.est.2023.109891>
22. Merrouche, W., Lekouaghet, B., Bouguenna, E.: Artificial search algorithm for parameters optimization of Li-ion battery electrical model. In: 2023 International Conference on Decision Aid Sciences and Applications (DASA), pp. 17–22. IEEE (2023). <https://doi.org/10.1109/DASA59624.2023.10286632>
23. Lekouaghet, B., Merrouche, W., Bouguenna, E., Himeur, Y.: Identifying the unknown parameters of ECM model for Li-ion battery using Rao-1 algorithm. In: The 4th International Electronic Conference on Applied Sciences session Energy, Environmental and Earth Science. MDPI (2023). <https://doi.org/10.3390/ASEC2023-15343>
24. Merrouche, W., Gaci, I., Ould-Amrouche, S., Boubézari, A.: PWM buck converter used in PV controller. In: Proceedings of 2019 7th International Renewable and Sustainable Energy Conference, IRSEC 2019. pp. 1–6. IEEE (2019). <https://doi.org/10.1109/IRSEC48032.2019.9078250>
25. Li, W., Rentemeister, M., Badeda, J., Jöst, D., Schulte, D., Sauer, D.U.: Digital twin for battery systems: cloud battery management system with online state-of-charge and state-of-health estimation. *J. Energy Storage*. **30**, 101557 (2020). <https://doi.org/10.1016/j.est.2020.101557>
26. Li, W., Chen, J., Quade, K., Luder, D., Gong, J., Sauer, D.U.: Battery degradation diagnosis with field data, impedance-based modeling and artificial intelligence. *Energy Storage Mater.* **53**, 391–403 (2022). <https://doi.org/10.1016/j.ensm.2022.08.021>



Quantum Recurrent Neural Networks for Soil Profiles Prediction in Türkiye

Yassine Drias¹ , Alaa Eddine Siouane², and Tuna Çakar¹

¹ MEF University, Istanbul, Turkey

{driasy,cakart}@mef.edu.tr

² University of Algiers, Algiers, Algeria

Abstract. In this article, we introduce a new approach for soil profile prediction using Quantum Recurrent Neural Networks (QRNNs). By harnessing the power of quantum computing, QRNNs present a promising solution to overcome the limitations of conventional soil mapping techniques. We begin by proposing a classical Recurrent Neural Networks (RNNs) architecture for soil profiles prediction, followed by the design of its quantum counterpart with QRNNs. Focusing on the application of our model in Türkiye, we leverage geospatial data from diverse sources, including climate, vegetation, and land relief data, to showcase the efficacy of QRNNs in soil classification and resource monitoring. Our results reveal a remarkable accuracy score and computational efficiency. Moreover, we delve into the broader implications of quantum computing for digital mapping and explore potential avenues for future research. Emphasizing the integration of quantum computing techniques with digital soil mapping, we foresee a promising advancement in sustainable soil management practices, aiding decision-making processes in agriculture, environmental planning, and natural resource management.

Keywords: Quantum Computing · Recurrent Neural Networks · Quantum Machine Learning · Digital Soil Mapping

1 Introduction

Soil mapping, an essential component of agricultural and environmental research, plays a crucial role in understanding soil characteristics and their impact on various ecosystems. The accurate assessment of soil properties is paramount for optimizing agricultural practices, mitigating environmental risks, and ensuring sustainable land management. Traditional soil mapping techniques, such as remote sensing, geographic information systems (GIS), and soil sampling, have long been the cornerstone of this field, providing valuable insights into soil properties and distributions. However, these methods often face challenges related to data resolution, spatial coverage, and time-consuming data processing, which can hinder their effectiveness in capturing the intricate spatial and temporal variations of soil attributes [1].

Recent years have witnessed remarkable progress in Artificial Intelligence (AI) and Machine Learning (ML), revolutionizing various scientific disciplines [2]. In the context of soil mapping, advanced ML techniques hold the potential to augment traditional methods and overcome their limitations. Quantum Computing (QC) is another groundbreaking field, which has been making significant strides in the realm of computing [3]. It harnesses the principles of quantum mechanics to process information in ways that defy the capabilities of classical computers. Its ability to process vast data and solve complex problems could overcome the limitations of traditional soil mapping techniques. Quantum algorithms might lead to more efficient and accurate soil maps, advancing land management and environmental practices. Although still in its early stages, quantum computing holds immense potential for transforming scientific fields, including soil mapping.

In this article, we propose a novel approach to Digital Soil Mapping based on Quantum Recurrent Neural Networks (QRNNs), which represents a synthesis of quantum computing principles and Recurrent Neural Networks (RNNs). The idea consists of building a model capable of predicting soil profiles for any region based on various features, including soil properties, climate, land cover, and land relief. By employing this comprehensive approach, we seek to advance digital soil mapping techniques and contribute to sustainable land management practices. The results hold significant potential for informed decision-making and efficient resource utilization in real-world applications.

This article is organized as follows: Sect. 2 delves into the background of Digital Soil Mapping and reviews related works in the field. In Sect. 3, we introduce and explain the architecture of our Quantum Recurrent Neural Networks for soil profiles prediction. Section 4 presents experimental results, evaluating the performance of the QRNNs model. Finally, in Sect. 5, we conclude this study and discuss some future directions.

2 Digital Soil Mapping

2.1 Background

Digital Soil Mapping (DSM) is an innovative approach that utilizes various technologies, data sources, and computational methods to create detailed and accurate representations of soil properties across vast geographical regions. Its overarching goal is to provide accurate and up-to-date soil information at regional and global scales, providing valuable insights for decision-making in various sectors, including agriculture, environmental management, urban planning, and natural resource conservation.

Unlike traditional soil mapping techniques that heavily rely on manual soil sampling and laborious field surveys, DSM leverages the power of remote sensing, geographical information systems, and artificial intelligence algorithms to generate high-resolution soil maps. The concept of DSM evolved as a response to the limitations of conventional soil mapping approaches, which often suffered

from spatial and temporal gaps due to the impracticality of exhaustive soil sampling across extensive landscapes. By integrating spatially explicit environmental covariates, such as terrain attributes, land use, climate data, and vegetation indices, DSM seeks to establish robust statistical relationships between these covariates and soil attributes.

The Scorpion model is one of the most popular models for Digital Soil Mapping. It serves as an empirical and quantitative correlation between a soil characteristic and its spatially implicit formative factors [4]. Additionally to soil attributes, the model considers observable soil factors that influence soil composition such as climate, vegetation, and relief. Formula 1 represents the Scorpion model equation where:

- ‘s’ represents the composition of the soil,
- ‘c’ is the climate such as precipitation and temperature,
- ‘o’ refers to organism, including vegetation, fauna, and human activities,
- ‘r’ describes the relief or the topography, including differences in elevation and slope,
- ‘p’ is the parent materials, which determine the soil profile development, like iron oxide index and magnetic susceptibility,
- ‘a’ gives information on the age or time,
- ‘n’ is the spacial or geographic position,
- ‘ ε ’ is added as an error term that could include the spatial trends that are not captured by the predictive factors.

$$S(x, y) = f(s, c, o, r, p, a, n) + \varepsilon \quad (1)$$

‘S’ can represent either the soil properties or soil classes to map, and ‘f’ is the function that links the Scorpion factors with the ‘S’ properties [5].

2.2 Related Works

In recent years, the integration of AI algorithms into DSM has garnered significant attention, leading to notable advancements in soil mapping accuracy and efficiency. Data Mining, Machine Learning, and Deep Learning algorithms have been employed to derive predictive models using input covariates derived from remote sensing data and soil point observations.

In this context, Data Warehouses have been studied for collecting environmental data, such as climate, hydrological, and agricultural data. In [6], the authors proposed a data warehouse architecture for analyzing and exploring spatial soil data in the Maghreb region. Their work focused on the analysis of organic carbon (CO), revealing positive spatial autocorrelation, indicating perfect spatial clustering across the entire Maghreb region.

In [7], the authors specifically utilized Convolutional Neural Network (CNNs) for DSM, demonstrating how this approach significantly improves soil mapping accuracy by incorporating contextual information surrounding observations. Deep learning models also offer considerable potential for DSM, automatically

extracting relevant features from data. Another work, in [8], explored the benefits of such models, including their ability to handle large datasets and identify complex patterns. However, this approach, along with the previously cited ones, face challenges, such as data quality for model training, appropriate variable selection for soil mapping, and other considerations related to implementing machine learning algorithms in DSM.

To overcome these challenges, integrating quantum computing presents a promising solution. In [9], the authors delve into Quantum Convolutional Neural Networks (QCNNs), discussing their architecture and the incorporation of quantum properties into CNNs. They also explore training using gradient descent and their relation to two well-known concepts in quantum information theory: multiscale entanglement renormalization (MERA) and quantum error correction (QEC). Similarly, in [10], the authors elaborate on QCNN architecture, adapting the structure of CNNs to quantum systems using qubits for parallel computations.

In the present article, we will harness this innovative approach by combining the advantages of Recurrent Neural Networks and Quantum Computing. Our approach aims to leverage the advanced capabilities offered by quantum computing to enhance the performance and efficiency of RNNs applied to digital soil mapping. The present work marks the inaugural application of quantum computing technology to the domain of digital soil mapping. To our best knowledge, the potential of Quantum Recurrent Networks in the realm of DSM remains unexplored.

3 Quantum Recurrent Neural Networks for Digital Soil Mapping

This study aims to develop a novel approach for predicting soil profiles by leveraging observable soil factors that significantly influence soil composition. The selection of these factors is based on the Scorpion model, as presented in the preceding section. Climate, vegetation, relief, and soil classes data are considered as features within our predictive framework. The primary advantage of this approach lies in its potential to predict soil profiles for non-covered regions where soil samples are unavailable.

We propose the integration of Machine Learning and Quantum Computing techniques to significantly expedite the prediction process and reduce associated costs, while ensuring the accuracy of soil data predictions. In the subsequent subsections, we first present our classical architecture utilizing Recurrent Neural Networks (RNNs), followed by the quantum variant employing Quantum Recurrent Neural Networks (QRNNs).

3.1 Classical Recurrent Neural Networks Architecture

RNNs have proven to be highly effective in capturing sequential patterns and temporal dependencies in data [11]. By employing RNNs, we aim to leverage

their capacity to model soil profiles based on the influential factors identified in the Scropan model. Figure 1 shows the architecture of our proposed RNN model with one input layer, one output layer and multiple hidden layers.

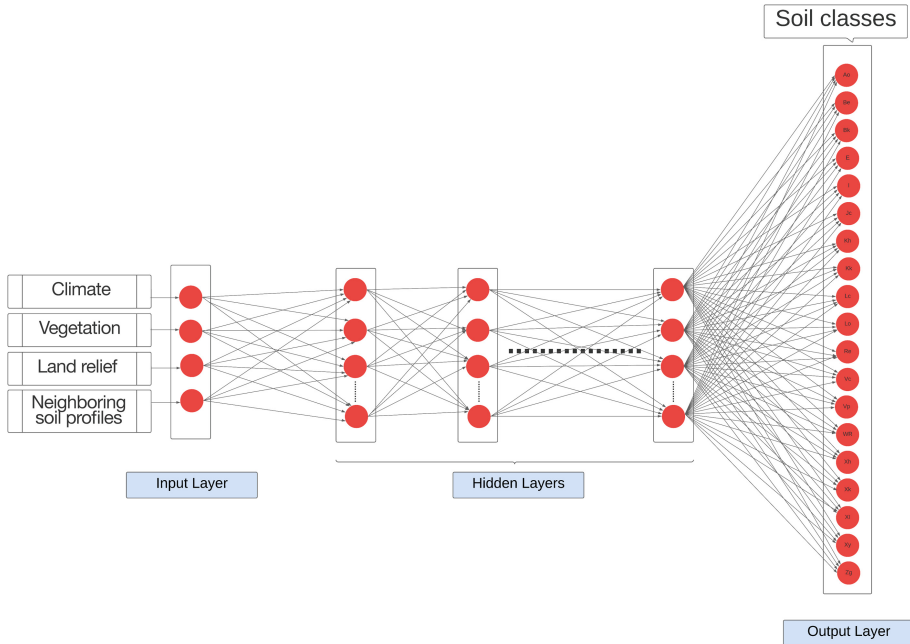


Fig. 1. The proposed RNN architecture for soil profiles prediction

The input layer incorporates data of the factors influencing soil composition. It is composed of the following four neurons:

- Climate: To obtain climate data, we adopted the widely used Köppen-Geiger climate classification system, which categorizes climates into five primary groups, each further subdivided based on seasonal precipitation and temperature patterns [12]. The five main climate groups are identified by the letters A (tropical), B (arid), C (temperate), D (continental), and E (polar). Each group and its subgroups are represented by a specific letter. In this classification system, all climates are assigned to a primary group denoted by the first letter. Additionally, climates in all groups except for polar are further categorized into seasonal precipitation subgroups indicated by the second letter. For climates in groups B, C, D, and E, the system also designates a temperature subgroup, indicated by the third letter for group B, C, and D climates, and by the second letter for group E climates. For example, a climate labeled as Cfb signifies an oceanic climate with mild winters and warm summers, with the letter b denoting the specific seasonal precipitation pattern.

- Vegetation: It is a fundamental component of the biosphere and interacts with other elements of the environment including soil. Vegetation plays a vital role in shaping the environment and supporting various ecosystems. It encompasses all types of plants, from small mosses and grasses to large trees and forests.
- Land relief: The slope and elevation of the land influence soil characteristics and the distribution of different soil types. Also known as terrain or topography, land relief refers to the variations in the elevation and surface features of the Earth’s land surface. It encompasses the arrangement of hills, mountains, valleys, plains, plateaus, and other physical landforms that shape the landscape.
- Neighboring soil profiles: The geographical space is divided into multiple regions, each defined by its unique shape, surface, latitude and longitude of its geometric center, climate, vegetation, topography, and soil profile. For each region, this neuron encompasses the information on the soil profiles of its neighboring regions if available.

Depending on the studied region, the output layer of our RNN can consist of as many nodes as there are soil profile classes. For illustration purposes, we represent 19 nodes in Fig. 1. We consider an architecture with at least one hidden layer. The exact number of hidden layers and nodes in each hidden layer are empirical parameters that should be fixed during experiments.

In the following subsections, we detail the integration of Quantum Computing with RNNs, and we unveil the quantum version of our architecture using QRNNs.

3.2 Fundamentals of Quantum Computing

In the realm of Quantum Computing, fundamental principles like superposition and entanglement take center stage, bringing forth a new era of lightning-fast calculations and parallel processing. This is achieved through cleverly designed algorithms that tackle intricate problems with remarkable efficiency. Key components in quantum computing include quantum bits, quantum gates, and quantum registers.

Quantum Bits. At the very heart of quantum computing lies the quantum bit, fondly known as the qubit. Unlike its classical counterpart, which can only embody states of either 0 or 1, a qubit exhibits the captivating phenomenon of superposition, allowing it to exist simultaneously in both states. The fundamental states of a qubit, conventionally denoted as $|0\rangle$ and $|1\rangle$, form the computational basis.

Mathematically, the state of a qubit $|\Psi\rangle$ is represented as $|\Psi\rangle = \alpha|0\rangle + \beta|1\rangle$, where α and β are complex numbers known as probability amplitudes. These probability amplitudes determine the likelihood of observing the qubit in states $|0\rangle$ or $|1\rangle$ upon measurement. In a broader context, a superposition of multiple states, symbolized as $|\Psi_1\rangle, \dots, |\Psi_n\rangle$, finds expression through $\sum_{i=1}^n \lambda_i |\Psi_i\rangle$, with λ_i being the complex coefficients denoting probability amplitudes.

Crucially, the squared sum of these amplitudes, $\sum_{i=1}^n \lambda_i^2 = 1$, ensures proper probabilities, rendering probabilistic predictions for each state within the superposition.

Quantum Registers. In the context of quantum computing, quantum registers are collections of qubits organized in a specific way to perform various computational tasks. They are analogous to classical registers in traditional computing, which store and manipulate data. The specific design and organization of quantum registers can vary depending on the quantum computer architecture and the task at hand.

Quantum Gates. Empowering quantum computation are the quantum gates, which are unitary operations that orchestrate transformations upon qubits, affecting their states. Among them are single-qubit gates, including the famous Pauli gates (X, Y, Z) for rotations and flips, and the versatile Hadamard gate that unlocks superposition. For more complex computations, controlled gates step into action, manipulating multiple qubits based on control qubits, leading to the phenomena of entanglement. Pivotal examples include the controlled-NOT (CNOT) gate and the Toffoli gate, instrumental in reversible classical computations and the simulation of classical logic circuits, paving the way for a quantum leap in computational power.

3.3 Quantum Recurrent Neural Networks Architecture

The combination of quantum computing and machine learning gives birth to Quantum Machine Learning, which is an emerging field that explores the application of quantum mechanics principles in machine learning algorithms. In this paper, we propose a DSM approach based on Quantum Recurrent Neural Networks (QRNNs). We believe that QRNNs present a promising approach for soil profile prediction in spatial regions, leveraging the principles of quantum mechanics to enhance the performance of traditional neural networks in this domain.

The fundamental advantage of QRNNs lies in their ability to exploit quantum computing's unique properties, such as superposition and entanglement, to handle large-scale and high-dimensional datasets more efficiently than classical ML algorithms [13]. Moreover, the integration of recurrent connections allows QRNNs to retain information from previous time steps or spatial locations, enabling the modeling of temporal trends and spatial correlations that are crucial in understanding soil attributes across landscapes. Figure 2 showcases our proposed Quantum Recurrent Neural Networks architecture for soil profiles prediction. It comprises three fundamental steps:

1. Data Loading: This essential step in Hybrid Quantum-Classical (HQC) approaches entails loading classical data into a quantum computer while also being associated with data encoding. The objective is to encode soil characteristics as qubits, enabling the QRNN to manipulate and process information in

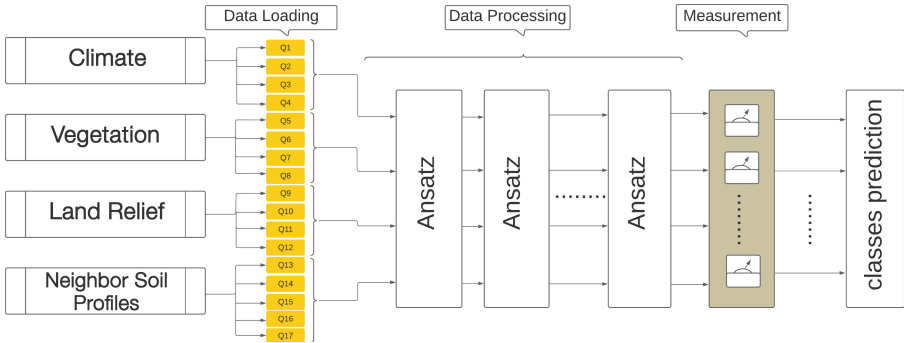


Fig. 2. QRNN architecture for soil profiles prediction

a quantum manner. The qubits represent specific soil composition influencing factor attributes, such as climate, vegetation, land relief, and neighboring soil profiles. For instance, considering the existence of 9 distinct climate classes in Türkiye, the climate information would be encoded using 4 qubits. This is achieved thanks to Basis Encoding, which is a technique used to represent classical information as quantum states with a specific basis or set of basis states [14]. It involves mapping classical bits (0 or 1) to corresponding quantum basis states, such as $|0\rangle$ and $|1\rangle$. It encodes an n-bit binary string x to an n-qubit quantum state $|x\rangle = |i_x\rangle$, where $|i_x\rangle$ is a computational basis state. For example, if $x = 1001$, the corresponding quantum state after basis encoding is $|1001\rangle$.

2. **Data Processing:** This stage enables manipulations on the qubits resulting from the previous step. These manipulations are carried out through quantum gates, which have equivalents to operations or functions used in classical neural networks. Quantum gates act upon the qubits to perform specific transformations. Their role in the QRNN is to provide non-linearity to the data, allowing for rapid parallel processing of information. The combination of these gates forms quantum circuits that describe the sequence of operations to be performed on the qubits. These circuits closely resemble the layers in traditional RNNs. Each one consists of adjustable parameters, often known as weights, which are fine-tuned to minimize the objective function. In our case, this function measures how close the predictions are to the actual soil profiles. This type of quantum circuits with parameters is also known as Ansatz [15]. Once the data is encoded, the quantum ansatz is applied to the qubits. The ansatz enables the capture of complex interactions among various soil characteristics. It functions as a data processing operation, transforming the initial state of qubits based on defined quantum relations, to represent long-term dependencies and non-linear relationships in sequential soil data.
3. **Measurement:** After the model is trained, quantum measurements are performed on certain qubits. Unlike the previous stages of the QRNN, where qubits were in superposition states, measurement compels the qubits to

“decide” on a definite state (either 0 or 1). Once the qubits are measured, the results are converted into classical bits, which can be interpreted to obtain the desired information about the predicted soil profile by the QRNN. Consequently, the model can classify soil types with extreme precision and speed based on the other considered features.

The QRNN architecture we propose for soil profiles prediction involves the encoding of soil data into qubits, processing using the quantum ansatz to capture long-term dependencies and non-linear relationships, memorizing previous states integrate contextual information, and measurement to obtain quantum predictions of soil profiles. This innovative approach provides a powerful methodology for predicting complex soil properties, facilitating more efficient and sustainable management of natural resources.

4 Experimental Results and Discussion

In this section, we present the results of our soil profiles prediction experiments conducted in Türkiye. We employed both classical Recurrent Neural Network (RNN) and Quantum Recurrent Neural Network (QRNN) implementations, utilizing the Python programming language. The quantum implementation was facilitated through the Qiskit library. It is important to note that, as an initial step in this study, the majority of experiments were conducted using the classical RNN approach.

Subsequently, in the following subsections, we introduce the datasets employed in our experiments and thoroughly present and discuss the achieved results.

4.1 Data Collection

To construct our dataset, we combined information from four distinct data sources. The soil profiles data were sourced from the FAO Digital Soil Map [16], which represents a digitized soil map of the world at a scale of 1:5 000 000. Within this dataset, we extracted 19 diverse soil profiles specifically pertaining to Türkiye: Orthic Acrisols (Ao), Eutric Cambisols (Be), Calcic Cambisols (Bk), Rendzina (E), Lithosol (I), Calcaric Fluvisols (Jc), Haplic Kastanozem (Kh), Calcic Kastanozem (Kk), Chromic Luvisols (Lc), Orthic Luvisols (Lo), Eutric Regosols (Re), Chromic Vertisols (Vc), Pellic Vertisols (Vp), Water Bodies (WR), Haplic Xerosols (Xh), Calcic Xerosols (Xk), Luvic Xerosols (XI), Gypsic Xerosols (Xy), and Gleyic Solonchaks (Zg).

For the climate data, we employed the World Map of the Köppen-Geiger Climate Classification [17]. Through this classification, we identified 9 distinctive climate classes existing in Türkiye, namely: Cold semi-arid (BSk), Humid subtropical (Cfa), Temperate oceanic (Cfb), Hot-summer Mediterranean (Cs), Warm-summer Mediterranean (Csb), Hot-summer humid continental (Dfa), Warm-summer humid continental (Dfb), Mediterranean-influenced hot-summer humid

continental (Dsa), and Mediterranean-influenced warm-summer humid continental (Dsb).

Moving on to vegetation, we relied on the FAO Global Land Cover Share Database [18] as a source of information, which offers insights into diverse vegetation types. Within the context of Türkiye, we identified the following 11 categories: Artificial Surfaces, Baresoil, Cropland, Grassland, Herbaceous vegetation, aquatic or regularly flooded, Shrubs Covered Areas, Snow and glaciers, Sparse vegetation, Tree Covered Areas, Waterbodies, and Others.

Finally, for land relief, we considered the FAO Terrain Slope Classes of the World [18], which distinguishes 8 classes that describe the inclination of the terrain within a given area. Each class represents a specific range of degrees of inclination.

Through the amalgamation of all the aforementioned data sources, a total of 136 554 distinctive regions emerged within Türkiye. Each of these regions possesses a unique combination of geographical position, climate, soil profile, vegetation, and land relief characteristics. To enhance the visualization of our findings, we created maps that display the data related to land relief, climate, and vegetation. Figure 3 illustrates these visualization outcomes for further reference.

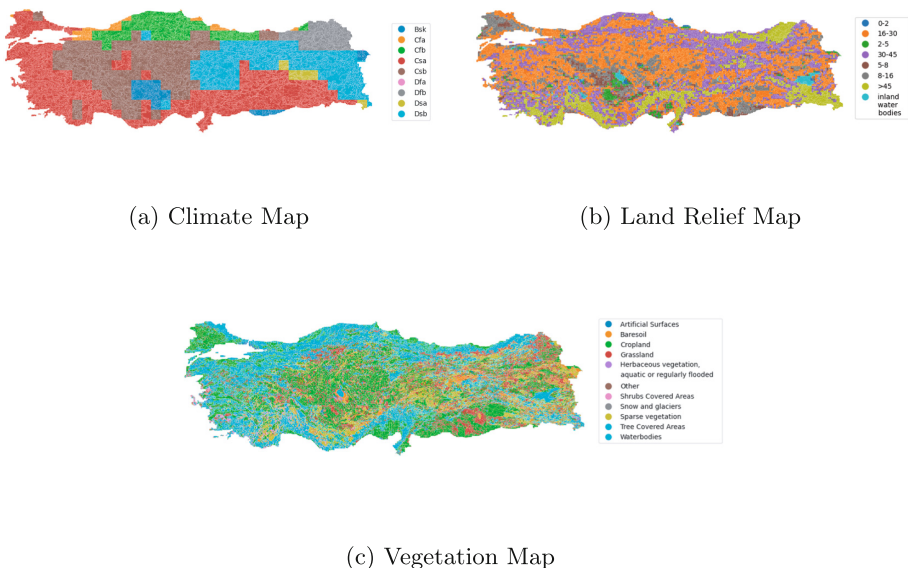


Fig. 3. Factors Influencing Soil Composition in Türkiye

4.2 Empirical Parameters Setting

Following extensive experiments, we configured our model with 3 hidden layers, each consisting of 64 neurons. The Rectified Linear Unit (ReLU) activation func-

tion was applied to these hidden layers. As for the output layer, we employed the Softmax activation function.

The data was partitioned, allocating 80% for the training set, resulting in 109,243 regions, and 20% for the test set, comprising 27,311 regions. Subsequently, 20% of the training data was utilized as a validation set. Table 1 provides a concise overview of the empirical parameter values.

Table 1. Best empirical parameters values

Parameter	Hidden layers	Neurons per hidden layer	Training set	Test set
Value	3	64	80%	20%

4.3 Soil Profiles Prediction Results

Figure 4a showcases the incomplete soil profiles data encompassing Türkiye, where 27 311 regions are depicted in white color to indicate missing information. These regions collectively cover an approximate total surface area of 140 000 km². Subsequently, in Fig. 4b, we present the outcomes of our soil profiles prediction approach. In this representation, each geographical region is associated with a corresponding soil profile selected from the 19 profiles listed in Subsect. 4.1.

The normalized confusion matrix, depicting the summary of predictions, is presented in Fig. 5. Notably, the majority of soil profiles have been accurately predicted, with 15 out of 19 achieving a rate higher than 80% on the matrix diagonal. However, there are 3 classes with prediction rates lower than 70%, namely: Water Bodies (WR), Gypsic Xerosols (Xy), and Gleyic Solonchaks (Zg).

The primary reason for the lower scores in these three profiles is their under-representation in our dataset. For instance, the Gypsic Xerosols class is present in only 21 regions out of 136,554 in Türkiye, resulting in an insufficient number of samples for the algorithm to generalize effectively, leading to a 0% prediction rate. Similarly, the other two profiles, Water Bodies and Gleyic Solonchak, have prediction rates of 63.93% and 58.82%, respectively, due to their limited presence in the dataset.

On the other hand, certain soil profiles demonstrate exceptionally high prediction rates, such as Luvic Xerosols (Xl) with 100% accuracy, Orthic Acrisols (Ao) with 99.89%, and Pellic Vertisols (Vp) with 98.68%. These impressive results are a testament to the model's capability in effectively predicting soil profiles covering vast geographical regions.

Figure 6a presents the accuracy curve of our model, and Fig. 6b illustrates the loss function curve. Notably, our approach attains an impressive overall accuracy of 0.91 and a loss value of 0.28. These compelling metrics serve as strong indicators of the effectiveness of our proposal and the commendable performance it can achieve. The high accuracy and relatively low loss signify the model's proficiency in accurately predicting soil profiles, thus bolstering confidence in the reliability of our methodology.

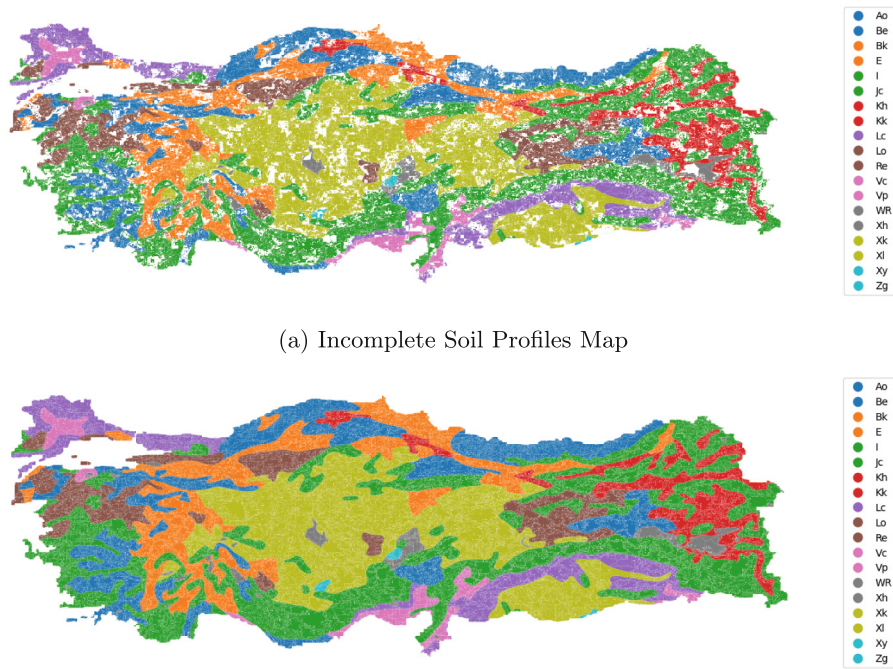


Fig. 4 Soil Profiles Map of TürkİYE

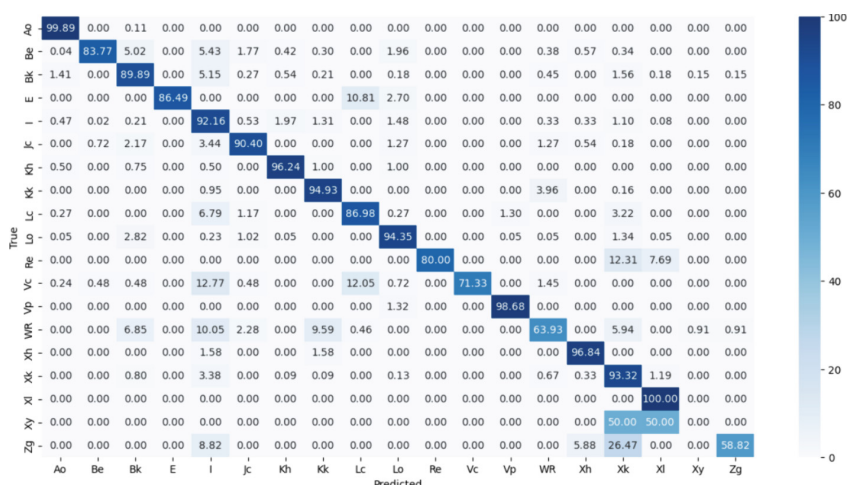


Fig. 5. Confusion matrix of soil profiles predictions

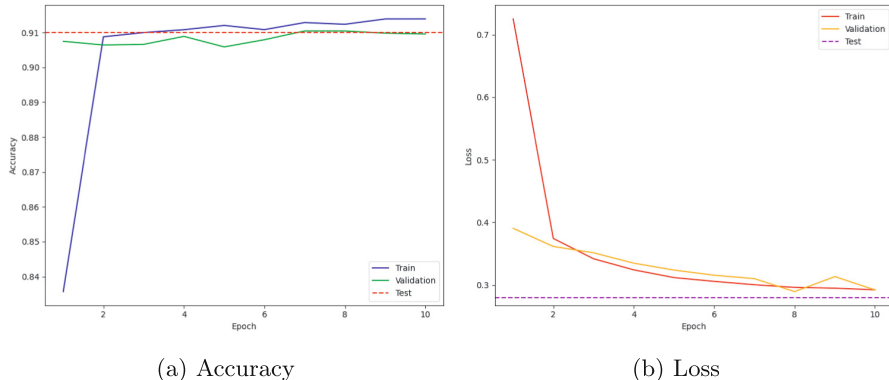


Fig. 6. Evaluation of the model performance based on accuracy and loss function

5 Conclusion and Future Directions

In this article, we introduced a novel approach to Digital Soil Mapping using Quantum Recurrent Neural Networks. We have demonstrated the power and potential of RNN in accurately predicting complex soil profiles. Through experiments, we have shown that our approach can capture long-term dependencies and non-linear relationships within soil data. We believe that the combination of quantum computing principles and recurrent neural networks opens up new horizons for addressing complex soil mapping challenges, providing valuable insights into soil properties and facilitating more sustainable resource management practices. The integration of quantum computing principles empowers the QRNN model to harness quantum parallelism, leading to accelerated computations and superior prediction capabilities. As the field of quantum computing continues to evolve, the potential for quantum-enhanced machine learning methods like QRNN to revolutionize soil science and environmental studies is truly exciting.

While this study showcases the promise of QRNN for soil profile prediction, there are exciting avenues for further exploration. Conducting extensive experiments with the QRNN model on larger datasets and comparing the outcomes with the classical RNN model will shed more light on its effectiveness across various scenarios. Additionally, investigating the potential of other hybrid approaches that combine classical and quantum algorithms could unlock even greater predictive power.

References

1. Belkadi, W.H., Drias, Y.: Advancements in digital soil mapping: from data acquisition to uncertainty estimation - a comprehensive review. In: Drias, H., Yalaoui, F., Hadjali, A. (eds.) AID 2022. CCIS, vol. 1852, pp. 162–177. Springer, Singapore (2023). https://doi.org/10.1007/978-981-99-4484-2_13
2. Drias, H., Drias, Y., Khennak, I.: A new swarm algorithm based on orcas intelligence for solving maze problems. In: Rocha, Á., Adeli, H., Reis, L.P., Costanzo, S., Orovic, I., Moreira, F. (eds.) WorldCIST 2020. AISC, vol. 1159, pp. 788–797. Springer, Cham (2020). https://doi.org/10.1007/978-3-030-45688-7_77
3. Drias, H., Drias, Y., Houacine, N.A., Bendimerad, L.S., Zouache, D., Khennak, I.: Quantum OPTICS and deep self-learning on swarm intelligence algorithms for COVID-19 emergency transportation. Soft. Comput. **27**, 13181–13200 (2023). <https://doi.org/10.1007/s00500-022-06946-8>
4. McBratney, A.B., Santos, M.L.M., Minasny, B.: On digital soil mapping. Geoderma **117**(1), 3–52 (2003). [https://doi.org/10.1016/S0016-7061\(03\)00223-4](https://doi.org/10.1016/S0016-7061(03)00223-4)
5. Dobos, E., Carre, F., Hengl, T., Reuter, H., Toth, G.: Digital soil mapping as a support to production of functional maps, vol. 22123 (2006)
6. Belkadi, W.H., Drias, Y., Drias, H.: A data warehouse for spatial soil data analysis and mining: application to the Maghreb region. In: Abraham, A., Plana, S., Casalino, G., Ma, K., Bajaj, A. (eds.) ISDA 2022. LNNS, vol. 716, pp. 160–170. Springer, Cham. (2023). https://doi.org/10.1007/978-3-031-35501-1_16
7. Padarian, J., Minasny, B., McBratney, A.B.: Using deep learning for digital soil mapping. Soil **5**(1), 79–89 (2019)
8. Wadoux, A., Minasny, B., McBratney, A.B.: Machine learning for digital soil mapping: applications, challenges and suggested solutions. Earth-Sci. Rev. **210** (2020). <https://doi.org/10.1016/j.earscirev.2020.103359>
9. Cong, I., Choi, S., Lukin, M.D.: Quantum convolutional neural networks. Nat. Phys. **1**(5), 1273–1278 (2019). <https://doi.org/10.1038/s41567-019-0648-8>
10. Oh, S., Choi, J., Kim, J.: A tutorial on quantum convolutional neural networks (QCNN). arXiv (2020). <https://doi.org/10.48550/arXiv.2009.09423>
11. Yu, Y., Si, X., Hu, C., Zhang, J.: A review of recurrent neural networks: LSTM cells and network architectures. Neural Comput. **31**(7), 1235–1270 (2019). https://doi.org/10.1162/neco_a_01199
12. Beck, H., Zimmermann, N., McVicar, T., Vergopolan, N., Berg, A., Wood, E.F.: Present and future Köppen-Geiger climate classification maps at 1-km resolution. Sci. Data **5**, 180–214 (2018). <https://doi.org/10.1038/sdata.2018.214>
13. Li, Y., et al.: Quantum recurrent neural networks for sequential learning. arXiv preprint (2023). <https://doi.org/10.48550/arXiv.2302.03244>
14. Schuld, M., Killoran, N.: Quantum machine learning in feature Hilbert spaces. Phys. Rev. Lett. **122**(4), (2019). <https://doi.org/10.1103/PhysRevLett.122.040504>
15. Verdon, G., Broughton, M., Biamonte, J.: A quantum algorithm to train neural networks using low-depth circuits. arXiv (2019). <https://doi.org/10.48550/arXiv.1712.05304>
16. FAO Digital Soil Map of the World. <https://www.fao.org/soils-portal/en/>. Accessed 4 June 2023
17. World Maps Of The Köppen-Geiger Climate Classification. <https://datacatalog.worldbank.org/search/dataset/0042325>. Accessed 4 June 2023
18. FAO Map Catalog. <https://data.apps.fao.org/map/catalog/>. Accessed 4 June 2023



Q-CODA: Co-designing Quantum Codes and Architectures for Hardware-Aware Quantum Error Correction

Pratik Thanharate¹ and Anurag Thanharate²

¹ SUNY, Binghamton, NY, USA

pthanth1@binghamton.edu

² University of Missouri, Kansas City, USA

adtmv7@mail.umkc.edu

Abstract. Quantum computers promise profound scientific advances, but their practical realization is impeded by ubiquitous errors. Quantum error correction (QEC) provides techniques to detect and correct errors, enabling reliable quantum computation. However, conventional QEC codes require prohibitive physical qubit overheads. This work introduces customized protocols to reduce QEC resource costs tailored for near-term superconducting hardware. We propose code constructions including optimized surface code geometries and concatenated inner code layers to improve qubit efficiency. A comprehensive noise modeling methodology is outlined to capture complex multi-qubit error processes using Lindblad master equation simulations of device Hamiltonians. The realistic device noise model is essential for evaluating tailored QEC protocols. Hardware-aware decoding algorithms based on recurrent neural networks can potentially further suppress logical faults by avoiding oversimplified assumptions. We introduce a modeling framework to quantify overhead reductions from our coordinated techniques. While considerable research remains to realize practical solutions, this work delineates promising directions by bridging hardware, software, and theory via code co-design, accurate noise models, and quantified gains. The tailored techniques offer the potential to progress toward viable fault tolerance in noisy intermediate-scale quantum devices.

Keywords: QEC · Fault Tolerant · Quantum Computing · Code Co-design · Quantum Error Correcting Codes · Resource Efficiency · Superconducting Qubits · NISQ devices · Hardware-Aware · Quantum Code

1 Introduction

The promise of quantum computing has captured widespread interest and investment from the scientific community, governments, and technology industry lead-

P. Thanharate—IEEE Member.

A. Thanharate—Senior IEEE Member.

ers. However, turning the immense possibilities into reality requires overcoming daunting challenges. Quantum systems are exponentially more fragile than conventional computing hardware. Myriad noise sources easily corrupt information encoded in intricate quantum states. Without new techniques to detect and correct these ubiquitous errors, quantum computations will swiftly degrade into meaningless noise.

QEC provides a path to mitigate errors and conduct reliable quantum operations. However, conventional techniques demand impractical levels of resources. To advance quantum computing from promise to reality necessitates optimized error correction protocols tailored to the constraints of current quantum hardware, known as Noisy Intermediate-Scale Quantum (NISQ) devices. Quantum information encoded in coherent superpositions of 0 and 1 can easily become corrupted from unwanted interaction with the environment or control flaws, resulting in noise-induced bit flips. Fragile quantum entanglement that provides an advantage also makes systems highly sensitive to perturbations. Without mitigating these ubiquitous errors, noisy quantum computations will swiftly degrade into meaningless classical mixtures.

QEC provides techniques to detect and correct errors, enabling reliable quantum computation even on noisy hardware. By encoding quantum information redundantly in carefully designed subspaces, errors can be identified and removed while preserving the encoded data. This opens a path to performing arbitrarily long quantum computations to arbitrary accuracy, provided errors remain below a threshold value. Constructing quantum error-correcting codes and associated fault-tolerant architectures is, therefore, critical for unlocking the profound capabilities of robust, general-purpose quantum computers. Recent years have witnessed tremendous advances in prototype quantum processors. Systems are rapidly approaching the scale required to demonstrate QEC practically. Superconducting quantum processors with dozens of qubits integrated into a chip now lead the charge. However, despite this remarkable progress, existing error correction protocols require a prohibitive overhead in additional physical qubits to reach the extremely low logical error rates needed for fault tolerance. Realizing practical error-corrected quantum computation demands more efficient codes tailored to the constraints of near-term hardware [1].

This work proposes techniques to optimize QEC tailored for near-term superconducting devices. We introduce code constructions to enhance efficiency and detailed noise models capturing complex processes in superconducting qubits. Quantifying resource savings is also critical to assess the real-world viability of our tailored techniques. Bridging across hardware, software, and theory via co-design, realistic models, and overhead analysis offers the potential to minimize costs. This cross-disciplinary approach aims to enable viable error correction in the Noisy Intermediate Scale Quantum (NISQ) era. There remains substantial research to realize solutions robust enough for noisy prototypes. However, by optimizing protocols for specific qubit technologies, we pave the path toward reliable, large-scale quantum computation.

1.1 Quantum Errors and Their Impact

Quantum information is subject to various error mechanisms that must be addressed. Relaxation errors occur when qubit states decay from higher to lower energy levels. Dephasing induces loss of quantum coherence between states without energy change. These effects are caused by unintended qubit interactions with the environment. Gate operations can also introduce errors by under or over-rotating qubit states. Crosstalk causes couplers between qubits to induce unwanted entanglement. Loss errors arise when qubit states leak out of the computational subspace. These quantum noise processes limit the number of sequential operations that can be performed coherently, known as the coherence time. Computational depth is constrained by coherence times, which must be exceeded by error correction frequencies to avoid information loss. Current superconducting processors have coherence times on the order of 10–100 μ s.

Gate errors arise from imperfect control pulses and calibration limitations. Typical gate error rates are on the order of 0.1–1%. Long algorithms require extremely low error rates per gate for accurate results. QEC codes can detect and correct a certain rate of errors, but higher error rates exceed code capacity. Errors compound rapidly in quantum systems due to the exponential state space. The information encoded in hundreds of faulty qubits will quickly become corrupted without error suppression. Mitigating errors to extend coherence times and reduce gate error rates is, therefore, critical. Encoding logically in error-correcting codes can detect and reverse discrete errors like bit flips. However, correlated noise from crosstalk or environmental coupling can defeat code assumptions and destroy encoded information. Realistic noise modeling is needed to evaluate code performance properly. Without sufficient error mitigation and encoding, computations involving more than a few dozen qubits will succumb to noise. QEC provides a path forward, but existing codes require large resource overheads. Efficient QEC protocols tailored to near-term hardware constraints are essential to progress beyond small demonstrator systems toward robust, fault-tolerant quantum computation.

1.2 Error Correction Code Design Advancements

Tremendous progress has been made in developing QEC codes and fault tolerance techniques over the past decades. However, realizing practical error-corrected quantum computation will require further improvements tailored to near-term hardware capabilities. This demands a multi-faceted approach combining refinements across all layers of the quantum computing stack. At the code level, overhead remains a major challenge. Topological codes like the surface code currently provide the most promising path to fault tolerance, but the resource costs are still daunting. For example, some estimates suggest a surface code quantum computer would require over a billion physical qubits to execute useful algorithms reliably. Reducing this overhead is imperative to make error correction viable in NISQ devices.

Several approaches to improve code efficiency show promise. Code deformation to remove unnecessary qubits has the potential to reduce surface code overhead significantly. Concatenation with specialized inner code layers could further optimize protection. Hardware-aware decoding algorithms that account for actual noise models may also decrease qubit costs. Detailed analysis is needed to quantify potential gains from these code refinements. At the hardware level, increasing qubit quality through advances in materials, fabrication, and controls will boost error correction prospects. Existing superconducting qubit platforms are rapidly maturing, with average gate fidelities now surpassing 99.9% in some devices. Further enhancing coherence properties and developing qubits with built-in noise protection could greatly ease error correction burdens. Increasing connectivity for 2D array fabrication is another critical milestone. Bridging between hardware and software, detailed noise characterization via techniques like quantum process tomography provides invaluable data for optimizing codes. Physics-based noise modeling can replicate non-Markovian and correlated error processes that impact multi-qubit codes. Validated simulators allow testing code improvements against real system performance to maximize robustness.

Finally, at the algorithm level, compiling techniques to optimize circuit mappings and gate sets for specific codes and hardware will help minimize resource overheads. Co-designing algorithms and error correction strategies will be essential to run meaningful applications efficiently. Attacking the fault tolerance challenge from all of these perspectives will accelerate progress beyond today's small demonstrator systems toward the goal of practical quantum computation. Continued research and innovation in error-correcting codes, hardware, modeling, and algorithms will pave the path forward through the era of NISQ devices toward robust and ubiquitous quantum computing.

1.3 Existing QEC Techniques

Various quantum error correcting codes and fault tolerance techniques have been developed, establishing the theoretical feasibility of error-protected quantum computation. The most prominent code family is stabilizer codes, which detect errors by measuring multi-qubit operators (stabilizers) that leave the code space invariant. Examples include Shor's 9-qubit code, surface codes, and color codes. Concatenated code structures further boost error suppression. These codes can protect arbitrary logical qubits by encoding each in a subspace of multiple physical qubits. If errors occur independently on subsets of physical qubits at low enough rates, they can be identified during stabilizer measurements and corrected by flipping appropriate qubits. This allows for recovering the original quantum information.

However, realistic physical errors often have spatial and temporal correlations that violate code assumptions. Correlated noise arising from effects like crosstalk and coupling to defects can accumulate over multiple code cycles and lead to logical failure modes. Codes must, therefore be evaluated under representative hardware noise models. Techniques like energy gap protection, dynamically corrected gates, and flag fault tolerance protocols help mitigate correlated errors.

But substantial overhead is still required to meet fault tolerance thresholds, especially for concatenated codes. State-of-the-art codes suggest surface codes likely provide the most viable path but still require prohibitive qubit overhead.

1.4 Challenges for Practical Implementation

While QEC is theoretically viable, near-term implementation faces steep challenges. Current superconducting quantum processors possess limited qubit numbers, connectivity, and coherence times. This restricts demonstrating codes beyond small stabilizer codes. To implement surface codes, processors require expanded qubit arrays with 2D connectivity. However, even a surface code logical qubit would demand thousands of physical qubits, given today's error rates. Managing such large entangled states poses control and design hurdles.

Hardware must therefore improve along multiple axes to become compatible with fault-tolerant codes. Increasing physical qubit quality and gate fidelities will reduce baseline error rates. Expanding to planar grid connectivity will enable 2D code layouts. Packaging and controls must scale while maintaining coherence. On the software side, decoding complex codes remains highly computationally demanding. Performing decoding within surface code cycle time constraints will require algorithmic optimizations leveraging emerging classical hardware like FPGAs. Most pressingly, reducing qubit and time overheads is imperative to make error correction imaginable with near-term devices. This necessitates co-designing solutions across the hardware and software stack.

1.5 Research Objectives and Outline

The overarching focus of this study is to devise targeted strategies for tailoring and optimizing QEC protocols, thereby minimizing resource overheads in the context of near-term quantum hardware. In pursuit of this objective, we delineate a cross-disciplinary framework that is finely attuned to the intricacies of superconducting qubits, encompassing the following key dimensions:

- 1. Code Constructions for Overhead Reduction** - A fundamental aspect of our approach involves innovating novel code constructions that harness the unique attributes of superconducting qubits. These customized codes aim to curtail the burdensome resource requirements, ultimately paving the way for enhanced efficiency in error correction.
- 2. Realistic Noise Characterization and Modeling** - To achieve robust error correction, an accurate understanding of noise is imperative. We introduce a comprehensive methodology for characterizing and modeling noise in superconducting qubits, transcending conventional simplifications and incorporating nuanced influences to ensure fidelity in our error correction strategies.
- 3. Resource Analysis Framework** - A pivotal aspect of our investigation entails the quantification of resource savings engendered by our tailored strategies. We introduce a versatile framework that systematically assesses

the efficiency gains achieved through the orchestrated interplay of our multi-faceted advancements.

By harmoniously amalgamating these meticulously designed enhancements across hardware, software, and theoretical underpinnings, our overarching ambition is to effectuate a substantial reduction in resource overheads. This holistic approach endeavors to render error correction viable and efficacious in the realm of NISQ devices. The ensuing sections expound upon the finer intricacies of these proposed contributions:

- 1. Optimized Code Parameters and Geometries** - We propose optimizing surface code parameters such as code distance and lattice geometry using a greedy algorithm to remove qubits along the lattice edges and corners selectively. This deformation minimizes overhead while retaining the code's error correction thresholds and properties. We analyze fault tolerance thresholds under these optimized parametrizations.
- 2. Realistic Noise Modeling Methodology** - Our noise modeling approach employs physics-based simulations of qubit device Hamiltonians using the Lindblad master equation formalism [2]. The simulator incorporates non-Markovian noise features, including relaxation, dephasing, crosstalk, and leakage. We extract key noise parameters like relaxation times T_1 , T_2 , gate error rates, and spatial correlations to construct realistic noise models.
- 3. Framework to Quantify Resource Savings** - Central to our approach is introducing a versatile framework that systematically quantifies the resource savings engendered by our orchestrated strategies, providing a tangible measure of their real-world utility.

The culmination of this tailored, co-designed endeavor holds the promise of ushering in an era of practical error-corrected quantum computation.

2 Related Work

Authors in [3] demonstrate a proof-of-concept QEC protocol using three beryllium ion qubits in a linear trap. By encoding a qubit across three physical qubits, detecting errors, and applying conditional recovery operations, they can improve state fidelity compared to no error correction. This shows the potential feasibility of scalable fault-tolerant quantum computation. E. A. Sete, et al. in [4] proposes a functional architecture for scalable superconducting quantum computing using transmon and fluxonium qubits arranged in a planar lattice. It introduces tuned DC-controlled two-qubit gates between the transmon and fluxonium qubits, enabling a universal gate set. This architecture allows the testing and optimization of quantum algorithms on a scalable platform.

In the dynamic realm of software development, Intelligent-Monitor [5] revolutionizes DevOps with real-time data, analytics, and AI for efficient issue resolution. The integration of Quantum Computing could provide enhanced security

and processing capabilities, offering a proactive solution to the evolving challenges within complex and ever-changing DevOps environments. In our other research [6], Addressing challenges in cloud-based testing, this paper introduces a distributed testing framework, reducing testing time by 18.75%, and a realistic simulation framework, enhancing accuracy. Integrating Quantum Computing could amplify testing capabilities, offering unparalleled performance and security insights in the dynamic landscape of cloud technologies, fostering reliability and innovation.

Authors in [7] paper proposes an approximate QEC scheme to boost the computational power of near-term quantum computers. It uses a greedy surface code decoding algorithm implemented in superconducting Single Flux Quantum (SFQ) logic to decode syndromes in real-time, avoiding exponential latency overheads of offline decoding. This expands the simple quantum volume, though it sacrifices some accuracy. SFQ implementation meets area and power constraints with fast decoding latency under 20ns. D. Copsey, et al. in [8] proposes a scalable silicon-based architecture for quantum computing using phosphorus atoms in silicon as qubits. It analyzes quantum wires for communication, finding swapping channels don't scale due to accumulating errors. Long-distance teleportation channels are proposed as a more scalable alternative. The paper also examines the layout and communication costs of QEC circuits under 2D fabrication constraints.

Authors in [9] shows that using qudits (d -dimensional quantum systems) with dimensionality satisfying $d \geq k + 1$, where k is the number of qudit connections, allows efficient implementation of multi-qubit gates. This relation enables substituting ancillas with higher qudit levels, significantly reducing the number of operations and circuit depth for realizing key quantum gates. The scheme is important for near-term noisy quantum devices to realize algorithms and error correction with fewer interactions between qubits. Authors in [10] introduces a multi-level reset protocol to remove leakage from higher qubit states in superconducting qubits. It is tested using the bit-flip stabilizer code, showing reset mitigates leakage-induced correlated errors. Reset improves logical error suppression, enhancing scaling with qubit numbers. The results demonstrate reset is critical for QEC by removing problematic correlated errors caused by leakage.

Authors in [11] present a low-latency hardware decoder for fault-tolerant quantum computers called AFS. It exploits sparsity in quantum error syndromes to compress data transmission, reducing bandwidth requirements. The decoder architecture shares resources across logical qubits to improve scalability while maintaining accuracy and performance. And authors in [12] presents Accurate, Fast, and Scalable error decoding algorithm (AFS), a hardware decoder for fault-tolerant quantum computers that is accurate, fast, and scalable. It uses a Union-Find decoding algorithm and a pipelined design. Conjoined-decoder architecture reduces hardware costs by sharing components across qubits. Syndrome Compression exploits sparsity to reduce syndrome transmission bandwidth. The research [13] addresses security testing and vulnerability detection within DevSecOps, emphasizing the need for automated tools. Our Python-based

solution comprises an automated security testing tool for the software development lifecycle and a vulnerability detection tool using Genetic Algorithm optimization. Simulated results validate its effectiveness, achieving a fitness score of 0.982. Automation fortifies software security, and our approach offers a promising avenue for advancing automated security testing and vulnerability detection within the DevSecOps paradigm. Integrating emerging technologies like Quantum Computing could further enhance the resilience of security practices in the ever-evolving landscape of software development.

Khan, Arif Ali, et al. in [14] present a systematic literature review on software architecture for quantum computing systems. It investigates architectural processes, modeling notations, patterns, tools, and challenges. The results show quantum software architecture is an emerging area leveraging classical software architecture concepts but require customization to address quantum-specific needs. Lau, Jonathan Wei Zhong, et al. in paper [15] reviews the current state of NISQ quantum computing. It gives an overview of the leading quantum computing platforms and algorithms that show promise for near-term quantum advantage. The concepts are explained accessibly for non-experts to provide context on recent developments and the timeline for quantum computing.

Authors in [16] review benchmarking techniques for evaluating the performance of quantum computers. It summarizes physical metrics like qubit number, gate fidelities, and coherence times. It discusses aggregated benchmarks like quantum volume and algorithmic qubits that aim to quantify overall performance. It also covers application benchmarks that test performance on real problems. The goal is to provide a systematic overview of quantum benchmarking approaches. Authors in [17] reviews a reference model for distributed quantum computing called D-NISQ. The model enables current NISQ devices to collaboratively solve problems by splitting the problem into sub-problems, solving each sub-problem on a quantum device, and fusing the results. It comprises four layers: decomposition, classical-to-quantum, quantum computation, and quantum information fusion. The model is tested on distributed implementations of Grover's algorithm and Grover's Adaptive Search. Experiments show that distributed algorithms have higher success rates than non-distributed versions, demonstrating D-NISQ can increase reliability and reduce noise. The paper introduces an important architecture for distributed quantum computation to overcome NISQ limitations.

J. D. Guimarães and C. Tavares in [18] propose a layered architecture for quantum error mitigation techniques to improve the fidelity of quantum computations on noisy intermediate-scale quantum computers. The authors implement a combination of techniques like zero noise extrapolation, randomized compiling, and dynamical decoupling in a quantum simulation of the Heisenberg model, achieving a 2.8x improvement in fidelity. B. McDonough et al. in [19] presents an automated software framework for quantum error mitigation using probabilistic error reduction. It combines Pauli noise tomography for noise characterization with partial inversion of the noise model to reduce overhead. The software

automates circuit generation, execution, and analysis to obtain error-mitigated results using extrapolation.

The research [20] focuses on enhancing health data management through ZeroTrustBlock, the emergence of quantum computing introduces potential opportunities and challenges. Quantum technology's computational power could impact cryptography methods employed in blockchain systems, necessitating adaptation for post-quantum security. Integrating quantum-resistant algorithms into ZeroTrustBlock would fortify its resilience against future quantum threats. However, the practical implementation and alignment of quantum technology with blockchain frameworks remain areas for exploration, requiring careful consideration of quantum-safe strategies in the evolving landscape of health information security.

While these works provide valuable foundations, realizing the immense potential of quantum computing necessitates continued research into efficient and robust error correction techniques compatible with near-term hardware constraints. This motivates the current paper's exploration of customized protocols to reduce resource overheads for quantum error correction in the NISQ era. The subsequent section introduces our core technical approach encompassing code constructions, comprehensive noise modeling, and resource analysis to realize viable solutions on noisy intermediate-scale quantum devices.

3 Proposed Techniques and Methodology

This research introduces new techniques for QEC code design, noise characterization, and mitigation strategies. Advanced codes and mitigation will be essential to achieving the low logical error rates required for fault-tolerant quantum computation. We propose code modifications to reduce overhead, tailored concatenation schemes, optimized decoding algorithms, and hardware-aware noise models. Detailed analysis and simulations will be required to evaluate the performance of these proposed techniques fully.

3.1 Code Constructions to Reduce Overhead

A major challenge for QEC is the large resource overhead required by codes like the surface code. We propose code modifications to reduce this overhead while maintaining fault tolerance thresholds. One approach constructs deformable surface code lattices by strategically altering the geometry. For a distance d surface code on a square lattice, the number of qubits is $O(d^2)$. By removing qubits along the edges and corners as shown in Algorithm 1, the lattice can conform to the limited connectivity of actual devices with $O(d^{1.5})$ qubits, providing up to a \sqrt{d} reduction in overhead. However, the modified lattice must be analyzed using the simulation framework to ensure it retains a threshold for fault-tolerant error correction.

Concatenating the surface code with small, specialized inner codes is another proposed technique to improve qubit efficiency. Tailored inner codes, like 4-qubit

stabilizer codes, require few additional qubits but can enhance protection against specific likely error modes. For instance, inner codes optimized for dephasing could supplement the surface code. Concatenated code thresholds can surpass individual code limits, but realizing this advantage depends on details of the inner code, decoding, and noise model.

Algorithm 1. Surface Code Lattice Deformation

```

MST  $\leftarrow$  MinimumSpanningTree(G)
procedure DEFORMLATTICE(L, D, MST)
    Input: L - original square lattice
    Input: D - desired distance
    Input: MST - minimum spanning tree of G
    for e in L edges do
        if e not in MST then
            Remove e from L
        end if
    end for
    Trim L to distance D
    return Deformed lattice L'
end procedure

```

The minimum spanning tree MST is constructed once from the connectivity graph G before calling the deformation procedure. An alternative approach is to directly construct the deformed lattice by starting from the MST edges rather than removing edges. This might be more efficient. The trim L to distance D step reshapes the lattice geometry to enforce the desired code distance D, since removing edges likely altered the distances between vertices. This shapes the lattice back into a valid error correction code with the right properties.

The algorithm takes as input the original square lattice L, the desired distance D for the deformed lattice, and the device connectivity graph G. It iterates through each edge e in the original lattice L. For each edge, it checks if that edge is part of the minimum spanning tree of the connectivity graph G. The minimum spanning tree is a subset of the edges of G that connects all vertices in G with the minimum total edge weight. If an edge e is not part of the minimum spanning tree of G, it means that the edge can be removed while still maintaining connectivity between all vertices. So, any such edges are removed from the lattice L. After iterating through all edges, the lattice L will have had extraneous edges removed. But its geometry may not match the desired distance D yet. So as a final step, the lattice is trimmed to force it to have the correct distance D. The minimum spanning tree of G essentially provides the most efficient set of edges to maintain connectivity between all qubits based on their connectivity and spacing on the physical device. Any edges not critical for connectivity can be safely removed to deform the lattice without impacting error correction performance. Trimming the lattice finalizes the deformation process to create a lattice L' with the topology matching the device connectivity G as closely as possible while

still maintaining the needed distance D for the desired level of error correction. This deformed lattice L' will have fewer physical qubits than the original square lattice, reducing resource overhead. The performance impact of this deformation needs to be analyzed by simulations, which is left for future work.

The algorithm illustrates a high-level algorithm for deforming the standard square surface code lattice by selectively removing edges to fit the target device topology better. Optimized decoding algorithms provide another avenue to reduce overhead. Most decoders make simplifying assumptions about independent errors. We propose developing decoders that explicitly leverage realistic device noise features like correlations, context dependence, and non-Markovian effects. Advanced decoders informed by the noise model can potentially maintain threshold fidelity with fewer physical qubits.

3.2 Noise Characterization and Modeling

To construct optimized error correction protocols, accurate noise modeling for superconducting qubits is imperative. We propose a comprehensive methodology for characterizing and simulating noise processes including relaxation, dephasing, crosstalk, and leakage. The modular approach incorporates the following steps:

1. Perform quantum process tomography on the device to extract initial noise parameters like T_1 , T_2 , gate fidelities, and process matrices.
2. Develop physics-based Hamiltonian simulations of the qubit system. For transmon qubits, this involves modeling the Hamiltonian [21]:

$$H = 4E_C(\hat{n} - n_g)^2 - E_J \cos \hat{\phi}$$

Where E_C is the charging energy, E_J is the Josephson energy, \hat{n} is the Cooper pair number operator, and $\hat{\phi}$ is the superconducting phase operator.

3. Simulate the device Hamiltonian while systematically varying parameters based on calibration data. Compare the simulated noise with tomography experiments.
4. Iteratively refine the noise model by tuning the simulator to match additional benchmarking results. This provides a validated model capturing complex noise features.

The validated simulator can then incorporate the optimized noise model to evaluate error correction protocols. By co-designing the noise model and correction codes, performance can be maximized for the target hardware. Key advantages of this approach include:

- Captures multi-qubit correlations absent in simplistic models
- Incorporates non-Markovian noise processes through time-dependent simulations
- Models device-specific noise features derived from physics principles
- Enables realistic assessment of code performance prior to hardware demonstration

Careful noise modeling is critical for developing error-corrected quantum architectures compatible with emerging NISQ technologies [22]. Our methodology leverages physics simulations, calibration data, and modular co-design to construct accurate noise models tailored to superconducting qubits. This will facilitate rigorous evaluation of optimized code constructions in future work. We propose an iterative noise model refinement algorithm to systematically tune the simulator to match empirical device noise data:

Algorithm 2. Iterative Noise Model Refinement Algorithm

```

procedure REFINEMODEL
    Perform device tomography for initial noise
    Simulate device Hamiltonian  $H$ 
    Extract noise parameters from  $H$ 
    Tune simulator to match tomography
    for range of parameters do
        Vary  $H$  simulator parameters
        Compare simulated noise to experiments
        Update noise model
    end for
    return Optimized noise model
end procedure
  
```

Algorithm 2 provides a high-level overview of the iterative approach to refine the noise model. The process begins by performing quantum process tomography on the target device to extract initial noise parameters. Next, the Hamiltonian is simulated and tuned to align with the tomography results. Then, the key step involves sweeping across a range of parameters in the simulator while comparing the simulated noise to additional benchmarking experiments. Any discrepancies are used to update the noise model parameters accordingly. By incrementally recalibrating the model to minimize discrepancies across diverse experiments, the model accuracy improves. This iterative refinement procedure results in a fully calibrated noise model capturing the nuances of the particular quantum hardware. The modularity enables adapting the technique to different qubit platforms. The validated simulator can then reliably evaluate code performance. This allows systematic refining of the noise model for code testing. Accurate models are critical for evaluating performance. The modular simulation framework models the encoding, decoding, error propagation, stabilization, and logical error rates. It flexibly incorporates different codes, decoders, devices, and noise models for characterization. Detailed code performance evaluation is left to future work.

3.3 Noise Mitigation Techniques

In addition to QEC, we propose using noise mitigation techniques to reduce physical error rates. Combining these approaches can further improve logical fault

tolerance thresholds. We identify control methods to mitigate dominant noise processes in superconducting qubits. Optimized pulse shapes can reduce leakage and crosstalk. Dynamical decoupling sequences tailored to device parameters suppress decoherence. Operating points are tuned based on energy relaxation and excitation rates. Validation experiments will quantify the reduction in noise achieved.

Another proposed technique is using subsystem codes. Stabilizer measurements in the subsystem code space can detect errors while reducing overhead compared to full QEC. Subsystem codes can potentially augment existing codes. Their compatibility with proposed code modifications and decoding algorithms needs investigation. Integrating these mitigation techniques with optimized codes and decoders is a promising approach to minimize the number of physical qubits needed for fault tolerance. However, considerable analysis is required to realize robust integrated solutions. The simulation framework provides a tool for this analysis as we work to improve QEC performance.

3.4 Hardware-Aware Decoding Algorithms

Most decoding algorithms for quantum error correcting codes make simplifying assumptions about independent error models [23]. However, realistic hardware exhibits complex noise features like correlations, context dependence, drift, and non-Markovian effects. We propose developing decoders optimized for actual device noise to improve performance. One approach trains machine learning models on simulated error data, including these effects. Neural networks can infer complex error patterns from syndrome measurements not identifiable by traditional algorithms. The decoder is tuned on code simulations under representative noise. We propose a recurrent neural network (RNN) decoder architecture utilizing long short-term memory (LSTM) units to capture complex temporal correlations in error patterns. The decoder is trained on an extensive dataset incorporating non-Markovian noise, drift, and spatial correlations generated from physics-based device Hamiltonian simulations. To realize the decoder, we map the trained neural network onto a compact hardware implementation comprising:

- Dense crossbar arrays for matrix multiplication
- Flash ADC (Analog-to-Digital Converter) units to digitize syndrome measurements
- A classical microcontroller for sequencing operations

The modular, scalable architecture will enable scaling the decoder to large code distances required for practical fault tolerance. The key advantage of these hardware-aware decoding schemes is reducing logical error rates by avoiding oversimplified noise assumptions. Even with a fixed code, more accurate decoding better suppresses logical faults. This reduces overhead by relaxing requirements on code distance, qubit quality, gate errors, etc., to reach a fault tolerance threshold. Careful benchmarking on empirical device noise data is critical to validate gains.

The key advantage of these hardware-aware decoding schemes is reducing logical error rates by avoiding over-simplified noise assumptions. Even with a fixed code, more accurate decoding better suppresses logical faults. This reduces overhead by relaxing requirements on code distance, qubit quality, gate errors, etc., to reach a fault tolerance threshold. Careful benchmarking on empirical device noise data is critical to validate gains.

While the recurrent neural network decoder architecture with LSTM units shows promise for capturing complex temporal error correlations, this approach remains a conceptual design yet to be implemented and tested [24]. The key next steps entail architecting the decoder components, training the neural network on extensive simulated noise model data sets, and quantifying improved logical error suppression. Significant research is required to realize a hardware-implemented neural network decoder capable of leveraging realistic noise characteristics to optimize quantum error correction.

3.5 Resource Analysis Framework

We propose developing a modeling framework to quantify the resource savings from proposed techniques compared to baseline schemes. The modular framework co-simulates hardware models, code/decoder implementations, and application benchmarks. Key code properties modeled include distance, lattice geometry, concatenation structure, and decoding algorithm. The simulated hardware model incorporates qubit connectivity, gate errors, noise parameters, and mitigation effects. Resource metrics, including the number of qubits, gates, time, and classical computing, are tracked. We propose tracking metrics including:

- Number of physical qubits
- Quantum gate count
- Circuit depth
- Classical runtime for decoding

The analysis will incorporate non-idealities like gate errors and crosstalk through device-specific noise modeling. We will validate the simulated resource costs using tailored experimental benchmarks. This modeling framework will allow predicting the resource overhead reductions from our techniques before intensive hardware demonstration. We anticipate substantial gains in qubit and time costs by co-optimizing codes, decoding, noise, and hardware constraints.

4 Limitations and Future Work

This work proposes techniques to enhance the efficiency of quantum error correction for near-term devices, yet substantial limitations and open questions persist, necessitating further research. The introduced code constructions, such as deformable surface code lattices and concatenated inner code layers, demand

extensive analysis and simulation for performance evaluation and potential overhead reductions. Validation of the noise modeling methodology against empirical device calibration data is essential across various parameters.

Hardware-aware decoding algorithms leveraging neural networks and machine learning, though promising in conceptual design, require implementation, training, and testing on representative quantum hardware to assess their effectiveness in suppressing logical faults. The resource analysis framework needs precise quantification of resource costs from both theoretical studies and experimental demonstrations.

While these techniques present promising directions to reduce resource overhead for quantum error correction, achieving practical fault tolerance in noisy near-term quantum processors demands continued research. Key next steps involve rigorous simulations to analyze proposed code constructions under realistic noise models, experiments to validate comprehensive noise characterization methodology on actual superconducting qubit devices, and integration of detailed resource cost metrics from small-scale prototype implementations into the modeling framework. Concurrently, the integration of quantum-resistant techniques into IoT security protocols presents an opportunity [25]. Quantum-safe encryption methods must be explored for securing IoT devices against potential quantum threats. Investigating the intersection of Quantum IoT Security and quantum error correction techniques could yield comprehensive solutions for securing both quantum and conventional information systems.

While the proposed code optimizations, noise modeling, and resource analysis methodologies offer promising directions, transforming these conceptual foundations into tangibly reduced overheads demands extensive research. Each technique introduced requires thorough investigation - simulating proposed code deformations under realistic noise models, validating the comprehensive error characterization methodology on actual superconducting devices, training and benchmarking hardware-aware decoder designs, and quantifying resource savings against baseline schemes. Addressing these open questions through rigorous analysis connects back to the overarching ambition of progressing quantum computing toward the fault tolerance thresholds necessary for reliable computation. By elucidating these gaps, this discussion spotlights that considerable work remains to evolve the proposed techniques from conceptual frameworks into demonstrable realizations. Ongoing research in error-correcting codes, noise characterization, decoding algorithms, and resource analysis tailored to near-term quantum hardware promises steady progress toward engineering practical fault tolerance.

5 Conclusion

Quantum computing promises revolutionary advances across science and industry, from drug discovery to machine learning. However, noise remains a central obstacle to realizing this profound potential. QEC provides a path to reliable quantum computation but requires exceedingly low physical error rates using conventional approaches.

This work introduces advanced techniques for efficient and viable quantum error correction customized for near-term noisy quantum hardware. The core techniques proposed encompass code constructions to reduce resource overhead through innovations like deformable surface code lattices and tailored concatenated inner code layers. To enable the co-design of optimized error correction protocols, the work outlines a comprehensive methodology for realistically modeling the intricate noise behaviors in superconducting qubits. Hardware-aware decoding algorithms based on data-driven machine learning techniques offer the potential to further boost performance by avoiding oversimplified assumptions. A flexible modeling framework provides systematic quantification of the overhead reductions achieved.

These contributions present an integrated approach strengthening the prospects for practical error correction in NISQ-era devices. While considerable research remains to construct solutions robust enough for implementation, this work delineates high-potential directions. Code optimizations must undergo rigorous analysis to validate gains. Comprehensive noise modeling requires extensive validation across diverse qubit platforms. Machine learning decoders need implementation and benchmarking on empirical error data sets. By elucidating promising techniques and quantifying their benefits, this research paves the path toward engineering quantum computers that finally fulfill the long-standing promise of scalable, fault-tolerant quantum computation.

References

1. de Andrade, M.G., Dai, W., Guha, S., Towsley, D.: A quantum walk control plane for distributed quantum computing in quantum networks. In: 2021 IEEE International Conference on Quantum Computing and Engineering (QCE), Broomfield, CO, USA, pp. 313–323 (2021). <https://doi.org/10.1109/QCE52317.2021.00048>.
2. Albert, V.V., Jiang, L.: Symmetries and conserved quantities in Lindblad master equations. Phys. Rev. A **89**(2), 022118 (2014). <https://doi.org/10.1103/PhysRevA.89.022118>
3. Chiaverini, J., Leibfried, D., Schaetz, T., et al.: Realization of QEC. Nature **432**, 602–605 (2004). <https://doi.org/10.1038/nature03074>
4. Sete, E.A., Zeng, W.J., Rigetti, C.T.: A functional architecture for scalable quantum computing. In: 2016 IEEE International Conference on Rebooting Computing (ICRC), San Diego, CA, USA, pp. 1–6 (2016). <https://doi.org/10.1109/ICRC.2016.7738703>.
5. Thantharate, P.: IntelligentMonitor: empowering devops environments with advanced monitoring and observability. In: 2023 International Conference on Information Technology (ICIT), Amman, Jordan, pp. 800–805 (2023). <https://doi.org/10.1109/ICIT58056.2023.10226123>.
6. Thantharate, P.: SCALE-IT: distributed and realistic simulation frameworks for testing cloud-based software. In: 2023 10th International Conference on Electrical Engineering, Computer Science and Informatics (EECSI), Palembang, Indonesia, pp. 300–306 (2023). <https://doi.org/10.1109/EECSI59885.2023.10295630>.

7. Holmes, A., Jokar, M.R., Pasandi, G., Ding, Y., Pedram, M., Chong, F.T.: NISQ+: boosting quantum computing power by approximating QEC. In: 2020 ACM/IEEE 47th Annual International Symposium on Computer Architecture (ISCA). Valencia, Spain, pp. 556–569 (2020). <https://doi.org/10.1109/ISCA45697.2020.00053>
8. Copsey, D., et al.: Toward a scalable, silicon-based quantum computing architecture. *IEEE J. Sel. Top. Quantum Electron.* **9**(6), 1552–1569 (2003). <https://doi.org/10.1109/JSTQE.2003.820922>
9. Kiktenko, E.O., et al.: Scalable quantum computing with qudits on a graph. *Phys. Rev. A* **101**(2), 022304 (2020). <https://doi.org/10.1103/PhysRevA.101.022304>
10. McEwen, M., Kafri, D., Chen, Z., et al.: Removing leakage-induced correlated errors in superconducting QEC. *Nat. Commun.* **12**, 1761 (2021). <https://doi.org/10.1038/s41467-021-21982-y>
11. Das, P., et al.: AFS: accurate, fast, and scalable error-decoding for fault-tolerant quantum computers. In: 2022 IEEE International Symposium on High-Performance Computer Architecture (HPCA). Seoul, Republic of Korea, pp. 259–273 (2022). <https://doi.org/10.1109/HPCA53966.2022.00027>
12. Russo, V., et al.: Testing platform-independent quantum error mitigation on noisy quantum computers. arXiv (2022). <https://doi.org/10.48550/arXiv.2210.07194>
13. Thantharate, P., Thantharate, A.: GeneticSecOps: harnessing heuristic genetic algorithms for automated security testing and vulnerability detection in DevSecOps. In: 2023 6th International Conference on Contemporary Computing and Informatics (IC3I), Gautam Buddha Nagar, India, pp. 2271–2278 (2023). <https://doi.org/10.1109/IC3I59117.2023.10398075>
14. Khan, A.A., et al.: Software architecture for quantum computing systems - a systematic review. *J. Syst. Softw.* **201**, 111682 (2023). <https://doi.org/10.1016/j.jss.2023.111682>
15. Lau, J.W.Z., Lim, K.H., Shrotriya, H., et al.: NISQ computing: where are we and where do we go? *AAPPS Bull.* **32**, 27 (2022). <https://doi.org/10.1007/s43673-022-00058-z>
16. Wang, J., Guo, G., Shan, Z.: SoK: benchmarking the performance of a quantum computer. *Entropy* **24**, 1467 (2022). <https://doi.org/10.3390/e24101467>
17. Acampora, G., et al.: D-NISQ: a reference model for distributed noisy intermediate-scale quantum computers. *Inf. Fusion* **89**, 16–28 (2023). <https://doi.org/10.1016/j.inffus.2022.08.003>
18. Guimarães, J.D., Tavares, C.: Towards a layered architecture for error mitigation in quantum computation. In: 2022 IEEE International Conference on Quantum Software (QSW), Barcelona, Spain, pp. 41–51 (2022). <https://doi.org/10.1109/QSW55613.2022.00022>
19. McDonough, B., et al.: Automated quantum error mitigation based on probabilistic error reduction. In: 2022 IEEE/ACM Third International Workshop on Quantum Computing Software (QCS), Dallas, TX, USA, pp. 83–93 (2022). <https://doi.org/10.1109/QCS56647.2022.00015>
20. Thantharate, P., Thantharate, A.: ZeroTrustBlock: enhancing security, privacy, and interoperability of sensitive data through ZeroTrust permissioned blockchain. *Big Data Cogn. Comput.* **7**, 165 (2023). <https://doi.org/10.3390/bdcc7040165>
21. Koch, J., et al.: Charge-insensitive qubit design derived from the Cooper pair box. *Phys. Rev. A* **76**, 042319 (2007)
22. Altman, E., et al.: Quantum simulators: architectures and opportunities. *PRX Quant.* **2**(1), 017003 (2021). <https://doi.org/10.1103/PRXQuantum.2.017003>

23. Wang, P., et al.: Cryogenic benchmarks of embedded memory technologies for recurrent neural network based quantum error correction. In: 2020 IEEE International Electron Devices Meeting (IEDM), San Francisco, CA, USA, pp. 38.5.1–38.5.4 (2020). <https://doi.org/10.1109/IEDM13553.2020.9371912>.
24. Bausch, J.: Recurrent quantum neural networks. In: Advances in Neural Information Processing Systems, vol. 33, pp. 1368–1379 (2020). proceedings.neurips.cc/paper/2020/hash/0ec96be397dd6d3cf2fecb4a2d627c1c-Abstract.html
25. Thantharate, P., Thantharate, A.: CYBRIA - pioneering federated learning for privacy-aware cybersecurity with brilliance. In: 2023 IEEE 20th International Conference on Smart Communities: Improving Quality of Life using AI, Robotics and IoT (HONET), Boca Raton, FL, USA, pp. 56–61 (2023). <https://doi.org/10.1109/HONET59747.2023.10374608>



Quantum Computing for Computer Vision: Applications, Challenges, and Research Tracks

Naoual El Djouher Mebtouche^{1(✉)} and Sarah Sahnoune²

¹ Laboratory of Research in Artificial Intelligence (LRIA), Faculty of Computer Science, University of Science and Technology Houari Boumediene (USTHB), Algiers, Algeria

nmebtouche@usthb.dz

² Faculty of Physics, University of Science and Technology Houari Boumediene (USTHB), Algiers, Algeria

Abstract. In the last few years, computer vision has achieved significant breakthroughs, largely due to the advances in deep learning models. However, despite these remarkable achievements, deep learning models for computer vision are already showing their limits. Quantum computing's capacity for parallelism and complex data processing presents a novel approach to tackling the computational demands of computer vision tasks. In this context, quantum computing emerges as a potential solution to the challenges in computer vision. Quantum principles have the potential to enhance computational efficiency and accuracy, opening doors to new horizons in solving complex computer vision problems. In this paper, we investigate the use of quantum computing for computer vision. First, we analyze quantum architectures and the evolution of quantum computing specifically for computer science. This analysis offers a foundational understanding of quantum computing and quantum techniques. Second, we study applied quantum computing research for computer vision through an extensive literature review. Simultaneously, we present an in-depth analysis of the existing limitations and challenges posed by quantum hardware and algorithms in computer vision applications as well as outline the potential research tracks for applied quantum computing in computer vision.

Keywords: quantum computing · computer vision · artificial intelligence · literature review

1 Introduction

Computer vision plays a crucial role in Artificial Intelligence. It gives machines the ability to understand and interpret visual information, much like how human eyes and brains process images. This has wide-ranging applications in areas like healthcare, self-driving cars, and security [39,41–44].

Over the past decade, the advent of deep learning has brought computer vision a series of high achievements. Deep learning models, particularly Convolutional Neural Networks (CNNs), have showcased exceptional results in tasks like image classification, object detection, and facial recognition. These advancements have enabled computers to recognize patterns and features within images with remarkable accuracy, almost rivaling human performance.

However, the remarkable results of deep learning models in computer vision are accompanied by challenging computational demands. Applications such as object detection [38, 40] require an immense amount of processing power to analyze vast datasets and make real-time decisions. This immense demand for computational resources poses challenges for scalability and the model's convergence of high semantic computer vision tasks.

Quantum computing has emerged as a promising alternative for addressing the challenges of classical computers, especially problems with high complexity [45]. Quantum computing has demonstrated remarkable successes in diverse domains of computer science, such as cryptographic security and optimization problems. These achievements highlight the transformative potential of quantum computation in revolutionizing algorithms and programs.

In the context of computer vision, the advent of quantum computing presents a promising prospect [46]. Its inherent capability for parallelism and data manipulation matches the computational demands of image analysis, object recognition, and visual pattern detection. The integration of quantum computing in computer vision raises a set of questions:

1. What type of problems can be solved by quantum computers?
2. How to effectively use quantum computing for computer vision tasks?
3. What are the inherent challenges of quantum computing in computer vision and how to potentially face them?

In this paper, we address these questions. First, we present the fundamental concepts of quantum computing as well as its evolution highlighting its transition from theoretical concepts to practical implementation. Furthermore, we present contemporary state-of-the-art quantum computing systems.

Second, we present a review of several academic works that integrate quantum computing into computer vision tasks. This extensive survey encapsulates a breadth of research papers that intersect these domains.

Last, we provide a structured presentation of challenges intrinsic to the application of quantum computing into computer vision. This taxonomy delineates obstacles surrounding quantum algorithm design, noise mitigation, and the orchestration of quantum-classical hybrid processing. Simultaneously, we outline prospective research directions of quantum computer vision.

The rest of this paper is organized as follows: Sect. 2 provides the basis for comprehensive principles of quantum computing, hardware implementation, and its evolution. Section 3 presents a review of quantum-based computer vision work and applications as well as the challenges and the research potential of quantum computing for computer vision tasks. Finally, Sect. 4 provides an exhaustive conclusion.

2 Quantum Computing: Principles and Evolution

2.1 History

Quantum computing was born in 1982 when the physicist and Nobel Laureate Richard Feynman proposed that classical computers struggled to simulate quantum systems efficiently. The idea he proposed was to design a machine that would run on quantum mechanics principles [1]. The idea took a significant leap forward in 1985 when David Deutsch formulated the quantum Turing machine. He envisioned a computer that could solve problems considered uncomputable for classical computers [2]. Far from theory, the very first application of quantum computing was proposed by Peter Shor in 1994 to factorize large numbers into their prime number. Later, in the early 2000s, experimental milestones followed with the hardware realization of basic quantum gates and qubits, the fundamental units of quantum information.

2.2 Qubit

A qubit is a quantum equivalent of a classical bit (qubit is short for “quantum bit”). Qubit is the fundamental unit of quantum information in quantum computing. Unlike classical bits, which can only represent values of 0 or 1, qubits use the quantum mechanics principle called superposition. Superposition means that the qubit can be either 0 or 1 or in the composition of both states (0 and 1) simultaneously. This unique property enables qubits to perform complex calculations and operations more efficiently than classical bits.

2.3 Superposition

A qubit $|\phi\rangle$ (this is called the Dirac's notation) can be in the state $|0\rangle$, $|1\rangle$ or any arbitrary superposition of both states. The qubit is then written as: $|\phi\rangle = \alpha|0\rangle + \beta|1\rangle$ where α and β are the probability amplitudes. The state of a qubit is unknown during computation and is only instantiated when measured this phenomenon is known as collapse in quantum mechanics. Specifically, if we measure a qubit $|\phi\rangle = \alpha|0\rangle + \beta|1\rangle$ it will collapse to either of the states $|0\rangle$ or $|1\rangle$. The probability that the obtained state is $|0\rangle$ is given by the amplitude $|\alpha|^2$ and the probability for the qubit to be $|1\rangle$ is given by the amplitude $|\beta|^2$. Superposition allows to run several computations at the same time whereas traditional computers perform tasks sequentially.

2.4 Entanglement

When generalizing to n qubits $|q1\rangle, |q2\rangle, \dots, |qn\rangle$, we need to define the qubits in the Hilbert space $\mathbb{C}^2 \otimes \mathbb{C}^2 \otimes \dots \otimes \mathbb{C}^2$ which is a superposition of 2^n basis states $|000\dots 0\rangle, |000\dots 1\rangle, \dots, |111\dots 1\rangle$. It is this exponential expansion of state spaces in the number qubits. Entanglement is a fundamental principle in quantum mechanics where the states of two or more qubits become intricately connected in

a way that the properties of one qubit cannot be described independently of the properties of the other qubits. Thus, measuring a single qubit can collapse the whole system of entangled qubits, and therefore, instantiate the measurement outcome [3]. Entanglement enables qubits to perform complex computations more efficiently by exploiting the interconnection of their states. It's a crucial resource for various quantum algorithms.

2.5 Quantum Gates

Quantum computation consists of transforming states to other states using gates. In other words, a quantum gate is a mapping from one state to another. Quantum gates are fundamental building blocks in quantum computing that perform operations on qubits, the quantum analogs of classical bits. These gates manipulate the quantum state of qubits to perform specific quantum operations, analogous to how classical logic gates manipulate classical bits to perform computations.

Quantum gates enable the execution of quantum algorithms and tasks. Concretely, they are represented by matrices. The combination of different quantum gates in a quantum circuit enables the execution of complex algorithms.

2.6 Universal Quantum Computer

Universal quantum computer is a theoretical type of quantum computer capable of simulating any other quantum system. Similar to how a classical universal computer can execute any classical algorithm, a quantum universal computer has the potential to execute any quantum algorithm and perform tasks that classical computers cannot efficiently achieve.

The concept of a universal quantum computer is the idea that quantum systems can exhibit complex behaviors that are challenging for classical computers to simulate. A universal quantum computer would have the ability to manipulate and control qubits using quantum gates, enabling it to execute a wide range of quantum algorithms, such as factorization, optimization, cryptography, and simulations of quantum systems.

The concept of a universal quantum computer was formalized by the mathematician and physicist David Deutsch [2] where he introduced the concept of a quantum Turing machine and demonstrated that a quantum computer could simulate any physical system, including other quantum systems.

Universal quantum computers can solve high-complexity problems beyond the capabilities of classical computers. However, building a practical quantum universal computer is a significant scientific and engineering challenge due to the delicate nature of qubits, their physical implementation, and the need for error correction.

In the following, we will review the evolution of quantum computers and provide a clear understanding of their advantages and limitations.

2.7 Evolution of Quantum Computers

Quantum computers are often classified into two types [48, 49]: gate-model computers and adiabatic quantum computers.

Quantum Gate-Based Computers

These are the most well-known types of quantum computers. They use quantum gates to manipulate qubits, which are the quantum analogs of classical bits. Qubits can exist in a superposition of states, allowing quantum gate operations to be performed in parallel. Examples include IBM's System [36] and Google's Bristlecone [37].

A Quantum gate-based computer is the equivalent of a classical computer in which the solutions (algorithms) are represented as a sequence of primitive quantum operations using quantum gates and qubits. This paradigm allows to design algorithms at low levels the way it is designed in boolean circuits.

Adiabatic Quantum Computers

Also known as a Quantum Annealer is a type of quantum computing model that operates based on the adiabatic theorem from quantum mechanics [47]. This model is designed to solve a certain category of problems: optimization problems by using the principles of quantum annealing. Adiabatic quantum computing consists of finding the lowest energy state of a physical system that corresponds to the solution of a given optimization problem.

The basic idea behind adiabatic quantum computing is to start with a quantum system in a simple initial state, which can be represented easily, and then slowly transform it into a final state that encodes the solution to the optimization problem. contrary to the quantum gate-based computers the transformation is carried out using a time-dependent Hamiltonian, which represents the energy of the system. In other words, we evaluate the solutions based on the evolution of the energy of a quantum system, not in a set of operations.

D-Wave Systems is a well-known company that has developed commercial adiabatic quantum computers based on superconducting qubits. These types of systems are designed to solve optimization problems and are particularly suitable for certain types of combinatorial optimization and machine learning tasks. While adiabatic quantum computers are not as universal as gate-based quantum computers in terms of the range of algorithms they can execute, they offer a specialized approach for solving certain optimization problems that can be mapped onto their quantum annealing computers.

These are some of the two main paradigms of quantum computing. Each type has its advantages, challenges, and potential applications. There are physical implementations that are based on other paradigms such as Rigetti hybrid quantum-classical system [34]. Rigetti offers a cloud-based quantum computing platform that includes both gate-based quantum and Quantum Virtual Machines for classical computation. Other paradigms also exist such as Quantum Cellular Automata [35], which is a computational model where a grid of cells interacts

based on certain rules. Quantum cellular automata have potential applications in quantum simulations. However, they are still in the theoretical research stages. The field of quantum computing is rapidly evolving, and new approaches and technologies are being developed over time.

3 Quantum Computer Vision: Research and Applications

3.1 Quantum Computer Vision (QCV)

In this section, we will delve into the exploration of quantum algorithms for computer vision. The integration of quantum computing into computer vision these last few years gives some perspective on how to use quantum computers for solving computer vision problems. However, before we delve into the existing literature, we first establish a simplified overview of computer vision pipelines and how this is important to understand the utilization of quantum algorithms. Fundamental concepts of computer vision help appreciate the specific challenges that quantum algorithms may help address and the innovative paths they may provide toward advancing computer vision tasks.

Computer Vision

Computer vision is a multidisciplinary field within artificial intelligence (AI) that focuses on enabling computers to interpret, analyze, and understand visual information from the world. Its primary goal is to replicate the human visual system's ability to perceive and comprehend visual data, enabling machines to recognize objects, scenes, and patterns, and even perform complex tasks based on visual input.

Computer vision can be visualized through a structured pipeline, as illustrated in Fig. 1. This pipeline serves as a generalized representation of the process of extracting information from visual data to serve various computer vision tasks.

This pipeline illustrates the general steps of computer vision tasks. Starting from an input source (step 1: data acquisition), which can be an image or a video, the pipeline guides the input data to an output task (step 3), this task ranges from segmentation, classification, or tracking. This transformation is applied by employing computer vision algorithms (step 2) tailored to the specific task we aim for.

Throughout this pipeline, computer vision algorithms can encompass a wide range of techniques, from traditional methods involving image processing, or more advanced approaches using machine learning, and deep learning.

It is therefore natural to consider the integration of quantum computing into computer vision algorithms (step 2) which consists of image processing algorithms or machine learning. The integration of quantum computing can be applied in two ways: either by substituting these algorithms (image processing algorithms and machine learning algorithms) or as a complement to existing

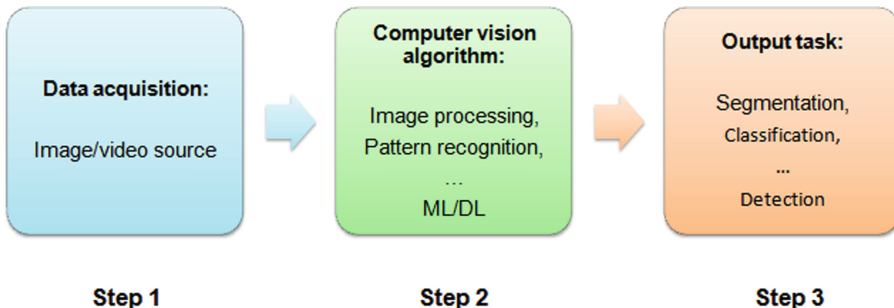


Fig. 1. Generic computer vision pipeline

algorithms by complementing their functionality with quantum-driven enhancements.

In the following, our focus will be directed towards a detailed examination of this integration process in image processing algorithms and machine learning algorithms. We aim to explore the synergy between quantum computing and the realm of computer vision, studying the potential benefits it can grant upon image processing and machine learning tasks.

Image Processing

Quantum image processing explores the utilization of quantum computing principles and techniques to enhance various aspects of image processing. There are several notable works and research directions that showcase the potential of quantum image processing:

Many quantum methods have been proposed for image processing over the last few years [4–7]. For problems such as shape matching [8–10], [8] applied quantum computing on point alignment, they have proved that low computer vision problems can be solved with adiabatic quantum computers. fundamental matrix estimation, point triangulation [11], and motion segmentation [12] all these works use adiabatic quantum computers (AQC). These works handle different types of image transformations [13,14], graph matching [15,16] mesh alignment [17], in tasks like image segmentation such as the work in [50] who used a specific set of gates to find dual thresholds for image segmentation. Geometric transformation (such as rotation) [18–20], Erosion and dilation operations [21], translation [22] and noise reduction [23]. [18] proposed an image encryption/decryption based on the quantum Fourier transform algorithm. All these works apply pure principles of quantum computers such as superposition, entanglement, quantum gates, or/and quantum annealing.

The integration of quantum computing in image processing is mainly used to replace traditionally complex computer vision algorithms, either by specific quantum circuits that mimic the behavior of certain algorithms or with the adiabatic approach for optimization.

The design of quantum algorithms introduces a unique set of characteristics based on the principles of superposition and entanglement, as well as the construction of intricate quantum circuits. Quantum algorithms are structured around these foundational concepts, enabling intermediate operations that can process information in multiple states simultaneously. This inherent parallelism and the potential for algorithm acceleration are among the defining features of quantum computing.

Deep Learning

Quantum deep learning is an emerging interdisciplinary field that aims to combine the principles of quantum computing with deep learning techniques. The number of publications on quantum deep learning has increased significantly over the last years. Quantum computing in deep learning aims to explore Quantum Convolutional Neural Networks (QCNNs) to address the limits of classical CNNs. The immense growth of data size as well as the models has been a significant obstacle in employing classical computers for complex computer vision tasks. QCNNs address this by employing qubits to represent data and using CNN in quantum computers.

QCNNs are based on the basic notions and structures of classical CNNs, but adjust them to quantum computers. In QCNNs, feature extraction is performed using quantum circuits (built of qubits and quantum gates). These circuits emulate the convolutions and pooling layers of CNN. The feature map is a set of qubits (generally one qubit). This qubit is then measured to give a prediction value (e.g.: classification task).

Many QCNN-based methods have been proposed for different computer vision tasks. Image recognition [24–26], Parthasarathy et al. [27] proposed to use quantum computing for efficient image recognition by creating a novel model, the quantum optical convolutional neural network (QOCNN). Their results showed the substantial potential of quantum computing for the development of recognition tasks.

Subsequently, Hur et al. [28] proposed a QCNN for the classification of the MNIST and Fashion MNIST datasets. Their results have shown that QCNN displayed high classification accuracy outperforming traditional CNN. Other researchers have also integrated quantum computing into deep learning, such as in [29] with a fully quantum perceptron.

Yen-chi et al. [30] proposed a hybrid quantum-classical model using a QNN coupled with a pre-trained CNN model. [30] Obtained an accuracy of 98.7% with the cats and dogs dataset and achieved a fast convergence. However, combining classical and quantum computing components in hybrid algorithms adds complexity and requires synchronization between the two computing paradigms.

Other computer-vision tasks based on quantum computing solutions have been lately proposed for object tracking [31,32], to Multi-Object Tracking [33]. Multiple object tracking is a particular task since it is an NP-hard problem in computer vision. Zaech et al. [33] proposed the first formulation of a quantum

adiabatic quantum computer to solve this type of task. the method achieved comparable results to the classical state of the art classical methods.

For image classification tasks, especially those involving deep learning and large datasets, gate-based quantum computers are currently more suitable due to their general-purpose nature and the availability of quantum machine learning algorithms. Quantum annealers might be considered for highly complex problems such as object detection or tracking.

The choice between the two depends on various factors such as the problem complexity, the specific quantum algorithms available, and the hardware's current capabilities.

It's important to note that quantum computing is still in its early stages, and both gate-based quantum computers and quantum annealers continue to advance. The suitability of each approach for specific tasks can change as quantum hardware and algorithms evolve.

As parallelism is at the core of both machine/deep learning and quantum computing, there is a natural alignment between the two. Machine learning fundamentally involves operations on matrices and vectors in multidimensional spaces, which closely mirrors the paradigm of quantum computing. This parallelism between the mathematical foundations of machine learning and quantum computing suggests that using quantum capabilities for machine learning and deep learning tasks could be highly beneficial.

The synergy arises from the shared mathematical underpinnings that enable efficient parallel processing in both domains. Quantum computers, with their inherent capacity to process information in superposition and entanglement, align well with the data-intensive computations prevalent in machine learning and deep learning tasks. This compatibility suggests that quantum computing has the potential to accelerate these computations by processing multiple paths of data simultaneously, effectively exploiting the parallelism that is integral to both quantum computing and machine learning.

3.2 Challenges

There is relatively less literature in quantum computing in computer vision compared to the application of quantum computing in other fields. While quantum computing has gained attention for its potential to revolutionize cryptography, optimization, and simulation, its integration into computer vision is starting to increase these last few years. There are many challenges regarding the use of quantum computing for computer vision.

Quantum Hardware

Quantum computers are still in the early stages of development, often facing limitations in terms of qubit coherence, error rates, and qubit connectivity. These constraints impact the feasibility of implementing complex algorithms efficiently.

Limited Quantum Resources: Quantum hardware resources are currently limited in terms of qubit count and coherence time. Mapping complex computer vision tasks onto these constrained resources requires innovative strategies.

Errors and Noise

Qubits are sensitive to noise, leading to errors in quantum computations this is due to various factors, including external interference and imperfections in the qubit hardware.

Another issue regards the entanglement. Quantum algorithms often leverage entanglement, which can be difficult to control and maintain in noisy quantum systems. Preparing qubits in desired states is also a challenge.

Algorithm Verification and Validation

Quantum algorithms can behave differently from classical algorithms, and verifying the correctness of quantum solutions is challenging. Validation methods need to be adapted for quantum contexts.

Quantum Scalability

Quantum algorithms can require a substantial number of quantum gates and circuits to achieve meaningful results. Implementing deep circuits and balancing the complexity of quantum algorithms with available resources is therefore a challenge. Also, designing efficient quantum gates and circuits adapted to computer vision tasks requires domain-specific prior in addition to new quantum optimization techniques.

Classical vs Quantum Computer Vision

Another issue when it comes to the use of quantum computing for computer vision is that we need to build novel algorithms and convert and recreate classical algorithms with the quantum paradigm. There are no bridges between existing classical algorithms and quantum algorithms, that can reduce the tedious task of building quantum algorithms from scratch. In addition to that it is non-trivial to map classical computer vision algorithms and their quantum counterparts due to differences in computation methods. This reduces the portability of the algorithms.

Quantum Computing for Image Processing

It is important to note that while quantum algorithms offer remarkable capabilities, their design and implementation can be intricate and demanding. In the context of image processing tasks, there are instances where the quantum approach might encounter challenges when compared to classical counterparts. The translation of a classical problem into a quantum algorithm often involves complex mathematical transformations. This process can be tedious and unnecessary an example would be the designing of a complex quantum algorithm for a simple task of image segmentation that can be held more efficiently in a classical computer.

Moreover, the parallelism inherent to quantum algorithms doesn't always lead to immediate advantages for all image processing tasks. The suitability of quantum algorithms for parallelism depends on the problem's nature.

Quantum Computing for Machine/Deep Learning

Despite the promising prospects of quantum deep learning, there are significant challenges that must be addressed. One notable challenge lies in the extraction of features from quantum machines. The process by which these features are derived in quantum settings remains largely unexplored within the current literature. This lack of discussion adds an additional layer of interpretability concerns to the existing challenge of the “black box” nature of deep learning algorithms.

Feature extraction is a crucial step in many machine learning tasks, including deep learning. It involves transforming raw data into a format that captures the relevant information for the task at hand. However, in the context of quantum deep learning, the methods and techniques for feature extraction are not well-established or widely understood. This opacity can impede our ability to comprehend how quantum features are identified and utilized in the learning process.

Deep learning’s success is largely attributed to its capacity to model intricate relationships within data through non-linear transformations enabled by activation functions like ReLU or sigmoid. Quantum computing, on the other hand, operates primarily through linear unitary transformations. This dichotomy between non-linearity in deep learning and the linear operations in quantum computing presents a challenge when adapting existing models to quantum-driven models it also reduces the model’s expression to only linear function.

3.3 Research Tracks

The exploration of quantum computing’s application in computer vision opens up several intriguing research tracks, each aimed at addressing the challenges and harnessing the potential of this emerging field. Some of the key research directions include:

Quantum Feature Extraction

Develop innovative techniques to extract features from quantum data representations, leveraging the unique properties of quantum states. This involves devising quantum versions of classical feature extraction methods, which could unlock new insights and enhance performance in tasks like image classification and object detection.

Quantum Activation Functions

Investigate the creation of quantum analogs to traditional non-linear activation functions used in deep learning. This involves exploring how quantum gates and operations can mimic non-linear transformations, potentially resulting in the development of novel activation functions tailored to quantum architectures.

Hybrid Quantum-Classical Models

Explore hybrid quantum-classical models that combine the strengths of quantum computing with classical deep learning approaches. This approach seeks to

leverage quantum computing's capabilities for certain sub-tasks while utilizing classical deep learning for others, ultimately enhancing the overall efficiency and accuracy of computer vision tasks.

Quantum Feature Selection and Dimensionality Reduction

Design quantum algorithms for feature selection and dimensionality reduction, aiming to mitigate the curse of dimensionality and improve the efficiency of training quantum models on high-dimensional image data.

Quantum Model Interpretability

Investigate methods for interpreting and visualizing the inner workings of quantum deep learning models. Developing techniques to elucidate the decision-making process of these models can enhance trust and understanding, addressing concerns related to interpretability.

Quantum Computing Hardware Optimization

Collaborate with quantum hardware developers to optimize quantum computing architectures for specific computer vision tasks. This includes exploring how quantum circuits can be tailored for the efficient execution of computer vision algorithms.

In conclusion, the integration of quantum computing into computer vision presents rich research opportunities. By addressing the challenges and taking advantage of the unique characteristics of quantum computing, innovative solutions can emerge that push the boundaries of computer vision applications.

4 Conclusion

In this paper, we have discussed the utilization of quantum computing for computer vision applications. First, we started by providing some background on quantum computing principles and quantum computing machines. Then, we reviewed the existing works and applications of quantum computing for computer vision. We have classified the work into two main categories: quantum image processing and quantum Machine/Deep learning applications. Most works reported in the literature use quantum annealers as they are more suitable for optimization purposes. Finally, we have discussed the challenges of quantum computing for computer vision from general quantum computing issues to specific ones related to image processing and Machine/Deep learning computer vision applications. Based on this analysis we also proposed some research tracks that have the potential to on one hand remedy the discussed challenges and on the other hand help advance quantum computer vision.

References

1. Feynman, R.P.: Simulating physics with computers. *Int. J. Theor. Phys.* **21**, 467–488 (1982)
2. Deutsch, D.: Quantum theory, the Church-Turing principle and the universal quantum computer. *Proc. Roy. Soc. London A Math. Phys. Sci.* **400**(1818), 97–117 (1985)
3. Griffiths, D.J., Schroeter, D.F.: *Introduction to Quantum Mechanics*, 3rd edn. Cambridge University Press, Cambridge (2018)
4. Caraiman, S., Manta, V.: Image processing using quantum computing. In: 2012 16th International Conference on System Theory, Control and Computing (ICSTCC), pp. 1–6. IEEE (2012)
5. Dendukuri, A., Luu, K.: Image processing in quantum computers. arXiv preprint [arXiv:1812.11042](https://arxiv.org/abs/1812.11042) (2018)
6. Venegas-Andraca, S.E., Bose, S.: Storing, processing, and retrieving an image using quantum mechanics. In: *Quantum information and computation*, vol. 5105, pp. 137–147. SPIE (2003)
7. Yan, F., Iliyasu, A.M., Venegas-Andraca, S.E.: A survey of quantum image representations. *Quantum Inf. Process.* **15**, 1–35 (2016)
8. Golyanik, V., Theobalt, C.: A quantum computational approach to correspondence problems on point sets. In: *Proceedings of the IEEE/CVF Conference on Computer Vision and Pattern Recognition*, pp. 9182–9191 (2020)
9. Meli, N.K., Mannel, F., Lellmann, J.: An iterative quantum approach for transformation estimation from point sets. In: *Proceedings of the IEEE/CVF Conference on Computer Vision and Pattern Recognition*, pp. 529–537 (2022)
10. Benkner, M.S., Lähner, Z., Golyanik, V., Wunderlich, C., Theobalt, C., Moeller, M.: Q-match: iterative shape matching via quantum annealing. In: *Proceedings of the IEEE/CVF International Conference on Computer Vision*, pp. 7586–7596 (2021)
11. Doan, A.D., Sasdelli, M., Suter, D., Chin, T.J.: A hybrid quantum-classical algorithm for robust fitting. In: *Proceedings of the IEEE/CVF Conference on Computer Vision and Pattern Recognition*, pp. 417–427 (2022)
12. Arrigoni, F., Menapace, W., Benkner, M.S., Ricci, E., Golyanik, V.: Quantum motion segmentation. In: Avidan, S., Brostow, G., Cissé, M., Farinella, G.M., Hassner, T. (eds.) *ECCV 2022. LNCS*, vol. 13689, pp. 506–523. Springer, Cham (2022). https://doi.org/10.1007/978-3-031-19818-2_29
13. Jiang, N., Wang, L.: Quantum image scaling using nearest neighbor interpolation. *Quantum Inf. Process.* **14**, 1559–1571 (2015)
14. Song, X.H., Wang, S., Abd El-Latif, A.A., Niu, X.M.: Quantum image encryption based on restricted geometric and color transformations. *Quantum Inf. Process.* **13**, 1765–1787 (2014)
15. Dörn, S.: Quantum algorithms for matching problems. *Theory Comput. Syst.* **45**(3), 613–628 (2009)
16. Benkner, M.S., Golyanik, V., Theobalt, C., Moeller, M.: Adiabatic quantum graph matching with permutation matrix constraints. In: *2020 International Conference on 3D Vision (3DV)*, pp. 583–592. IEEE (2020)
17. Amenta, N., Bern, M., Eppstein, D.: Optimal point placement for mesh smoothing. *J. Algorithms* **30**(2), 302–322 (1999)
18. Yang, Y.G., Xia, J., Jia, X., Zhang, H.: Novel image encryption/decryption based on quantum Fourier transform and double phase encoding. *Quantum Inf. Process.* **12**, 3477–3493 (2013)

19. Le, P.Q., Iliyasu, A.M., Dong, F., Hirota, K.: Fast geometric transformations on quantum images. *IAENG Int. J. Appl. Math.* **40**(3) (2010)
20. Le, P.Q., Iliyasu, A.M., Dong, F., Hirota, K.: Strategies for designing geometric transformations on quantum images. *Theoret. Comput. Sci.* **412**(15), 1406–1418 (2011)
21. Yuan, S., Mao, X., Chen, L., Xue, Y.: Quantum digital image processing algorithms based on quantum measurement. *Optik* **124**(23), 6386–6390 (2013)
22. Wang, J., Jiang, N., Wang, L.: Quantum image translation. *Quantum Inf. Process.* **14**(5), 1589–1604 (2015)
23. Treps, N., Delaubert, V., Maître, A., Courty, J.M., Fabre, C.: Quantum noise in multipixel image processing. *Phys. Rev. A* **71**(1), 013820 (2005)
24. Neven, H., Denchev, V.S., Rose, G., Macready, W.G.: QBoost: large scale classifier training with adiabatic quantum optimization. In: Asian Conference on Machine Learning, pp. 333–348. PMLR. (2012)
25. Neven, H., Rose, G., Macready, W.G.: Image recognition with an adiabatic quantum computer I. Mapping to quadratic unconstrained binary optimization. arXiv preprint [arXiv:0804.4457](https://arxiv.org/abs/0804.4457) (2008)
26. O’Malley, D., Vesselinov, V.V., Alexandrov, B.S., Alexandrov, L.B.: Nonnegative/binary matrix factorization with a D-wave quantum annealer. *PLoS ONE* **13**(12), e0206653 (2018)
27. Parthasarathy, R., Bhowmik, R.T.: Quantum optical convolutional neural network: a novel image recognition framework for quantum computing. *IEEE Access* **9**, 103337–103346 (2021)
28. Hur, T., Kim, L., Park, D.K.: Quantum convolutional neural network for classical data classification. *Quantum Mach. Intell.* **4**(1), 3 (2022)
29. Potok, T.E., et al.: A study of complex deep learning networks on high-performance, neuromorphic, and quantum computers. *ACM J. Emerg. Technol. Comput. Syst. (JETC)* **14**(2), 1–21 (2018)
30. Chen, S.Y.C., Yoo, S.: Federated quantum machine learning. *Entropy* **23**(4), 460 (2021)
31. Misra, R., Ray, K.S.: Object tracking based on quantum particle swarm optimization. In: 2017 Ninth International Conference on Advances in Pattern Recognition (ICAPR), pp. 1–6. IEEE (2017)
32. Yu, C.H., Gao, F., Liu, C., Huynh, D., Reynolds, M., Wang, J.: Quantum algorithm for visual tracking. *Phys. Rev. A* **99**(2), 022301 (2019)
33. Zaech, J.N., Liniger, A., Danelljan, M., Dai, D., Van Gool, L.: Adiabatic quantum computing for multi object tracking. In: Proceedings of the IEEE/CVF Conference on Computer Vision and Pattern Recognition, pp. 8811–8822 (2022)
34. Karalekas, P.J., Tezak, N.A., Peterson, E.C., Ryan, C.A., Da Silva, M.P., Smith, R.S.: A quantum-classical cloud platform optimized for variational hybrid algorithms. *Quantum Sci. Technol.* **5**(2), 024003 (2020)
35. Lent, C.S., Tougaw, P.D., Porod, W., Bernstein, G.H.: Quantum cellular automata. *Nanotechnology* **4**(1), 49 (1993)
36. Cross, A.: The IBM Q experience and QISKit open-source quantum computing software. In: APS March Meeting Abstracts, vol. 2018, p. L58-003 (2018)
37. Kelly, J., Chen, Z., Chiaro, B., Foxen, B., Martinis, J., Team, Q.H.T.: Operating and characterizing of a 72 superconducting qubit processor “Bristlecone”: part 1. In: APS March Meeting Abstracts (2019)
38. Mebtouche, N.E.-D., Baha, N.: Robust object detection based on deep neural network and saliency features from visible and thermal images. In: AI2SD 2020. AISC,

- vol. 1418, pp. 529–540. Springer, Cham (2022). https://doi.org/10.1007/978-3-030-90639-9_43
- 39. Stephen, O., Sain, M., Maduh, U.J., Jeong, D.U.: An efficient deep learning approach to pneumonia classification in healthcare. *J. Healthc. Eng.* (2019)
 - 40. Mebtouche, N.E.D., Baha, N., Kaddouri, N., Zaghdar, A., Redjil, A.B.E.: Improving thermal object detection for optimized deep neural networks on embedded devices. In: Drias, H., Yalaoui, F., Hadjali, A. (eds.) *AID 2022. CCIS*, vol. 1852, pp. 83–94. Springer, Singapore (2023). https://doi.org/10.1007/978-981-99-4484-2_7
 - 41. Kumra, S., Kanan, C.: Robotic grasp detection using deep convolutional neural networks. In: *2017 IEEE/RSJ International Conference on Intelligent Robots and Systems (IROS)*, pp. 769–776. IEEE (2017)
 - 42. Zhou, W., Dou, P., Su, T., Hu, H., Zheng, Z.: Feature learning network with transformer for multi-label image classification. *Pattern Recogn.* **136**, 109203 (2023)
 - 43. Mebtouche, N.E.D., Baha, N.: Robust UAV detection based on saliency cues and magnified features on thermal images. *Multimed. Tools Appl.* (2023)
 - 44. Abed, M., Ibrikci, T.: Sleep apnea events detection using deep learning techniques. *J. Sleep Disord. Treat. Care* (2023)
 - 45. Harrow, A.W., Montanaro, A.: Quantum computational supremacy. *Nature* **549**(7671), 203–209 (2017)
 - 46. Ruan, Y., Chen, H., Tan, J., Li, X.: Quantum computation for large-scale image classification. *Quantum Inf. Process.* **15**, 4049–4069 (2016)
 - 47. Kato, T.: On the adiabatic theorem of quantum mechanics. *J. Phys. Soc. Jpn.* **5**(6), 435–439 (1950)
 - 48. McGeoch, C.C.: *Adiabatic Quantum Computation and Quantum Annealing: Theory and Practice*. Springer, Cham (2022). <https://doi.org/10.1007/978-3-031-02518-1>
 - 49. Yulianti, L. P., Surendro, K.: Implementation of quantum annealing: a systematic review. *IEEE Access* (2022)
 - 50. López, L.O., Orts, F., Ortega, G., et al.: Fault-tolerant quantum algorithm for dual-threshold image segmentation. *J. Supercomput.* **79**, 12549–12562 (2023)



A Multiparty Efficient Semi-quantum Secret Sharing Protocol of Specific Bits

Mustapha Anis Younes¹(✉), Sofia Zebboudj², and Abdelhakim Gharbi¹

¹ Université de Bejaia, Faculté des Sciences Exactes, Laboratoire de Physique Théorique, 06000 Bejaia, Algérie

{mustaphaanis.younes, abdelhakim.gharbi}@univ-bejaia.dz

² ENSIBS, Université Bretagne Sud, 56000 Vannes, France

sofiazebboudj@gmail.com

Abstract. Recently, Tian et al. [22] introduced a protocol enabling quantum Alice to securely share a specific secret with classical Bob and Charlie using Bell states. In this protocol, Alice has full control over the shared secret message and the percentage of detection qubits, resulting in remarkable efficiency compared to existing approaches. However, the protocol has two main limitations: Firstly, it is restricted to only two participants. Secondly, the proposed approach suggests using photon number splitter (PNS) and wavelength filter (WF) to address Trojan horse attacks, which deviates from the fundamental purpose of semi-quantum cryptography. In this study, we propose a generalization of the protocol of Tian et al. [22] to accommodate n classical parties. Additionally, we demonstrate that this new protocol is robust against the Trojan horse attacks without the need for costly quantum devices, aligning with the original intent of the semi-quantum environment. Moreover, we offer a succinct summary of semi-quantum secret sharing, discussing the different challenges and domain-specific concerns, and presenting potential research avenues for further investigation.

Keywords: Quantum cryptography · Semi-quantum secret sharing · Trojan horse attack · Bell states · Entangled states

1 Introduction

Secret sharing, pioneered by Adi Shamir [19] and George Blakley [1] in 1979, is a fundamental procedure for dividing a secret into multiple shares and distributing them among participants. The goal is to ensure that individual participants have no intelligible knowledge of the secret, but when a sufficient number of shares are combined, the original secret can be reconstructed. However, classical secret sharing protocols face significant challenges with the advancement of current technology. To address these limitations, Hillery et al. [8] introduced “quantum secret sharing” (QSS) in 1999, based on the use of Greenberger-Horne-Zeilinger (GHZ) states, leading to the development of the pioneering HBB99 protocol.

Inspired by the quantum key distribution (QKD) protocol BB84, Karlsson et al. [10] presented a QSS protocol utilizing two-particle quantum entanglement. Unlike classical methods, the secret is distributed, transmitted, and recovered through quantum operation, so its security is based on the fundamental principle of quantum physics.

One of the issues in quantum cryptography lies in the assumption that all participants in quantum communication possess full quantum capabilities. Quantum information technology research is still in its early stages, with high-priced and complex quantum devices. The challenges of quantum state preparation, storage, and transmission further add to the complexity [6]. It is unrealistic to expect all participants to afford such expensive devices and execute such intricate operations. In response, Boyer et al. [3] introduced the concept “semi-quantum cryptography” in 2007. This approach allows one party to have full quantum capability, while the other’s quantum capacity is limited, enabling secure communication between a quantum and a classical user. To be more precise, a participant possessing the capability to perform the following operations is referred to as a quantum participant: (a) generating any quantum states; (b) performing any quantum measurements; (c) storing qubits in quantum memory. A participant with the capacity to perform the following operations is known as a classical participant: (a) generating qubits with the computational basis $\{|0\rangle, |1\rangle\}$; (b) measuring qubits with the computational basis $\{|0\rangle, |1\rangle\}$; (c) reflecting qubits without disturbance; (d) reordering qubits. This simplifies quantum communication realisation while maintaining security. Initially developed for key distribution, semi-quantum research has expanded, with new protocols [9], security proofs [18][12][34], experimental implementations [9][2], and broader cryptographic applications beyond key distribution [36][17][20].

Recently Tian et al. [22] introduced a protocol that enables quantum Alice to share a specific secret with classical Bob and Charlie using Bell states. Notably, this protocol exhibits exceptional resilience against well-known attacks and achieves remarkable efficiency compared to similar approaches and existing schemes. However, a limitation of the protocol is its applicability only to two participants. In this study, we extend the protocol to accommodate multiple classical parties, generalizing it for n participants. Additionally, we demonstrate the protocol’s robustness against the Trojan horse attacks without the need for costly quantum devices, aligning with the original intent of the semi-quantum environment. Furthermore, we provide a concise overview of semi-quantum secret sharing, addressing challenges and field-specific issues, while also highlighting potential research directions for future exploration.

The subsequent sections are structured as follows: Sect. 2 provides a concise overview of semi-quantum secret sharing, addressing the challenges faced by SQSS protocols and presenting open questions for further investigation. Section 3 reviews Tian et al.’s protocol [22]. In Sect. 4, we present the generalized protocol for multiple parties. Section 5 demonstrates the protocol’s resilience against Trojan horse attacks without compromising the intent of the semi-quantum environment. The article concludes with a final summary.

2 Background

In 2010, Li et al. [14] extended the concept of semi-quantum to secret sharing by introducing two SQSS protocols: randomization-based SQSS protocol and measure-resend SQSS protocol, employing maximally entangled GHZ-type states. However, in 2012, Lin et al. [16] discovered security vulnerabilities in the eavesdropping check phase of both protocols, making them susceptible to intercept-resend and Trojan horse attacks. Two potential solutions were proposed to fix those weaknesses. Later, in 2013, Qiu et al. [13] introduced a two-party SQSS protocol based on product states, offering a more practical and feasible approach compared to entangled states using current technologies. In 2015, Xie et al. [27] presented a multiparty SQSS protocol focused on specific bits, which allowed direct sharing of secret messages, a significant advancement over existing methods at the time. However, Yin et al. [32] identified a security weakness susceptible to intercept and resend attacks in this protocol, and though they proposed a solution, it deviated from the semi-quantum condition. In contrast, Gao et al. [7] introduced a new protocol in 2017 that resolved the security issue while adhering to the semi-quantum condition and improved efficiency. Additionally, in 2017, Yin et al. [33] presented an efficient SQSS protocol based on Bell states.

Semi-quantum cryptography was initially introduced to address the theoretical question of how much quantum capability is needed to surpass the classical counterpart. Therefore, exploring how resource requirements can be minimized and how this impacts security remains an intriguing aspect of the field. In 2018, Ye et al. [28] proposed a circular transmission protocol, departing from the traditional tree-type approach, and eliminated the need for measurements by classical parties. In the same year, Li et al. [15] introduced a resource-efficient SQSS protocol, relieving participants from performing measurements. In 2019, Xiang et al. [26] presented a novel protocol based on multi-level systems, reducing participants' capacities while ensuring strong security. This approach eliminated the need for Alice to access quantum memories and for classical users to perform measurements, offering remarkable efficiency by optimizing quantum resources in eavesdropping detection and increasing the amount of information carried by each particle.

In recent years, several notable advancements have been made in the field of semi-quantum secret sharing (SQSS). In 2019, Tsai et al. [24] introduced a three-party SQSS protocol based on W-states. In 2020, Zhi-Gang [35] presented an enhanced version of Gao et al.'s protocol, achieving higher qubit efficiency and reduced classical communication by utilizing two-particle entangled states. In 2021, Tian et al. [22] proposed a new SQSS protocol, efficiently sharing specific secret information. Concurrently, Yin and Chen [31] introduced a protocol with identity authentication, using GHZ-type states to verify communication partners' identification. During the same year, Ye et al. [29] introduced a multiparty SQSS protocol based on measure-flip and reflect operations. These developments demonstrate the remarkable progress in SQSS, with researchers proposing diverse protocols [30] [5] [4] [21], leveraging various quantum resources to address specific

security, efficiency, or feasibility concerns. So far, semi-quantum communication schemes appear to encompass most of the desired features in a protocol. However, as referenced in prior works [11] [9] [23] [25], such protocols face two significant limitations:

- Only the user with full quantum capabilities can share a secret. This aligns with practicality, but it sparks interest in exploring how a classical user could share their secret and remain protected from a dishonest quantum user.
- Most of SQSS protocols adopt a two-way quantum communication scheme, making them exceedingly vulnerable to Trojan horse attacks. Consequently, all classical participants must equip themselves with additional quantum devices such as photon number splitters and optical wavelength filters to fend off these attacks. However, incorporating these devices may deviate from the original intent of the semi-quantum environment, which aimed to demonstrate the design of low-cost and limited-capability protocols comparable in security to fully quantum ones.

The primary limitation was first tackled in 2015 [11] when Krawec introduced the concept of “mediated semi-quantum key distribution” (MSQKD) in his article. This model involves two classical users, namely Alice and Bob, aiming to establish an exclusive secret key between them. To achieve this, they enlist the assistance of an untrusted quantum server responsible for executing all the necessary quantum operations in the protocol. However, this quantum server may pose a potential risk, as it could attempt various attacks to gain access to Alice and Bob’s secret key. Subsequently, in 2019, Tsai and Yang [23] addressed the second limitation by proposing an MSQKD protocol designed to mitigate the Trojan horse threat. They devised a one-way communication protocol and granted classical users the ability to perform the Hadamard operator.

In 2021, these same authors further extended these concepts to semi-quantum secret sharing [25]. Their article introduced a multiparty mediated quantum secret sharing (MQSS) protocol based on GHZ states, which enables restricted quantum users to share secrets with the assistance of a potentially untrustworthy third-party (TP) with full quantum capabilities. Additionally, apart from the four allowed operations for classical users we have seen in the introduction, they included the Hadamard operation. By adopting a one-way communication approach, this protocol exhibits robustness against Trojan horse attacks, relieving limited quantum participants of the need to invest in costly quantum devices. This aligns with the fundamental purpose of semi-quantum cryptography. To our knowledge, Tsai et al.’s [25] protocol stands as the sole MSQSS protocol that addresses the above limitations for SQSS protocols.

This avenue of research presents intriguing possibilities for future studies, expanding the realm of options in semi-quantum quantum secret sharing. Notably, it demonstrates that classical users can benefit from quantum physics tools to securely share sensitive information, even in the presence of internal quantum adversaries. Furthermore, this concept holds practical significance, as it opens a scenario where untrusted servers play a facilitating role for classi-

cal users, assisting them to implement SQSS protocols (or other cryptographic schemes) within their communication infrastructure.

3 Review of Tian et al.'s Protocol

The protocol [22] is based on Bell states, providing Alice with the flexibility to determine both the content of the shared secret message and the number of detected particles. By controlling the percentage of detection qubits, she can effectively regulate the protocol's efficiency. Alice utilizes the two Bell states: $|\phi^-\rangle = \frac{1}{\sqrt{2}}(|00\rangle - |11\rangle)$ and $|\psi^+\rangle = \frac{1}{\sqrt{2}}(|01\rangle + |10\rangle)$, representing the bit “0” and “1”, respectively.

For the eavesdropping detection process, Bob and Charlie have the option to choose between two operations: **Measure and Resend**, where they measure the received qubits in the Z -basis and return newly generated qubits with the same states to Alice, or **Reflect**, where they simply reflect the qubits without any disturbance. Meanwhile, for the remaining qubits, Bob and Charlie conduct measurements in the Z -basis. To ensure the validity of the shared secrets, test bits come into play, allowing Bob and Charlie to perform exclusive-OR operations and compare their results with Alice. When both Bob and Charlie measure their qubits in the Z -basis, their measurements reveal a distinctive correlation:

$$0 = r_B \oplus r_C \quad (\text{If the shared state is } |\phi^-\rangle) \quad (1)$$

$$1 = r_B \oplus r_C \quad (\text{If the shared state is } |\psi^+\rangle) \quad (2)$$

In these equations, r_B and r_C represent the outcomes of measurements conducted in the Z -basis by Bob and Charlie, respectively. Additionally, the protocol employs decoy photons to detect potential attackers, while the test bits play a crucial role in verifying the authenticity and integrity of the shared secrets. The protocol is described by the following steps:

1. Alice prepares N entangled particle pairs. If the classical bit she intends to share is “0”, she prepares the Bell state

$$|\phi^-\rangle_{bc} = \left(\frac{1}{\sqrt{2}}\right)(|00\rangle - |11\rangle)_{bc}. \quad (3)$$

Else she prepares

$$|\psi^+\rangle_{bc} = \left(\frac{1}{\sqrt{2}}\right)(|01\rangle + |10\rangle)_{bc}. \quad (4)$$

Alice obtains two sequences of particles, S_B and S_C , that need to be transmitted to Bob and Charlie, respectively. Additionally, she possesses a random bit sequence K_A that corresponds to her preparation of the entangled states.

2. Alice generates a set of decoy photons, randomly choosing from the states $\{|0\rangle, |1\rangle, |+\rangle, |-\rangle\}$, and then inserts them into the sequences S_B and S_C at random positions. Alice obtains two new sequences which are represented by S'_B and S'_C .
3. Alice sends the new sequences S'_B and S'_C to Bob and Charlie, respectively. After they confirm receipt, Alice discloses the positions of the decoy photons she inserted earlier.
4. Alice, Bob, and Charlie perform the eavesdropping checks using the decoy photons. Subsequently, Bob and Charlie randomly decide between **Measure and Resend** or **Reflect**. Alice's subsequent operations are based on Bob and Charlie's choices.
 - In the event that both Bob and Charlie opt for **Measure and Resend**, Alice measures the received particles using the Z -basis and then compares the measurements with those made by Bob and Charlie.
 - Should either Bob or Charlie choose the **Reflect** operation, Alice will compare the measurements of the reflecting particles with the initial states she prepared.
5. After the eavesdropping checks, Bob and Charlie measure their respective qubits in sequences S_B and S_C with the Z -basis, obtaining binary bit strings denoted as K_B , and K_C . To verify the shared secret, Bob and Charlie extract test bits from K_B and K_C , perform the exclusive-OR operation, and compare with Alice's corresponding bits. Finally, using the remaining bits of K_B and K_C , Bob and Charlie calculate Alice's secret keys as $K_A = K_B \oplus K_C$.

4 The Proposed Generalized Protocol

In the multiparty case, Alice encodes her classical messages in two entangled states: $|\psi_0\rangle = \frac{1}{\sqrt{2}}(|+\rangle^{\otimes n} + |-\rangle^{\otimes n})$ and $|\psi_1\rangle = \frac{1}{\sqrt{2}}(|+\rangle^{\otimes n} - |-\rangle^{\otimes n})$, where

$$|+\rangle = \frac{1}{\sqrt{2}}(|0\rangle + |1\rangle), \quad |-\rangle = \frac{1}{\sqrt{2}}(|0\rangle - |1\rangle). \quad (5)$$

Here, $|\psi_0\rangle$ represents the classical bit “0” and $|\psi_1\rangle$ represents the classical bit “1”. When all classical participants measure their qubits in the Z -basis, their measurement results exhibit the following correlation:

$$0 = r_1 \oplus r_2 \oplus \cdots \oplus r_n, \quad (\text{If the shared state is } |\psi_0\rangle) \quad (6)$$

$$1 = r_1 \oplus r_2 \oplus \cdots \oplus r_n, \quad (\text{If the shared state is } |\psi_1\rangle) \quad (7)$$

Here, r_i represents the result of the measurement performed by the i -th classical participant in Z -basis. Now, let's describe our protocol:

1. Alice prepares N entangled states, each of which is

$$|\psi_0\rangle = \frac{1}{\sqrt{2}}(|+\rangle^{\otimes n} + |-\rangle^{\otimes n}), \quad (8)$$

or

$$|\psi_1\rangle = \frac{1}{\sqrt{2}}(|+\rangle^{\otimes n} - |-\rangle^{\otimes n}) \quad (9)$$

Where N is the length of the string of binary bit Alice wants to share and n is the number of classical participant. Based on Alice's preparation of entangled states, she generates a random bit sequence denoted as K_A . For each entangled state, Alice will transmit one to each of the n participants. She possesses n sequences of particles denoted as $S_i = (p_i^1, p_i^2, \dots, p_i^N)$, where $1 \leq i \leq n$, and she sends each sequence to the corresponding participant. Each sequence $(p_1^j, p_2^j, \dots, p_n^j)$, where $1 \leq j \leq N$, comprises entangled particles.

2. Alice generates a set of decoy photons, randomly choosing from the states $\{|0\rangle, |1\rangle, |+\rangle, |-\rangle\}$, and then inserts them into the sequences S_i at random positions. It's worth noting that only Alice is aware of the positions and states of these decoy photons. As a result, she obtains n new sequences denoted as S'_i .
3. Alice proceeds to transmit the sequences S'_i to each of the n participants individually. It is worth noting that Alice doesn't keep any sequence of particles to herself. Upon receiving their respective sequences, each participant publicly announces the receipt of their sequence.
4. Alice declares the positions of the decoy photons, which she inserted before.
5. During the eavesdropping checking phase, Alice and the n participants collectively perform the necessary procedures. Based on Alice's declaration, each participant selects decoy photons and randomly chooses between two operations: **Measure and Resend** or **Reflect**. Subsequently, Alice's operations are determined according to the choices made by each participant.
 - If all participants choose **Measure and Resend**, Alice will measure the received particles in the Z -basis and compare the results with the measurements of each participant. The error rate will indicate whether there is an eavesdropper. If there is no eavesdropper, the measurement results should match those of the participants. Any discrepancy in the measurement results indicates the presence of an eavesdropper. If the error rate exceeds a predefined threshold, the protocol is terminated; otherwise, they proceed to the next step.
 - If $m \geq 1$ participants choose the **Reflect** operation, Alice will compare the measurements of the reflecting particles with the initial states she prepared. Any deviation from the initial qubits she sent indicates the presence of an eavesdropper. If the error rate exceeds the threshold, the communication is aborted; otherwise, they proceed to the next step.

After that, the sequences S_i are lifting in participants' hands, respectively.

6. After the eavesdropping check, each participant measures all qubits in their sequences S_i using the Z -basis and records the measurement results in their respective key sequences K_i , where $1 \leq i \leq n$. The measurement result $|0\rangle$ corresponds to the classical bit “0”, and $|1\rangle$ corresponds to the classical bit “1”. These sequences K_i serve as the keys containing the measurement results of the qubits for each participant. To verify the validity of the shared secret, participants select test bits from their K_i sequences and perform exclusive-OR operations on them. Then, they compare the results with the values of the corresponding bits in Alice’s sequence K_A . It’s worth noting that Alice reveals the values of these particular bits via the public channel, without disclosing the entire sequence K_A , but solely the relevant test bits. If the two values match, the shared secret is considered valid. Finally, the participants calculate Alice’s secret keys with the rest of the K_i by

$$K_A = K_1 \oplus K_2 \oplus \cdots \oplus K_n. \quad (10)$$

5 Security Analysis

In this section, we show that the proposed protocol is robust against the Trojan horse attacks. There exists two types of Trojan horse attacks. The first type involves using a “delayed photon”, where the attacker intercepts and probes a qubit with an undetectable photon inserted in a shorter time window. The attacker gains information about the participant’s operation by measuring the probing photon after the participant performs their operation. The second type involves attaching an “invisible photon” to each qubit sent to the participant, remaining undetected. When the participant performs an operation on the qubit, the invisible photon also undergoes the same operation simultaneously. In both methods, the attacker can extract full information about the participant’s operations when retrieving the Trojan horse photons.

Most SQSS Protocols adopt a two-way or circular communication which makes them most vulnerable to Trojan horse attacks, as the attacker has a chance to retrieve malicious photons. On the other hand, one-way communication protocols [23] are robust against these attacks since no qubits are returned, making them less susceptible to Trojan horse attacks. To avoid these attacks, most SQSS protocols equip the classical participants with additional costly quantum devices such as the photon number splitters and the optical wavelength filters, which violates the original assumption of the semi-quantum environment. Even highly efficient multiparty protocols such as Ye et al. [29] protocol display this issue. In contrast, our newly proposed multiparty protocol demonstrates resilience against Trojan horse attacks without necessitating the deployment of these costly quantum devices among classical participants.

In our proposed protocol, two communication methods are employed over the quantum channel: a two-way communication system for decoy photons used in eavesdropping checks and a one-way communication system for the qubits

involved in sharing the specific secret message and verifying its validity. Let's consider a simple scenario involving three parties, with Charlie as the potential dishonest participant. He intercepts the transmission between Alice and Bob and attaches invisible photons to each particle of the sequence S'_B sent from Alice to Bob, along with inserting delay photons within the same time window for each particle of S'_B .

During the eavesdropping checks, Bob can choose either the **Measure and Resend** or **Reflect** operation in response to Alice's announcements about the positions of the decoy photons in the sequence S'_B . For the **Measure and Resend** photons, their corresponding spy photons vanish after being replaced by newly produced ones. On the other hand, Bob directly reflects the **Reflect** photons without any disturbance to Alice. Consequently, when Charlie intercepts the returning sequence of decoy photons (from Bob to Alice), he can distinguish between the **Measure and Resend** photons and the **Reflect** photons within the decoy photon sequence.

For the **Measure and Resend** photons, Charlie can easily perform a Z -basis measurement and resend them to Alice without any further action. Since Alice will also perform a Z -basis measurement on these photons from Bob, their measurement results will match. Consequently, the **Measure and Resend** photons used for the eavesdropping checks cannot detect the presence of Charlie as an attacker. However, with the **Reflect** photons, Charlie's detectability is different. If he chooses to measure the reflected photons in the Z -basis, he will be detectable half of the time. For instance, if Bob reflects the state $|+\rangle$, Alice will expect this same state. If Charlie measures it in the Z -basis, Alice will know there is an eavesdropper. However, if Bob reflects a state in the computational basis, Charlie will remain unnoticed. Therefore, to avoid detection during the eavesdropping checks, Charlie must retrieve the spy photons and let the reflected photons go undisturbed without knowing their states. This way, Charlie can only obtain information about the **Measure and Resend** photons without being noticed.

Regarding the qubits in the sequences S_B , which are used to determine Alice's secret message, Charlie has no means of obtaining any information about Bob's secret shadow. Even if Charlie inserts spy photons into each transmitted qubit, he cannot retrieve information about Bob's secret shadow bits since the spy photons are not sent out after being received by Bob. This one-way communication nature safeguards the protocol against the Trojan horse attacks, ensuring robustness even when an attacker like Charlie remains undetected during the eavesdropping checks.

6 Conclusion

This paper addresses two key limitations of Tian et al.'s protocol. We begin by providing a succinct overview of the field of quantum secret sharing, delving into the challenges and limitations faced by existing SQSS protocols, and identifying promising areas for future research. Subsequently, we propose a generalized

protocol that extends Tian et al.'s approach to accommodate multiple parties, thereby enhancing the protocol's practicality and applicability. Furthermore, we demonstrate that our protocol remains robust against the Trojan horse attack without requiring classical participants to invest in costly quantum devices, in accordance with the principles of semi-quantum cryptography. Nevertheless, further investigations into the security and efficiency aspects of our protocol merit careful consideration in future studies.

References

1. Blakley, G.R.: Safeguarding cryptographic keys. In,: International Workshop on Managing Requirements Knowledge (MARK). IEEE (1979). <https://doi.org/10.1109/mark.1979.8817296>
2. Boyer, M., Katz, M., Liss, R., Mor, T.: Experimentally feasible protocol for semi-quantum key distribution. *Phys. Rev. A* **96**(6), 062335 (2017)
3. Boyer, M., Kenigsberg, D., Mor, T.: Quantum key distribution with classical bob, vol. 99, no. 14, p. 140501 (2007). <https://doi.org/10.1103/physrevlett.99.140501>
4. Chen, Y., Ye, T.Y.: Semiquantum secret sharing by using -type states, vol. 137, no. 12 (2022). <https://doi.org/10.1140/epjp/s13360-022-03521-w>
5. Chong-Qiang, Y., Tian-Yu, Y., De, H., Zhi-Gang, G.: Multiparty semi-quantum secret sharing with d-level single-particle states. *Int. J. Theor. Phys.* **58**(11), 3797–3814 (2019). <https://doi.org/10.1007/s10773-019-04248-8>
6. Cirac, J.I.: Quantum computing and simulation, vol. 10, no. 1, pp. 453–456 (2020). <https://doi.org/10.1515/nanoph-2020-0351>
7. Gao, X., Zhang, S., Chang, Y.: Cryptanalysis and improvement of the semi-quantum secret sharing protocol. *Int. J. Theor. Phys.* **56**(8), 2512–2520 (2017). <https://doi.org/10.1007/s10773-017-3404-9>
8. Hillery, M., Bužek, V., Berthiaume, A.: Quantum secret sharing. *Phys. Rev. A* **59**(3), 1829–1834 (1999). <https://doi.org/10.1103/physreva.59.1829>
9. Iqbal, H., Krawec, W.O.: Semi-quantum cryptography. *Quant. Inf. Process.* **19**(3), 97 (2020). <https://doi.org/10.1007/s11128-020-2595-9>
10. Karlsson, A., Koashi, M., Imoto, N.: Quantum entanglement for secret sharing and secret splitting. *Phys. Rev. A* **59**(1), 162–168 (1999). <https://doi.org/10.1103/physreva.59.162>
11. Krawec, W.O.: Mediated semiquantum key distribution. *Phys. Rev. A* **91**(3), 032323 (2015). <https://doi.org/10.1103/physreva.91.032323>
12. Krawec, W.O.: Security proof of a semi-quantum key distribution protocol. In: 2015 IEEE International Symposium on Information Theory (ISIT), pp. 686–690. IEEE (2015)
13. Li, L., Qiu, D., Mateus, P.: Quantum secret sharing with classical bobs. *J. Phys. A: Math. Theor.* **46**(4), 045304 (2013). <https://doi.org/10.1088/1751-8113/46/4/045304>
14. Li, Q., Chan, W.H., Long, D.Y.: Semiquantum secret sharing using entangled states. *Phys. Rev. A* **82**(2), 022303 (2010). <https://doi.org/10.1103/physreva.82.022303>
15. Li, Z., Li, Q., Liu, C., Peng, Y., Chan, W.H., Li, L.: Limited resource semiquantum secret sharing. *Quant. Inf. Process.* **17**(10), 1–11 (2018). <https://doi.org/10.1007/s11128-018-2058-8>

16. Lin, J., Yang, C.W., Tsai, C.W., Hwang, T.: Intercept-resend attacks on semi-quantum secret sharing and the improvements. *Int. J. Theor. Phys.* **52**(1), 156–162 (2012). <https://doi.org/10.1007/s10773-012-1314-4>
17. Nie, Y.Y., Li, Y.H., Wang, Z.S.: Semi-quantum information splitting using GHZ-type states. *Quant. Inf. Process.* **12**(1), 437–448 (2012). <https://doi.org/10.1007/s11128-012-0388-5>
18. Scarani, V., Bechmann-Pasquinucci, H., Cerf, N.J., Dušek, M., Lütkenhaus, N., Peev, M.: The security of practical quantum key distribution. *Rev. Mod. Phys.* **81**(3), 1301 (2009)
19. Shamir, A.: How to share a secret. *Commun. ACM* **22**(11), 612–613 (1979). <https://doi.org/10.1145/359168.359176>
20. Thapliyal, K., Sharma, R.D., Pathak, A.: Orthogonal-state-based and semi-quantum protocols for quantum private comparison in noisy environment. *Int. J. Quant. Inf.* **16**(05), 1850047 (2018). <https://doi.org/10.1142/s0219749918500478>
21. Tian, Y., Bian, G., Chang, J., Tang, Y., Li, J., Ye, C.: A semi-quantum secret-sharing protocol with a high channel capacity. *Entropy* **25**(5), 742 (2023). <https://doi.org/10.3390/e25050742>
22. Tian, Y., Li, J., Chen, X.B., Ye, C.Q., Li, H.J.: An efficient semi-quantum secret sharing protocol of specific bits. *Quant. Inf. Process.* **20**(6), 217 (2021). <https://doi.org/10.1007/s11128-021-03157-2>
23. Tsai, C.W., Yang, C.W.: Lightweight mediated semi-quantum key distribution protocol with a dishonest third party based on bell states. *Sci. Rep.* **11**(1), 23222 (2021). <https://doi.org/10.1038/s41598-021-02614-3>
24. Tsai, C.W., Yang, C.W., Lee, N.Y.: Semi-quantum secret sharing protocol using w-state. *Mod. Phys. Lett. A* **34**(27), 1950213 (2019). <https://doi.org/10.1142/s0217732319502134>
25. Tsai, C.W., Yang, C.W., Lin, J.: Multiparty mediated quantum secret sharing protocol. *Quant. Inf. Process.* **21**(2), 63 (2022). <https://doi.org/10.1007/s11128-021-03402-8>
26. Xiang, Y., Liu, J., Bai, M.Q., Yang, X., Mo, Z.W.: Limited resource semi-quantum secret sharing based on multi-level systems. *Int. J. Theor. Phys.* **58**, 2883–2892 (2019). <https://doi.org/10.1007/s10773-019-04171-y>
27. Xie, C., Li, L., Qiu, D.: A novel semi-quantum secret sharing scheme of specific bits. *Int. J. Theor. Phys.* **54**(10), 3819–3824 (2015). <https://doi.org/10.1007/s10773-015-2622-2>
28. Ye, C.Q., Ye, T.Y.: Circular semi-quantum secret sharing using single particles. *Commun. Theor. Phys.* **70**(6), 661 (2018). <https://doi.org/10.1088/0253-6102/70/6/661>
29. Ye, C., Li, J., Chen, X., Yuan, T.: Multi-party semi-quantum secret sharing protocol based on measure-flip and reflect operations (2021)
30. Yin, A.H., Tong, Y.: A novel semi-quantum secret sharing scheme using entangled states. *Mod. Phys. Lett. B* **32**(22), 1850256 (2018). <https://doi.org/10.1142/s0217984918502561>
31. Yin, A., Chen, T.: Authenticated semi-quantum secret sharing based on GHZ-type states. *Int. J. Theor. Phys.* **60**(1), 265–273 (2021). <https://doi.org/10.1007/s10773-020-04688-7>
32. Yin, A., Fu, F.: Eavesdropping on semi-quantum secret sharing scheme of specific bits. *Int. J. Theor. Phys.* **55**(9), 4027–4035 (2016). <https://doi.org/10.1007/s10773-016-3031-x>

33. Yin, A., Wang, Z., Fu, F.: A novel semi-quantum secret sharing scheme based on bell states. *Mod. Phys. Lett. B* **31**(13), 1750150 (2017). <https://doi.org/10.1142/s0217984917501500>
34. Zhang, W., Qiu, D., Mateus, P.: Security of a single-state semi-quantum key distribution protocol. *Quant. Inf. Process.* **17**, 1–21 (2018)
35. Zhi-Gang, G.: Improvement of Gao et al.’s semi-quantum secret sharing protocol. *Int. J. Theor. Phys.* **59**, 930–935 (2020). <https://doi.org/10.1007/s10773-019-04378-z>
36. Zou, X., Qiu, D.: Three-step semiquantum secure direct communication protocol. *Sci. China Phys. Mech. Astron.* **57**(9), 1696–1702 (2014). <https://doi.org/10.1007/s11433-014-5542-x>



Quantum Convolution for Convolutional Neural Networks

Mustapha Bourahla^(✉)

Computer Science Department, University of M'Sila, M'Sila, Algeria
mustapha.bourahla@univ-msila.dz

Abstract. Quantum machine learning has garnered a lot of attention recently due to the quick advancement of quantum technologies. For enhancing the performance of classical neural networks, a family of hybrid quantum-classical neural networks made up of both classical and quantum components has received extensive study. A new design of quantum convolutional neural networks (QCNNs), is what we propose in this research. With the help of our technique, the idea of convolution, which is frequently used in contemporary deep learning algorithms, is developed with quantum operations to be used in designing the quantum convolutional neural networks (QCNNs). While lowering the computational cost, the suggested QCNNs are able to capture more context throughout the quantum convolution process. We conduct practical studies on the keras digits dataset to perform image recognition and show that QCNN models generally outperform existing quantum convolutional neural networks (QCNNs) in terms of accuracy and loss computation.

Keywords: Convolutional Neural Network · Quantum Neural Network · Quantum Convolution · Parameterized Quantum Circuits · PennyLane

1 Introduction

Convolutional neural networks (CNNs) [1], are one of the most potent deep learning techniques. The primary benefit of CNNs is their ability to reliably and automatically learn critical characteristics from the data without any human supervision by using numerous feature extraction steps. This advantage has allowed CNNs to achieve outstanding results in a wide range of challenging computer vision tasks, including as image recognition [2–5], object detection [6–8], and image segmentation [9–11]. With the advancement of deep learning in recent years, CNNs have also shown promising results in a variety of machine learning applications, including speech recognition [12], time series forecasting [13], and recommendation systems [14].

Parallel to this, the field of quantum machine learning has drawn considerable interest and sparked a tremendous amount of effort due to recent advances in quantum technology (e.g., noisy intermediate-scale quantum (NISQ) processors

are already accessible). The goal of quantum machine learning is to use quantum mechanical phenomena like superposition and entanglement to enhance the efficiency of machine learning algorithms. Despite the fact that quantum machine learning is a relatively new field, classical machine learning issues like support vector machines (SVM), clustering (Clustering), and principal component analysis (PCA) have seen a number of successful quantum extensions.

Quantum convolutional neural networks (QCNNs), often referred to as hybrid quantum-classical convolutional neural networks, are a family of variational quantum algorithms that have most recently attracted a lot of attention in the scientific community. The fundamental concept behind QCNNs is to build a quantum convolutional layer inside artificial neural networks based on parameterized quantum circuits to estimate complex kernel functions in high dimensional Hilbert space. Liu et al. [15] proposed the first QCNN model and applied it for image recognition, drawing inspiration from CNNs. The QCNN model was then further examined in a number of works [16–21]. Recent research in [22] has shown that QCNN models can also produce promising outcomes in speech recognition.

QCNNs are successful, however there are computational bottlenecks that make training them time-consuming. First, unitary matrices of dimension $2^n \times 2^n$, which expand exponentially with the size of quantum circuits, are needed to perform quantum operations on n -qubit quantum circuits. Additionally, when QCNNs are trained on a real quantum device, the calculation of gradients as a result of the parameter-shift rule [23,24], leads to additional quantum circuit executions.

For each training sample, a quantum filter with p trainable parameters will execute 2^p additional quantum circuits in order to compute the necessary gradients. QCNNs will inevitably encounter another difficulty, even though this one can be lessened by using quantum simulators that provide back-propagation [25,26], and adjoint differentiation method [27] for more efficient gradient computing.

Due to local connectivity in CNNs, a convolutional layer executes numerous element-wise matrix multiplication operations. The size of the feature map will have a considerable impact on the computational cost. Fortunately, vectorization approaches can be used to solve this computational problem in CNNs [28,29]. The issue is the same for QCNNs, which are CNNs' equivalents. Contrary to CNNs, the majority of modern quantum devices, including quantum simulators and hardware, do not enable vectorization. Despite the existence of better developed quantum devices in the NISQ period, it would generally be impracticable to execute a significant number of quantum circuits.

1.1 Related Work

Several studies have been conducted to look into ways to make QCNNs less complex to run. The first family of studies uses classical data pre-processing techniques to lower the dimension of the input characteristics fed into the quantum (convolutional) layer, resulting in the tiny number of qubits needed for the quantum circuit. For instance, Hur et al. [31] use autoencoding (AutoEnc) for

the dimensionality reduction, whereas Pramanik et al. [30] use PCA to lower the VGG-16 features for the variational quantum classifier (VQC). However, as demonstrated in [30], the restricted expressive capacity of the reduced features is likely to impair the performance of the model trained in this way.

The second series of research focuses on effective quantum state encoding of classical data. The amplitude encoding for variational quantum circuits is proposed and implemented by Schuld and Killoran [32], and it is further discussed in [33] for the Flexible Representation of Quantum Images (FRQI). This kind of encoding technique is effective in terms of the number of qubits needed to encode data, but it is impractical for NISQ devices because it depends on extremely deep quantum circuits. A new approach is suggested by several recent researchers [21], who suggest angle encoding (also known as qubit encoding) and its variations, such as dense angle encoding, which employ a constant quantum circuit depth for state preparation.

This encoding method is inefficient for high-dimensional input features since it uses one qubit to encode just one or a small number of the input feature vector's components. Hur et al. [31] further create a hybrid encoding approach to trade off these two encoding techniques, using a shorter quantum circuit depth than the amplitude encoding and fewer qubits than the angle encoding. A threshold-based encoding technique is also used by Henderson et al. [17] to condense the input-state space and enable access to the output feature map via a look-up table during the quantum convolution procedure without repeatedly running the same quantum circuit on image segments. Although this method is simple to use, genuine quantum devices cannot support it, as stated in [17].

After reviewing all of these issues and advancements, we suggest a novel quantum architecture in this paper. Our method, which is inspired by the convolution in deep learning, is another approach of the designs provided in [15, 17]. Compared to the aforementioned methods, it helps lower the computational cost of QCNNs in a unique way. The suggested QCNN can generally increase the computational efficiency of conventional QCNNs while obtaining improved task performance.

We propose a unique architecture for a quantum convolutional neural network based on a quantum convolution operation. This is a summary of our work's contributions. This study attempts to incorporate variational quantum circuits with the idea of convolution. Using the digits dataset, we perform experiments to show that these QCNN models perform better than existing QCNN models.

The rest of this paper is organized as follows. In Sect. 2, we present preliminaries on convolution and correlation procedures that are used in this work. The design of the new QCNN is detailed in Sect. 3. Section 4 presents its implementation and experimental results with overall performance evaluation. At the end, we conclude this paper by conclusions and perspectives.

2 Preliminaries

For classification applications like image identification, convolutional neural networks (CNNs) provide a viable machine learning architecture. Typically, a CNN

is made up of several (interleaved) layers of image processing, each of which creates a feature map (a 2-D array of pixels) from the previous layer. The convolution layers calculate new pixel values $features_{i,j}^{(\ell)}$ from a linear combination of nearby pixels in the previous map $features_{i,j}^{(\ell)} = \sum_{k,l=1}^W weights_{k,l} \times features_{i+k,j+l}^{(\ell-1)}$, where the weights $weights_{k,l}$ form a $W \times W$ matrix.

Thus, a key component of CNNs is the convolutional layer, which conducts an operation known as a “convolution”. A convolution is a linear procedure that includes multiplying a set of weights with the features (input) in the context of convolutional networks. A feature extractor, also known as a kernel or filter, for a convolution operation is a two-dimensional (2-D) array of learnable weights. Receptive field, a patch of the input image with the size of a filter, is subjected to a filter, and a product is created between its pixels and the filter’s weight values.

The filter then moves to the next patch using a step size referred to as stride, and repeats the procedure above until it has covered the entire image. A feature map is the result of a sequence of products between the values below the filter and the filter weights. Let’s represent the input image by F and the output feature map by M . Applying a filter h to the input image F produces the feature map M in the 2-D convolution process:

$$M[i, j] = \sum_{u=-k}^k \sum_{v=-k}^k h[u, v] \times F[i - u, j - v] \quad (1)$$

where i and j are the position indices for M . Due to the convolution technique, the output feature map typically has a lower spatial resolution than the original image. By using the zero padding approach, which involves putting a border of pixels with a value of zero around the edges of the input image before applying a filter, this drop in dimensions can be avoided. To specify how many zero values to add to the image’s border, a hyper-parameter called padding can be defined. Typically, the spatial resolution m_w and m_h of the final feature map, which a $m \times n$ kernel extracts from an $i_w \times i_h$ input image, may be determined as:

$$m_w = \frac{i_w - m + 2 \times p}{s} + 1, \quad m_h = \frac{i_h - n + 2 \times p}{s} + 1 \quad (2)$$

where the padding is denoted by p , and the stride is denoted by s .

The correlation is another operation used for the forward and backward propagation in CNNs. The correlation formula is the same as the convolution except that it does shifting in the opposite direction, so the formula of convolution is modified to be

$$M[i, j] = \sum_{u=-k}^k \sum_{v=-k}^k h[u, v] \times F[i + u, j + v] \quad (3)$$

which means that we can obtain the same result if we rotate the filter (kernel) matrix by an angle of 180° .

By taking the maximum value from a small number of adjacent pixels, for example, pooling layers reduce the size of feature maps between successive convolutional layers, where nonlinear (activation) function can be applied. When the size of the feature map is small enough, the final result is calculated using a function that depends on every last pixel (fully connected layer).

By training on huge data sets, the weights and fully connected function are optimized. Contrarily, for a certain CNN, parameters like the number of convolution and pooling layers, as well as the size W of the weight matrices, are fixed. Thus, translationally invariant convolution and pooling layers, each with a fixed set of parameters (regardless of system size), and sequential data size reduction (i.e., a hierarchical structure), are CNN's main characteristics.

3 Design of Quantum Convolutional Neural Network

In tasks like image recognition, recommender systems, and sound classification, the traditional CNNs have demonstrated outstanding performance. Convolutions and pooling operations are used by the family of neural networks known as “classical CNNs” to provide an inductive bias that favors invariances to spatial transformations including translation, rotation, and scaling. A convolutional layer is made up of a small kernel (a window) that sweeps through a 2-D array representation of an image and extracts local information while sharing parameters across the spatial dimensions. To minimize the quantity of the input and provide a technique for summing up data from a neighborhood of input values, pooling layers are often used in addition to convolutional layers. These layers offer the benefit of making the model independent of certain transformations like scaling and rotation in addition to reducing dimensionality. These two kinds of layers are repeatedly applied in alternation.

We present a quantum circuit model that extends these essential qualities to the quantum realm in response to this construction. Our design of quantum convolutional neural network is based on quantum circuit (we followed the principle of PennyLane [34] for designing the quantum circuits) that differs from classical convolutional neural networks and typically consists of three modules (Fig. 1): the encoding module, the entanglement module, and the decoding module.

In the encoding module, the classical data are transformed into a quantum state and then processed further in the following modules of the quantum CNN circuit. There are several different encoding techniques, including basis, amplitude, and angle encoding [35]. For this work we used the amplitude encoding, which encodes data in a compact manner that do not require calculations. A numerical input data vector must be encoded for quantum computing. Since the squared modulus of the amplitudes of a quantum state must add up to L , we employ amplitudes to encode the data. As a result, the input vector must be normalized to a length of L .

To associate each amplitude with a component of the input vector, the dimension of the vector must be equal to a power of two because the vector space of an n qubit register has dimension 2^n . If this is not the case, the input vector can

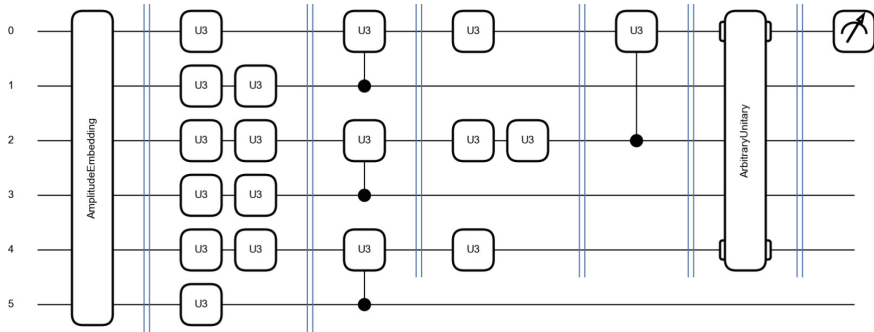


Fig. 1. QCNN circuit for features shape of $(8,8,1)$ and QCNN depth of 2. The two vertical blue lines are used to separate the QCNN layers: The first is an input layer, the second and the fourth are convolution layers, the third and fifth are pooling layers, the sixth is a fully connected layer and the last is an output layer.

be padded with additional zeros to increase the dimension of it. For an arbitrary state represented by n qubits (which represents 2^n data values), it is known that at least $2^n/n$ parallel operations are needed [36]. Current state preparation routines perform slightly better than 2^n operations [36]. However, depending on the data it may still be possible to realize an encoding in a logarithmic runtime. For example, a uniform superposition can be created by applying a Hadamard gate to each of the n qubits, which can be done in parallel and thus in a single step.

It must be noted that if the output is also encoded in the amplitude, multiple measurements must be taken to obtain a good estimate of the output result. The number of measurements scales with the number of amplitudes, as n qubits contain 2^n amplitudes, this is costly [36]. The encoding is more compact (in terms of qubits) than basic and angle encoding. Amplitude encoding is required by many quantum machine learning algorithms [38]. The pre-condition that the data values can be normalized is a common assumption in machine learning [37], e.g. in support vector machine.

The previous module's encoded quantum state is subjected to a set of single and multiple qubit gates in the entanglement module, where, we will build a convolutional and pooling layer in a quantum circuit. Local correlations will be extracted by the first layer, and the second layer will allow the feature vector's dimensionality to be reduced. In a quantum circuit, the convolutional layer is a two-qubit unitary that correlates nearby qubits and consists of a kernel swept along the entire image. We'll employ a single-qubit unitary that is conditioned on the measurement of a nearby qubit for the pooling layer. Then, using an all-to-all unitary gate, we utilize a fully connected layer to entangle every qubit of the final state.

The two-qubit unitary's updated weights, which are input into the convolutional layer at each training step, should be used. This arbitrary two-qubit unitary is modeled in PennyLane using a specific set of gates, two single-qubit U_3

gates, each parametrized by three parameters and each interaction parametrized by one parameter. A QCNN to classify n -qubit input states is thus characterized by $O(\log_2(n))$ parameters. This corresponds to doubly exponential reduction compared to a generic quantum circuit-based classifier and allows for efficient learning and implementation.

The weights of the single-qubit conditional unitaries, in this case U_3 gates, are the inputs of the pooling layer. We next apply these conditional measurements to half of the unmeasured wires, which results in a reduction in the size of our system. By mixing both layers and modeling a fully connected layer with an arbitrary unitary, we can create a QCNN. A set of features (the image) will be input, encoded using an embedding map, subjected to rounds of convolutional and pooling layers, before the necessary measurement statistics of the circuit are finally output.

4 Implementation and Experimental Results

We have used PennyLane [34], which is a cross-platform Python library for programming quantum computers to implement and test the quantum convolutional neural networks (QCNNs). PennyLane is a Python-based open source framework, which makes it possible to automatically differentiate for quantum-classical computations. It features a robust ecosystem of plugins and is inter-operable with popular machine learning frameworks like TensorFlow and PyTorch, which gives users access to a wide range of quantum devices (i.e., simulators and hardware) from a variety of manufacturers, such as IBM, Google, Microsoft, Rigetti, and QunaSys.

Due to its differentiable programming paradigm, quantum programs can be run and trained on a variety of backends. PennyLane makes sophisticated machine learning frameworks like NumPy’s autograd, JAX, PyTorch, and TensorFlow quantum-aware by connecting them to quantum computers. The management of quantum computations, including the assessment of circuits and the computing of their gradients, is its primary function. By sending this data to the classical framework, programs can use seamless quantum-classical pipelines.

According to PennyLane’s design principle, circuits can operate without modification on a variety of hardware simulators or devices because the difficult task of enhancing communication with the devices, compiling circuits for the backend, and selecting the best gradient strategies is handled. The library has built-in simulators, but it also has excellent integration with third-party tools for running quantum circuits, like IBM’s Qiskit, Google’s Cirq, Rigetti’s Forest, and Xanadu’s Strawberry Fields.

To evaluate the efficiency of the proposed QCNN, we implemented Python classes for convolutional, pooling and fully connected layers in addition to input and output layers to define quantum network models. Quantum node objects are used in PennyLane to describe quantum computations, which entail the use of one or more quantum circuits. The quantum circuit is declared using a quantum node, which also links the computation to the particular hardware used to carry

it out. One must first choose a computing equipment before running and then optimizing a quantum circuit. The device is a member of the *Device* class and can represent a hardware or a simulator.

The device loader can be used to instantiate them, for instance, in the definition `device = qml.device('default.qubit', wires=num_wires)`, the ‘default.qubit’, ‘default.mixed’, ‘lightning.qubit’, and ‘default.gaussian’ simulators are some of the fundamental devices available in PennyLane; further devices can be added as plugins. It should be noted that the choice of a device has a considerable impact on calculation performance as well as the choices that can be supplied to the device loader. A quantum node, also known as a *QNode* object, is made up of a quantum function and a device that encapsulates and connects the two. The following code will explicitly build a *QNode* circuit:

```
circuit = qml.QNode(quantum_fun, dev_wires).
```

The *QNode* can be used to compute the result of a quantum circuit as if it was a Python function. It takes the same arguments as the original quantum function: `@qml.qnode(qml.device('default.qubit', wires=nw), interface='jax')`. By including an extra interface argument when establishing a *QNode*, *QNodes* can interface with any of the supporting numerical and machine learning libraries: NumPy, PyTorch, TensorFlow, and JAX. The quantum circuit may easily combine with optimizers and data structures that are specialized to a given library (such as NumPy and JAX arrays or Pytorch/TensorFlow tensors). A unique Python function called a quantum circuit function, or simply a quantum function, is used to build a quantum circuit: `def circuit(weights, features)`.

Through interfaces to automatic differentiation libraries, PennyLane offers a link between the quantum and classical worlds. The supporting libraries at the moment are NumPy, PyTorch, JAX, and TensorFlow. Each of these libraries becomes quantum-aware thanks to PennyLane, enabling the treatment of quantum circuits as any other process. We can select any automatic differentiation framework using any device.

For the input layer (the encoding layer), a loading procedure for amplitude encoding [34], is provided by PennyLane. A routine for preparing arbitrary states is also included in the library. A state preparation technique that approximates the required amplitude encoding encodes 2^n features into the amplitude vector of n qubits and needs an exponential number of operations to encode 2^n data values.

```
qml.AmplitudeEmbedding(features=self.features, wires=self.wires,
                        normalize=True, pad_with=0.5)
```

Features (the layer self data) are automatically padded to dimension 2^n when `pad_with` is set to a real or complex value, where n is the number of qubits used in the embedding. The L2-norm of features must equal one in order to constitute a legitimate quantum state vector. To automatically equalize the characteristics, set the option `normalize` to *True*.

If automatic padding and normalization are both employed, padding is carried out first. A normalized 2^n -dimensional feature vector is encoded using ampli-

tude embedding into the state of $n = \text{self.wires}$ qubits, which is the layer self data representing its number of wires.

The features argument is generally not distinguishable since non-trivial classical processing was required to build the state preparation circuit. If the feature input is not normalized, the template will produce an error. To automatically normalize it, set $\text{normalize} = \text{True}$.

If the feature vector's dimension is less than the total number of amplitudes, the `pad_with` option will automatically add a constant to make up for the missing dimensions.

The second layer is the quantum convolutional layer, which is used for extracting local correlations. In a quantum circuit, the convolutional layer is a two-qubit unitary U_3 that correlates nearby qubits and consists of a kernel swept along the entire image.

This quantum gate performs on one wire an arbitrary (generalized) rotation, which is given by a unitary matrix using three parameters: a polar angle, an azimuthal angle and a quantum shift phase.

```
n_wires = len(self.wires)
for x, w in enumerate(self.wires):
    if x < n_wires - 1:
        qml.U3(*self.weights[3*x:3*(x+1)], wires=[w])
        qml.U3(*self.weights[3*x:3*(x+1)], wires=[self.wires[x+1]])
```

The third layer is the pooling layer, which will allow the feature vector's dimensionality to be reduced. We will employ a single-qubit unitary that is conditioned on the measurement of a nearby qubit for the pooling layer. The quantum gate “`qml.measure`” performs a mid-circuit measurement in the computational basis on the supplied qubit.

This measurement outcomes can be obtained and used to conditionally apply operations. If a device doesn't support mid-circuit measurements natively, then the QNode will apply the `defer_measurements()` transform. The used wires by this gate can be reused after measurement. Moreover, measured wires can be reset to the $|0\rangle$ by setting its option `reset` to the value `True`.

The QNode “`qml.cond`” conditions a quantum operation on the results of mid-circuit qubit measurements, where the support for using “`cond()`” is device-dependent. If a device doesn't support mid-circuit measurements natively, then the QNode will apply the `defer_measurements()` transform. Its parameters are the condition (`MeasurementValue`), which is a conditional expression involving a mid-circuit measurement value.

The second argument, which is a quantum function of PennyLane operation will be applied if the condition is `True`, else it will apply the quantum function represented by the third argument or none if it is not present. This QNode returns a new function that applies the conditional equivalent of true function. The returned function takes the same input arguments as true function.

```

n_wires = len(self.wires)
for x, w in enumerate(self.wires):
    if x % 2 == 0 and x < n_wires-1:
        m_cond = qml.measure(self.wires[x + 1])
        qml.cond(m_cond, qml.U3)(*self.weights, wires=self.wires[x])

```

Then, using an all-to-all unitary gate, we utilize a fully connected layer to entangle every qubit of the final state. For this layer, an arbitrary unitary is applied on the specified wires. An arbitrary unitary on n wires is parametrized by $4^n - 1$ independent real parameters. This template uses “Pauli” word rotations to parametrize the unitary. Its first parameter is the weights (tensor like), which represents the angles of the “Pauli” word rotations, needed to have length $4^n - 1$, where n is its second parameter (the number of wires the template acts upon).

```
qml.ArbitraryUnitary(self.weights, self.wires)
```

The output layer uses the function “`qml.probs()`” to instruct the *QNode* to return a probability of each computational basis state. This measurement function accepts either a wire specification or an observable. Passing wires to the function instructs the *QNode* to return a flat array containing the probabilities $| \langle i | \psi \rangle |^2$ of measuring the computational basis state $|i\rangle$ given the current state $|\psi\rangle$. Marginal probabilities may also be requested by restricting the wires to a subset of the full system; the size of the returned array will be $[2^{len(wires)}]$.

```
return qml.probs(wires=self.output_wires)
```

In addition to these classes of QCNN layers, a main Python class called QCNN is defined for declaring model objects to make up QCNN models, which has methods for fitting the model using data sets and predicting outputs of given inputs. The fitting function uses the AdamOptimizer to optimize and update weights by calculating loss and accuracy using jax, which supports just-in-time (jit) compilation and jax.vmap to vectorize the execution of the QCNN model over all input states.

4.1 Comparison with Classical CNN

On a local machine with a 4-core CPU (2.3 GHz), experiments are carried out using PennyLane. We defined two models using the different coded classes, the first is a classical CNN model (*cmodel*) using the different Keras classes representing CNN layers and the second is a QCNN model (*qmodel*) using the different QCNN layers classes implemented in this work. These two models are trained on the same keras dataset of digits. The following is the Python code for the QCNN model.

```

x_train, y_train, x_test, y_test = load_digits_data(num_train=150, num_test=100)
model = QCNN(features_shape=x_train.shape, QCNN_depth=2) # x_train.shape = (8,8,1)
device = qml.device('default.qubit', wires=model.num_wires)
@qml.qnode(device, interface='jax')
def circuit(weights, features):
    model.layers = []
    model.weights = weights
    model.features = features
    model.add(InputLayer(model.features, model.wires))
    model.add(BarrierLayer(model.wires))
    model.add(ConvolutionalLayer(model.weights[:,0][::3*(model.num_wires-1)], model.wires))
    model.add(BarrierLayer(model.wires))
    model.add(PoolingLayer(model.weights[:,0][3*(model.num_wires-1)::], model.wires))
    model.add(BarrierLayer(model.wires[::2]))
    model.add(ConvolutionalLayer(model.weights[:,1][::3*(model.num_wires-1)], model.wires[::2]))
    model.add(BarrierLayer(model.wires[::2]))
    model.add(PoolingLayer(model.weights[:,1][3*(model.num_wires-1)::], model.wires[::2]))
    model.add(BarrierLayer(model.wires[::2][::2]))
    model.add(FCLayer(model.FCweights(), model.wires[::2][::2]))
    model.add(BarrierLayer(model.wires[::2][::2]))
    model.add(OutputLayer(model.wires[0]))
    return model.circuit()
history = model.fit(x_train, y_train, x_test, y_test, epochs=200)

```

We will tackle a challenge where $8 \times 8 = 64$ attributes must be encoded in our quantum state. As a result, each feature value must be encoded in the amplitude of each computational basis state using six qubits ($\log_2(64) = 6$). We categorize the numbers 0 and 1 from the traditional digits data set (keras digits dataset). Each handwritten digit image is represented as a 8×8 array of pixels. In order to make the digits data set from sklearn.dataset more convenient, we construct a load_digits_data function that will generate random training and testing sets from the data set.

In this experiment, we were interested to evaluate the performance with regard to both validation loss and accuracy. In light of the quantum convolutional neural network, it provides up to 11.74% lower validation loss and up to 3% higher validation accuracy, compared with the classical CNN model (Fig. 2). This observed model performance boost stems mainly from the contextual information at larger scales captured by the QCNN design.

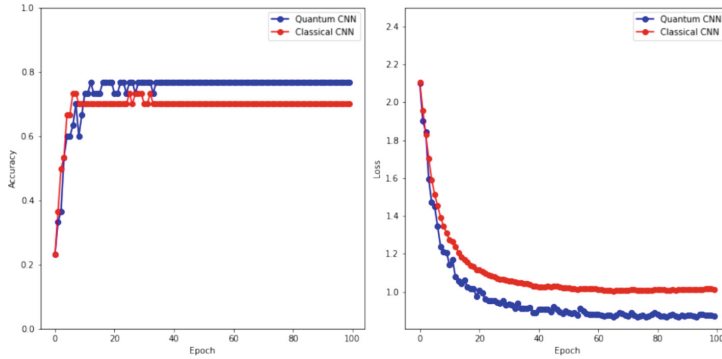


Fig. 2. Comparison of validation loss and accuracy

4.2 Overall Performance Evaluation

Making precise predictions based on unobserved data is the ultimate objective of quantum machine learning (QML). To verify its bound with respect to its

complexity, we compute the accuracy error for this. We strive to maximize a machine-learning model's performance over the relevant data distribution (for example, images of various classes) when optimizing it, whether it be classical or quantum. However, in reality, we are only given a finite set of data, which is why it is important to consider how well our model works with fresh, previously unexplored data. The accuracy error, which measures how well the model has learned to predict unseen data, is the difference between the model's performance on the genuine data distribution and the performance calculated from our training data.

For overall performance evaluation, we begin by outlining the conventional QML model data processing pipeline. A mapping called $x \mapsto \zeta(x)$ is used to first encode a classical data input, x , in a quantum state. Then, this encoded state is processed through a quantum channel with learnable parameters named $Q_\alpha(\zeta(x))$. The final forecast is obtained by doing a measurement on the outcome state. Our model's performance on fresh data is now measured by minimizing the anticipated loss over the data-generating distribution D . For a loss function ℓ , the anticipated loss, denoted by L , can be calculated mathematically by using the formula $L(\alpha) = Q_{(x,y) \sim D}[\ell(\alpha; x, y)]$, where x stands for the features, y for the labels, and D for their combined distribution.

In reality, this amount must be calculated from a limited set of data because the combined distribution D is typically unknown. Given a training set $S = \{(x_i, y_i)\}_{i=1}^N$ with N samples, we estimate the performance of QCNN model by calculating the average loss over the training set $L_S(\alpha) = 1/N \sum_{i=1}^N \ell(\alpha; x_i, y_i)$, which is referred to as the training loss and is an unbiased estimate of $L(\alpha)$. This is merely a proximate representation of the genuine quantity of interest $L(\alpha)$; the difference between the two is known as the accuracy error, or $AE(\alpha) = L(\alpha) - L_S(\alpha)$, and it is this quantity that we will be focusing on.

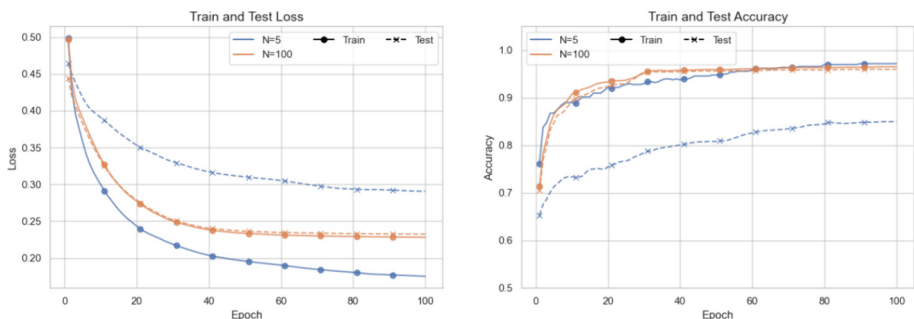


Fig. 3. Train and test losses and accuracies of two datasets, $N = 5$ and $N = 100$

As may be seen here, training for various training set sizes results in various accuracy levels. The overall test accuracy increases as the size of the training data increases. We will compare the model's test and train accuracy by plotting the loss and accuracy for the training and testing sets across all training

epochs (Fig. 3). Some quantum learning models may produce high-fidelity predictions with only a small amount of training data. We have trained the QCNN to discriminate between handwritten digits of 0s and 1s using six qubits. We developed a model with an accuracy of more than 97 percent using 100 samples and 200 training epochs.

Additionally, we examined the test and train accuracy of this model for various training sample counts and discovered that the error scaling is consistent with our intuitive understanding that the accuracy error scales inversely with the quantity of training samples N and rises with the quantity of parametrized gates G . With this, we can see that QCNNs require a training set of size N to satisfy this inequality $AE(\alpha) \leq \sqrt{G/N}$, which means $N \sim O(\text{poly}(\log(n)))$, where n is the circuit size. The accuracy errors of different sizes of datasets are shown in Fig. 4.

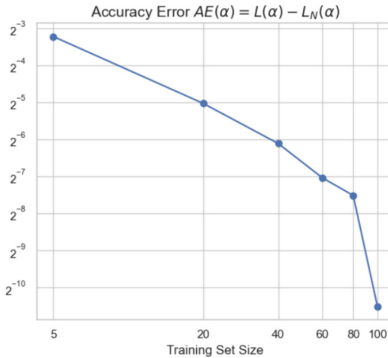


Fig. 4. Accuracy errors of different sizes of datasets

5 Conclusions and Perspectives

In this study, we proposed a brand-new quantum machine learning model that applies the convolutional neural network from deep learning to the quantum network. We provide empirical data to demonstrate that, in terms of recognition accuracy and loss validation, the suggested QCNN model performs better than the recently developed QCNN approach. We specifically discover that a better model performance is often aided by the quantum convolution. In the field of deep learning, convolution has received a great deal of attention, but research on it in the context of quantum machine learning has been sparse. A starting step in this approach is our effort. Our QCNN technique merits more research in the future given the encouraging results on the digits dataset.

References

1. LeCun, Y., Bottou, L., Bengio, Y., Haffner, P.: Gradient-based learning applied to document recognition. Proc. IEEE **86**(11), 2278–2324 (1998)
2. Krizhevsky, A., Sutskever, I., Hinton, G.E.: ImageNet classification with deep convolutional neural networks. In: Proceedings of Advance Neural Information Processing System (NIPS), vol. 25, pp. 1097–1105 (2012)
3. Simonyan, K., Zisserman, A.: Very deep convolutional networks for large-scale image recognition. [arXiv:1409.1556](https://arxiv.org/abs/1409.1556) (2014)
4. Szegedy, C., et al.: Going deeper with convolutions. In: Proceedings of IEEE Conference on Computer Vision Pattern Recognition (CVPR), pp. 1–9 (2015)
5. He, K., Zhang, X., Ren, S., Sun, J.: Deep residual learning for image recognition. In: Proceedings of IEEE Conference on Computer Vision Pattern Recognition (CVPR), pp. 770–778 (2016)
6. Girshick, R., Donahue, J., Darrell, T., Malik, J.: Rich feature hierarchies for accurate object detection and semantic segmentation. In: Proceedings of IEEE Conference on Computer Vision Pattern Recognition, pp. 580–587 (2014)
7. Girshick, R.: FastR-CNN. In: Proceedings of IEEE International Conference on Computer Vision (ICCV), pp. 1440–1448 (2015)
8. Redmon, J., Divvala, S., Girshick, R., Farhadi, A.: You only look once: unified, real-time object detection. In: Proceedings of IEEE Conference on Computer Vision Pattern Recognition (CVPR), pp. 779–788 (2016)
9. He, K., Gkioxari, G., Dollár, P., Girshick, R.: Mask R-CNN. In: Proceedings of IEEE International Conference on Computer Vision, pp. 2961–2969 (2017)
10. Ronneberger, O., Fischer, P., Brox, T.: U-Net: convolutional networks for biomedical image segmentation. In: Navab, N., Hornegger, J., Wells, W., Frangi, A. (eds.) MICCAI 2015, vol. 9351, pp. 234–241. Springer, Heidelberg (2015). https://doi.org/10.1007/978-3-319-24574-4_28
11. Chen, L.C., Zhu, Y., Papandreou, G., Schroff, F., Adam, H.: Encoder-decoder with atrous separable convolution for semantic image segmentation. In: Proceedings of the European Conference on Computer Vision (ECCV), pp. 801–818 (2018)
12. van den Oord, A., et al.: WaveNet: a generative model for raw audio. [arXiv:1609.03499](https://arxiv.org/abs/1609.03499) (2016)
13. Borovykh, A., Bohte, S., Oosterlee, C.W.: Conditional time series forecasting with convolutional neural networks. [arXiv:1703.04691](https://arxiv.org/abs/1703.04691) (2017)
14. Yuan, F., Karatzoglou, A., Arapakis, I., Jose, J.M., He, X.: A simple convolutional generative network for next item recommendation. In: Proceedings of the 12 ACM International Conference on Web Search and Data Mining, pp. 582–590 (2019)
15. Liu, J., Lim, K.H., Wood, K.L., Huang, W., Guo, C., Huang, H.-L.: Hybrid quantum-classical convolutional neural networks. [arXiv:1911.02998](https://arxiv.org/abs/1911.02998) (2019)
16. Cong, I., Choi, S., Lukin, M.D.: Quantum convolutional neural networks. Nat. Phys. **15**(12), 1273–1278 (2019)
17. Henderson, M., Shakya, S., Pradhan, S., Cook, T.: Quanvolutional neural networks: powering image recognition with quantum circuits. Quant. Mach. Intell. **2**(1), 1–9 (2020)
18. Oh, S., Choi, J., Kim, J.: A tutorial on quantum convolutional neural networks (QCNN). In: 2020 International Conference on Information and Communication Technology Convergence (ICTC), pp. 236–239. IEEE (2020)
19. Chen, S.Y.C., Wei, T.-C., Zhang, C., Yu, H., Yoo, S.: Quantum convolutional neural networks for high energy physics data analysis. [arXiv:2012.12177](https://arxiv.org/abs/2012.12177) (2020)

20. Houssein, E.H., Abohashima, Z., Elhoseny, M., Mohamed, W.M.: Hybrid quantum convolutional neural networks model for COVID-19 prediction using chest X-ray images. [arXiv:2102.06535](https://arxiv.org/abs/2102.06535) (2021)
21. Alam, M., Kundu, S., Topaloglu, R.O., Ghosh, S.: Iccad special session paper: quantum-classical hybrid machine learning for image classification. arXiv preprint [arXiv:2109.02862](https://arxiv.org/abs/2109.02862) (2021)
22. Yang, C.-H.-H., et al.: Decentralizing feature extraction with quantum convolutional neural network for automatic speech recognition. In: Proceedings of IEEE International Conference on Acoustics, Speech Signal Processing (ICASSP), pp. 6523–6527 (2021)
23. Mitarai, K., Negoro, M., Kitagawa, M., Fujii, K.: Quantum circuit learning. Phys. Rev. A **98**(3), 032309 (2018)
24. Schuld, M., Bergholm, V., Gogolin, C., Izaac, J., Killoran, N.: Evaluating analytic gradients on quantum hardware. Phys. Rev. A **99**(3), 032331 (2019)
25. Linnainmaa, S.: Taylor expansion of the accumulated rounding error. In: BIT, vol. 16, pp. 146160 (1976)
26. Rumelhart, D.E., Hinton, G.E., Williams, R.J.: Learning representations by back-propagating errors. Nature **323**(6088), 533–536 (1986)
27. Jones, T., Gacon, J.: Efficient calculation of gradients in classical simulations of variational quantum algorithms. [arXiv:2009.02823](https://arxiv.org/abs/2009.02823) (2020)
28. Chellapilla, K., Puri, S., Simard, P.: High performance convolutional neural networks for document processing. In: Proceedings of 10th International Workshop Frontiers Handwriting Recognition, pp. 1–5 (2006)
29. Renand, J., Xu, L.: On vectorization of deep convolutional neural networks for vision tasks. In: Proceedings of Conference on Artificial Intelligent, pp. 1840–1846 (2015)
30. Pramanik, S., et al.: A quantum-classical hybrid method for image classification and segmentation. [arXiv:2109.14431](https://arxiv.org/abs/2109.14431) (2021)
31. Hur, T., Kim, L., Park, D.K.: Quantum convolutional neural network for classical data classification. [arXiv:2108.00661](https://arxiv.org/abs/2108.00661) (2021)
32. Schuld, M., Killoran, N.: Quantum machine learning in feature Hilbert spaces. Phys. Rev. Lett. **122**(4), 040504 (2019)
33. Mattern, D., Martyniuk, D., Willems, H., Bergmann, F., Paschke, A.: Variational quanvolutional neural networks with enhanced image encoding. [arXiv:2106.07327](https://arxiv.org/abs/2106.07327) (2021)
34. Bergholm, V., et al.: PennyLane: automatic differentiation of hybrid quantum-classical computations. [arXiv:1811.04968](https://arxiv.org/abs/1811.04968) (2018)
35. Weigold, M., Barzen, J., Leymann, F., Salm, M.: Data encoding patterns for quantum computing. In: Proceedings of Conference on Pattern Language Programming, pp. 1–11 (2019)
36. Schuld, M., Petruccione, F.: Supervised Learning with Quantum Computers. Springer, Heidelberg (2018). <https://doi.org/10.1007/978-3-319-96424-9>
37. Schuld, M., Fingerhuth, M., Petruccione, F.: Implementing a distance-based classifier with a quantum interference circuit. EPL (Europhys. Lett.) **119**, 6 (2017). <https://doi.org/10.1209/0295-5075/119/60002>
38. LaRose, R., Coyle, B.: Robust data encodings for quantum classifiers. [arXiv:2003.01695](https://arxiv.org/abs/2003.01695) [quant-ph] (2020)



A Quantum-Inspired Deep Learning Models for Skin Lesion Classification

Mohamed Ait Mehdi¹ , Khadidja Belattar² , and Feryel Souami¹

¹ LRIA, USTHB, Algiers, Algeria

{maitmehdi,f.souami}@usthb.dz

² Computer Science Department, University of Algiers, Algiers, Algeria
k.belattar@univ-alger.dz

Abstract. The present study explores the application of quantum machine learning for classifying skin lesion images as melanoma, nevus, or basal cell carcinoma. Using hybrid classical-quantum neural networks with transfer learning, we demonstrate the potential advantages of the four proposed variants in generalizing on complex data. Our models yield improved outcomes compared to conventional deep learning models such as ResNet-18, DenseNet-121, RegNetX-1.6GF, and EfficientNetV2-small. Specifically, we achieve accuracy rates of 82.04%, 85.0%, 84.90% and 86.94% as opposed to 80.0%, 84.08%, 81.63% and 84.49%, respectively. The experiments are conducted on the default PennyLane simulator using the ISIC dataset, demonstrating the practical applicability of quantum machine learning for computer-aided diagnosis applications. Despite these encouraging findings, the study highlights the need for further research to comprehensively understand quantum machine learning approaches and optimize their performance.

Keywords: Quantum machine learning · Deep learning · Convolutional neural networks · Transfer learning · Skin lesion classification

1 Introduction

Image classification [6] is advancing rapidly, marked by increasingly complex applications. These applications span a range of fields, including medical diagnosis [10], face recognition [33], and sign language recognition [2], among others. However, conventional machine learning [17] struggles to effectively address image classification due to its inherent complexity, particularly in high-dimensional data. The process of manual feature extraction in such approaches proves to be time-consuming and lacks adaptability to varying datasets, thus limiting accuracy and generalization capabilities.

In response to these issues, Convolutional Neural Networks (CNN) were proposed, drawing inspiration from the human brain's neural networks, to provide powerful models for deep learning [11]. Despite their wide adoption for real-world challenges, recent progress has revealed limitations of CNN architectures,

especially when handling massive datasets. These limitations arise from the significant computational demands during training and the need for storage, rendering them computationally intensive, and their performance often hinges on the availability of large datasets, potentially restricting applications with limited data.

Concurrently, quantum computing [18], based on the standards on quantum mechanics, shows promise in reducing algorithmic complexity and achieving faster computation processes. This efficiency arises from the inherent parallelism in quantum computing. Such a computational capacity can be exploited to address challenging computational tasks.

While the development of efficient quantum machines is in progress, alternative strategies, such as simulating quantum algorithms on classical computers or integrating them with conventional methods, offer avenues to explore quantum advantages while awaiting advancements in quantum computing systems.

The combination of machine learning algorithms and principles from quantum computing, known as Quantum Machine Learning (QML) [23], has proven to be useful in addressing a wide range of problems [16], including the image classification problem [30], image processing problem [34], regression problem [26], clustering [25], and more. The goal of QML is to enhance the capabilities of each paradigm through mutual inspiration. Within this context, this paper introduces quantum-inspired deep learning models designed to tackle the skin lesion classification problem. The core principle of this hybrid approach lies in enhancing the conventional CNN-based transfer learning architectures (ResNet-18, DenseNet-121, RegNetX-1.6GF, and EfficientNetV2-small) with a variational quantum circuit.

The structure of the paper is as follows. Section 2 provides an overview of the current state of computer-aided diagnosis, with a distinct emphasis on the application of quantum machine learning models for the classification of skin lesions. In Sect. 3, we design and evaluate four pre-trained CNN models inspired by quantum computing for classifying skin lesions using the ISIC image database. Section 4 presents the experimental outcomes and corresponding discussions. Finally, Sect. 5 concludes the study, summarizing the findings, and emphasizes the potential future directions.

2 Related Work

Quantum computing is efficient for complex calculations, requiring specialized machines. While awaiting such devices, quantum-inspired computing has emerged, employing novel algorithms on standard computers with quantum concepts. These methods simplify intricate problem-solving via quantum principles, resulting in a reduction of computational complexity.

Beyond this, quantum machine learning applies quantum algorithms to diverse machine learning tasks, capitalizing on the distinctive attributes of quantum computing, such as superposition and entanglement. These features provide notable advantages, including: 1) Achieving exponential speedup in specific

machine learning tasks [28], **2)** Generating probabilistic outcomes through QML algorithms which are particularly well-suited for classification problems [9], and **3)** Operating within exponentially larger search spaces, consequently leading to significant performance improvements [20, 21, 31].

Among the four emerging variants of QML, including the Classical-to-Classical (CC), Classical-to-Quantum (CQ), Quantum-to-Classical (QC), Quantum-to-Quantum (QQ), the CQ and CC strategies have attracted more attention and exploration in the QML field. The CQ approach involves using classical models, often deep learning models, as feature extractors. Subsequently, these extracted features undergo processing on a quantum computer or circuit. In the QC scenario, pre-trained quantum circuits or models act as feature extractors, generating an output vector of numerical values corresponding to the input. A classical network then further post-process these extracted features for the specific problem at hand. The QQ approach employs trainable quantum models for both feature extraction and subsequent feature post-processing.

In the context of skin lesion classification through CC approaches, a recent study conducted by Belattar et al. [7] undertook a comparative analysis of widely used CNN architectures. This study also summarized the prevailing deep learning-driven approaches to skin lesion classification that were employed between 2020 and 2022.

Consequently, this section presents a comprehensive outline of the most recent quantum-inspired deep neural network strategies in the scope of CQ approaches, all aimed at advancing the field of skin lesion classification. A restricted yet set of proposed techniques has emerged in this context. The inception of this concept can be traced back to [15], where Iyer et al. put forth the idea of developing a 2-qubit hybrid quantum system specifically aimed at classifying skin lesion images. The system is based on the variational classifier model [29]. It involves the following steps: **1)** dimensionality reduction of the input images using an Autoencoder to fit them into the quantum circuit, **2)** the output compressed vectors are encoded into quantum amplitudes, **3)** the encoded quantum representation is used as input data for classification within the quantum circuit, **4)** gradient descent is employed to optimize the classification parameters. To assess the performance of the developed system, a dataset comprising 1000 skin lesion images (including melanoma and melanocytic nevi) is used. The algorithm achieves an average training accuracy of 52%, while the validation accuracy reaches a maximum of 60%.

Later, Li et al. [19] proposed an enhanced quantum Inception-ResNetV1 model for the multi-classification of skin lesion images. This classification system incorporates data augmentation and weighted random sampling techniques to address the challenges posed by imbalanced data distributions. The resulted image dataset is then feed into the enhanced quantum Inception-ResNetV1 model for both training and test steps. The proposed model introduces significant modifications. Notably, the fully connected layer of the network was removed, and instead, an SVM was employed as the classifier. Additionally, the backbone network stem utilizes a quantum convolution layer for feature extraction.

This layer employs multiple parameterized quantum filters, including CNOT (controlled NOT) gates and rotary gates. As a result of these refinements, the achieved classification accuracy rate attains 98.765% when tested on the ISIC 2019 dataset, which comprises eight distinct classes of skin lesions.

In light of the studies mentioned earlier, it becomes apparent that the outcomes of the first work exhibit limited performance, as it focuses on binary classification. In contrast, the second study presents a multi-classification model with strong generalization performance. However, it does not provide insights into computational efficiency aspects such as training time and parameter count. Additionally, it lacks a demonstration of any improvements over the baseline model.

When it comes to medical images, there has been a noticeable rise in interest in utilizing quantum machine learning techniques [35]. This trend has led to the development of innovative approaches that aim to improve the quality of computer-aided diagnosis. Prominent examples include [1] and [4], both dedicated to COVID-19 detection, along with [24], which focuses on classifying distinct levels of retinopathy and instances of pneumonia infections. Moreover, [5] introduces a method for breast cancer diagnosis, while [3] pertains to the classification of brain cancer.

3 Proposed Approach

In this section, we present a classical-to-quantum system as a solution to accurately differentiate between three types of skin lesions, namely nevus (N), melanoma (M), and basal cell carcinoma (BCC).

Inspired by the research of Mari et al. [22], we have experimentally adapted a 5-qubit dressed quantum circuit model known as DressedQNet. To train this adapted DressedQNet model and perform predictions on skin lesion images, the utilization of transfer learning is essential.

The transfer concept involves considering two models: the pre-trained CNN model, serving as the feature extractor, and the DressedQNet model, designed to act as the classifier. The transfer process is outlined as follows:

1. Initiate the process by pre-training the source CNN model on ImageNet dataset encompassing 1000 classes. The chosen pre-trained models include ResNet-18 [12], DenseNet-121 [13], RegNetX-1.6GF [27], and EfficientNetV2-small (EfficientNetV2-S) [32] architectures. These specific models have been selected due to their resulted compact feature vector dimensions and proven effectiveness.
2. Construct a target model that has the same the configuration as the pre-trained CNN model.
3. In the target model, introduce a trainable output layer (referred to as Dressed-QNet) to the pre-trained model, excluding its final fully connected layer (acting as a classifier for the feature extractor component).
4. Train the target model using the training dataset of skin lesion images, enabling the update of both the extractor's weights and those of the DressedQNet model.

As illustrated in Fig. 1, the DressedQNet model takes an input feature vector z with dimensions of M (512, 1024, 912, 1280 for ResNet-18, DenseNet-121, RegNetX-1.6GF, and EfficientNetV2-S, respectively). Once the adapted model is trained, it becomes capable of conducting inferences on input skin lesion images. During the model inference, it generates the corresponding prediction y for the given skin lesion image.

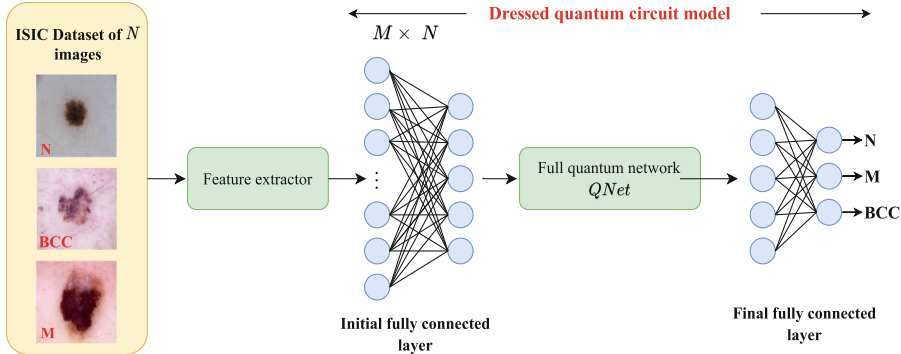


Fig. 1. The adapted 5-qubit dressed quantum circuit model for skin lesion classification

In terms of its architectural components, the DressedQNet model comprises the following elements:

(1) **An initial fully connected layer:** This layer is responsible for reducing the feature dimension (M) of the output obtained from pre-trained CNN models down to 5-qubit. This layer is specifically indicated in Eqs. 5–8 as $fc_{M \rightarrow 5}$.

(2) **A full quantum network (QNet):** This network consists of the initial embedding (\mathcal{E}) layer, the variational quantum circuit (\mathcal{VQC}) of depth d and the final measurement (\mathcal{M}) layer. These constituents are represented by Eq. 1 and Fig. 2 illustrates the circuit diagram of the full quantum network.

$$QNet = \mathcal{M} \circ \mathcal{VQC} \circ \mathcal{E} \quad (1)$$

In accordance with Fig. 2, the $QNet$ is constructed from:

- **Embedding layer:** This layer maps the real vector x into a quantum state using a specified embedding map. The latter prepares each qubit in a balanced superposition of $|0\rangle$ and $|1\rangle$ state using a Hadamard gate H . Subsequently, it performs a rotation around the Y-axis of the Bloch sphere, parameterized by a classical vector $x = (x_1, x_2, \dots, x_5)$.

$$\mathcal{E}(x) = \bigotimes_{i=1}^5 \left(R_y(x_i \frac{\pi}{2}) H \right) |00000\rangle \quad (2)$$

- **Variational quantum circuit:** Is a sequence of d quantum layers. In our case, d is fixed at a value of 4. This circuit is designed to carry out the task of skin lesion classification. Conceptually, a \mathcal{VQC} can be understood as a composition of multiple unitary matrices, each characterized by specific weights (w). The structure of the \mathcal{VQC} can be represented as:

$$\mathcal{VQC} = \mathcal{L}_4 \circ \mathcal{L}_3 \circ \mathcal{L}_2 \circ \mathcal{L}_1 \quad (3)$$

Here, \mathcal{L}_i denotes a quantum layer. It can be defined as unitary operation performed by \mathcal{VQC} . This operation transforms the input state $|x\rangle$ of n_qubit or quantum subsystems into the output state $|y\rangle$. Mathematically, the quantum layer \mathcal{L} can be expressed using Eq. 4:

$$\mathcal{L}(w) : |x\rangle \rightarrow |y\rangle = K \bigotimes_{i=1}^5 R_y(w_i)|x\rangle \quad (4)$$

Where K represents an entangling unitary operation comprising four CNOT gates.

- **Measurement layer:** In this stage, the output states are measured using the Pauli-Z matrix, which converts them into classical states (0 or 1) based on their quantum probabilities. These measured outcomes are then recorded in a classical register, which is a memory unit for storing classical information. The data from the classical register is subsequently passed to the final fully connected layer, facilitating the translation of quantum outcomes into a format that can be used for further computation and analysis in classical models.

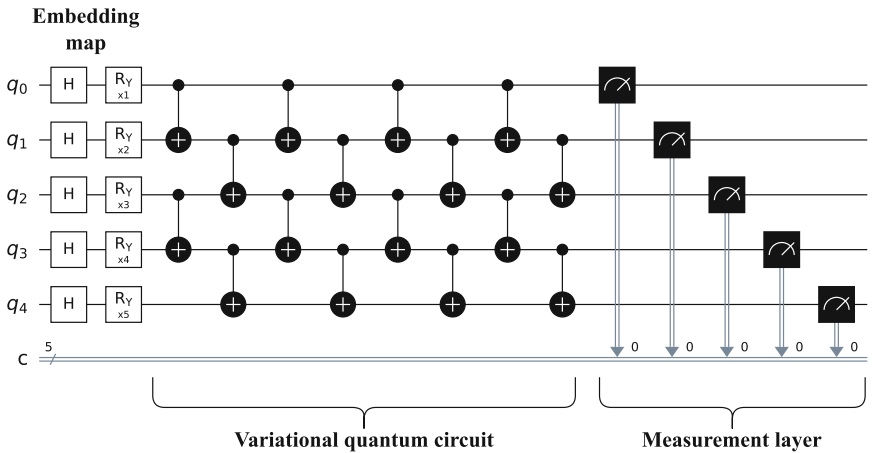


Fig. 2. Circuit diagram of the full quantum network

- (3) **A final fully connected layer ($fc_{5 \rightarrow 3}$):** Serves as the classification stage, where the decision for classifying the input image is based on determining the

index with the highest value in the output vector $y = (y_1, y_2, y_3)$ produced by the dressed quantum circuit.

Mathematically, the DressedQNet model is formulated through Eqs. 5–8, which are derived from the specific pre-trained models used. This has led to the development of four distinct variants of the DressedQNet model.

$$\text{DressedQNet_ResNet} = fc_{5 \rightarrow 3} \circ QNet \circ fc_{512 \rightarrow 5} \quad (5)$$

$$\text{DressedQNet_DenseNet} = fc_{5 \rightarrow 3} \circ QNet \circ fc_{1024 \rightarrow 5} \quad (6)$$

$$\text{DressedQNet_RegNetX} = fc_{5 \rightarrow 3} \circ QNet \circ fc_{912 \rightarrow 5} \quad (7)$$

$$\text{DressedQNet_EfficientNet} = fc_{5 \rightarrow 3} \circ fc \circ QNet \circ fc_{1280 \rightarrow 5} \quad (8)$$

4 Experimental Results and Discussion

To evaluate the effectiveness of our proposed approach, we used the Python programming language and the Google Colaboratory platform, which featured 16 GB of memory and utilized the free T4 GPU for enhanced computational capabilities. Furthermore, we conducted several tests and comparisons with different variants of the DressedQNet model using the default PennyLane [8] quantum simulator.

Concerning the dataset, we used the ISIC dataset, which can be accessed through the provided link¹. This dataset encompasses a total of 2357 dermoscopic labelled images, showcasing a variety of classes including actinic keratosis, basal cell carcinoma, dermatofibroma, melanoma, nevus, pigmented benign keratosis, seborrheic keratosis, squamous cell carcinoma, and vascular lesion.

From the entirety of the dataset, we made a selection of 1219 skin lesion images that are representative of three basic classes: melanoma, nevus, and basal cell carcinoma. However, the original dataset demonstrated an imbalance, which led us to create a more balanced dataset. This rebalancing was achieved by selecting randomly 373 nevus images, 454 melanoma images, and 392 basal cell carcinoma images.

After constructing the dataset, we proceeded to split it into separate training, validation, and test sets. The distribution of data samples across the three classes used in our study within these sets is outlined in Table 1.

In the process of establishing the empirical parameter configurations, an extensive series of tests was carried out to meticulously fine-tune the hyperparameters of both the classical deep learning and DressedQNet models. The objective was to identify specific values that would lead to the effective skin lesion predictions. Table 2 lists the corresponding values that we were selected for this purpose.

¹ <https://www.kaggle.com/datasets/nodoubtome/skin-cancer9-classesisisic>.

Table 1. Distribution of the ISIC dataset among training, validation, and test sets

Classes	Training set	Validation set	Test set
Nevus (N)	261	37	75
Melanoma (M)	317	46	91
Basal cell carcinoma (BCC)	274	39	79
Total	852	122	245

Table 2. Empirical hyperparameter settings

Optimizer	Initial lr	Momentum	Epoch	lr Scheduler	Milestones	Gamma	Batch size
SGD	$1e - 3$	0.9	30	MultiStepLR	[7, 11]	0.1	4

Quantitatively speaking, Tables 3, 4, 5, and 6 provide a visual representation of the confusion matrices corresponding to DressedQNet.ResNet, Dressed QNet.DenseNet, DressedQNet.RegNetX and DressedQNet.EfficientNet models. These matrices were generated during the inference stage using the PennyLane simulator (PL.Sim).

Table 3. Confusion matrix for the DressedQNet.ResNet Model using PL.Sim

		Predicted		
		N	M	BCC
Actual	N	50	22	3
	M	7	80	4
	BCC	5	3	71

Table 4. Confusion matrix for the DressedQNet.DenseNet Model using PL.Sim

		Predicted		
		N	M	BCC
Actual	N	54	18	3
	M	5	81	5
	BCC	4	1	74

Table 5. Confusion matrix for the DressedQNet_RegNetX Model using PL_Sim

		Predicted		
		N	M	BCC
Actual	N	52	19	4
	M	4	85	2
	BCC	5	3	71

Table 6. Confusion matrix for the DressedQNet_EfficientNet Model using PL_Sim

		Predicted		
		N	M	BCC
Actual	N	58	16	1
	M	6	82	3
	BCC	4	2	73

As indicated by the confusion matrices, the DressedQNet_EfficientNet model achieved a high accuracy rate by correctly classifying 58 out of 75 nevus, 82 out of 91 melanoma, and 73 out of 79 basal cell carcinoma skin lesions. Upon analyzing the classification outcomes of the DressedQNet_RestNet model, we can observe that it exhibits the lowest true classification rate and the highest misclassification rate across all skin lesion types when compared to the other models.

Furthermore, we have presented the classification loss curves for the four different variants of the simulated DressedQNet model, alongside ResNet-18, RegNetX-1.6GF, DenseNet-121, and EfficientNetV2-S, as shown in Fig. 3.

Overall, the analysis of loss curves reveals distinct characteristics among the models: RegNetX-1.6GF and DressedQNet_RegNetX models exhibit consistent and stable learning trends, EfficientNetV2-S outperforms with notably lower loss values, converging to 0.23 for training and 0.32 for validation after 30 epochs, while ResNet18 lags behind with relatively higher loss values, reaching 0.48 for training and 0.41 for validation.

For the sake of completeness, we present details on the number of trainable parameters and training times (measured in seconds/epoch) for various models. This includes ResNet-18, RegNetX-1.6GF, DenseNet-121, and EfficientNetV2-S, all of which operate as feature extractors. Moreover, we provide insights into the ResNet-18, RegNetX-1.6GF, DenseNet-121, and EfficientNetV2-S-based classical neural network (classical-NN), each of which consists of fully connected layer(s) for skin lesion classification. Additionally, we are including information about the four distinct variants of the simulated DressedQNet model. These details are summarized in Table 7.

When considering the numbers of trainable parameters, it's noteworthy that pre-trained CNN feature extractors exhibit high numbers of trainable parameters

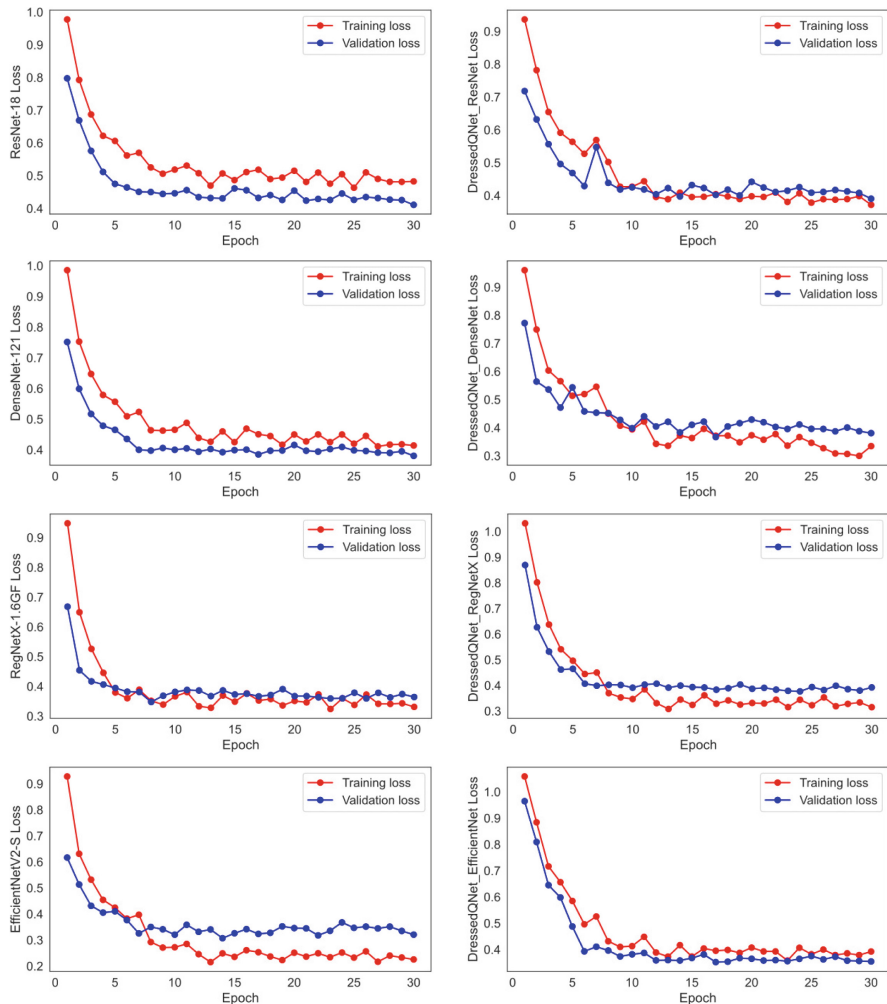


Fig. 3. Loss curves of the skin lesion classification models

Table 7. Comparing trainable parameters and training time of the skin lesion classification models

Model	Trainable parameters			Training time	
	Feature extractor	Classical-NN	DressedQNet	Classical-NN	DressedQNet
ResNet-18 [12]	11176512	1539	2603	6	64
DenseNet-121 [13]	6953856	3075	5163	13	69
RegNetX-1.6GF [27]	8277136	2739	4603	10	66
EfficientNetV2-S [32]	20177488	3843	6443	15	68

compared to classical-NN and DressedQNet models. This can be justified by deep and complex architectures characterized by intricate, multi-layered structures in these feature extractors. Among them, EfficientNetV2-S boasts the highest count, followed by ResNet-18, RegNetX-1.6GF, and DenseNet-121. In contrast, the classical-NN models possess significantly fewer trainable parameters, with the lowest tally found in ResNet-18, followed by RegNetX-1.6GF, DenseNet-121, and EfficientNetV2-S. This difference arises from the simplified architectures of classical-NN models, typically composed of fully connected layers. Concerning the DressedQNet models themselves, the trainable parameter counts also differ, with the lowest in ResNet-18, followed by RegNetX-1.6GF, DenseNet-121, and EfficientNetV2-S. The integration of quantum components in DressedQNet models introduces additional quantum layers and operations, increasing parameter number. Consequently, DressedQNet models exhibit a higher number of trainable parameters compared to conventional CNNs.

In regard to training time, the classical-NN models demonstrate the shortest training duration, with ResNet-18 being the fastest. Conversely, the training time for the DressedQNet models themselves is longer, where ResNet-18 stands out as the most efficient model. This discrepancy can be attributed to various factors, including the well-developed and optimized classical hardware, the inherent complexities and overheads of quantum computations, and the existing scalability challenges in quantum technologies. As an alternative solution, one could run the DressedQNet models on real quantum processors and leverage parallelism in computations, potentially further enhancing training time.

Based on the obtained results, it is clear that the classical-NN using ResNet and the DressedQNet_ResNet variant stand out as the lightweight architectures and the most efficient models in terms of computational speed. These architectures employ skip connections, which are known to alleviate the vanishing gradient problem and consequently reduce the number of parameters.

Table 8 reports the skin lesion classification performance for the purpose of comparison. It includes metrics such as sensitivity (%), precision (%), specificity (%), F1-score, accuracy (%), and inference time (ms). These evaluations are conducted for the simulated DressedQNet models and the pre-trained CNN models. The comparison is based on the results obtained using both the default PennyLane simulator and the `ibmq_asmq_simulator` [14] (IBM_Sim).

After conducting a thorough comparison of the classification model results, several important observations emerge:

- The DressedQNet variants in both the default PennyLane simulator and the `ibmq_qasm_simulator` consistently show improved generalization results compared to the deep learning models across different architectures. The variants seem to improve sensitivity, precision, specificity, F1-score, and accuracy performance while introducing additional complexity in terms of inference time. This predictive prowess is attributed to the adaptation of quantum computing concepts within the DressedQNet models.
- The simulated DressedQNet models in the default PennyLane often demonstrate similar or slightly improved predictive performance compared to

those tested in the `ibmq_qasm_simulator`. This is due to PennyLane's use of sophisticated algorithms optimized for accuracy and the absence of noise models, resulting in more deterministic outcomes. In contrast, the `ibmq_qasm_simulator` introduces variability through noise and error models to mimic real quantum hardware. Furthermore, the PennyLane simulator excels in circuit optimization and is well-suited for less complex circuits, contributing to its quicker inference times. The resource allocation and efficiency differences between the two simulators also play a role in the observed performance variations.

- When considering the trade-off between predictive performance and computational time, the `DressedQNet_EfficientNetPL-Sim` demonstrates high performance metrics (sensitivity, precision, specificity, F1-score, accuracy) while maintaining a moderate increase in computational time compared to the `EfficientNetV2-S` model.

Table 8. Comparison of the adapted DressedQNet models with pre-trained CNN models for skin lesion classification

Models	Sensitivity	Precision	Specificity	F1-Score	Accuracy	Time
ResNet-18	79	80.91	89.74	78.82	80	4
DressedQNet_ResNet _{PL-Sim}	81.48	82.62	90.83	81.69	82.04	36
DressedQNet_ResNet _{IBM-Sim}	81.48	82.62	90.83	81.69	82.04	3449
DenseNet-121	83.49	84.63	91.88	83.7	84.08	16
DressedQNet_DenseNet _{PL-Sim}	84.89	85.65	92.52	85.1	85	49
DressedQNet_DenseNet _{IBM-Sim}	84.89	85.65	92.52	85.1	85	3714
RegNetX-1.6GF	80.79	82.93	90.56	80.62	81.63	9
DressedQNet_RegNetX _{PL-Sim}	84.2	85.63	92.27	84.45	84.9	43
DressedQNet_RegNetX _{IBM-Sim}	83.76	85.3	92.05	84	84.49	3456
EfficientNetV2-S	83.87	85.55	92.02	84.19	84.49	17
DressedQNet_EfficientNet _{PL-Sim}	86.62	87.37	93.34	86.86	86.94	51
DressedQNet_EfficientNet _{IBM-Sim}	86.17	87.02	93.12	86.43	86.53	3562

5 Conclusion

In this study, we have introduced an innovative approach, a classical-to-quantum system, for the task of skin lesion classification. This novel solution involves adapting a 5-qubit dressed quantum circuit model and using four pre-trained CNN models (ResNet-18, DenseNet-121, RegNetX-1.6GF, and EfficientNetV2-S) as feature extractors. This adaptation has given rise to four unique variants of the model, each leveraging a different architecture.

Our evaluation process encompassed thorough testing on the ISIC image dataset, employing the default PennyLane simulator. The results of these extensive tests highlight the remarkable generalization capabilities of our proposed classical-to-quantum system compared to deep learning models.

In the future, we plan to expand our research by using diverse medical image datasets that contain a wider range of classes. Additionally, we are interested in running the adapted dressed quantum circuit model on IBM quantum processors and using parallelism in computations. This ultimately enhances the efficiency of our medical diagnosis process. Another promising direction involves exploring quantum-to-quantum machine learning approaches.

References

1. Acar, E., Yilmaz, İ.: Covid-19 detection on ibm quantum computer with classical-quantum transfer learning. medRxiv (2020). <https://doi.org/10.1101/2020.11.07.20227306>
2. Adeyanju, I., Bello, O., Adegbeye, M.: Machine learning methods for sign language recognition: a critical review and analysis. Intell. Syst. Appl. **12**, 200056 (2021). <https://doi.org/10.1016/j.iswa.2021.200056>
3. Ajlouni, N., Özyavaş, A., Takaoglu, M., Takaoglu, F., Ajlouni, F.: Medical image diagnosis based on adaptive hybrid quantum cnn (2023). <https://doi.org/10.21203/rs.3.rs-3037666/v1>
4. Amin, J., Sharif, M., Gul, N., Kadry, S., Chakraborty, C.: Quantum machine learning architecture for covid-19 classification based on synthetic data generation using conditional adversarial neural network. Cogn. Comput. **14**(5), 1677–1688 (2022). <https://doi.org/10.1007/s12559-021-09926-6>
5. Azevedo, V., Silva, C., Dutra, I.: Quantum transfer learning for breast cancer detection. Quant. Mach. Intell. **4**(1), 5 (2022). <https://doi.org/10.1007/s42484-022-00062-4>
6. Bajić, F., Job, J.: Review of chart image detection and classification. Int. J. Doc. Anal. Recogn. (IJDAR) (2023). <https://doi.org/10.1007/s10032-022-00424-5>
7. Belattar, K., Adjadj, M., Bakir, M., Ait Mehdi, M.: A comparative study of cnn architectures for melanoma skin cancer classification (2022). <http://hdl.handle.net/20.500.12188/25340>
8. Bergholm, V., et al.: Pennylane: automatic differentiation of hybrid quantum-classical computations. arXiv preprint [arXiv:1811.04968](https://arxiv.org/abs/1811.04968) (2018)
9. Bokhan, D., Mastiukova, A.S., Boev, A.S., Trubnikov, D.N., Fedorov, A.K.: Multiclass classification using quantum convolutional neural networks with hybrid quantum-classical learning. Front. Phys. **10**, 1069985 (2022). <https://doi.org/10.3389/fphy.2022.1069985>
10. Dey, N. (ed.): Classification techniques for medical image analysis and computer aided diagnosis. In: Advances in Ubiquitous Sensing Applications for Healthcare. Academic Press (2019). <https://doi.org/10.1016/B978-0-12-818004-4.00003-0>
11. Goodfellow, I., Bengio, Y., Courville, A.: Deep Learning. MIT press, Cambridge (2016)
12. He, K., Zhang, X., Ren, S., Sun, J.: Deep residual learning for image recognition (2015)
13. Huang, G., Liu, Z., van der Maaten, L., Weinberger, K.Q.: Densely connected convolutional networks (2018)
14. IBM, I.: Migration guide from qiskit-ibmq-provider to qiskit-ibm-provider. https://qiskit.org/ecosystem/ibm-provider/tutorials/Migration_Guide_from_qiskit-ibmq-provider.html

15. Iyer, V., Ganti, B., Am, H., Namboori, D.K., Iyer, S.: Hybrid quantum computing based early detection of skin cancer. *J. Interdisc. Math.* **23**, 347–355 (2020). <https://doi.org/10.1080/09720502.2020.1731948>
16. Jadhav, A., Rasool, A., Gyanchandani, M.: Quantum machine learning: scope for real-world problems. *Procedia Comput. Sci.* **218**, 2612–2625 (2023). <https://doi.org/10.1016/j.procs.2023.01.235>
17. Janiesch, C., Zschech, P., Heinrich, K.: Machine learning and deep learning. *Electron. Mark.* **31**(3), 685–695 (2021). <https://doi.org/10.1007/s12525-021-00475-2>
18. Ladd, T.D., Jelezko, F., Laflamme, R., Nakamura, Y., Monroe, C., O’Brien, J.L.: Quantum computers. *Nature* **464**(7285), 45–53 (2010)
19. Li, Z., et al.: A classification method for multi-class skin damage images combining quantum computing and inception-resnet-v1. *Front. Phys.* **10**, 1046314 (2022). <https://doi.org/10.3389/fphy.2022.1046314>
20. Lloyd, S.: Universal quantum simulators. *Science* **273**(5278), 1073–1078 (1996). <https://doi.org/10.1126/science.273.5278.1073>
21. Lloyd, S., Mohseni, M., Rebentrost, P.: Quantum algorithms for supervised and unsupervised machine learning (2013). <https://doi.org/10.48550/arXiv.1307.0411>
22. Mari, A., Bromley, T.R., Izaac, J., Schuld, M., Killoran, N.: Transfer learning in hybrid classical-quantum neural networks. *Quantum* **4**, 340 (2020). <https://doi.org/10.22331/q-2020-10-09-340>
23. Martín-Guerrero, J.D., Lamata, L.: Quantum machine learning: a tutorial. *Neurocomputing* **470**, 457–461 (2022). <https://doi.org/10.1016/j.neucom.2021.02.102>
24. Mathur, N., et al.: Medical image classification via quantum neural networks (2022)
25. Pastorello, D.: Quantum clustering, pp. 57–68. Springer, Singapore (2023). https://doi.org/10.1007/978-981-19-6897-6_6
26. Perelshtain, M., et al.: Practical application-specific advantage through hybrid quantum computing (2022)
27. Radosavovic, I., Kosaraju, R.P., Girshick, R., He, K., Dollár, P.: Designing network design spaces (2020)
28. Schuld, M., Fingerhuth, M., Petruccione, F.: Implementing a distance-based classifier with a quantum interference circuit. *EPL (Europhys. Lett.)* **119**(6), 60002 (2017). <https://doi.org/10.1209/0295-5075/119/60002>
29. Schuld, M., Petruccione, F.: Supervised Learning with Quantum Computers. Springer, Cham (2018). <https://doi.org/10.1007/978-3-319-96424-9>
30. Senokosov, A., Sedykh, A., Saginalieva, A., Melnikov, A.: Quantum machine learning for image classification (2023)
31. Shor, P.: Algorithms for quantum computation: discrete logarithms and factoring. In: Proceedings 35th Annual Symposium on Foundations of Computer Science, pp. 124–134 (1994). <https://doi.org/10.1109/SFCS.1994.365700>
32. Tan, M., Le, Q.V.: Efficientnetv2: smaller models and faster training (2021)
33. Taskiran, M., Kahraman, N., Erdem, C.E.: Face recognition: past, present and future (a review). *Digital Signal Process.* **106**, 102809 (2020). <https://doi.org/10.1016/j.dsp.2020.102809>
34. Wang, Z., Xu, M., Zhang, Y.: Review of quantum image processing. *Arch. Comput. Methods Eng.* **29** (2021). <https://doi.org/10.1007/s11831-021-09599-2>
35. Wei, L., et al.: Quantum machine learning in medical image analysis: a survey. *Neurocomputing* **525**, 42–53 (2023). <https://doi.org/10.1016/j.neucom.2023.01.049>

Author Index

A

- Achouri, Youssouf 1
Ait Mehdi, Mohamed 194

B

- Belattar, Khadidja 194
Belhadeff, Hacene 15
Belkadi, Widad Hassina 91
Bendjeghaba, Omar 38
Boughaci, Dalila 50
Bouguenna, Elouahab 107
Bourahla, Mustapha 179

C

- Çakar, Tuna 120

D

- Djellab, Rima 1
Drias, Habiba 77, 91
Drias, Yassine 91, 120

G

- Gharbi, Abdelhakim 167

H

- Hamouid, Khaled 1

I

- Ishak Boushaki, Saida 38

K

- Kali Ali, Selma 50
Kamel, Nadjet 38
Khelfa, Celia 77
Khennak, Ilyes 77

L

- Lariane, Mohcene Mouad 15
Lekouaghet, Badis 107

M

- Mebtouche, Naoual El Djouher 152
Merazi-Meksen, Thouraya 32
Merrouche, Walid 107
Moulai, Hadjer 65

S

- Sahnoune, Sarah 152
Salhi, Dhai Eddine 38
Siouane, Alaa Eddine 120
Souami, Feryel 194

T

- Thantharate, Anurag 134
Thantharate, Pratik 134

Y

- Younes, Mustapha Anis 167

Z

- Zebboudj, Sofia 167